Computational Modelling of the Degradation of Poly-L-lactide for a Bioresorbable Polymeric Stent

Rosa Connor Shine B.E. (2014)

A thesis submitted to the National University of Ireland as fulfilment of the requirements for the Degree of Doctor of Philosophy.

January 2020

Discipline of Biomedical Engineering,

School of Engineering,

National University of Ireland Galway

Primary Supervisor Prof. Peter E. McHugh

Co-Supervisor Dr. William Ronan

Abstract

The interest in biodegradable polymers for the design of bioresorbable stents, temporary vascular scaffolds designed to restore patency to obstructed vessels, has witnessed a dramatic growth over the last ten to fifteen years. While bioresorbable polymeric stents (BPS) offer possibilities to help address the long-term complications (e.g. in-stent restenosis, stent thrombosis) associated with permanent devices, in-vivo degradation behaviours are not yet fully understood. The application of computational modelling, for example finite element analysis (FEA), to predict and analyse BPS degradation behaviour provides a means to investigate in-vivo performance and further enhance BPS design. Current computational modelling techniques for the degradation of BPS predominately focus on the phenomenological aspects of degradation, with little emphasis given to the inherent microstructure changes (bulk degradation, crystallisation) which occur in the degrading polymer.

This research aims to advance the computational modelling techniques for examination of BPS degradation behaviours, though development of co-simulation techniques which are applied to evaluate the physio-chemical degradation of BPS and assess the impacts of material, design and degradation product boundary condition on the physio-chemical degradation, and on the subsequent mechanical performance and scaffolding ability of the device.

Physio-chemical degradation of BPS geometries and materials is simulated through adaptation of the heat equation in FE. Model predictions reveal a significant dependency of degradation on the imposed degradation product boundary conditions. Predictions indicate that BPS design does not have a significant impact on molecular weight reduction rates; however, material

crystallinity and heterogeneities in crystallinity emerge as key contributors to device performance. Consideration of the device mechanical boundary conditions shows a reliance of the scaffolding ability of degrading BPS on the imposed initial loading. This research proposes considerations for the modelling requirements surrounding BPS regulatory approval.

In conclusion, the work performed in this thesis has led to an enhanced understanding of the in-vivo degradation behaviours and mechanical performance of BPS. This work has generated new insight into the expected clinical performance of BPS and presents a solid framework for the development of further design and analysis techniques for BPS.

Acknowledgements

Firstly I want to express my sincere gratitude and thanks to my supervisors Prof. Peter McHugh and Dr. William Ronan for their constant support, knowledge, guidance and encouragement. I'd like to thank them for always ensuring that I had access to the best facilities, expertise and support available during the creation and execution of the work presented in this thesis.

I wish to acknowledge funding through the College of Engineering, NUI Galway, Postgraduate Scholarship Scheme, from the National University of Ireland, and from Fulbright Ireland. I'd like to also acknowledge the SFI/HEA funded Irish Centre for High End Computing (ICHEC) for the provision of computational facilities and support. I would like to thank Dr Nicola Kelly for her support and guidance during the early stages of the research, and to acknowledge Dr. Reyhaneh Neghabat Shirazi and Dr. Caoimhe Sweeney for their advice and support on the project.

I wish to thank the staff and my fellow postgraduate students in the Biomedical and Mechanical departments, in particular Prof. Laoise McNamara, Dr. Ted Vaughan, Mr. David Connolly, Mr. William Kelly, Ms. Jane Bowman and to Donnacha, Enda, Sinead and members of the McHugh and Ronan research groups. I'd like to thank and acknowledge Dr. Claire Conway and Prof. Elazer Edelman for their support and valued insights on the project during my time in Boston; thanks to all at Fulbright Ireland and all in the Edelman lab, especially to Dr. Natalie Artzi, Pei-jiang, Eric, Vicky and Kim.

Finally, I want to acknowledge the constant support and encouragement I received from my parents, family and friends over the last few years, and in particular thank Dearbhla, Lisa, Paddy, Aaron, Saoirse, Sean, Padraig, Beano

and everyone involved with NUI Galway soccer and Corrib Rangers, and to volunteers and friends at Teach Solais, GOSSIP, and AMACH, especially Mary, Vivienne, Jenny, Sarah, Cameron and Cúán for always making themselves available for a cup of tea and a chat during Saturday drop-in.

For Amelia Perry, thank you for always being your wonderful true self and for continuing to inspire me every day.

List of Publications

The work presented in this thesis has appeared in the following publications:

Chapter 2: Boland, E.L., Shine, R., Kelly, N., Sweeney, C.A., McHugh, P.E., 2016b. A Review of Material Degradation Modelling for the Analysis and Design of Bioabsorbable Stents. Ann. Biomed. Eng. 44, 341–356. https://doi.org/10.1007/s10439-015-1413-5

Chapter 4: Shine, R., Shirazi, R.N., Ronan, W., Sweeney, C.A., Kelly, N., Rochev, Y.A., McHugh, P.E., Modelling of Biodegradable Polyesters with Applications to Coronary Stents (ASME Journal of Medical Devices, Volume 11 (2), May 2017) https://doi.org/10.1115/1.4035723

The work presented in this thesis has directly contributed to a number of conference presentations (oral presentations):

"*Finite element modelling of crystallization and its effects on the mechanical performance of bio-erodible polymeric scaffolds (BPS)*"

R. Shine, P.E. McHugh, W. Ronan

10th European Solid Mechanics Conference, July 2-6 2018, Bologna, Italy

"Finite element analysis of bioresorbable polymers using a thermo-mechanical co-simulation model"

R. Shine, R.N. Shirazi, C.A. Sweeney, N. Kelly, P.E. McHugh

General session on mechanical properties of biomaterials, 10th World Biomaterials Congress, May 17-22nd 2016 Montréal, Canada

"A co-simulation degradation model for the computational analysis of a bioresorbable Poly-(L-lactide) stent"

R. Shine, C.A. Sweeney, N. Kelly, P.E. McHugh

22nd Bioengineering in Ireland Conference, Jan 22nd 2016, Galway, Ireland

General Abbreviations

BMS	bare metal stent
BPS	bioresorbable polymeric stent
BRMS	bioresorbable magnesium stents
BVS	Bioresorbable Vascular Scaffold
CAD	coronary artery disease
CVD	cardiovascular disease
DAPT	dual anti-platelet therapy
DES	drug-eluting stent
FDA	Food and Drug Administration
FE	finite element
FEA	finite element analysis
FIM	first in man
GPC	gel permeation chromatography
ISR	in-stent restenosis
IVUS	intravascular ultrasound
LA	lactic acid
MI	myocardial infarction
NIR	neo-intimal remodelling
OCT	optical coherence tomography
PAE	poly-anhydride ester
PBS	phosphate buffer solution
PBS*	poly(butylene succinate)
PCI	percutaneous coronary intervention
PCL	poly (e-caprolactone)
PDLA	poly-D-lactide
PDLGA	poly-D,L-lactide-co-glycolide
PDLLA	poly-D,L-lactide
PDS	poly (dioxanone)
PGA	poly-glycolic acid
PLA	poly-lactide
PLLA	poly-L-lactide
PLGA	poly-lactide-co-glycolic acid
POBA	plain old balloon angioplasty
PTCA	percutaneous transluminal coronary angioplasty
QLV	quasi-linear viscoelastic
SFE	stent fully embedded
SFS	stent free surface
SIFS	strut inner surface free
SMC	smooth muscle cell
SPE	strut partially embedded
TLR	target lesion revascularisation
UMAT	user material subroutine
UMATHT	user material subroutine for thermal behaviour
USDFLD	user subroutine for redefining field variables

Nomenclature

b	dimensionless Knowles constant
$\boldsymbol{B}$	left Cauchy-Green deformation tensor
$\boldsymbol{B_e}$	shape function matrix
$\widehat{\boldsymbol{B}}$	global shape function gradient matrix
C_c	specific energy
C_e	mole concentration of ester bonds of polymer chains
C_{e0}	initial mole concentration of ester bonds of polymer chains
$\bar{C}_e$	normalised mole concentration of ester bonds of polymer chains
$\hat{C}_e$	Non-dimensional form of ester bond concentration
C_m	mole concentration of monomers
$\hat{C}_m$	Non-dimensional form of monomer concentration
C_{ij}	Material parameter for HGO model
C_{ol}	mole number of ester bonds in oligomers per unit volume
$\bar{C}_{ol}$	normalised mole concentration of oligomers
C_p	specific heat
$\boldsymbol{C_m}$	diffusive flux of monomers
$\boldsymbol{C}$	right Cauchy-Green deformation tensor
$\overline{\boldsymbol{C}}$	modified right Cauchy-Green deformation tensor
d	degradation parameter
D	effective diffusion coefficient
D_1	inverse of material bulk modulus
D_a	diffusion coefficient of oligomers in amorphous polymer (Arrhenius temperature dependant constant)
D_i	Material parameter for HGO model

D_{matrix}	diffusion coefficient in the polymer matrix
D_o	intrinsic diffusion coefficient
D_{pore}	diffusion coefficient in liquid-filled pores
e	element in the finite element mesh
E	Young's modulus
E_0	initial value of Young's modulus
E_{k1}	activation energy for hydrolysis
E_{k2}	activation energy for autocatalysis
E_{max0}	activation energy for maximum crystallinity
$\boldsymbol{E}$	Green-Lagrangian strain tensor
$\mathbf{f}$	heat flux vector
$\boldsymbol{F}$	deformation gradient
$\boldsymbol{G}$	global force balance
H	hydrolysis reaction
I_1, I_2, I_3	First, second and third invariants of strain tensor
$\bar{I}_1, \bar{I}_2$	First and second invariants of the modified right Cauchy Green strain tensor
$\boldsymbol{I}$	identity tensor
J	Jacobian
J_m	material flux
k_1	reaction rate constant for hydrolysis
k_{10}	temperature dependant pre-exponential constant for hydrolysis
k_2	reaction rate constant for autocatalysis
k_{20}	temperature dependant pre-exponential constant for autocatalysis
k_m	modulus degradation rate constant

K	material bulk modulus
$\mathbf{k}$	thermal conductivity matrix
$\boldsymbol{K}$	Kirchhoff stress tensor
L	length of representative unit of material
l_{diff}	diffusion length parameter
l_e	characteristic element length
m	average number of repeating units of the oligomers
M_n	number average molecular weight
M_{n0}	initial number average molecular weight
$\bar{M}_n$	normalised number average molecular weight
$\bar{M}_n^V$	volume averaged number average molecular weight
M_0	molar mass of a repeating unit of the polymer
M_w	weight average molecular weight
$\bar{M}_w$	normalised value of weight average molecular weight
$\bar{M}_w^V$	volume averaged weight average molecular weight
M_{w0}	initial value of weight average molecular weight
n	acid dissociation constant
n_i	iteration number (for FE iteration)
n_h	dimensionless hardening parameter
$\boldsymbol{n}$	outward unit vector normal to the surface S_A
$\hat{\boldsymbol{n}}$	outward unit vector normal to the surface
N	number of polynomial terms used in a series
$\widehat{\boldsymbol{N}}$	global shape function matrix

N_{chains}	initial molar concentration of the polymer chains
$\boldsymbol{N_e}$	matrix of shape functions for a defined element e
p_h	hydrostatic pressure component
p	porosity
P	point in the reference configuration
P'	deformed point in the current configuration
$\boldsymbol{P}$	first Piola-Kirchhoff stress tensor
P_x	probability of chain scission nucleating to a crystal
q	heat flux per unit area of a body
Q	second point in reference configuration
r	heat supplied externally into the body per unit volume
R	universal gas constant
R_{ol}	mole number of oligomers per unit volume
R_s	molar number of chain-scissions per unit volume
$\boldsymbol{R}$	orthogonal rotation tensor
S	equilibrium surface
S_A	surface area
$\boldsymbol{S}$	deviatoric stress component
t	time step
$\hat{t}$	normalised time
$\boldsymbol{t}$	thickness of PLLA film
$\tilde{\boldsymbol{t}}$	traction acting on a surface
T	temperature (K)

$\boldsymbol{u}$	displacement vector
$\boldsymbol{u_e}$	nodal displacement vector for element e
U	volumetric component of strain energy density
$\dot{U}$	material time rate of the internal thermal energy
U_c	chemical energy
$\boldsymbol{U}$	symmetric material stretch tensor
V	volume
V_c	finite volume of crystal growth
$\boldsymbol{V}$	symmetric spatial stretch tensor
$\bar{W}$	isochoric component of strain energy density
W_e	strain energy density potential
$\bar{x}$	non-dimensional distance through film thickness
$\boldsymbol{x}$	updated position vector of new deformed point P'
$\boldsymbol{X}$	original position vector of reference point P
X_c	volume fraction degree of crystallinity
X_{c0}	initial value of the volume fraction degree of crystallinity
X_{ext}	volume fraction extended degree of crystallinity
X_{max}	maximum degree of crystallinity
X_{max0}	Arrhenius pre-exponential constant for crystallinity
Y_1, Y_2, Y_3	unknown trial functions of normalised time
α_2	empirical parameter for crystallinity theory
β	empirical parameter for crystallinity theory
δ_{ij}	Kronecker delta

$\delta\boldsymbol{\varepsilon}$	virtual strain vector
$\delta\boldsymbol{u}$	virtual displacement vector
$\boldsymbol{\varepsilon}$	infinitesimal strain tensor
θ	temperature
λ	Lamé elastic constant
λ_i	principle stretches of deformation
ϕ_L	lumen diameter
η_a	Avogadro's constant
ψ	Helmholtz potential
ρ	density
$\boldsymbol{\sigma}$	Cauchy stress tensor
$\bar{\sigma}$	Von Mises equivalent stress
$\boldsymbol{\tau}$	second Piola-Kirchhoff stress tensor
τ_D	characteristic degradation time
μ	shear modulus
μ_0	initial value of shear modulus
ν	Poisson's ratio
ω	inverse molar volume of the crystalline phase

1 Introduction

The treatment of atherosclerotic heart disease was revolutionised by the introduction of coronary stents in the early 1990s. Early stents were metallic devices, which became known as ‘bare metal’ stents (BMS). Later came polymer coated drug-eluting stents (DES), designed to deliver anti-proliferative drugs and lessen incidence of acute stent thrombosis. While the use of BMS and DES is now relatively mature, significant scientific and technological challenges still remain, particularly in tackling the complications associated with long-term placement of the device. This has given rise to the design and development of biodegradable stents, for which bioresorbable polymer materials have been revealed to be favourable materials. Biodegradable stents made from bioresorbable polymers provide the focus for the work of this thesis.

The firm establishment of bioresorbable polymeric stents (BPS) in clinical practice has not yet been realised, which may be due in part to a lack of understanding of the impact of the material degradation on the long-term mechanical performance of the device, and also the dependence of such material degradation on the in-vivo loading environment. The design of bioresorbable stents has recently progressed to reflect the multifaceted aspects of their performance in-vivo, which has proven to be much more complex than first believed. Insight into this complex performance and the key challenges which remain for BPS can be gained through use of computational modelling techniques, which present a powerful means of examining and predicting device behaviour and performance.

1.1 Chapter Summary

A brief overview of cardiovascular disease is given in Section 1.2. The advancement of treatments for this disease and the evolution of stenting technologies are discussed in Section 1.3. An overview of the developments of commercial BPS devices is given in Section 1.4. Certain aspects of BPS design, which are identified as the key challenges to the successful widespread use of such next generation devices, are outlined and summarised in Section 1.5. Computational modelling as a tool for the design and testing of medical devices is reviewed in Section 1.6, with the importance of modelling for the analysis of stents highlighted. Finally, thesis motivation and aims are presented in Sections 1.7 and 1.8, respectively.

1.2 Cardiovascular Heart Disease

Cardiovascular disease (CVD) remains the most common form of death worldwide, with recent mortality statistics for Europe showing 45% of deaths attributed to this illness, amounting to 4 million deaths every year [1]. CVD can often manifest in coronary artery disease (CAD), where the narrow vessels responsible for delivering oxygenated blood to the heart muscles experience a build-up of fatty deposits in the artery wall, which can result in blockage of the artery and ultimately, cardiac ischemia, i.e. restricted blood supply to the heart muscles. CAD can lead to heart pain, or angina, and in severe cases it can result in death of the surrounding cardiac tissue and myocardial infarction (MI). The walls of healthy arteries are made up of three distinct layers known as the intima, the media and the adventitia. Cells present in each of these layers control the healthy functioning and the regular repair of the arteries. If, as a result of CAD, plaques or fatty-deposits build up over time in the artery wall, the lumen (or cross-sectional area) of the artery available for blood flow can

become blocked. This is known clinically as atherosclerosis, and often results in rupture of the intimal layer, leading to the formation of blood clots which may further restrict blood flow, or even migrate to other areas of the heart.

1.3 Advancement of Treatments

1.3.1 Percutaneous coronary intervention

Percutaneous coronary intervention (PCI) is a non-surgical procedure which has been developed and refined over the last three decades for the treatment of CAD. The introduction of coronary angioplasty was first reported by Gruntzig, who successfully performed the first percutaneous transluminal coronary angioplasty (PTCA), or plain old balloon angioplasty (POBA), in 1977, which revolutionised the treatment of CAD [2]. In a coronary angioplasty procedure, a guide catheter is inserted through an incision in the femoral artery, and directed to the site of obstruction in the coronary vasculature. Next, using a guide wire, a balloon catheter (flexible plastic tube) is led along to the blockage site, where the balloon is inflated to compress the plaque and reopen the vessel. This was seen as an attractive alternative to coronary artery bypass surgery; however, angioplasty presented its own shortcomings, with several studies reporting acute complications and high rates of restenosis [3]–[5]. Restenosis, which is most commonly defined as a more than 50% narrowing of the treated vessel lumen [6], is triggered by re-narrowing of the artery (due to elastic vessel recoil), constrictive remodelling of the arterial tissue and neo-intimal hyperplasia [7]. In an effort to reduce the high incidence of restenosis observed for PTCA, the era of coronary stenting was established.

1.3.2 Bare metal stents (BMS)

Stents were first designed as tubular structures of metals such as stainless steel or cobalt chromium, and were designed with the principal intent of keeping the treated artery patent (or open) after percutaneous intervention [8]. Stent implantation is achieved using techniques similar to those used in a POBA procedure; the artery is expanded using a balloon, which deploys the metallic stent structure into the vessel, where it remains in place as a permanent scaffold (**Figure 1.1**). The mechanical properties of the materials chosen for the early bare metal stents (BMS) were a defining factor in the early device design [9]. While the introduction of BMS was shown to significantly lessen the incidence of restenosis and the resultant adverse events of this [10], [11], device failure through stent thrombosis, in-stent restenosis (ISR) or due to strut fracture was nonetheless observed [12], [13].

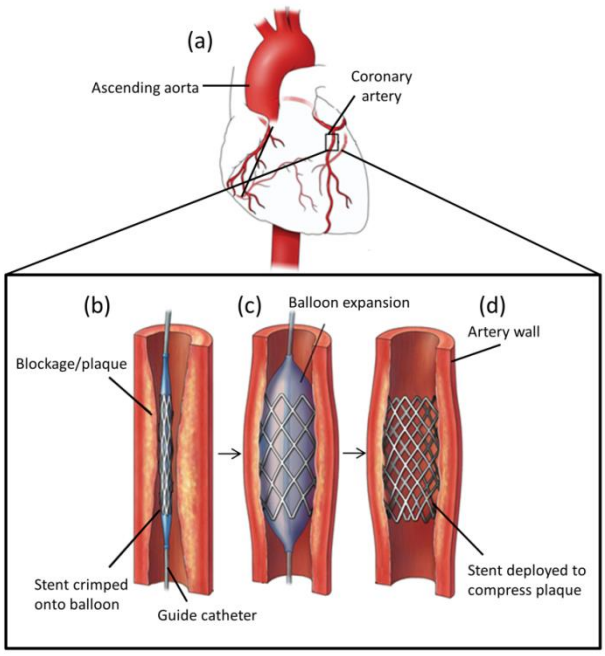

Figure 1.1 Deployment of a stent in a coronary artery during a PCI procedure, showing (a) the location of the coronary arteries, (b) stent crimped onto a deflated balloon catheter at treatment site, (c) balloon expansion to deploy stent and compress the artery, (d) expanded stent remains to provide scaffolding support to the vessel wall while balloon and guide catheter are removed (Adapted from [14]).

As the surface of the stent becomes exposed to the arterial wall, anti-inflammatory reactions are triggered and anti-thrombotic events are elicited [15]. The formation of new tissue, or neointima, directly around the stent struts gives rise to ISR, a process facilitated by the activation, proliferation and migration of smooth muscle cells to the site of treatment, where expedited neointima formation occurs to re-obstruct the vessel. High rates of ISR for BMS devices [16] brought about the performance of target lesion revascularisation (TLR) procedures, which typically involve repeat surgeries to restore vessel patency. Modifications to stent devices which were introduced to further combat high rates of ISR and thrombosis involved the inclusion of pharmaceutical agents on the outer surfaces of the stent, often through the means of a polymeric coating, as now discussed.

1.3.3 Drug eluting stents (DES)

The successful administration of pharmaceutical agents to surrounding arterial tissues, which helps to combat the risk of ISR and stent thrombosis following stent deployment, was achieved with the development and design of drug-eluting stents (DES). Drug-eluting stents have been applied for the treatment of coronary artery disease since 2000 [17], and such technologies have resulted in substantial reductions in the incidence in ISR and in the frequency of TLR procedures [18]. The anti-proliferative drugs, the most established for DES being paclitaxel or sirolimus, are often bonded to thin polymer coatings on the outer surfaces of the stent device [19], [20]. Polymer coatings for DES can be fabricated using either durable polymers or biodegradable polymers [21]. The fast degradation times of the biodegradable polymers commonly investigated as coatings, for example poly-lactide-co-glycolic acid (PLGA), can facilitate drug release during initial deployment and throughout the early stages of device implantation. DES have been adopted into widespread

clinical practice [22] and are now used for approximately three-quarters of all revascularisation procedures in the US [12].

1.3.4 Bioresorbable stents

Research into biodegradable stents was undertaken to present alternatives to the permanent devices discussed above, which remain in the body indefinitely, and which may present difficulties for the realisation of future clinical procedures. Several variations in the terminology used to describe biodegradable stents (for example, bioresorbable, bioabsorbable, bio-erodible, or the use of 'scaffold' to describe a temporary stent) are observed throughout the literature. A precise understanding of the various terms helps to distinguish between different types of degradable devices. Biodegradable refers to materials which break-down in the body and whose subsequent degradation products remain in tissues long-term. Bioresorbable, however, relates to materials that degrade in-vivo into non-toxic degradation products, which are either eliminated from the body or metabolised therein, whereas bioabsorbable is a more specific term which signifies both degradation facilitated by a biological system, and resultant erosion of the material via natural absorption of non-toxic degradation products [23]. The terms 'bioresorbable stent', recently accepted for coronary stents by the European Association of Percutaneous Coronary Interventions task force [24] and 'bioresorbable polymeric stent' (BPS), to signify devices of the polymer variation, are used in this thesis going forward.

Bioresorbable stents represent the newest generation of stenting technologies for the treatment of CAD. The development of stents which will break down and dissolve from the artery, after the initial necessary scaffolding period of 6-9 months [25], has come under intense investigation since the early 2000s

[25], [26]. To date, bioresorbable stents have been designed from either bioresorbable metal or bioresorbable polymer materials.

The earliest development of the bioresorbable stent technology was in the design of biodegradable coatings on permanent drug eluting metal stents (as discussed above). The use of bioresorbable materials for stents offers possibilities for devices which would slowly degrade, eventually freeing the vessel wall, and potentially eliminating the risk of late and very-late stent thrombosis and in-stent restenosis [27], [28]. The use of fully degradable devices is believed to restore vessel vasomotion and facilitate positive arterial remodelling, and would also permit the use of repeat treatments (surgical or percutaneous) to the same site [29]. Bioresorbable stents also present many advantages for use in areas of complex anatomy, where a conventional stent would permanently obstruct side branches [29], [30], and in treating paediatric patients, where a non-biodegrading device has the potential to become mechanically unstable in growing vessels [31].

The biodegradable metals which have come under the most investigation for the stent application include magnesium alloys [31]–[33] and iron alloys [34], [35]. These materials present attractive characteristics for use in bioresorbable stents, including suitable mechanical stiffness properties, excellent biocompatibility, and degradation products which are low in toxicity [36], [37].

For the bioresorbable polymers, there have been an extensive number of polymer materials investigated for this application. The main focus has been on aliphatic polyester materials, e.g. poly-lactide (PLA) and its different stereoisomer variations (poly-L-lactide (PLLA), poly-D-lactide (PDLA) and poly-D,L-lactide (PDLLA)) [38], [39]. Poly-ϵ-caprolactone (PCL), poly-anhydride ester (PAE) and tyrosine-derived polycarbonates have also come

under investigation [40]. The majority of these polymer materials degrade via hydrolytic degradation, where water molecules penetrate the material and cleave the polymer backbone chains into smaller fragments, which eventually diffuse out of the device and are naturally metabolised [41]. The very first report of PLLA being investigated for the purposes of stenting was in the Duke stent, which was developed in the late 1980s [42], [43]. The work of Tamai *et al*. [26], who reported the successful implantation of PLLA stents in humans in 2000, is often believed to have rekindled the interest in fully bioresorbable polymeric stents for clinical use.

While both classes of materials have potential in this application, the focus of this thesis is on polymer-based bioresorbable stents. Bioresorbable polymers have advantages over magnesium and iron alloys, in that there is a reduced likelihood that their degradation products will elicit an inflammatory response [44], and they also offer possibilities to tailor their degradation rates and mechanical properties through a range of processing techniques. A brief overview of BPS is now given.

1.4 Overview of Bioresorbable Polymeric Stents (BPS)

Bioresorbable polyesters such as PLLA have been extensively investigated for medical applications since the 1970's [45] due to their excellent biocompatibility and physio-chemical properties, which can be easily tuned through manufacturing processes [46]. As shown in **Table 1.1**, PLLA has emerged as one the main materials employed in the design of bioresorbable polymeric stents (BPS). A large number of the current BPS also feature drug eluting polymer coatings on their surfaces (**Table 1.1**). The microstructural properties of degradable polymer materials make them ideal drug carriers for the purpose of controlled drug release, which was in itself a contributing factor in the development of polymer coatings on permanent DES [47].

Table 1.1 Summary of the BPS that have undergone and/or are still in clinical evaluation (table published in [38], version shown here updated to show just the BPS).

Device name (Company)	Strut material	Strut thickness	Radio-opacity	Drug eluting	Crossing Profile	Radial Support	Resorption time	Current Status
Igaki-Tamai (Kyoto Medical)	Poly-L-lactide	170 µm	Gold markers	×	N/A	6 months	24 months	CE Mark (Peripheral device)
ABSORB BVS 1.0 (Abbott Vascular)	Poly-L-lactide & poly-D-lactide coating	156 µm	Platinum markers	✓ - Everolimus	1.4 mm	Weeks	18-24 months	Discontinued
ABSORB BVS 1.1 (Abbott Vascular)	Poly-L-lactide & poly-D-lactide coating	156 µm	Platinum markers	✓ - Everolimus	1.4 mm	6 months	18-24 months	CE Mark FDA approval** (2016)
ABSORB GT1 (Abbott Vascular)	Poly-L-lactide	156 µm	Platinum markers	✓ - Everolimus	1.4 mm	6 months	18-24 months	CE Mark
REVA (Reva Medical)	Poly-tyrosine derived polycarbonate	200 µm	Stent	×	1.7 mm	3-6 months	24 months	Discontinued
ReZolve (Reva Medical)	Poly-tyrosine derived polycarbonate	200 µm	Stent	✓ - Sirolimus	1.5 mm	4-6 months	24 months	Discontinued
Fantom Encore (Reva Medical)	Poly-tyrosine derived polycarbonate	125 µm	Stent	✓ - Sirolimus	1.5 mm	4-6 months	24 months	CE Mark
Pure Bioresorbable Scaffold (ART)	Poly-D,L-lactide	170 µm	×	×	N/A*	3-6 months	3-18 months	CE Mark

Table 1.1 Table continued

Device name (Company)	Strut material	Strut thickness	Radio-opacity	Drug eluting	Crossing Profile	Radial Support	Resorption time	Current Status
Fortitude (Amaranath Medical)	Poly-L-lactide	120-200 µm	×	×	N/A*	3-6 months	3-6 months	In clinical trials
DESolve and DESolve 100 (Elixir)	Poly-L-lactide	120-150 µm	Metallic markers	✓-Myolimus	1.5 mm	N/A	12-24 months	CE Mark
Ideal BTI (Xenogenics)	Poly-L-lactide and salicylates	200 µm	×	✓-Sirolimus	1.5-1.7 mm	3 months	6-9 months	FIM completed. Discontinued
Ideal BioStent (Xenogenics)	Poly-L-lactide and salicylates	150 µm	×	✓-Sirolimus	1.5-1.7mm	3 months	6-9 months	Pre-clinical stage
Acute BRS (Orbus Neich)	Poly-L-lactide-, poly-D-lactide and e-caprolactone	150 µm	distal and proximal	✓-EPC and sirolimus	N/A	N/A	>6 months	Pre-clinical stage
Xinsorb (Huaan Biotech)	Poly -L-lactide	160 µm	distal and proximal	✓-Sirolimus	N/A	N/A	N/A	Pre-clinical stage

BVS: Bioresorbable Vascular Scaffold, *CE*: Conformité Européenne, *N/A*: not applicable, *FDA*: Food and Drug Administration, *GT1:* GlideTrack catheter, *ART*: Arterial remodelling technologies, *FIM*: first in man, *6-Fr compatible, ** Warning letter sent out re clinical use

Following the introduction of the Igaki Tamai bioresorbable stent in the early 2000s [26], [48], a number of devices have since entered the BPS arena, and have shown promise as suitable candidates for use as the next generation of coronary artery treatment. However, even with the ever increasing interest in bioresorbable stents (particularly in the last 5-10 years) the emergence of BPS onto the market has been a slow process, with as of May 2018, only four polymeric devices having obtained CE (Conformité Européenne) marking for use in Europe.

The BPS devices which have received CE mark approval for use on the European market include three devices from companies in the USA: the Absorb Bioresorbable Vascular Scaffold (BVS) (Abbott Vascular, Santa Clara, CA, USA), DESolve (Elixir Medical Corporation, Sunnydale, California, USA), Fantom (REVA Medical, Inc., San Diego, CA, USA), and one from Japan, the ART Pure Bioresorbable Scaffold (Arterial Remodelling Technologies, Tokyo, Japan). The Absorb BVS also received approval by the Food and Drug Administration (FDA) in July 2016 for its use in the USA, however, a letter was subsequently sent by the FDA to healthcare professionals regarding recommendations for its use. More recently, use of the BVS has also been constrained in Europe, after the European regulatory agency restricted it to clinical registries in May 2017. Due to such challenges, as described for the Absorb device, the current usage of BPS has experienced significant limitations in recent years, with several of the BPS shown in **Table 1.1** also having recently been discontinued. An overview of the main advancements and developments of this technology from the perspective of the CE mark approved polymeric devices is given in **Chapter 2**.

1.5 Challenges for BPS

Each of the bioresorbable devices that were granted market approval has faced challenges during the design, development, preclinical and clinical testing stages. Various difficulties in wholly overcoming such challenges have no doubt slowed the progression of BPS onto the widespread clinical market. A number of key aspects of BPS design which require further research in this regard are identified and briefly outlined below.

1.5.1 Degradation time

The degradation timeline of the polymer material(s) used in the design of a BPS is a key factor in the device's subsequent success or failure. Polyester materials exhibit degradation times ranging from as little as 30 days up to a number of years [49]. For the BPS application, in order for the stent to provide adequate radial support to the healing vessel, it must degrade at an "optimal rate", which is generally believed to be around 24 months [50]. Bioresorbable stents undergo three main stages of degradation in-vivo namely, revascularisation, restoration and resorption. The length and nature of the specific events which occur during each of these stages are highly dependent on the stent material, and design, and on the physiological in-vivo environment. Therefore, due to the considerable variation in materials, design and patient populations, it is impossible to identify a single optimal rate for the general degradation of BPS. To date, the polyester PLLA, which has a disappearance time in-vivo of 2 years [51], is currently the most widely investigated material for the BPS application.

1.5.2 Thicker struts

It has been widely noted in the literature that the thickness of stent struts has a large bearing on the performance of the device in-vivo, in particular on the

rates of restenosis [52], and also on the mechanical performance (i.e. flexibility, stress/strain, and radial support properties [53]–[55]). Polymeric stents are often manufactured with much thicker struts than their permanent metallic counterparts, due to the lower mechanical stiffness of PLLA, and other aliphatic polyesters when compared to metals. However, thinner stent struts lead to more flexible devices, which along with a reduction in the overall cross sectional profile, has beneficial consequences for localised blood flow and the endothelial shear stresses experienced in-vivo [56]–[58]. The extensively investigated Absorb BVS has relatively thick struts (150 μm), and efforts are underway to design the next generation BVS with sub-100 μm struts [59].

1.5.3 Strut fracture

Successful deployment of polymeric devices during an angioplasty procedure is dependent on a number of factors, including ductility of the polymer stent, and presence of calcified atheroma [60]. Polymer materials are complex materials in terms of their mechanical behaviour. PLLA exhibits highly non-linear mechanical behaviour, which is greatly dependent on temperature, molecular weight, orientation, crystallinity and physical aging features (as discussed further in **Chapter 2**).

Occurrence of strut fracture has been reported for PLLA based BPS [61]. Microscope and optical coherence tomography (OCT) measurements, along with point force mechanical testing of stent struts, were used to identify and investigate incidence of strut fracture and strut disconnections following excessive expansion [61]. Risk of strut fracture coincides with other device challenges that show a strong dependence on the mechanical properties of the backbone polymer material, for example the minimum elastic recoil, which is now discussed.

1.5.4 Recoil/Radial strength

Following deployment and implantation, a polymeric stent provides mechanical support to the vessel, which ideally heals over a timeframe similar to that of device degradation. The initial period of vessel scaffolding is often of the greatest interest to device designers [29]; therefore, the polymer materials used in the BPS application are often modified using processing techniques which enhance their mechanical properties, in order to provide adequate strength for initial vessel support [40]. The in-vivo loading experienced by the stent (due to the actions of pulsatile blood flow and pressure exerted by the vessel) may impact on the time-dependent characteristics of the polymer and lead to excessive recoil before complete endothelialisation has occurred; a consequence which can result in late stent thrombotic events [62], [63]. The mechanical properties of the polymer material are a key consideration in the fundamental scaffolding performance of the degrading device, as is discussed further in **Chapter 2**.

1.6 Computational Modelling

The advent of computational modelling applied to the design and analysis of medical devices meant that a powerful methodology had become available to describe and examine the physical behaviour of the device, and predict its real-life performance. For stents, the use of in-silico techniques to examine and predict device performance is now well-established, and methods such as finite element analysis (FEA) are needed to provide timely and accurate insights into possible device failure mechanisms [64], [65]. FEA is commonly employed as the numerical modelling method for coronary stents, as it presents a powerful means through which to simulate complex angioplasty procedures and examine the structural performance of the device [66]. FEA presents many benefits for stent design:

- It facilitates the examination of several design criteria, for example flexibility and recoil, which govern the device deliverability and deployment, respectively
- It provides the means to include a representative physiological environment and examine its impact on the device
- It lessens the dependence on complex and repetitive experimental testing in the design and development of the device
- It allows for analysis of the mechanical stress-strain performance of the device
- It can provide insight into the resulting stress response experienced by the arterial tissue
- It facilitates assessment of the long term device behaviour under a range of different conditions, which may not be practical to replicate experimentally.

According to the guidelines published by the FDA in the United States, FEA is required as part of the stent design process. However specific guidelines relating to bioresorbable stents have not yet been established [67]. Specifications for bioresorbable stent design are also lacking in the directives which govern attainment of CE marking approval. In recent years, a large number of publications have examined and predicted the in-vivo mechanical performance of bioresorbable polymeric stents using computational methods [68]–[78]. One of the key considerations for the in-vivo performance of bioresorbable devices is the device degradation, which as indicated above, depending on the polymer material utilised, is thought to take place over a period ranging from 6 months to 5 years [39]. Computational modelling studies of polymer degradation can provide vital information on the impact of degradation on both the properties of the device and also on the surrounding

tissues [38], [79]. The development of more advanced and multi-physics modelling techniques for degradation, merged with enhanced computational platforms for coronary stent analysis, would undoubtedly aid the advancement of regulatory guidelines for bioresorbable polymeric stents.

1.7 Thesis Aims

Improvements in the design and analysis of the next generation of medical devices for the treatment of coronary artery disease are undoubtedly dependant on improvements in computational modelling techniques which examine their expected in-vivo performances. Given the current clinical challenges faced by BPS, as described in Section 1.4, a better understanding of BPS behaviour, which can be achieved through improved modelling of devices, is needed to aid the advancement of devices in the clinical arena. Therefore, given the stated focus of this thesis work on BPS, thesis aims are:

- to present a critical review of the state of the art in computational modelling techniques for BPS degradation. The main achievements and limitations of such works to date are highlighted and presented alongside a review of the relevant literature on the use of PLLA for the BPS application (**Chapter 2**).
- to develop a computational modelling framework to predict the physio-chemical degradation of polymer materials (achieved through implementation of physio-chemical degradation equations into FEA, as described in **Chapter 3**)
- to apply this framework to simulate the in-vivo degradation of a range of BPS geometries (**Chapter 4**).

- to update the developed model to allow changes in material crystallinity to be captured and provide an insight into the diffusion characteristics of degrading semi-crystalline polymers (**Chapter 5**)
- and finally, to evaluate the mechanical performance (in terms of scaffolding ability) of various BPS with degradation under a range of loading and boundary conditions

By achieving each of these specific aims, insights into the in-vivo degradation behaviours of BPS are given, including the dependence on and influence of stent geometry, in-vivo loading conditions and material properties.

1.8 Thesis Overview

Chapter 2 of this thesis presents an overview of the polyester material PLLA which is predominantly employed in the BPS application. A critical review of the existing in-silico modelling techniques used to examine the degradation of BPS then follows. The details of the physio-chemical degradation equations adapted to simulate and examine the degradation of BPS in an FEA framework are given in **Chapter 3**, alongside the remaining theoretical and numerical methods which are used in the thesis.

The organisation of the modelling work encompassed in this thesis is summarised in **Figure 1.2**. In **Chapter 4**, a computational modelling study is presented, in which the degradation and mechanical behaviour of a number of BPS devices are investigated in terms of their molecular weight and stiffness. An investigation into the effects of stent geometry, material properties and in-vivo boundary conditions is described and the advantages of developing FEA methods to simulate the physio-chemical aspects of polymer degradation are highlighted. In **Chapter 5**, the inclusion of equations governing the crystallinity behaviour of bioresorbable polymeric devices is described and a study of the degradation, crystallisation and diffusion behaviours of PLLA based BPS is

presented. **Chapter 6** presents a co-simulation modelling framework to examine the dual degradation and mechanical performance (through their scaffolding ability) of BPS under a range of loading and boundary conditions. Finally, in **Chapter 7**, the main outcomes and conclusions of the previous chapters are summarized and briefly discussed. A number of key recommendations for the use of computational modelling in the design, analysis and regulatory approval process of BPS are outlined, and possible future perspective for this area is provided.

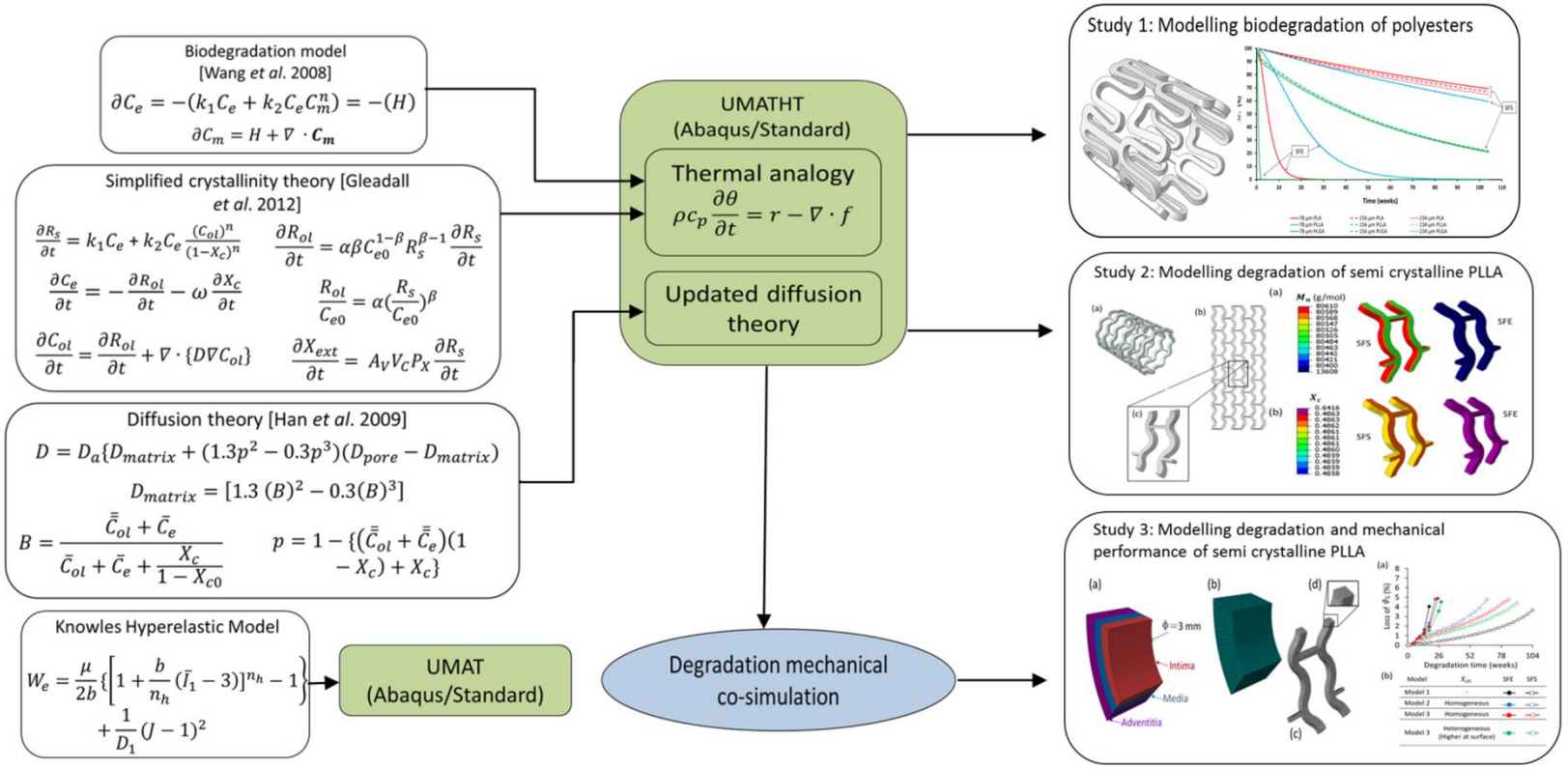

Figure 1.2 Flowchart which gives an overview of the work presented in this thesis.

References

[1] N. Townsend, L. Wilson, P. Bhatnagar, K. Wickramasinghe, M. Rayner, and M. Nichols, “Cardiovascular disease in Europe: Epidemiological update 2016,” *Eur. Heart J.*, vol. 37, no. 42, pp. 3232–3245, 2016.

[2] A. R. Grüntzig, Å. Senning, and W. E. Siegenthaler, “Nonoperative Dilatation of Coronary-Artery Stenosis,” *N. Engl. J. Med.*, vol. 301, no. 2, pp. 61–68, Jul. 1979.

[3] K. Detre *et al.*, “Percutaneous transluminal coronary angioplasty in 1985-1986 and 1977-1981. The National Heart, Lung, and Blood Institute Registry.,” *N. Engl. J. Med.*, vol. 318, no. 5, pp. 265–270, Feb. 1988.

[4] R. J. Ivanhoe *et al.*, “Percutaneous transluminal coronary angioplasty of chronic total occlusions. Primary success, restenosis, and long-term clinical follow-up.,” *Circulation*, vol. 85, no. 1, pp. 106–115, Jan. 1992.

[5] S. Glagov, “Current Perspectives Intimal Hyperplasia , Vascular Modeling , and the Restenosis Problem,” pp. 2888–2891, 1994.

[6] C. Landau, R. A. Lange, and L. D. Hillis, “Percutaneous transluminal coronary angioplasty.,” *N. Engl. J. Med.*, vol. 330, no. 14, pp. 981–993, Apr. 1994.

[7] G. S. Mintz *et al.*, “Arterial remodeling after coronary angioplasty: a serial intravascular ultrasound study.,” *Circulation*, vol. 94, no. 1, pp. 35–43, Jul. 1996.

[8] J. Al Suwaidi, P. B. Berger, and D. R. J. Holmes, “Coronary artery stents.,” *JAMA*, vol. 284, no. 14, pp. 1828–1836, Oct. 2000.

[9] A. Sakamoto, H. Jinnouchi, S. Torii, R. Virmani, and A. V Finn, “Understanding the Impact of Stent and Scaffold Material and Strut Design on Coronary Artery Thrombosis from the Basic and Clinical Points of View,” pp. 1–19, 2018.

[10] P. W. Serruys *et al.*, “A comparison of balloon-expandable-stent implantation with balloon angioplasty in patients with coronary artery disease. Benestent Study Group.,” *N. Engl. J. Med.*, vol. 331, no. 8, pp. 489–495, Aug. 1994.

[11] D. L. Fischman *et al.*, “A Randomized Comparison of Coronary-Stent Placement and Balloon Angioplasty in the Treatment of Coronary Artery Disease,” *N. Engl. J. Med.*, vol. 331, no. 8, pp. 496–501, Aug. 1994.

[12] G. Maluenda, G. Lemesle, and R. Waksman, “A Critical Appraisal of the Safety and Efficacy of Drug-Eluting Stents,” *Clin. Pharmacol. Ther.*, vol. 85, no. 5, pp. 474–480, May 2009.

[13] D. R. J. Holmes *et al.*, “Stent thrombosis.,” *J. Am. Coll. Cardiol.*, vol. 56, no. 17, pp. 1357–1365, Oct. 2010.

[14] “Nucleus Medical Media,” *Nucleus medical media: Medical video, animation, illustration.* [Online]. Available: http://catalog.nucleusmedicalmedia.com/. [Accessed: 15-Jan-2019].

[15] R. A. Schatz *et al.*, “Clinical experience with the Palmaz-Schatz coronary stent. Initial results of a multicenter study.,” *Circulation*, vol. 83, no. 1, pp. 148–161, Jan. 1991.

[16] D. J. Moliterno, “Healing Achilles — Sirolimus versus Paclitaxel,” *N. Engl. J. Med.*, vol. 353, no. 7, pp. 724–727, Aug. 2005.

[17] J. Wiebe, H. M. Nef, and C. W. Hamm, “Current status of bioresorbable

scaffolds in the treatment of coronary artery disease," *J. Am. Coll. Cardiol.*, vol. 64, no. 23, pp. 2541–2551, 2014.

[18] D. Ardissino *et al.*, "Sirolimus-eluting vs uncoated stents for prevention of restenosis in small coronary arteries: a randomized trial.," *JAMA*, vol. 292, no. 22, pp. 2727–2734, Dec. 2004.

[19] G. W. Stone *et al.*, "One-year clinical results with the slow-release, polymer-based, paclitaxel-eluting TAXUS stent: the TAXUS-IV trial.," *Circulation*, vol. 109, no. 16, pp. 1942–1947, Apr. 2004.

[20] J. Schofer *et al.*, "Sirolimus-eluting stents for treatment of patients with long atherosclerotic lesions in small coronary arteries: double-blind, randomised controlled trial (E-SIRIUS).," *Lancet (London, England)*, vol. 362, no. 9390, pp. 1093–1099, Oct. 2003.

[21] G. G. Stefanini *et al.*, "Long-term clinical outcomes of biodegradable polymer biolimus-eluting stents versus durable polymer sirolimus-eluting stents in patients with coronary artery disease (LEADERS): 4 year follow-up of a randomised non-inferiority trial," *Lancet*, vol. 378, no. 9807, pp. 1940–1948, Dec. 2011.

[22] F. Saia, A. Marzocchi, and P. W. Serruys, "Drug-eluting stents. The third revolution in percutaneous coronary intervention.," *Ital. Heart J.*, vol. 6, no. 4, pp. 289–303, Apr. 2005.

[23] J. F. da S. Soares, "Constitutive modeling for biodegradable polymers for application in endovascular stents," Texas A&M University, 2008.

[24] R. A. Byrne *et al.*, "Report of a European Society of Cardiology-European Association of Percutaneous Cardiovascular Interventions task force on the evaluation of coronary stents in Europe: Executive summary," *Eur. Heart J.*, vol. 36, no. 38, pp. 2608–2620, 2015.

[25] S. Saito, "New horizon of bioabsorbable stent.," *Catheterization and cardiovascular interventions : official journal of the Society for Cardiac Angiography & Interventions*, vol. 66, no. 4. United States, pp. 595–596, Dec-2005.

[26] H. Tamai *et al.*, "Initial and 6-month results of biodegradable poly-l-lactic acid coronary stents in humans," *Circulation*, vol. 102, no. 4, pp. 399–404, 2000.

[27] R. Waksman, "Promise and challenges of bioabsorbable stents," *Catheter. Cardiovasc. Interv.*, vol. 70, no. 3, pp. 407–414, Sep. 2007.

[28] S. H. Im, Y. Jung, and S. H. Kim, "Current status and future direction of biodegradable metallic and polymeric vascular scaffolds for next-generation stents," *Acta Biomater.*, vol. 60, pp. 3–22, 2017.

[29] J. a. Ormiston and P. W. S. Serruys, "Bioabsorbable coronary stents," *Circ. Cardiovasc. Interv.*, vol. 2, no. 3, pp. 255–260, 2009.

[30] J. Iqbal, Y. Onuma, J. Ormiston, A. Abizaid, R. Waksman, and P. Serruys, "Bioresorbable scaffolds: Rationale, current status, challenges, and future," *Eur. Heart J.*, vol. 35, pp. 765–776, 2014.

[31] P. Zartner, R. Cesnjevar, H. Singer, and M. Weyand, "First successful implantation of a biodegradable metal stent into the left pulmonary artery of a preterm baby.," *Catheter. Cardiovasc. Interv.*, vol. 66, no. 4, pp. 590–4, Dec. 2005.

[32] M. Haude *et al.*, "Safety and performance of the drug-eluting absorbable metal

scaffold (DREAMS) in patients with de-novo coronary lesions: 12 month results of the prospective, multicentre, first-in-man BIOSOLVE-I trial.," *Lancet*, vol. 381, no. 9869, pp. 836–44, Mar. 2013.

[33] R. Waksman *et al.*, "Early- and Long-Term Intravascular Ultrasound and Angiographic Findings After Bioabsorbable Magnesium Stent Implantation in Human Coronary Arteries," *JACC Cardiovasc. Interv.*, vol. 2, no. 4, pp. 312–320, Apr. 2009.

[34] M. Peuster *et al.*, "A novel approach to temporary stenting: Degradable cardiovascular stents produced from corrodible metal - Results 6-18 months after implantation into New Zealand white rabbits," *Heart*, vol. 86, no. 5, pp. 563–569, 2001.

[35] R. Waksman, R. Pakala, R. Baffour, R. Seabron, D. Hellinga, and F. O. Tio, "Short-term effects of biocorrodible iron stents in porcine coronary arteries.," *J. Interv. Cardiol.*, vol. 21, no. 1, pp. 15–20, Mar. 2008.

[36] H. Hermawan, D. Dubé, and D. Mantovani, "Developments in metallic biodegradable stents.," *Acta Biomater.*, vol. 6, no. 5, pp. 1693–7, May 2010.

[37] Y. F. Zheng, X. N. Gu, and F. Witte, "Biodegradable metals," *Mater. Sci. Eng. R Reports*, vol. 77, pp. 1–34, 2014.

[38] E. L. Boland, R. Shine, N. Kelly, C. A. Sweeney, and P. E. McHugh, "A Review of Material Degradation Modelling for the Analysis and Design of Bioabsorbable Stents," *Ann. Biomed. Eng.*, vol. 44, no. 2, pp. 341–356, 2015.

[39] S. McMahon *et al.*, "Bio-resorbable polymer stents: a review of material progress and prospects," *Prog. Polym. Sci.*, vol. 83, pp. 79–96, 2018.

[40] L. Da Hou, Z. Li, Y. Pan, M. I. Sabir, Y. F. Zheng, and L. Li, "A review on biodegradable materials for cardiovascular stent application," *Front. Mater. Sci.*, vol. 10, no. 3, pp. 238–259, 2016.

[41] Y. Wang, J. Pan, X. Han, C. Sinka, and L. Ding, "A phenomenological model for the degradation of biodegradable polymers," *Biomaterials*, vol. 29, no. 23, pp. 3393–3401, 2008.

[42] R. S. Stack *et al.*, "Interventional cardiac catheterization at Duke Medical Center," *Am J Cardiol*, vol. 62, no. 10 Pt 2, pp. 3F-24F, 1988.

[43] R. S. Gammon *et al.*, "Mechanical features of the duke biodegradable intravascular stent," *Journal of the American College of Cardiology.*, vol. 17, no. 2. [New York, N.Y.] :, p. A235, 1991.

[44] M. Bartkowiak-Jowsa, R. Będziński, A. Kozłowska, J. Filipiak, and C. Pezowicz, "Mechanical, rheological, fatigue, and degradation behavior of PLLA, PGLA and PDGLA as materials for vascular implants," *Meccanica*, vol. 48, no. 3, pp. 721–731, 2013.

[45] P. Tormala, T. Pohjonen, and P. Rokkanen, "Bioabsorbable polymers: materials technology and surgical applications," *Proc Inst Mech Eng H*, vol. 212, no. 2, pp. 101–111, 1998.

[46] A. J. R. Lasprilla, G. A. R. Martinez, B. H. Lunelli, A. L. Jardini, and R. M. Filho, "Poly-lactic acid synthesis for application in biomedical devices — A review," *Biotechnol. Adv.*, vol. 30, no. 1, pp. 321–328, 2012.

[47] J. G. Murphy, R. S. Schwartz, K. C. Huber, and D. R. Holmes Jr., "Polymeric stents: modern alchemy or the future?," *J Invasive Cardiol*, vol. 3, no. 3, pp. 144–148, 1991.

[48] S. Nishio *et al.*, “Long-term (>10 Years) clinical outcomes of first-in-human biodegradable poly-l-lactic acid coronary stents: Igaki-Tamai stents,” *Circulation*, vol. 125, no. 19, pp. 2343–2352, May 2012.

[49] L. S. Nair and C. T. Laurencin, “Biodegradable polymers as biomaterials,” *Prog. Polym. Sci.*, vol. 32, no. 8, pp. 762–798, 2007.

[50] C. Collet, R. J. de Winter, Y. Onuma, and P. W. Serruys, “The Absorb bioresorbable vascular scaffold for the treatment of coronary artery disease.,” *Expert Opin. Drug Deliv.*, vol. 13, no. 10, pp. 1489–1499, Oct. 2016.

[51] D. Garlotta, “A Literature Review of Poly (Lactic Acid),” vol. 9, no. 2, 2002.

[52] A. Kastrati *et al.*, “Intracoronary stenting and angiographic results: strut thickness effect on restenosis outcome (ISAR-STEREO) trial.,” *Circulation*, vol. 103, no. 23, pp. 2816–2821, Jun. 2001.

[53] S. Mishra, “A fresh look at bioresorbable scaffold technology: Intuition pumps,” *Indian Heart J.*, vol. 69, no. 1, pp. 107–111, 2017.

[54] B. P. Murphy, P. Savage, P. E. McHugh, and D. F. Quinn, “The stress-strain behavior of coronary stent struts is size dependent.,” *Ann. Biomed. Eng.*, vol. 31, no. 6, pp. 686–691, Jun. 2003.

[55] P. Savage, B. P. O’Donnell, P. E. McHugh, B. P. Murphy, and D. F. Quinn, “Coronary stent strut size dependent stress-strain response investigated using micromechanical finite element models.,” *Ann. Biomed. Eng.*, vol. 32, no. 2, pp. 202–211, Feb. 2004.

[56] K. Kolandaivelu *et al.*, “Stent thrombogenicity early in high-risk interventional settings is driven by stent design and deployment and protected by polymer-drug coatings.,” *Circulation*, vol. 123, no. 13, pp. 1400–1409, Apr. 2011.

[57] K. C. Koskinas, Y. S. Chatzizisis, A. P. Antoniadis, and G. D. Giannoglou, “Role of Endothelial Shear Stress in Stent Restenosis and Thrombosis: Pathophysiologic Mechanisms and Implications for Clinical Translation,” *J. Am. Coll. Cardiol.*, vol. 59, no. 15, pp. 1337–1349, 2012.

[58] E. Tenekecioglu *et al.*, “Strut protrusion and shape impact on endothelial shear stress: insights from pre-clinical study comparing Mirage and Absorb bioresorbable scaffolds,” *Int. J. Cardiovasc. Imaging*, vol. 33, no. 9, pp. 1313–1322, 2017.

[59] D. Regazzoli, P. P. Leone, A. Colombo, and A. Latib, “New generation bioresorbable scaffold technologies: an update on novel devices and clinical results,” *J. Thorac. Dis.*, vol. 9(Suppl 9), pp. S979–S985, 2017.

[60] C. Conway, J. P. McGarry, and P. E. McHugh, “Modelling of Atherosclerotic Plaque for Use in a Computational Test-Bed for Stent Angioplasty,” *Ann. Biomed. Eng.*, vol. 42, no. 12, pp. 2425–2439, 2014.

[61] N. Foin *et al.*, “Bioabsorbable vascular scaffold overexpansion: insights from in vitro post-expansion experiments.,” *EuroIntervention J. Eur. Collab. with Work. Gr. Interv. Cardiol. Eur. Soc. Cardiol.*, vol. 11, no. 12, pp. 1389–1399, Mar. 2016.

[62] A. V Finn *et al.*, “Pathological correlates of late drug-eluting stent thrombosis: strut coverage as a marker of endothelialization.,” *Circulation*, vol. 115, no. 18, pp. 2435–2441, May 2007.

[63] N. Grabow, D. P. Martin, and K. Sternberg, “Absorbable polymer stent technologies for vascular regeneration Niels Grabow , a ∗ David P . Martin , b

Klaus-Peter Schmitz a," vol. 2009, no. September 2009, pp. 744–751, 2010.

[64] D. Martin and F. J. Boyle, "Computational Structural Modelling of Coronary Stent Deployment : A Review," pp. 331–348, 2011.

[65] S. Morlacchi and F. Migliavacca, "Modeling stented coronary arteries: where we are, where to go.," *Ann. Biomed. Eng.*, vol. 41, no. 7, pp. 1428–1444, Jul. 2013.

[66] F. Gervaso, C. Capelli, L. Petrini, S. Lattanzio, L. Di Virgilio, and F. Migliavacca, "On the effects of different strategies in modelling balloon-expandable stenting by means of finite element method," vol. 41, pp. 1206–1212, 2008.

[67] Food and Drug Administration, "ASTM-FDA Workshop on Absorbable Medical Devices:Lessons Learned from Correlations of Bench Testing and Clinical Performance," *U.S Food and Drug Administration - Public Workshop*, 2012. [Online]. Available: http://www.fda.gov/MedicalDevices/NewsEvents/WorkshopsConferences/ucm312601.htm. [Accessed: 30-Apr-2015].

[68] N. Paryab, D. Cronin, P. Lee-Sullivan, X. Ying, F. Y. C. Boey, and S. Venkatraman, "Uniform Expansion of a Polymeric Helical Stent," *J. Med. Device.*, vol. 6, no. 2, p. 021012, 2012.

[69] N. Debusschere, P. Segers, P. Dubruel, B. Verhegghe, and M. De Beule, "A finite element strategy to investigate the free expansion behaviour of a biodegradable polymeric stent," *J. Biomech.*, vol. 48, no. 10, pp. 2012–2018, 2015.

[70] H. Li *et al.*, "Multi-Objective optimizations of biodegradable polymer stent structure and stent microinjection molding process," *Polymers (Basel).*, vol. 9, no. 1, 2017.

[71] R. G. Pauck and B. D. Reddy, "Computational analysis of the radial mechanical performance of PLLA coronary artery stents," *Med. Eng. Phys.*, vol. 37, no. 1, pp. 7–12, 2015.

[72] A. C. Bobel, S. Petisco, J. Ramon Sarasua, W. Wenxin, and P. E. McHugh, "Computational Bench Testing to Evaluate the Short-Term Mechanical Performance of a Polymeric Stent," *Cardiovasc. Eng. Technol.*, 2015.

[73] A. C. Bobel and P. E. McHugh, "Computational Analysis of the Utilisation of the Shape Memory Effect and Balloon Expansion in Fully Polymeric Stent Deployment," *Cardiovasc. Eng. Technol.*, vol. 9, no. 1, pp. 60–72, 2018.

[74] R. Naseem, L. Zhao, Y. Liu, and V. V. Silberschmidt, "Experimental and computational studies of poly-L-lactic acid for cardiovascular applications: recent progress," *Mech. Adv. Mater. Mod. Process.*, vol. 3, no. 1, p. 13, 2017.

[75] A. Schiavone, C. Abunassar, S. Hossainy, and L. G. Zhao, "Computational analysis of mechanical stress–strain interaction of a bioresorbable scaffold with blood vessel," *J. Biomech.*, vol. 49, no. 13, pp. 2677–2683, 2016.

[76] A. Schiavone, T.-Y. Qiu, and L.-G. Zhao, "Crimping and deployment of metallic and polymeric stents -- finite element modelling," *Vessel Plus*, vol. 1, no. 1, pp. 12–21, 2017.

[77] Q. Wang, G. Fang, Y. Zhao, G. Wang, and T. Cai, "Computational and experimental investigation into mechanical performances of Poly-L-Lactide Acid (PLLA) coronary stents," *J. Mech. Behav. Biomed. Mater.*, vol. 65, pp. 415–427, 2017.

[78] P.-J. Wang *et al.*, “Effect of working environment and procedural strategies on mechanical performance of bioresorbable vascular scaffolds,” *Acta Biomater.*, pp. 1–10, 2018.

[79] T. Qiu, R. He, C. Abunassar, S. Hossainy, and L. G. Zhao, “Effect of two-year degradation on mechanical interaction between a bioresorbable scaffold and blood vessel,” *J. Mech. Behav. Biomed. Mater.*, vol. 78, no. November 2017, pp. 254–265, 2018.

2. Background

2.1 Chapter Summary

This chapter aims to provide an overview of the main topics relevant to the work presented in this thesis. Bioresorbable materials have huge potential for the future development of implantable medical devices. A significant interest has emerged over the last 10-15 years in the use of biodegradable materials, in particular bioresorbable polymers (reviewed in Section 2.2), for use in the coronary stent application. Lessons learned from the development of permanent metallic stents, in particular in relation to favourable stent design characteristics are summarised in Section 2.3.

The biodegradable aliphatic polyester poly-L-lactide, (PLLA) has emerged as a promising material for the design of BPS. Degradation mechanisms of PLLA are reviewed (Section 2.4.1), and an overview of its clinical performance in BPS is given (Section2.4.2). The mechanical behaviour of PLLA is outlined in Section 2.4.3, with a focus on the mechanical properties applicable for its use in BPS. Polyesters are generally considered to exhibit plastic as well as non-linear viscoelastic material behaviour, which is in turn highly dependent on a number of factors. The key factors which govern the mechanical properties and degradation behaviour of PLLA for its use in the BPS application are reviewed in Section 2.4.4.

A review of the state of the art in computational modelling techniques for BPS degradation is given in Section 2.5, with the main advancements and limitations of each technique highlighted. This review has been published in [1], with slight amendments made to the text here for chapter formatting.

Finally, conclusions from the review of the literature, and a suggested focus for further research, are presented in Section2.6.

2.2 Biodegradable Polymers

Biodegradable polymers can be categorised as biologically derived polymers, natural polymers, and synthetic polymers [2]. Biologically derived polymers, for example materials originating from natural polysaccharides, have principally been examined for the design of biodegradable suture materials [3], [4]. Although natural biodegradable polymer materials, for example collagen, have a long history of being successfully used in medical applications [5], [6], the biological activities of these materials can lead to undesirable side-effects in-vivo. These side-effects can include unwanted immunological responses and a risk of transmitted infections to the host tissue [7]. It has also proven difficult to predict the degradation rates of the biologically derived and natural polymers, and to tailor their mechanical and chemical properties for degradation and erosion [8]. Therefore, biodegradable synthetic polymers have become the materials of choice for medical device applications.

Synthetic biodegradable polymers have been examined for use in medical device applications since the 1960s, and more specifically, biodegradable aliphatic polyesters have shown success in a number of areas over the last two decades, including for biodegradable sutures [9], bioresorbable orthopaedic fixation devices [10], [11], tissue engineered scaffolds and drug delivery devices [12], [13], and in bioresorbable coronary stents [14]. The particular chemical composition of synthetic aliphatic polyesters, or poly (α-esters), as shown in **Figure 2.1**, is what makes them highly suitable for use in biodegradable medical devices [15]. The synthetic poly (α-esters) materials include poly (e-caprolactone) (PCL), poly (dioxanone) (PDS), polylactide

(PLA) and poly-glycolic acid (PGA), and their co-polymers. The reader is directed to a number of works which have been published on biodegradable polymers, and the evolution of their use in medical device applications [2], [15]–[20]. Given that it is the most extensively investigated polymer material for the BPS application (as discussed briefly in **Chapter 1**), PLLA is characterised below (Section 2.4) for this application in terms of its defining physiochemical and mechanical properties.

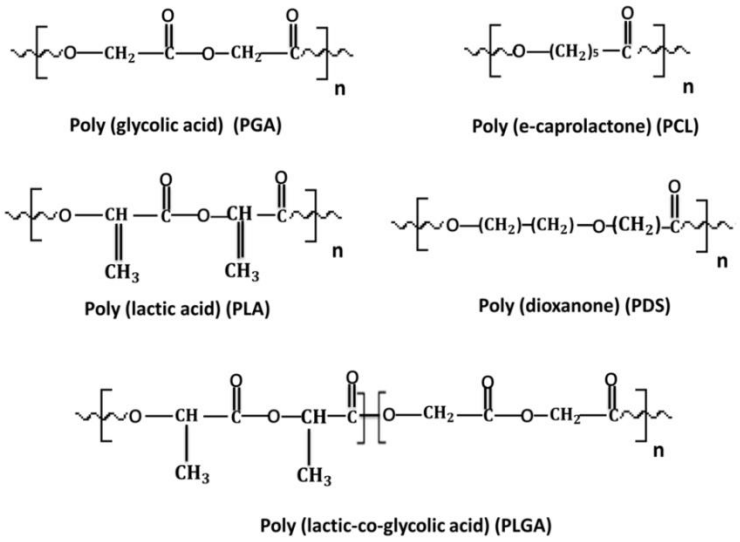

Figure 2.1 Chemical structure of the polyester materials commonly used for biodegradable medical device applications.

2.3 Developments in Metallic Stents – Lessons Learned

Before focusing on the characterisation of PLLA, it is useful to briefly review the development of permanent metallics stents, focusing on particular on what has been learned concerning favourable stent design attributes.

Since the first clinical application of coronary stents in the 1980's, stent design has evolved, and gradual improvements in the design have been introduced (as reviewed in [21]). Stainless steel was among the early materials used in commercial balloon expandable stents (e.g. 316L for the Medtronic DRIVER

device). Such alloys possess a relatively high elastic modulus, ultimate tensile strength and elongation at break (typical values of 193 GPa, 670 MPa and 48% respectively for 316L steel alloy [22]), all which enable these materials to be used in the load bearing stent application.

Developments in stent design focused on reducing the risks of ISR and stent thrombosis through the generation of devices with thinner struts, motivated by findings from the ISAR-STEREO clinical trial in the early 2000's [23], [24]. Strut thickness in early DES designed from 316L was within a range of 97-140 µm [21]. Following the introduction of cobalt chromium (CoCr) and platinum chromium (PtCr) alloys in DES design, strut thickness was initially reduced down to 81 µm, and then as low as 40 µm in the case of CoCr devices (values as stated for the XIENCE V stent from Abbott Vascular [21] and the Meril MITSU stent platform respectively [25]); whereas a strut thickness of 81 µm was achieved for a PtCr device (the ELEMENT stent from Boston Scientific [26]). The higher strengths of CoCr and PtCr alloys over 316L steel (e.g. ultimate tensile strengths of 1000 MPa for CoCr L605 alloy [22], and 834 MPa for PtCr [27]) helps the stents to maintain their ability to resist collapse under applied external pressure (i.e. radial strength) when thinner struts are used.

The design of stents with thinner struts also improved the overall flexibility and crossing profile of devices, to facilitate device delivery and placement. Early stent design was based on hoops of wire in sinusoidal patterns (which were welded to form junctions), braiding or knitting thin wires together, or laser cutting of thin walled tubing. Successful expansion of a stent in the artery is facilitated by the opening of these hinge-like regions in the stent's profile, which leads to plastic (irreversible) deformation of the material at the hinge area and allows the stent to largely retain its shape. Suitable material

biocompatibility and radiopacity are further important considerations for successful stent design.

The attributes of material stiffness and strength, enabling the minimisation of strut thickness, while still allowing for the achievement of stent radial strength, combined with biocompatibility, have helped guide the choice of biodegradable polymers for the BPS application, and have led to the use of PLLA in particular.

2.4 Review of PLLA for the BPS Application

2.4.1 Degradation mechanisms of PLLA

Poly-L-lactide (PLLA) is a synthetic poly (α-ester) which is currently well established as the principal material in the vast majority of bioresorbable polymeric stents (BPS). PLLA is formed from the biodegradable, compostable thermoplastic PLA, which is typically produced from either lactide through ring-opening polymerisation or lactic acid, through random polymerisation techniques [15]. PLA is the common abbreviation for the resulting poly (lactic acid) and polylactide materials. Polymerisation of PLA which uses a controlled mixture of the L-isomers of lactic acid (**Figure 2.2**), leads to the production of the isotactic, high molecular weight semi-crystalline compound PLLA.

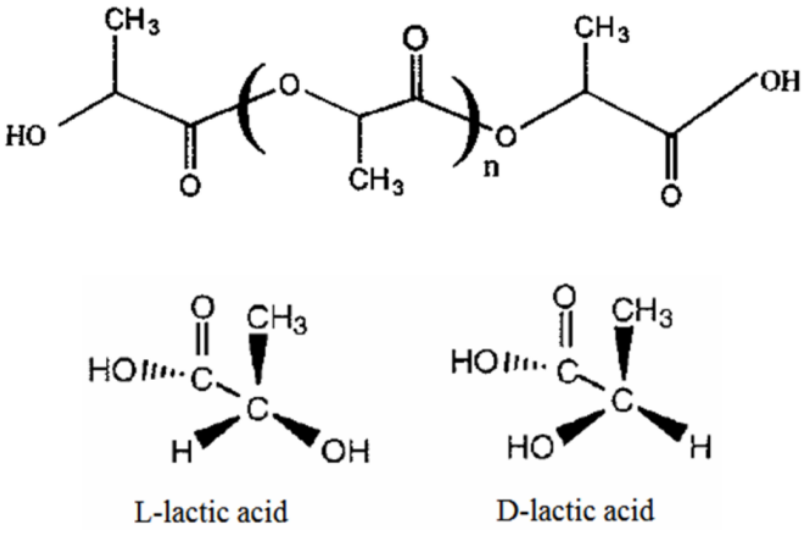

Figure 2.2 Chemical structure of high-molecular-weight PLA (top) and the L- and D-enantiomers of lactic acid used to form PLLA and its stereoisomer PDLA (adapted with permission from [19]).

The basic structure of polymeric materials is characterised by tangled interconnected chains, which are able to conform to a large number of chain arrangements. Polyester materials used in biomedical applications are degraded in-vivo by hydrolysis, when water molecules diffuse into the material and cause scission, or cleavage, of the polymer backbone chains. Carbon, hydrogen and oxygen atoms comprise the repeating polymer units of PLLA [28]. During hydrolysis, water molecules hydrolyse the ester bonds linking these repeating units in the amorphous regions of the material. PLLA undergoes degradation in what is essentially a two phase process. In the first phase, the vulnerable ester linkages in the polymeric chain react with water molecules and are broken down through chemical hydrolysis into oligomers (shorter chains) and finally into monomer fragments [29]. Chain cleavage through such hydrolysis is an irreversible process, and it produces changes at the molecular scale that have consequences for the overall material. Hydrolysis of PLLA is associated with a phenomenon known as autocatalysis, that is, when the scission of the polymer chains gives rise to the formation of

carboxyl chain end groups, which increase the acidic environment within the polymer matrix and therefore accelerate the rate of further hydrolytic breakdown [30]. Active metabolism of the monomer products formed through hydrolysis comprises the events of the second phase in the degradation. The monomer fragments formed as a result of PLLA hydrolysis are lactic acids, non-toxic compounds which are natural by-products of the Kreb's cycle, and are therefore easily eliminated from the body through normal cellular reactions [31]. As shown in **Figure 2.3**(a), degradation of biodegradable polymeric materials occurs through either bulk erosion or surface erosion mechanisms. The total degradation, or disappearance time, of PLLA in-vivo is thought to be approximately 2 years [32], which is believed to be favourable for the time required for superior vessel remodelling to occur [33].

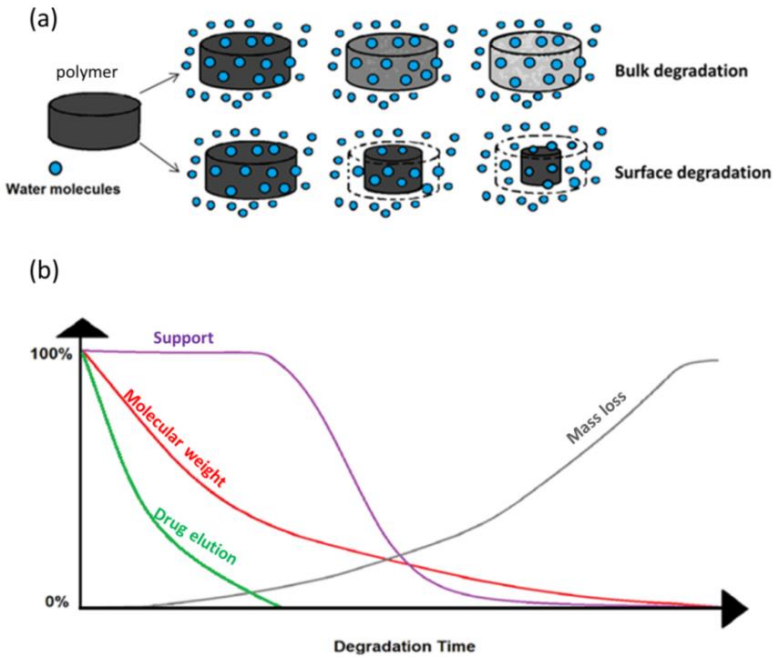

Figure 2.3 PLLA primarily undergoes bulk degradation (shown in schematic (a), as compared to surface degradation). The main events involved in the degradation of a typical PLLA based BPS, and their relative time scales are shown in (b). The decrease in the molecular weight and support capacity of the device show gradual trends, as does the mass loss behaviour of the device. This is in comparison to the more rapid reduction observed for drug elution from the device.

PLLA degrades primarily through bulk degradation [34], which results in an overall mass loss and decrease in the molecular weight of the material (as depicted in the typical paradigm for BPS degradation shown in **Figure 2.3**(b)). Degradation of polymer materials is commonly measured by tracking the evolution in the material's molecular weight (either the number average, or the weight-averaged form). As a result of the chain scission which occurs during degradation, the molecular weight of a polymer decreases (i.e. the lengths of the polymer chains decrease). While the initial stages of polyester degradation (uptake of water molecules into the material) are often considered a passive process, that shows little dependence on enzymes or other chemical factors [35], the hydrolysis mechanisms of the polymer chains are governed by many chemical and physical features [36].

The structure of PLLA exhibits a number of hierarchical length scales, which start at the atomic monomer level (10^{-9} m), up to the individual polymeric chains, which form the polymeric network of backbone chains, and which generate the bulk material (10^{-2} - 10^{1} m) [37]. Polymer degradation behaviour has numerous consequences for the overall material at a macro-scale, micro-scale and nano-scale level. The effects of degradation at the macro-scale are considered through analysis of the physical structure of the polymer, the evolution of its mechanical properties and the associated physio-chemical changes which occur within the material. Changes in the inherent microstructural properties and chain compositions of degrading polyesters are generally viewed as effects which occur at a micro-scale level [38]. Nano-scale effects of degradation occur at a molecular level in the material, where the behaviours of the atomistic structures present are influenced by the breaking of the molecular bonds, crystallisation of the polymer chains and diffusion of the monomer products formed [37]. Further understanding of each

of these complex chemical and physical effects, and how they translate across length scales, is required to fully understand the global degradation of polyester materials such as PLLA.

2.4.2 Overview of PLLA-based BPS

An overview of the main advancements and developments of the CE mark approved PLLA BPS devices is now given. **Figure 2.4** presents a comparison between several BPS which have emerged in preclinical or clinical use.

Abbott Vascular (Absorb BVS)

The first generation Absorb Bioresorbable Vascular Scaffold (BVS) 1.0 was designed from PLLA with a strut thickness of 156 μm and a 1.4 mm crossing profile (maximum diameter which exists between the proximal end of the balloon and the distal tip of the delivery catheter) [39]–[41]. The BVS 1.0 was composed of out of phase zig-zag hoops and comprised of a 2-4 μm thick conformal poly-D,L-lactic acid (PDLLA) coating. The zig-zag struts were modified to be slightly thinner (150 μm), and had an alternative in-phase design in the next generation BVS 1.1 (**Figure 2.4**) [40], [42].

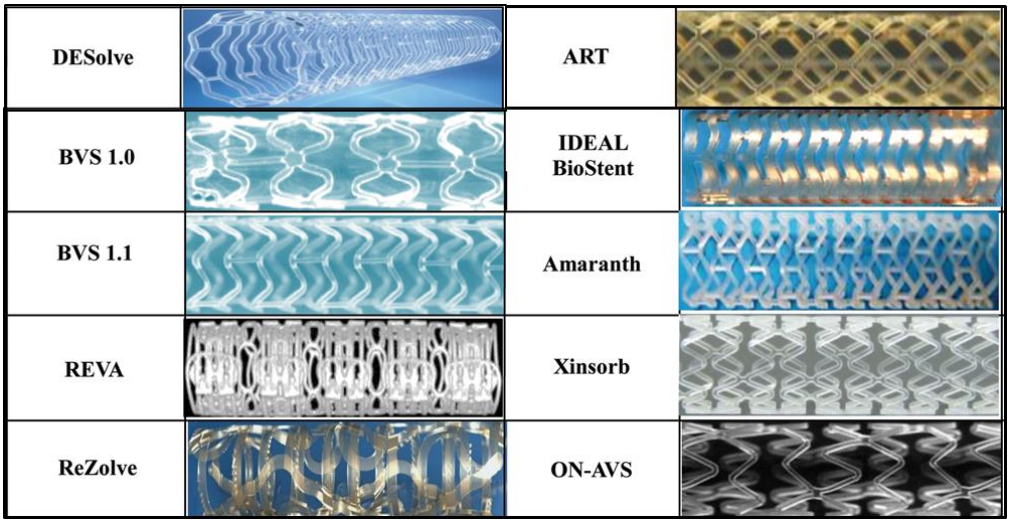

Figure 2.4 Comparison of several bioresorbable polymeric stents for clinical or preclinical use (figure adapted with permission from [35]).

The registry and clinical trial experience with the BVS devices is extensive, and several randomised clinical trials have been performed to test the safety and efficacy of both generations of the device. A detailed overview of the clinical trials and key findings for BVS 1.0 and 1.1 can be found in a number of recent articles [43]–[45]. Some of the key outcomes from these studies were that the BVS performed similarly to an already established DES (Xience DES, Abbott Vascular) during the early stages of investigation, with the emergence of adverse events occurring during long-term follow up of the device [46].

In ABSORB III, one of the more recently completed investigations (which compared the BVS to Xience in over 2000 patients), the bioresorbable stent was found to be non-inferior to Xience for the primary endpoint of target lesion failure (TLF) after 1 year [47]. However, after 2 years, rates of reported TLF significantly increased for the BVS compared to Xience (11% compared to 7.9%), with an increase in cardiac death and ischemia also observed [47]. Similarly, recent early stage results published from the Amsterdam Investigator-initiated Absorb Strategy All-comers (AIDA) trial highlighted issues with the BVS, which showed higher rates of device thrombosis when compared to a metallic DES [48]. The Absorb BVS was approved for use in Europe in 2011, in the US in July 2016, and in Japan in December 2016. However, following the disappointing results of ABSORB III, the FDA sent a recommendation letter to healthcare professionals on the use of the device. The European regulatory agency restricted use of the device to clinical registries only in May 2017, before the manufacturers were forced to stop production due to low sales.

Another device which is currently undergoing development at Abbott Vascular, the Falcon BVS, is yet another PLLA based stent, believed to comprise of <

100 μm struts [49]. Currently there is very little clinical data on the Falcon BVS available in the literature [45], [50].

Reva Medical (Reva, ReZolve, Fantom)

Reva Medical initially developed and trialled REVA, a bioresorbable stent composed of poly-tyrosine derived polycarbonate, and with struts measuring 200 μm in thickness [51]. REVA was evaluated for its clinical performance in the RESORB study [52]. Later generations of the device, ReZolve, and ReZolve 2, included a slide-and-lock mechanism and a polymer coating for the controlled release of sirolimus [53]. Data from two clinical trials examining the safety and efficacy of the ReZolve devices RESTORE and RESTORE-II, showed a need to reduce the profile of the device (following occurrences of late lumen loss and acute vessel recoil) [54].

Following these clinical results, the company's subsequent device, Fantom, was developed and tested in the FANTOM II trial (which evaluated the device in up to 240 patients) [55]. A low percentage (4.2%) of major adverse cardiac events was reported after 12 months [56], [57], and the device achieved CE mark approval soon after (April 2017). Fantom is designed using the same poly-tyrosine derived polycarbonate material as the previous devices, with key differences being its thin 125 μm struts, radiographic visibility features, improved expansion properties, and non-specific requirements for storage or handling [45], [58].

Elixir Medical (DESolve)

Elixir Medical have developed and tested a series of BPS devices, beginning with their DESolve, followed by the DESolve 100 (which achieved CE mark approval in May 2014), the DESolve Nx, DESolve Cx and the DESolve Amity

[59], [60]. Similarly to the Absorb BVS, the DESolve family are once again balloon-expandable PLLA-based devices, with polymeric coatings designed to elute anti-proliferative drugs during the early stages of implantation. Initially this drug was myolimus, but then changed to novolimus in the second generation DESolve 100 [60], [61]. Key features of the DESolve 100 include self-expansion properties (i.e. the stent self-corrects itself up to a nominal diameter in the occurrence of a malapposition between the struts and vessel wall, which is distinct to the continuous long-term loading exerted by self-expanding metallic stents [60], and which is achieved for the DESolve 100 device through proprietary processing techniques of the polymer), and significant device degradation in the first year, with complete resorption reported by 2 years [59]. Most noticeably, the DESolve 100 has a strut thickness of 100 μm, and it is believed that the polymer undergoes additional processing in the manufacture of the device to allow it to maintain the mechanical strength required for such thin struts [59], [61]. Approval was granted in Europe, following the results published for the DESolve first-in-man trial (which showed no stent thrombosis, or no major adverse cardiac events after 1 year) [61] and favourable results have so far also been observed in ongoing clinical trials of next generation DESolve devices, DESOLVE Nx and DESOLVE Cx [62]–[64].

Arterial Remodeling Technologies and Terumo (ART)

The Pure Bioresorbable Scaffold (PBS) received CE mark approval in May 2015. A PLA polymer was utilised for the initial design of the PBS device (strut thickness of 170 μm) which showed early degradation after just 3 months, followed by full resorption at 24 months [65], [66]. A mixed PDLLA polymer, incorporating a drug eluting coating (developed by Terumo Corporation

technology), is used in the design of the second generation ART 18Z device [67]. The first in man (FIM) clinical trial, Arterial Remodeling Transient Dismantling Vascular Angioplasty (ARTDIVA) was conducted to establish the safety and efficacy of the second generation device, with no incidents of MI or stroke observed, and 1 case of ischemic-driven TLR reported after 6 months [68]. There is no other clinical results available to date for the drug eluting ART 18Z.

Devices in the pipeline

Outside of these commercially available devices, a significant research effort is being made by numerous companies and research institutions to better the design of BPS, with a focus on a number of key areas, seen as the main challenges for this technology.

Devices which are currently under development, in preclinical testing or are being evaluated in ongoing clinical trials include:

- Abbott's latest generation Falcon BVS (Abbott Vascular, Santa Clara, CA, USA)
- A series of PLLA based devices from Amaranth medical (Amaranth Medical, Mountain View, USA) Fortitude, Aptitude and Magnitude
- Ideal BioStent, developed from a poly-lactide anhydride mixed with salicylic acid (Xenogenics Corp, Canton, MA, USA)
- Xinsorb (Huaan Biotech, Upper Heyford, UK)
- Renuvia (Boston Scientific, Marlborough, MA, USA)
- MeRes and MeRes 100 (Meril Life Science, Gujarat, India)
- Mirage bio-resorbable micro-fiber scaffold (Manli Cardiology, X Singapore)
- ReNATURAL (Cardionovum GmbH, Bonn, Germany)

- ON-AVS (OrbusNeich, Fort Lauderdale, FL, USA)
- and Firesorb (Microport, Shanghai, China).

2.4.3 Mechanical properties of PLLA

PLLA is a thermoplastic material which exhibits highly non-linear behaviour when subjected to loading. The standard elastic modulus for PLLA at room temperature is between 3-4 GPa, which is often reported alongside a low (<10%) elongation to failure [69]. Typical stress strain behaviour for PLLA is shown in **Figure 2.5** (adapted with permission from [70] and [71]).

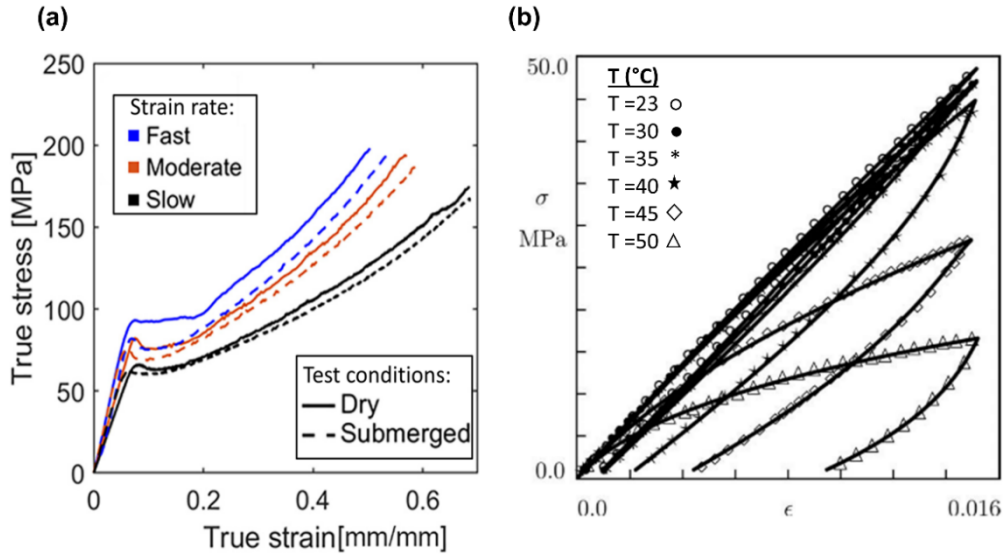

Figure 2.5 Mechanical stress-strain behaviour for PLLA under a number of testing conditions is shown (a) alongside behaviour for PLLA injection moulded specimens at different temperatures (b) (plots adapted with permission from [70] and [71]).

The main characteristics of the loading behaviour observed in **Figure 2.5** are an initial elastic response at low strains, a defined yield point for each of the different testing conditions examined in **Figure 2.5**(a) (with a secondary yield point observed for the dry material tested under high strain rates) and an increase in stress with increasing strain. The loading and unloading curves reported by Dusunceli *et al*. for PLLA examined under uniaxial loading and temperatures ranging from 35°C to 50°C (**Figure 2.5**(b)) highlight both the

non-linear viscoelastic behaviour and the dependence on testing temperature, with an increased temperature effect seen for T > 40°C. Differences in the yield behaviour are evident between the testing data shown **Figure 2.5**(a) and (b), which may in part be explained by the different crystallinities of the materials examined (11% [71] compared to 44% [70]). Generally, the unloading behaviour of PLLA is not well reported in the literature. Bobel *et al*. recently discussed the unloading characteristics of PLLA specimens and also reported an observed temperature effect in their experimental investigation of PLLA pre-degradation mechanical characteristics [72].

Polymers consist of long chains, made up of hundreds or thousands of monomer repeating units. PLLA is a semi-crystalline material in which chains may take an amorphous (random, entangled) or crystalline (aligned, highly structured) configuration. The crystalline regions of PLLA contain high interatomic bonds between the closely packed chains, which results in the high stiffness observed for PLLA compared to the amorphous polyesters. When loaded, the interconnected backbone chains in the amorphous regions unwind and conform to extended arrangements, which allow for large deformation behaviours (as observed in **Figure 2.5**). Upon the removal of external load, backbone chains will return to their initial configuration, unless they are fixed through manufacturing or processing methods; this is what provides PLLA with its ability to recover from large deformations. The mechanical behaviour of thermoplastics includes plastic as well as non-linear viscoelastic behaviour. PLLA is well known to possess non-linear viscoelastic material behaviour (as seen in **Figure 2.5**) and it demonstrates both stress relaxation and creep characteristics under long-term loading.

There have been numerous experimental studies investigating the mechanical properties of PLLA for use in the coronary stent application, which have been performed both in the absence and presence of material degradation (the latter of which are reviewed in the next section). In terms of the mechanical characteristics most often reported in such works, the Young's modulus and tensile strength are the properties which are most often considered [70], [72]–[76]. The radial stiffness, collapse pressure and creep resistance of PLLA based stents have also been reported for a number of studies [75], [77]–[79].

The initial mechanical properties of PLLA fibres for use in BPS were extensively investigated by Zilberman *et al*., who demonstrated a clear yield point for tested fibres, along with high tensile strength, high modulus and moderate strain to failure (967 MPa, 5 GPa and 50% strain respectively) [73]. The initial radial compression strength of the PLLA fibre stents (which took the form of a helical coil with longitudinal reinforcing fibres) was reported to be greater than 200 kPa [73]. The plastic response of PLLA was considered as being more critical relative to its viscoelastic or strain-rate dependence behaviour in the in-vitro characterisation of bilayer helical coiled stents (composed from PLLA and PLGA materials) [74]. Tensile testing revealed that PLGA did not contribute significantly to the structural performance of the devices investigated and the measured elongation at break of PLLA was found to exceed 50% [74].

One of the earliest studies into the mechanical properties of PLLA for use in BPS was carried out by Agrawal *et al*. (1992), who examined the effects of various processing techniques on the collapse pressure of the pioneering bioresorbable Duke stent [77]. In-vitro testing was performed to evaluate the impact of fibre draw ratio and thermal processing methods on the mechanical

behaviour of monofilament PLLA stents; the fibre draw ratio and stent diameter were found to inversely influence the collapse pressure [77]. More recent work by Venkatraman *et al*. followed a similar approach to measure the collapse pressure of helical PLLA stent prototypes [79]. The collapse pressure showed little dependence on the molecular weight of the polymers used in fabrication; however a change in the stent design, and the addition of a 5 wt% loading of a hydrophobic drug, both resulted in a significant difference in the pressure values measured [79].

The pre-degradation characteristics of PLLA for its use in BPS have recently been examined by Bobel *et al*. through tensile testing of solvent cast PLLA samples at two different temperatures (37°C, 42°C) [72]. The temperature and strain-rate dependency of the material were investigated, and a softer and more compliant behaviour was observed for PLLA under tensile testing at higher temperatures, with a significant viscoelastic strain recovery noted for the material during load-unload testing [72] (performed over a strain-rate range representative of that experienced during stent deployment [80]). The importance of investigating the complex pre-degradation mechanical behaviours of PLLA for the BPS application was highlighted in this study. Utilising this and other experimental data, the short term mechanical performance [81], and the benefits of incorporating a shape memory effect on the recoil characteristics of a PLLA based BPS were computationally evaluated by Bobel and co-workers [82].

As discussed above, the microstructure of polymers materials has a strong bearing on their mechanical behaviour. Both the degree of crystallinity and the molecular orientation of PLLA have a strong influence on its properties, in particular on stiffness and ductility. The impact of processing techniques on

PLLA mechanical properties has been reviewed by a number of groups [83]–[85]. Tensile data reported for various PLLA specimens at room temperature are compared in **Figure 2.6** (adapted with permission from [69]). The high variation in reported tensile response is due to the final form of the molecular orientation, crystallinity and condition of the tested specimens. Typical values of Young's modulus for extruded PLLA fibres are given between 3 and 4 GPa [69], with annealed or fibre-orientated variations exhibiting values up to 11 GPa [85].

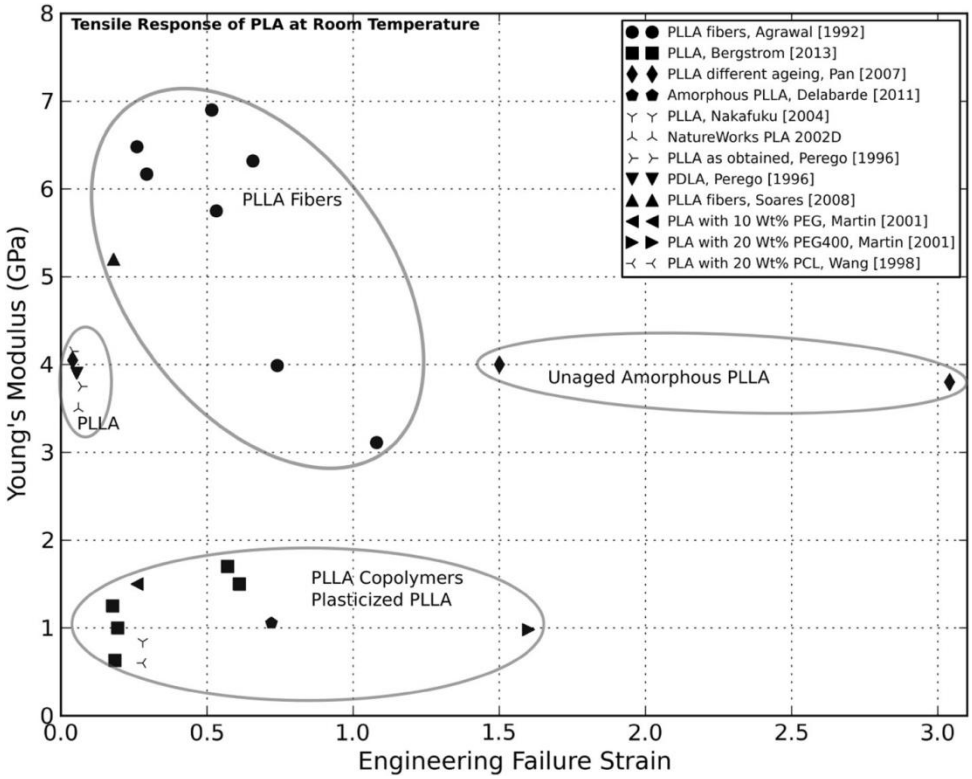

Figure 2.6 The tensile response of a number of PLA specimens is compared above. There is a high variation in the measured Young's modulus of different PLA and PLLA fibres (adapted with permission from [69]).

There have been numerous attempts at modifying PLLA or creating blends of PLLA and other biodegradable polyesters, specifically for use in BPS [75], [86]–[88]. A number of studies by Grabow *et al*. examined the mechanical and thermo-mechanical properties of pure PLLA, and several modified forms of

PLLA, for the BPS application [75], [76], [87]. In the first of these, the addition of a plasticiser (triethylcitrate (TEC)) to PLLA micro specimens, and the subsequent laser cutting and sterilisation of the specimens, were all shown to have a significant influence on the molecular weight, elastic modulus, tensile strength and elongation at break of the tested specimens [76]. The effects of TEC plasticising also had a noticeable impact on the glass transition temperature, and on the observed creep behaviour of the specimens [76].

Knowledge of the instantaneous strength of poly-lactide materials has been found to be insufficient in predicting their long-term performance [89]. PLLA is known to experience creep when applied strains are lower in value than the material's yield strain [90]. Further work of Grabow *et al*. [75] involved determining and comparing the initial tensile properties and creep response of PLLA for use in a balloon-expandable slotted tube stent design, to the tensile and creep properties of a plasticised blend of PLLA and PCL for the same application [75]. PLLA specimens were found to have higher elastic modulus but similar tensile strengths, when compared to the plasticised blend of PLLA and PCL [75]. A more gradual creep response was also observed for the pure PLLA stents, when stents were tested in a custom made pressure chamber, and subjected to external pressure loads of 100 mm Hg [75].

Quite a number of research groups have looked at using nano-fillers and other composite materials to enhance the mechanical strength and expansion properties of PLLA based BPS [91], [92]. In one such study, nanocomposite biomaterials based on inorganic barium sulphate (BaS04) and PLLA were formulated and fabricated, and the corresponding effects of nano-filler loading on the mechanical performance of the BPS devices were investigated, with improvements in the tensile modulus and strength of the devices observed

[91]. As expected, the ageing state of the polymer material is also thought to have a strong effect on its mechanical properties. PLLA, like all glassy polymers, will undergo physical ageing, i.e. a gradual rearrangement in its microstructure to reduce the overall system enthalpy. The use of thermal treatment, via annealing, has been seen to induce reorientation and realignment of fibre crystalline structures in PLLA fibre-based stents, with a favourable influence on the stress-strain characteristics observed [93]. Bergstorm and Hayman recently presented a detailed overview of the mechanical properties of PLA, which includes a focus on the temperature dependence and physical ageing characteristics of PLLA materials [69].

There are extensive studies reported in the literature for the in-vitro mechanical behaviour of the commercially available PLLA stents. Two recent studies, which have focused on the radial performance of BPS, [94], [95] are highlighted here. The expansion behaviour of three commercially available stents (Absorb BVS, DESolve and the magnesium based Magmaris) were examined and compared, with the Absorb BVS and Elixir's DESolve both exhibiting time-dependent recoil characteristics [94]. In other work, the recoil behaviour and crossing profile of the Absorb and DESolve device were investigated and found to be greater than that observed for a typical metallic DES [95]. The radial strength of the polymeric devices, however, showed a reduction when compared to the metallic stent (which also had a smaller crossing profile) [95].

The interactions between elastic modulus, yield strength and other important physical properties, for example molecular weight, orientation and crystallinity (as discussed below) are oftentimes the key focus of experimental studies investigating PLLA for use in the BPS application. Such experimental data is

valuable to device designers, and it may be beneficial in the development of better computational modelling techniques to aid the design and development of PLLA-based BPS (as discussed in Section 2.5).

2.4.4 Key factors in the mechanical and degradation behaviour of PLLA

From the perspective of designing next generation BPS, the phenomenon of biodegradation, through the bulk degradation behaviour observed for PLA polymers, adds significant complications, in comparison to permanent stents. Specific to bioresorbable stents, designed from polymeric materials, the interactions between molecular weight, crystallinity, degradation time, mechanical strength and external loading are of interest to the community. **Table 2.1** presents an overview of some of the relevant in-vitro degradation studies of PLLA for use in the BPS application, where the main data that were obtained from such studies are highlighted. As discussed above, hydrolysis of polyesters causes reduction in their chain lengths, and as a result the molecular weight of the polymer decreases. The molecular weight of PLLA is very often used as a key indicator of its degradation behaviour, and there has been much research carried out to provide an understanding of how changes in molecular weight may influence the stiffness, strength and ductility of PLLA for its use in BPS. The entanglement of polymer chains is dependent on their respective length, therefore the number of chain entanglements that require breaking has an influence on the measured strength, and on the elongation-at-break of PLLA. The direct relationship between molecular weight and elastic modulus of degrading polymers, as reviewed in [96], is often of interest when designing biodegradable devices. Experimental studies of PLLA for the BPS application frequently examine the molecular weight (using gel permeation

chromatography (GPC), which determines the molecular weight distribution of a polymer for chains within a given molecular weight range), alongside the elastic and tensile properties of the material (**Table 2.1**).

Table 2.1 In-vitro degradation studies that have investigated PLLA for its use in the BPS application. Sample type, data obtained and the degradation conditions are highlighted for each study.

Sample Type	Data obtained	Degradation conditions	Ref.
Braided PLLA stents	Molecular weight, mechanical properties, mass loss, crystallinity	Degradation at 37°C (six fibres and 4 stents tested) for 104 weeks. Samples were gamma sterilised prior to degradation.	[97]
PLLA and PLLA helical stents	Tensile properties, glass transition temperature, molecular weight, collapse pressure (stents)	PLLA tensile specimens degraded in a saline environment at 37°C for 3 months. Stents immersed in similar conditions for 5 weeks	[79]
PLLA fibres and coiled PLLA stents	Mass loss, tensile properties, radial compression strengths (stents)	Fibres degraded in PBS at 37°C for 6 weeks. PLLA stents were investigated for 20 weeks in the same conditions.	[73]
PLLA/P4HB slotted tube stent	Molecular weight, stent collapse pressure	Stents degraded in Sørensen's buffer solution at 37°C for up to 48 weeks.	[87]
PLLA slotted tube stent	Molecular weight, stent collapse pressure	Stents degraded in Sørensen's buffer solution at 37°C for up to 24 weeks.	[75]
PLLA fibres	Mass loss, tensile properties, stress relaxation properties	Degradation under static loading studied for a total of 12 months in PBS at 37°C.	[98]
PLLA, PLGA, PDLGA injected moulded samples	Tensile, fatigue, creep and DMTA properties, pH measurements	Degradation periods of 24 (PLLA), 7 (PLGA) and 1 (PDLGA) month(s) in distilled water at 37°C.	[99]
PLLA, PLLA/PBS* (injection moulded dog-bone)	Molecular weight, tensile properties, ductility, creep properties	Degradation in PBS at 37°C for 24 weeks.	[88]

Table 2.1 Table 2.1 continued

Sample Type	Data obtained	Degradation conditions	Ref.
PLLA scaffolds	Molecular weight, radial strength, thermal properties	Degradation in a customised in-vitro system (consisting of pump, artificial vasculature). Scaffolds immersed for 6 months and examined under applied pressure and fluid flow.	[100]
Extruded PLLA fibres	Tensile properties, crystallinity, thermal properties	Degradation in PBS at accelerated temperature (45°C) to represent 15 months of degradation. Static and dynamic loading applied using free-hanging weights and dynamic force transducer.	[101]
PLLA tubes	Molecular weight, crystallinity	PLLA tubes were degraded in PBS (control) or in a mock vessel (under pulsatile flow) at 37°C for 6 months.	[102]
PLLA stent subunits	Tensile properties, molecular weight, crystallinity	Simulated degradation of sub-units under fatigue loading, and in static conditions. Degradation carried out at 42°C in both cases.	[103]
PLLA scaffolds and sheets	Molecular weight, crystallinity	Degradation in PBS under static conditions at 37°C for 110 days.	[104]

PBS: phosphate buffer solution, *P4HB*: poly (4-hydroxybutyrate), *PDLGA*: poly-D,L-lactide-co-glycolide, *PBS**: poly(butylene succinate), *DMTA*: dynamic mechanical thermal analysis.

Changes in the crystalline regions of semi-crystalline PLLA have an effect on its mechanical behaviour. Polymer crystallinity is characterised by the highly-ordered compact structures which exist for semi-crystalline polymers, which can experience degradation-induced changes or transformations, that ultimately modifies these organised arrangements [105], [106]. Such transformations take the form of chain alignment events, when regions of amorphous polymer (composed of entangled polymer chains) undergo hydrolysis; with the chain-scission reactions providing the polymer chains with extra mobility, allowing them to pack closely together in crystallite regions. It has been well documented in the literature that polyester materials such as PLLA experience changes in crystallinity during the hydrolytic degradation process [105], [107]–[109], and also that such microstructural effects play a significant role in the changing mechanical properties which can be observed for these materials [108]–[111]. Such alterations in the degree of polymer crystallinity are a key consideration in the analysis and design of bioresorbable polymeric stents, and as highlighted in **Table 2.1**, a number of studies have looked at the changing crystallinity of BPS devices in experimental investigations of their long-term behaviour. Recent understanding of how changes in the percentage crystallinity of PLLA impacts on the mechanical function of a stent is becoming more developed [101], [109], [112]. Recently, Wang *et al*. have examined the changes in material crystallinity for PLLA stents degraded for 110 days and reported higher values of crystallinity on the outer surface of the stent compared to the core, which provides valuable insight into the heterogeneous nature of the degradation [104].

Another key determinant of a polymer's mechanical behaviour is its glass transition temperature, given as approximately 60°C for PLLA [28]. The microstructure of PLLA is dramatically different above and below this

temperature; below 60°C, PLLA is considered to be in a glassy state, and will exhibit quite brittle characteristics, whereas above 60°C, PLLA takes on rubbery characteristics, and is more able to withstand high deformation loading [85]. As stated earlier, the effects of both temperature and hydration on the mechanical performance of PLLA have been found to be significant, which is due to a large extent on the induced changes which occur in the material microstructure [70], [74].

The influence of molecular weight on both the stress-strain and the creep response of PLA materials was recently examined, and a modified form of the Eyring energy activation model was developed to describe the observed stress-dependent and molecular weight-dependent lifetime of the polymer materials [113]. The influence of factors such as molecular weight, stent design and incorporation of drugs on the measured mechanical behaviour of PLLA stent prototypes for a degradation period of 5 weeks has been examined [79]. Three PLLA materials of different molecular weight were used to fabricate helical stents, for which the measured collapse pressure remained almost constant (at 2.0-2.8 bars) for the three molecular weights over the 5 weeks. Incorporation of drugs and differences in stent design were initially shown to have a significant impact on collapse pressure values measured, however whether either factor had any further influence on the degradation rates of the stents mechanical properties was not evident [79].

In a similar study, the effects of long-term degradation on the mechanical stiffness, molecular weight and mass loss of PLLA fibres, and self-expanding fibre braided stents, were investigated for an immersion period of up to 104 weeks [97]. A 50% reduction in stiffness occurred for the PLLA stents after 30 weeks of degradation, and full loss of structural integrity was observed for the

stents after 36 weeks. A sharp increase in the material crystallinity (from 62%, to 82% at 52 weeks) was also observed for the tested stents [97].

Following investigation after a long term in-vitro degradation period, PLLA fibres showed almost no change in mechanical properties and demonstrated excellent radial compression endurance [73]. Values of radial compression strength of at least 150 kPa were reported for the PLLA fibre-based stents, following a degradation period of 20 weeks [73]. The influence of stent design on the values of compression strength measured was also investigated, with double-fibre stents exhibiting enhanced mechanical performance when compared to the single-fibre design [73]. More recently, a study by Bartkowiak-Jowsa and co-workers stated the need for more comprehensive data on the degradation dynamics of established biodegradable polymers, for use in the design and development of bioresorbable stents [99]. Comprehensive data from the degradation of the fundamental polymer materials would provide an excellent basis to enable the modification and development of enhanced polymer blends and composites for the BPS application. In an attempt to provide such data, the static and dynamic mechanical properties, thermomechanical, rheological and fatigue properties, and the rate of degradation product release were all analysed for PLLA, PLGA and poly-D,L-lactide-co-glycolide (PDLGA) specimens [99]. A significant influence of hydration on the mechanical parameters was observed for PLLA, and an initial slight decrease in the measured values of Young's modulus, tensile strength and deformability occurred with degradation [99]. After 15 months, however, there was a clear increase in the mechanical properties measured; Young's modulus and tensile strength were observed to be 60% higher than the initial undegraded values [99]. PLLA was identified as a favourable material for the coronary stent application, due to the less than

10% decrease in mechanical properties which were observed over the 24 month degradation period. PLLA also showed the slowest rate of pH change, an observation which is in line with the belief that there is a reduced likelihood of inflammatory reactions for this material [99]. Although the above mentioned study did not measure polymer crystallinity, they have attributed the observed increase in Young's modulus to recrystallisation of the polymer chains with degradation. This phenomenon of increasing mechanical stiffness with degradation has also been reported in a number of other studies for PLLA ([103], [108], [114]–[117]).

The in-vivo pressure loading imparted on an implanted stent from vessel dilation causes the device to recoil, i.e. it experiences a gradual reduction in diameter. Such loading occurs throughout the lifetime of the device in the vessel. Therefore, consideration of the long-term creep behaviour of PLLA and other materials utilised is important for the design and analysis of BPS [118]. The long-term creep of PLLA stents has been investigated in a number of studies [87], [88]. In one such recent study, the change in creep characteristics and other mechanical properties of PLLA and PLLA/Poly-butylene succinate (PBS) blends with degradation were examined [88]. Dog-bone specimens of PLLA and PLLA/PBS materials were immersed for 24 weeks and creep tests were performed directly after the samples were removed from the degradation buffer. The creep resistance of neat PLLA samples showed an increase over the first 2 months of degradation, as did the strength and elastic modulus of the neat material [88]. Creep resistance of the polymer samples was evaluated, with the creep resistance of PLLA showing a critical decrease after 16 weeks of degradation, compared to just a few weeks for the PLLA/PBS blend [88]. The impact of PBS content on the ductility of the

polymer blended samples was also evaluated in this study; with the ductility greatly increased for blends containing 4% or more PBS [88].

Alongside their studies on the mechanical and thermo-mechanical properties of pure PLLA, and several modified forms of PLLA for the stent application, Grabow and co-workers also examined the in-vitro degradation behaviours [75], [87]. Stents composed of polymer blends of PLLA and poly(4-hydroxybutyrate) (P4HB) showed a decrease in molecular weight by 82% after 48 weeks, alongside an initial increase in collapse pressure (maximum at 4 weeks degradation) [87]. An increase in collapse pressure was once again observed for balloon-expandable BPS, in this case manufactured from PLLA, and a blend of PLLA, PCL and TEC, and degraded for a period of 24 weeks [75]. The final measured values of collapse pressure for the PLLA stents were well above the initial values, and similar trends of molecular weight reduction were observed for the balloon-expandable devices; less than 30% of the material molecular weight remained after 24 weeks [75].

Experimental studies as outlined for PLLA for the BPS application, have generally examined the mechanical and chemical properties of PLLA during degradation in the absence of any loading or external stimuli. The degradation rates of polyesters used in bioresorbable medical devices are known to be closely linked to the in-vivo environment. A review of the means through which mechanical loading is believed to impact on degradation rates of polyesters is given in [119]. An early investigation into the impact of cyclic compressive loading on the mechanical properties and in-vitro release characteristics of a 50:50 PLLA/PLGA implant demonstrated that the applied loading had a significant impact on the stiffness, as well as the molecular weight, and on the release of protein from the tested implants over 6 weeks [120]. More recent

results for the effects of loading on the degradation rate of PLLA copolymers and polyorthoesters show an increase in the degradation rates under applied loading [121]–[123]. However, the impact of the specific in-vivo loading conditions experienced by BPS (fatigue, pressure, fluid flow) on the degradation rates of PLLA has only recently come under focus in the design of experimental protocols.

For the BPS application, preliminary experimental data on the influence of static loading conditions on PLLA fibre degradation has been provided by Soares *et al*. [98], [124]. Tensile loading was applied to PLLA fibres by the inclusion of dead-weights (50 g or 100 g), which were attached to the fibres using metallic crimps. Loaded and unloaded fibres were immersed in PBS at 37°C for a total period of 12 months after which the mass loss and the elastic and stress-relaxation response of the fibres were measured. Following the inconclusive results of this study, however, degradation times greater than 1 year were deemed necessary to fully investigate the impact of loading on the degradation in material properties [124]. A similar experimental approach was recently used by Hayman *et al*. [101] to examine the effect of both static and dynamic loading conditions on the long-term (15 month) degradation of PLLA fibres for use in the cardiovascular application [101]. Degradation of the tensile mechanical properties of the PLLA fibres was seen to increase with application of an increasing static load, and the same pattern was observed for dynamic loading [101]. Alongside tensile properties, the percent crystallinity of the PLLA fibres was investigated; material crystallinity was observed to increase with the degradation, and a linear relationship between crystallinity and the fibre rigidity constant, β, employed in the modelling work presented, was established [101]. Further examination of the effects of dynamic loading on the degradation in mechanical properties and the changes in material

crystallinity of PLLA would help to provide relevant insights into possible expected degradation behaviours of BPS in-vivo.

Recent ISO technical standards for absorbable cardiovascular implants (ISO TS 17137) presented suggestions for tackling some of the complex problems which have arisen for the durability testing of bioresorbable coronary stents [125]. The fatigue behaviour of bioresorbable devices was identified as a key consideration, however little guidelines were given on how best to simulate fatigue loading for such devices. The effects of fatigue on the mechanical and chemical degradation behaviours of model stent sub-units were recently investigated by Dreher *et al*. [103]. PLLA stent sub-units were custom made and degraded under an accelerated temperature (42°C) for 100 or 191 days, and subjected to fatigue conditions, representative of one year of in-vivo loading [103]. Fatigue loading of sub-units resulted in a statistically significant increase in the measured stiffness at designated degradation time points when compared to control samples (degradation under no load). The molecular weight of the fatigue-tested sub-units also showed noticeable differences to the control group [103]. Similar differences in degradation behaviour were observed for PLLA tubes degraded in a pulsatile flow loop in an earlier study from this group [102]. A significantly different degradation pattern was observed for the molecular weight and crystallinity of the PLLA tubes under each loading condition [102].

The morphology, radial stiffness and molecular weight of PLLA coronary stents degraded for 6 months using a custom made in-vitro test rig (designed to provide testing conditions similar to that of the in-vivo environment) were recently investigated [100]. No apparent collapse behaviour was observed with SEM, and the measured values of radial force showed a slight increase

after the 6 months of in-vitro testing: from 259 ± 17 kPa to 275 ± 14 kPa [100]. A noticeable decrease however, was observed in the molecular weight of the PLLA stents, with 68.5% of the initial value of weight-averaged molecular weight observed after the 6 month period; the weight-averaged molecular weight was believed to be a very important factor in evaluating the support capabilities of the stents [100]. These results were consistent with the measured values of radial force and molecular weight obtained in the concurrent in-vivo study which was undertaken (using a swine model), showing that the designed testing rig was effective in predicting the degradation trends observed for the examined devices in-vivo [100].

2.5 Review of Computational Modelling of BPS Degradation

As outlined briefly in the preceding chapter, the use of computational modelling for the analysis and design of next generation bioresorbable stents is required under FDA guidelines. In recent years, a substantial number of publications have looked at examining BPS behaviour and predicting their in-vivo performance using computational methods [74], [80]–[82], [119], [126]–[128]. As discussed above, an in-depth understanding of the mechanical behaviour of PLLA, and how factors such as degradation, microstructure, and external loading, among others, impact on such behaviour is required for the successful design of BPS. Mathematical models that represent the mechanical and degradation behaviour of PLLA have been developed, and reviews of these models are presented in [69], [129], [130]. The modelling techniques that have specifically been applied to BPS, to describe and predict degradation, and which can be categorised as either phenomenological or physio-chemical (**Table 2.2**) [1], are now reviewed.

Table 2.2 Summary of material degradation models that have been used to investigate the degradation performance of BPS.

Model Type	Brief Description	Key Equations	Code	Ref.
Phenomenological -damage based	Degradation parameter related to the strain invariants of the deformation (I_1, I_2). Model incorporates degradation through degradation dependent material properties	$\frac{d}{dt}d(t) = C(1-d(t))[(I_1-3)^2+(I_2-3)^2]^{\frac{1}{2}}$ $\mu = \mu_0(1-d)$	Abaqus Standard (UMAT)	[124]
Phenomenological -damage based	Modified viscoelastic QLV model used to represent the material behaviour. Degradation function was defined in terms of the strain magnitude and concentration of water in the device and was related to the material modulus *E*.	$P(d,t) = \int_0^t E(d,\varphi^t-\varphi^s)\frac{dF}{d\varepsilon}\frac{d\varepsilon}{ds}ds$ $E(d,t) = E_\infty(1-\lambda_i d)+\sum_{n=1}^{N}E_n(1-\lambda_n d)e^{-\frac{t}{\tau_{RN}}}$	Abaqus Standard (UMAT)	[131]
Phenomenological -damage based	Damage based model developed using combined Maxwell and Ogden-type models. Strain energy density ψ related to free energy of a single element, ψ^{el} of the ith Maxwell element ψ_i and the degradation parameter *d*.	$\psi(\boldsymbol{F},\boldsymbol{F}_i^{\nu},d) = \psi^{el}(\boldsymbol{F},d)+\sum_{i=1}^{N}\psi_i(\boldsymbol{F}\boldsymbol{F}_i^{\nu-1},d)$	Abaqus Standard (UMAT)	[132]

Table 2.2 Table 2.2 continued

Model Type	Brief Description	Key Equations	Code	Ref.
Phenomenological -damage based	Model incorporated a degradation degree which was described using an exponential function. Material constants (*a, b, c, m, n*) were obtained by fitting to experimental data.	$D = D(\varepsilon, t) = a(b + c \times \varepsilon^n) \times t^m$	Abaqus Standard (USDFLD)	[133]
Physio-chemical	First order degradation model developed based on transient diffusion-reaction equations for each polymer species S $_{(1\text{-}5)}$. Each species was described as a function of the hydrolysis *K*, autocatalysis effects K_a and its stoichiometric coefficient $n_{1\text{-}5}$. LA concentrations C_0^s examined using diffusion based model.	$S_1 \rightarrow n_2 S_2 \rightarrow n_3 S_3 \rightarrow n_4 S_4 \rightarrow n_5 S_5$ $\frac{\partial C_x^s}{\partial t} = \mathbf{f}(K, K_a, C_{1-5}, n_{1-5})$ $\frac{\partial C_0^s}{\partial t} = \nabla \cdot (D_0^s \nabla C_0^s) + 2\sum_{m=1}^{n} K C_m^s K_a$	COMSOL (Multiphysics)	[134], [135]
Physio-chemical	Simultaneous model of the biodegradation and drug release for a PLLA based stent coating. Presented four equations in terms of transport of the polymer (C_P shown on right),water molecules, oligomers and LA's	$\frac{\partial C_P}{\partial t} = \frac{\partial}{\partial x}(D_P \frac{\partial C_P}{\partial x}) - k_{PW} C_P C_W (1 + \alpha C_L)$	Not specified	[136]

QLV: Quasi-linear viscoelastic, *LA*: Lactic acid

2.5.1 Phenomenological modelling of BPS

Phenomenological modelling approaches have been applied to BPS with a primary focus of simulating the changing mechanical performance of the device and examining its scaffolding ability. These methods have involved a continuum damage mechanics (CDM) approach, where a degradation parameter, d, is introduced to represent the degradation driven loss of mechanical integrity. Following on from the phenomenological degradation theory proposed by Rajagopal and Wineman in the early nineties [137], Rajagopal *et al*. [138] developed a thermodynamically consistent model for the strain-induced degradation of rubbery polymers. Scission and healing (reformation of the networks) of the polymer chains were considered to be equally dependent on a state variable, which measured the extent of local degradation. This theory was further developed by Soares *et al*. [98], [124], [139]–[141] who reported a number of studies focusing predominantly on PLLA BPS and their weakening mechanical properties. Variations in mechanical response due to degradation are captured through evolution of material parameters present in the chosen constitutive law. In their initial work [98], [124], [139], a preliminary model was developed to describe the mechanical behaviour of a loaded, cylindrical structure composed of a linear degradable polymeric material. A degradation parameter d, ($d = 0 \leftrightarrow$ no degradation; $d = 1 \leftrightarrow$ maximum degradation) was used. It was hypothesised that the rate of change of degradation was dependent on the applied strain, the current state of degradation, and implicitly dependent on both spatial location and time, through the following relationship:

$$\frac{\mathrm{d}}{dt}\, d(t) = C\big(1 - d(t)\big)[(I_1 - 3)^2 + (I_2 - 3)^2]^{0.5} \tag{2.1}$$

where C is a time constant and I_1 and I_2 are the first and second strain invariants [98]. In the constitutive model for the material, the strain energy was related to the degradation parameter through damage based evolution of the shear modulus μ as follows:

$$\mu = \mu_0(1 - d) \tag{2.2}$$

where μ_0 is the initial shear modulus [98], [139].

Results from experiments involving homogenous uniaxial extension of PLLA were then used to assess the predictions of the model. The model was first proposed for conditions of linear elastic behaviour and extended, in a follow up study [140], to explain the non-linear response for finite deformations. As part of other work [141] based on the results of experimental extension tests on un-degraded PLLA fibres, a specific form of the Helmholtz potential, ψ, was used to represent the mechanical behaviour:

$$\rho\psi(I_1, d) = \lambda(d)e^{-(I_1-3)}(I_1 - 3) + \mu(d)\ln\left[1 + a(I_1 - 3)\right] \tag{2.3}$$

where μ and λ are material properties, that are both considered to be functions of the degradation d, ρ is the density and a is a material constant. This was then implemented in the finite element code Abaqus/Standard with user subroutines USDFLD and UHYPER to examine the behaviour of a BPS based on the Cypher stent geometry (Error! Reference source not found.**Figure 2.7**) and the effects of pressure on the degradation were explored [140]. This model was then extended by Muliana and Rajagopal [131] to describe materials which show viscoelastic characteristics in the absence of degradation. The degradation rate was modified to include the effects of water diffusion through the material [142] and an adaptation of the quasi-linear viscoelastic (QLV) model [143] was used to form the constitutive law. Material

parameters were calibrated and degradation of a PLLA BPS was examined using Abaqus/Standard and a UMAT user subroutine. The response of the polymer to quasi-static loading was examined and it was found that coupling between the stent and a viscoelastic arterial wall had a significant effect on the degradation response of the stent [131]. While this model presented an advanced methodology for studying the effects of degradation on the material's mechanical performance, the governing equation for water diffusion through the device was based on simple Fickian diffusion and a constant value was used for the water concentration, limiting the model's ability to accurately describe internal hydrolysis reactions.

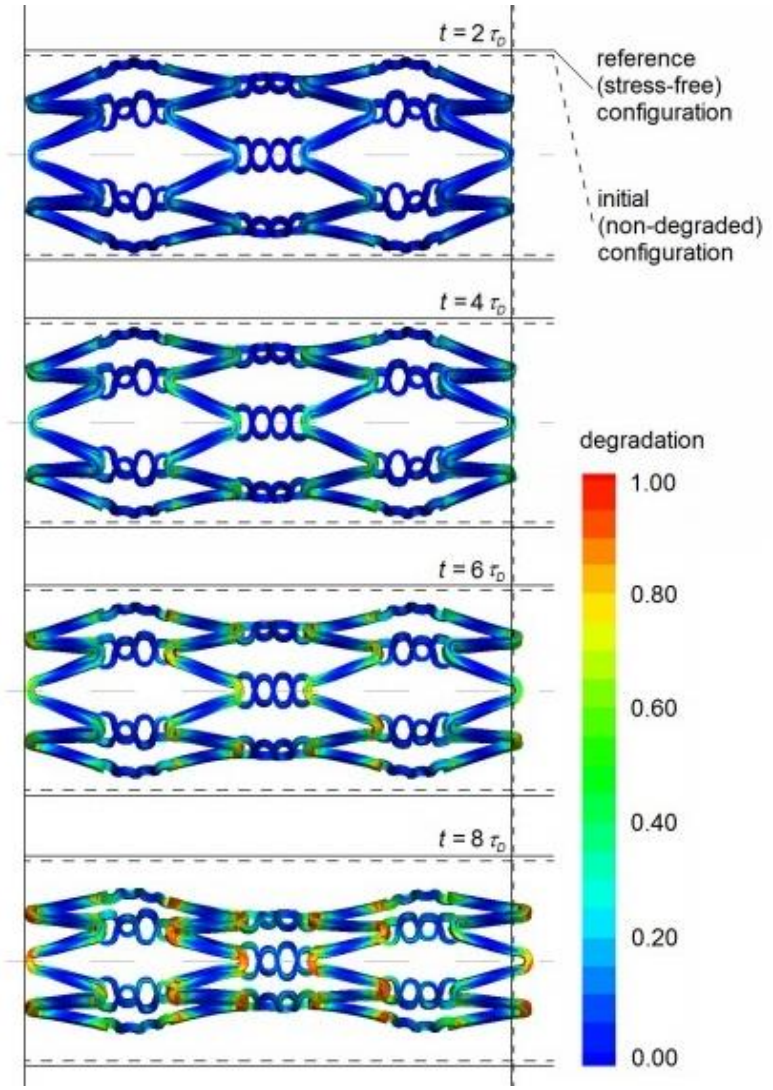

Figure 2.7 A biodegradable version of the Cypher stent was used to investigate the effects of pressurisation on the magnitude and locations of degradation in a BPS, where time t is related to a characteristic degradation time τ_D [140].

A phenomenological model has also been presented by Luo *et al*. [133] who utilised combined experimental and numerical techniques to investigate the degradation behaviour of high molecular weight PLLA BPS [100], [133]. Changes in the diameters of PLLA stents were measured following in-vitro experimental testing and the ratios of elongation before and after degradation were used to define the degree of degradation [133]. Finite element simulations using Abaqus/Standard (through user subroutine USDFLD) were performed on a stent geometry; the principal stress and strain distributions were seen to accumulate mainly at central locations of the stent, and initial

values reported for strain were related to the degradation rate of the material [133].

Khan and El-Sayed [132] utilised the previously described degradation parameter in the development of a non-linear viscoplastic model to predict the mechanical response of BPS under time-dependent loading conditions. The model was implemented in Abaqus/Standard and a study of two cylindrical annuli suggested that inhomogeneous deformations can occur in a BPS [132]. More recently, Hayman *et al*. [101] experimentally investigated how static and dynamic loading influenced the degradation of PLLA fibres and suggested exponential equations based on their results to describe the evolution of material properties for a Knowles's strain energy potential. In another recent publication, Qiu *et al*. modelled the degradation in the mechanical properties of a BPS using a phenomenological approach, and examined the mechanical interactions between the stent and a remodelling vessel over a two-year period [144]. Experimental measurements of BPS radial stiffness and strength were used in the model development, and simulations on a geometry representative of the Absorb BVS were performed. A reduction in maximum Von Mises stress from 115.16 MPa to 43.67 MPa was reported for the degrading BPS after 545 days [144].

While the above models account for material degradation, and when implemented in finite element software have demonstrated great capability for simulating the mechanical performance and scaffolding ability of a BPS, the formulations are phenomenological and rely for the most part on calibration of material parameters to macroscopic experimental material degradation data, and do not explicitly represent the internal physiochemical processes involved in the material degradation. This can be considered as a limitation, since

elucidating the influence of these processes is a very important part of understanding BPS in-vivo behaviour and is necessary for driving future BPS design. Physio-chemical based models where such processes have been more explicitly represented are now discussed and summarised

2.5.2 Physio-chemical modelling of BPS

Farrar and Buchanan [145] previously provided a summary of physio-chemical polymer degradation models and described how complex hydrolysis of the backbone bonds in biodegradable polyesters occurs at a molecular level within the material. Efforts have been made to model the most dominant physio-chemical processes involved in this phenomenon using continuum theory, and in particular, established first-order kinetic equations have been proposed of the form used in [146], to describe the diffusion of esters, monomers and water molecules. A recent example is the general degradation model of Wang *et al*. [147], where the evolution of ester bond and monomer concentrations are described by non-linear first-order rate equations, which incorporate autocatalytic rate constants, and where monomer diffusion is based on Fick's law.

Expanding on such an approach, Shazly *et al*. [134] presented a reaction-transport modelling framework to describe how the hydrolytic degradation of a tissue-embedded BPS affects the by-products released (implemented in COMSOL Multiphysics™). A 3D model was used to assess how the degradation rate, as well as arterial remodelling and metabolic activity rates, influenced the concentration of lactic acid (LA) present within arterial tissue. Degradation was modelled as a chain scission process and the concentrations

of different polymer species C_{1-5}^{s} (assuming five species) were related to the hydrolysis, K and its autocatalytic effects, K_a, using equations of the form:

$$\frac{\partial C_i^s}{\partial t} = \mathrm{f}\,(K, K_a C_i, n_i), \qquad i = 1,2,3,4,5 \tag{2.4}$$

where n_i is the stoichiometric coefficient of each species. As part of further work, Ferdous *et al*. [135] explored the effects of stent structure and composition on the fate of the LA's and on the kinetics of the polymer degradation and erosion. Kinetic equations incorporating diffusion of the stent constituents were proposed, for example where C_j^s and D_j^s are the soluble constituent concentrations and the diffusion coefficient respectively, for a constituent with j ester bonds and where k and A represent hydrolysis degradation and autocatalysis effects respectively, as follows:

$$\frac{\partial C_j^s}{\partial t} = \nabla \cdot (D_j^s \nabla C_j^s) - jkC_j^s A + 2\sum_{m=j+1}^{n} kC_m^s A \qquad 0 < j < 8 \tag{2.5}$$

where n and C_m^s are, respectively, the number of ester bonds, and any constituent's concentration with the number of ester bonds between n and $j+1$ in the stent. A 2D computational model was developed using COMSOL (**Figure 2.8**) with transport of soluble constituents through the arterial wall and the lumen governed by Eq. (2.5). Results from experimental degradation studies on poly-dispersed PLLA were then used to validate the model. Stent degradation kinetics was found to have a major influence on the performance of PLLA-based BPS. In terms of the material degradation models which have been developed for drug eluting polymer stents, Alexis [148] described the main factors that affect biodegradation and drug-release rate in the early 2000s. A number of research groups [136], [149], [150] have modelled the dual process of biodegradation and drug release for biodegradable stent

coatings and BPS, using transport-reaction formulations, which accounted for the main physical–chemical parameters involved. Arosio *et al.* [150] used a "shrinking core" approach to develop a twinned drug release and degradation model, which was combined with a mechanical strength model for the analysis of bioresorbable polymer materials loaded with drugs. Decay of the polymer's mechanical properties, bending strength and tensile modulus, were related to the resistant section-area decrease and the molecular weight decrease respectively; however, this work was not specific to BPS.

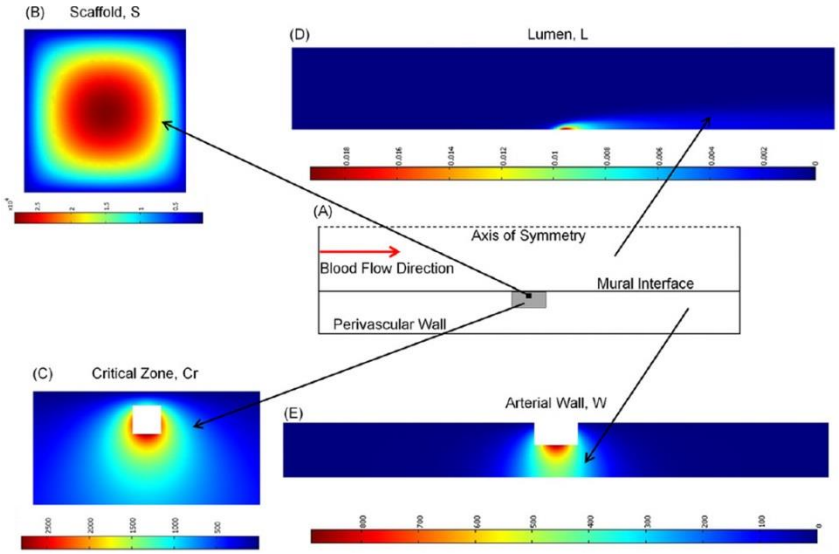

Figure 2.8 The schematic above shows the components of the two dimensional geometry used by Ferdous *et al*. [135] to represent a tissue-embedded PLLA stent. In the study [135], a diffusion reaction model was developed by the authors to investigate the degradation kinetics of the stent and the accumulation of lactic acids within the surrounding tissues. Reproduced with permission from [135].

In general, the most advanced physio-chemical polymer degradation models that have been reported have predominantly been utilised for the analysis and design of general degradable polymeric devices and implants [151]–[155] other than BPS, as evidenced by the small number of studies of this type listed in **Table 2.2**. Therefore, additional work is needed to further develop the equivalent modelling techniques for BPS. A model which encapsulates the

dominant aspects of the hydrolytic degradation, while providing insight into the impact on the stent's mechanical integrity, would be of benefit to BPS development. At present, while the computational modelling techniques used to describe the degradation of polyester and other polymer materials consider the principle hydrolysis mechanisms or the phenomenological effects of degradation on the materials mechanical behaviour [1], further work is needed to develop more comprehensive, multi-physics and multi-scale modelling frameworks that combine the accuracy of the physio-chemical approach with the robust practicality of the phenomenological approach. Development of multi-faceted models which can offer further insight into and capture the effects of the complex in-vivo environment (for example, dynamic loading, blood flow, tissue remodelling etc.) on the rates of device degradation would provide opportunities for enhancement of the analysis and design tools for bioresorbable devices, and also on the development of the regulatory guidelines.

2.6 Conclusions

The bioresorbable polyester PLLA has emerged as the dominant material to date for the BPS application. This is due in part to its high biocompatibility, reasonable rates of degradation and physical and chemical attributes, which are highly adaptable through processing techniques, and which therefore offer many mechanisms to tailor PLLA for use in a coronary stent.

PLLA exhibits a wide range of mechanical properties, which are highly dependent on the manufacturing techniques used during device fabrication. A number of BPS devices composed of PLLA have reached the clinical market. However, overall results for the long-term performance of these devices have

proven disappointing, and while efforts are currently underway to develop new devices from other biodegradable polymers, a great deal of research is also ongoing to provide improved insights into the degradation aspects of PLLA for this application. From review of the relevant literature surrounding PLLA, and following on from the successful attributes of permanent metallic stents, as discussed in Section 2.3, it is possible to identify several key areas which could form part of the renewed research focus into PLLA stents for coronary interventions. In summary, the following aspects of PLLA's degradation and mechanical behaviour are of interest:

- Molecular weight

The reduction in molecular weight is very often investigated in experimental studies of BPS, alongside its dependence on various factors (e.g. degradation environment, material processing techniques). However, oftentimes the impact of molecular weight on the mechanical properties of biodegradable polyesters does not become apparent until a critically low value of molecular weight has been reached [156], [157]. Therefore, knowledge of the long-term molecular weight behaviour of degrading PLLA based BPS, would aid enhanced device design.

- Thermal properties (crystallinity, glass transition temperature)

The impact of physical ageing and degradation induced crystallisation on PLLA materials for use in the BPS application has far reaching consequences for the mechanical performance of the device. Crystallinity relates to changes in the precise microstructure of the material, which act to alter its mechanical behaviour. Additionally, mechanical testing of PLLA materials is highly

dependent on the testing conditions, and in particular the temperature conditions used.

- Mechanical properties (tensile strength, viscoelasticity, creep)

Whether it is necessary to provide mechanical support to a remodelling artery or simply deliver drugs to an identified site of treatment, the mechanical strength, flexibility and creep performance of the material used in device design are all important considerations.

PLLA is a relatively stiff polymer, however its ultimate tensile strength is lower than that of the high strength alloys traditionally used in the development of coronary stents, prompting the need for thicker stent struts in PLLA BPS devices (as discussed in **Chapter 1**).

PLLA also experiences local yielding and exhibits plastic and non-linear viscoelastic behaviours. Therefore, singular examination of the Young's modulus of PLLA during degradation is insufficient to provide adequate information on its full mechanical performance. Creep deformation of PLLA is an important consideration for the design of BPS. Creep may occur early on in the scaffolding period (before a noticeable drop in Young's modulus for example), and this may result in the device losing contact with the artery wall, which could lead to incomplete endothelialisation and ultimately trigger late stent thrombosis [158]. In-vitro testing and modelling of polylactides for spinal cage devices has revealed time-dependency effects that were found to be responsible for the premature failure of the devices under loading [89]. Janssen *et al*. highlighted a relationship between the fatigue life of thermoplastics and their creep behaviour [159]. A detailed knowledge of the creep characteristics of PLLA and other applicable polyesters would aid the

development of the regulatory guidelines and standards for assessing the durability of BPS. Given that quite a number of factors have an influence on the mechanical behaviour of PLLA (for example the processing and testing temperatures, the applied strain rates, the long-term loading experienced and the initial material microstructure) the use of computational modelling, where enhanced constitutive laws for material behaviour may be implemented, presents an attractive means to examine the mechanical performance of PLLA based devices.

- Tailoring the mechanical properties

Additionally, it is possible to enhance the mechanical capabilities of PLLA for use in BPS through thermal processing or other ageing techniques. This has also been investigated through the blending of PLLA with other degradable polymers, and the use of rigid fillers to form composite materials. The successful application of modified PLLA blends or PLLA-based composites may allow for thinner struts to be employed in device design , similar to the early efforts made for permanent stents to mitigate the risk of restenosis. This ability to tailor the mechanical properties of PLLA during the manufacturing process is possibly one of the key reasons it has emerged as a highly suitable material for this application.

- Impact of mechanical loading

The impact of mechanical loading on the degradation rates and in-vivo performance of PLLA based BPS has consequences for the design and development of this next generation technology. More work is needed in this regard to understand the precise influences of long-term cyclic loading and

fluid flow on the degradation rates, microstructure and mechanical performance of PLLA BPS.

- Computational models – (usefulness, mechanical behaviour, degradation)

Due to the complexity and the long-term time dependence of the experimental studies that are needed to provide a fully comprehensive insight into the degradation mechanisms and resulting behaviour of PLLA based BPS, the development and enhancement of computational modelling techniques for investigating and predicting degradation, and its effects on mechanical behaviour, would undoubtedly aid device design.

From review of the existing computational techniques used to examine BPS degradation, there is little evidence of physio-chemical models being developed with a focus on the structural degradation of the BPS. Understanding how the mechanical behaviour of the polymer is impacted by the variations to chain lengths, the formation of crystallisation structures, or the diffusion of degradation products, would be aided with a robust computer simulation framework. The development of a rigorous finite element framework for studying BPS degradation is of necessary importance for furthering the progression of the next generation treatments for coronary artery disease.

In light of this, physio-chemical models of polymer degradation are adapted and developed in this thesis for PLLA based BPS, with a specific focus on the interactions between molecular weight, material crystallinity and long-term mechanical performance of the stent.

References

[1] E. L. Boland, R. Shine, N. Kelly, C. A. Sweeney, and P. E. McHugh, “A Review of Material Degradation Modelling for the Analysis and Design of Bioabsorbable Stents,” *Ann. Biomed. Eng.*, vol. 44, no. 2, pp. 341–356, 2015.

[2] L. S. Nair and C. T. Laurencin, “Biodegradable polymers as biomaterials,” *Prog. Polym. Sci.*, vol. 32, no. 8, pp. 762–798, 2007.

[3] I.-Y. Kim *et al.*, “Chitosan and its derivatives for tissue engineering applications,” *Biotechnol. Adv.*, vol. 26, no. 1, pp. 1–21, 2008.

[4] G. G. d’Ayala, M. Malinconico, and P. Laurienzo, “Marine derived polysaccharides for biomedical applications: chemical modification approaches,” *Molecules*, vol. 13, no. 9, pp. 2069–2106, 2008.

[5] W. Khan, D. Yadav, A. J. Domb, and N. Kumar, “Collagen,” in *Biodegradable Polymers in Clinical Use and Clinical Development*, John Wiley & Sons, Inc., 2011, pp. 59–89.

[6] A. Mandal, S. Panigrahi, and C. Zhang, “Collagen as Biomaterial for Medical Application--Drug Delivery and Scaffolds for Tissue Regeneration: A Review,” *Biol. Eng. Trans.*, vol. 2, no. 2, pp. 63–88, 2010.

[7] B. D. Ulery, L. S. Nair, and C. T. Laurencin, “Biomedical Applications of Biodegradable Polymers,” *J. Polym. Sci. B. Polym. Phys.*, vol. 49, no. 12, pp. 832–864, Jun. 2011.

[8] M. I. Sabir, X. Xu, and L. Li, “A review on biodegradable polymeric materials for bone tissue engineering applications,” *J. Mater. Sci.*, vol. 44, no. 21, pp. 5713–5724, 2009.

[9] J. H. Solhaug and P. Heimann, “Polyglycolic acid (PGA, Dexon) sutures in neck surgery.,” *Acta Chir. Scand.*, vol. 141, no. 5, pp. 326–328, 1974.

[10] F. A. Barber, “Resorbable fixation devices: a product guide,” *Orthop. Spec. Ed.*, vol. 4, pp. 1111–1117, 1998.

[11] J. C. Middleton and A. J. Tipton, “Synthetic biodegradable polymers as orthopedic devices.,” *Biomaterials*, vol. 21, no. 23, pp. 2335–2346, Dec. 2000.

[12] Shive and Anderson, “Biodegradation and biocompatibility of PLA and PLGA microspheres.,” *Adv. Drug Deliv. Rev.*, vol. 28, no. 1, pp. 5–24, Oct. 1997.

[13] M. Sokolsky-Papkov, K. Agashi, A. Olaye, K. Shakesheff, and A. J. Domb, “Polymer carriers for drug delivery in tissue engineering.,” *Adv. Drug Deliv. Rev.*, vol. 59, no. 4–5, pp. 187–206, May 2007.

[14] L. Da Hou, Z. Li, Y. Pan, M. I. Sabir, Y. F. Zheng, and L. Li, “A review on biodegradable materials for cardiovascular stent application,” *Front. Mater. Sci.*, vol. 10, no. 3, pp. 238–259, 2016.

[15] I. Manavitehrani, A. Fathi, H. Badr, S. Daly, A. Negahi Shirazi, and F. Dehghani, “Biomedical Applications of Biodegradable Polyesters,” *Polymers* , vol. 8, no. 1. 2016.

[16] P. J. Flory, *Principles of Polymer Chemistry*. Cornell University Press, 1953.

[17] F. Rodriguez, C. Cohen, C. K. Ober, and L. Archer, *Principles of Polymer Systems 5th Edition*. Taylor & Francis, 2003.

[18] A. L. Sisson, M. Schroeter, and A. Lendlein, “Polyesters,” in *Handbook of Biodegradable Polymers*, Wiley-VCH Verlag GmbH & Co. KGaA, 2011, pp. 1–21.

[19] P. A. Gunatillake and R. Adhikari, “BIODEGRADABLE SYNTHETIC POLYMERS FOR TISSUE ENGINEERING,” vol. 5, pp. 1–16, 2003.

[20] C.-C. Chu, “Biodegradable Polymeric Biomaterials: An Updated Overview,” *Biomed. Eng. Handb.*, pp. 1–22, 2000.

[21] S. Garg and P. W. Serruys, “Coronary stents: Current status,” *J. Am. Coll. Cardiol.*, vol. 56, no. 10, pp. S1–S42, 2010.

[22] P. Poncin and J. Proft, “Stent tubing: Understanding the desired attributes,” *Med. Device Mater. - Proc. Mater. Process. Med. Devices Conf. 2003*, no. September, pp. 253–259, 2003.

[23] A. Kastrati *et al.*, “Intracoronary Stenting and Angiographic Results:Strut Thickness Effect on Restenosis Outcome (ISAR-STEREO) Trial,” *Circulation*, vol. 103, no. 23, pp. 2816–2821, 2001.

[24] J. Pache *et al.*, “Intracoronary stenting and angiographic results: strut thickness effect on restenosis outcome (ISAR-STEREO-2) trial.,” *J. Am. Coll. Cardiol.*, vol. 41, no. 8, pp. 1283–1288, Apr. 2003.

[25] A. Seth, “Interventional cardiology moving towards biomimicry - the development of the novel BioMime Sirolimus-eluting coronary stent system,” *Am. J. Cardiol.*, vol. 107, no. 8, pp. 1A-2A, Apr. 2011.

[26] S. Garg and P. W. Serruys, “Coronary stents: looking forward.,” *J. Am. Coll. Cardiol.*, vol. 56, no. 10 Suppl, pp. S43-78, Aug. 2010.

[27] B. J. O’Brien, J. S. Stinson, S. R. Larsen, M. J. Eppihimer, and W. M. Carroll, “A platinum–chromium steel for cardiovascular stents,” *Biomaterials*, vol. 31, no. 14, pp. 3755–3761, 2010.

[28] H. Tsuji, “Poly(lactide) stereocomplexes: Formation, structure, properties, degradation, and applications,” *Macromol. Biosci.*, vol. 5, no. 7, pp. 569–597, 2005.

[29] A. Gopferich, “Mechanisms of polymer degradation and erosion,” *Biomaterials*, vol. 17, no. 2, pp. 103–114, 1996.

[30] C. G. Pitt, F. I. Chasalow, Y. M. Hibionada, D. M. Klimas, and A. Schindler, “Aliphatic polyesters II. The degradation of poly (DL-lactide), poly (epsilon-caprolactone), and their copolymers in vivo,” *J. Appl. Polym. Sci.*, vol. 26, no. 11, pp. 3779–3787, 1981.

[31] A. Gopferich and R. Langer, “Modeling monomer release from bioerodible polymers,” *J. Control. Release*, vol. 33, no. 1, pp. 55–69, 1995.

[32] D. Garlotta, “A Literature Review of Poly (Lactic Acid),” vol. 9, no. 2, 2002.

[33] S. Saito, “New horizon of bioabsorbable stent.,” *Catheterization and cardiovascular interventions : official journal of the Society for Cardiac Angiography & Interventions*, vol. 66, no. 4. United States, pp. 595–596, Dec-2005.

[34] H. Antheunis, J.-C. van der Meer, M. de Geus, W. Kingma, and C. E. Koning,

"Improved Mathematical Model for the Hydrolytic Degradation of Aliphatic Polyesters," *Macromolecules*, vol. 42, no. 7, pp. 2462–2471, 2009.

[35] N. A. Weir, F. J. Buchanan, J. F. Orr, and G. R. Dickson, "Degradation of poly-L-lactide. Part 1: in vitro and in vivo physiological temperature degradation," *Proc Inst Mech Eng H*, vol. 218, no. 5, pp. 307–319, 2004.

[36] A. Gleadall, J. Pan, M. A. Kruft, and M. Kellomaki, "Degradation mechanisms of bioresorbable polyesters. Part 1. Effects of random scission, end scission and autocatalysis," *Acta Biomater*, vol. 10, no. 5, pp. 2223–2232, 2014.

[37] Y. Li *et al.*, "A predictive multiscale computational framework for viscoelastic properties of linear polymers," *Polymer (Guildf).*, vol. 53, no. 25, pp. 5935–5952, Nov. 2012.

[38] J. L. Bouvard, D. K. Ward, D. Hossain, S. Nouranian, E. B. Marin, and M. F. Horstemeyer, "Review of Hierarchical Multiscale Modeling to Describe the Mechanical Behavior of Amorphous Polymers," *J. Eng. Mater. Technol.*, vol. 131, no. 4, p. 41206, Sep. 2009.

[39] J. A. Ormiston, M. W. Webster, and G. Armstrong, "First-in-human implantation of a fully bioabsorbable drug-eluting stent: the BVS poly-L-lactic acid everolimus-eluting coronary stent," *Catheter Cardiovasc Interv*, vol. 69, no. 1, pp. 128–131, 2007.

[40] Y. Onuma and P. W. Serruys, "Bioresorbable scaffold: the advent of a new era in percutaneous coronary and peripheral revascularization?," *Circulation*, vol. 123, no. 7, pp. 779–797, 2011.

[41] B. D. Gogas, V. Farooq, Y. Onuma, and P. W. Serruys, "The ABSORB bioresorbable vascular scaffold: an evolution or revolution in interventional cardiology," *Hell. J Cardiol*, vol. 53, no. 4, pp. 301–309, 2012.

[42] S. Garg and P. Serruys, "Biodegradable stents and non-biodegradable stents.," *Minerva Cardioangiol.*, vol. 57, no. 5, pp. 537–565, Oct. 2009.

[43] D. J. Kereiakes, Y. Onuma, P. W. Serruys, and G. W. Stone, "Bioresorbable Vascular Scaffolds for Coronary Revascularization," *Circulation*, vol. 134, no. 2, pp. 168–182, 2016.

[44] J. Iqbal, Y. Onuma, J. Ormiston, A. Abizaid, R. Waksman, and P. Serruys, "Bioresorbable scaffolds: Rationale, current status, challenges, and future," *Eur. Heart J.*, vol. 35, pp. 765–776, 2014.

[45] D. Capodanno, "Bioresorbable scaffolds in coronary intervention: Unmet needs and evolution," *Korean Circ. J.*, vol. 48, no. 1, pp. 24–35, 2018.

[46] P. W. Serruys *et al.*, "Comparison of an everolimus-eluting bioresorbable scaffold with an everolimus-eluting metallic stent for the treatment of coronary artery stenosis (ABSORB II): a 3 year, randomised, controlled, single-blind, multicentre clinical trial," *Lancet*, vol. 388, no. 10059, pp. 2479–2491, 2016.

[47] S. G. Ellis *et al.*, "Everolimus-eluting bioresorbable scaffolds for coronary artery disease," *N. Engl. J. Med.*, vol. 373, no. 20, pp. 1905–1915, 2015.

[48] J. Wykrzykowska *et al.*, "Bioresorbable scaffolds versus metallic stents in routine PCI: the plot thickens," *J. Thorac. Dis.*, vol. 9, no. 8, pp. 2296–2300, 2017.

[49] R. J. Rapoza, “Next generation Absorb: a workhorse BVS,” in *Transcatheter Cardiovasc Therapeutics*, 2016.

[50] D. Regazzoli, P. P. Leone, A. Colombo, and A. Latib, “New generation bioresorbable scaffold technologies: an update on novel devices and clinical results,” *J. Thorac. Dis.*, vol. 9(Suppl 9), pp. S979–S985, 2017.

[51] M. Pollman, “Engineering a bioresorbable stent: REVA programme update,” *EuroIntervention*, vol. 5, no. F, pp. F54–F57, Dec. 2009.

[52] E. Strandberg, J. Zeltinger, D. G. Schulz, and G. L. Kaluza, “Late Positive Remodeling and Late Lumen Gain Contribute to Vascular Restoration by a Non-Drug Eluting Bioresorbable Scaffold,” *Circ. Cardiovasc. Interv.*, vol. 5, no. 1, pp. 39–46, 2012.

[53] E. Grube, “Bioabsorbable stent: the Boston Scientific and REVA technology,” in *Euro PCR*, 2009.

[54] R. Costa, “REVA ReZolve clinical program update,” in *Transcatheter Cardiovascular Therapeutics*, 2012.

[55] G. Stone, “FANTOM: A radio-opaque desaminotyrosine polycarbonate-based scaffold,” in *Transcatheter Cardiovasc Therapeutics*, 2016.

[56] N. Frey, “FANTOM II trial: clinical results from the Fantom sirolimus-eluting BRS,” in *EuroPCR*, 2016.

[57] A. Abizaid *et al.*, “6-Month Clinical and Angiographic Outcomes of a Novel Radiopaque Sirolimus-Eluting Bioresorbable Vascular Scaffold: The FANTOM II Study,” *JACC Cardiovasc. Interv.*, vol. 10, no. 18, pp. 1832–1838, Sep. 2017.

[58] A. Abizaid, “Sirolimus-eluting bioresorbable scaffold,” in *EuroPCR*, 2015.

[59] S. Verheye *et al.*, “TCT-563 Multi-Center, First-In-Man Evaluation of the Myolimus-Eluting Bioresorbable Coronary Scaffold: 6-Month Clinical and Imaging Results,” *J. Am. Coll. Cardiol.*, vol. 60, no. 17, p. B163, 2012.

[60] H. M. Nef *et al.*, “A new novolimus-eluting bioresorbable coronary scaffold: Present status and future clinical perspectives,” *Int. J. Cardiol.*, vol. 227, pp. 127–133, 2017.

[61] S. Verheye *et al.*, “A next-generation bioresorbable coronary scaffold system: From bench to first clinical evaluation: 6- and 12-month clinical and multimodality imaging results,” *JACC Cardiovasc. Interv.*, vol. 7, no. 1, pp. 89–99, 2014.

[62] A. Mattesini *et al.*, “The DESolve novolimus bioresorbable Scaffold: from bench to bedside,” *J. Thorac. Dis. Vol 9, Suppl. 9 (August 2017) J. Thorac. Dis. (Bioresorbable Vasc. Scaffolds Treat. Coron. Artery Dis.*, 2017.

[63] S. Verheye *et al.*, “TCT-16 Prospective, Multi-Center Evaluation of the DESolve Novolimus-Eluting Bioresorbable Coronary Scaffold: Imaging Outcomes and 5-Year Clinical and Imaging Results,” *J. Am. Coll. Cardiol.*, vol. 70, no. 18 Supplement, p. B7 LP-B8, Oct. 2017.

[64] A. Abizaid *et al.*, “Serial Multimodality Imaging and 2-Year Clinical Outcomes of the Novel DESolve Novolimus-Eluting Bioresorbable Coronary Scaffold System for the Treatment of Single De Novo Coronary Lesions,” *JACC Cardiovasc. Interv.*, vol. 9, no. 6, pp. 565–574, 2016.

[65] E. Durand *et al.*, “Head-to-head comparison of a drug-free early programmed dismantling polylactic acid bioresorbable scaffold and a metallic stent in the porcine coronary artery: six-month angiography and optical coherence tomographic follow-up study.,” *Circ. Cardiovasc. Interv.*, vol. 7, no. 1, pp. 70–79, Feb. 2014.

[66] K. Yahagi *et al.*, “Comparison of a Drug-Free Early Programmed Dismantling PDLLA Bioresorbable Scaffold and a Metallic Stent in a Porcine Coronary Artery Model at 3-Year Follow-Up.,” *J. Am. Heart Assoc.*, vol. 6, no. 6, Jun. 2017.

[67] J. Fajadet, “The ART, stent: design and early first-in-man experiences,” in *Transcatheter Cardiovasc Therapeutics*, 2012.

[68] A. Lafont, “ARTDIVA,” in *BRS 2014*, 2014.

[69] J. S. Bergström and D. Hayman, “An Overview of Mechanical Properties and Material Modeling of Polylactide (PLA) for Medical Applications,” *Ann. Biomed. Eng.*, vol. 44, no. 2, pp. 330–340, 2016.

[70] P.-J. Wang *et al.*, “Effect of working environment and procedural strategies on mechanical performance of bioresorbable vascular scaffolds,” *Acta Biomater.*, pp. 1–10, 2018.

[71] N. Dusunceli, A. D. Drozdocv, and N. Theilgaard, “Influence of Temperature on Viscoelastic–Viscoplastic Behavior of Poly(lactic acid) Under Loading–Unloading,” *Polym. Eng. Sci.*, vol. 57, no. 3, pp. 239–247, 2016.

[72] A. C. Bobel, S. Lohfeld, R. N. Shirazi, and P. E. McHugh, “Experimental mechanical testing of Poly (L-Lactide) (PLLA) to facilitate pre-degradation characteristics for application in cardiovascular stenting,” *Polym. Test.*, vol. 54, pp. 150–158, 2016.

[73] M. Zilberman, K. D. Nelson, and R. C. Eberhart, “Mechanical properties and in vitro degradation of bioresorbable fibers and expandable fiber-based stents,” *J. Biomed. Mater. Res. - Part B Appl. Biomater.*, vol. 74, no. 2, pp. 792–799, 2005.

[74] N. Paryab, D. Cronin, P. Lee-Sullivan, X. Ying, F. Y. C. Boey, and S. Venkatraman, “Uniform Expansion of a Polymeric Helical Stent,” *J. Med. Device.*, vol. 6, no. 2, p. 021012, 2012.

[75] N. Grabow, C. M. Bünger, K. Sternberg, S. Mews, K. Schmohl, and K.-P. Schmitz, “Mechanical Properties of a Biodegradable Balloon-expandable Stent From Poly(L-lactide) for Peripheral Vascular Applications,” *J. Med. Device.*, vol. 1, no. 1, p. 84, 2007.

[76] N. Grabow, M. Schlun, K. Sternberg, N. Hakansson, S. Kramer, and K.-P. Schmitz, “Mechanical Properties of Laser Cut Poly(L-Lactide) Micro-Specimens: Implications for Stent Design, Manufacture, and Sterilization,” *J. Biomech. Eng.*, vol. 127, no. 1, pp. 25–31, Mar. 2005.

[77] C. M. Agrawal, K. F. Haas, D. A. Leopold, and H. G. Clark, “Evaluation of poly(L-lactic acid) as a material for intravascular polymeric stents,” *Biomaterials*, vol. 13, no. 3, pp. 176–182, 1992.

[78] R. S. Gammon *et al.*, “Mechanical features of the duke biodegradable intravascular stent,” *Journal of the American College of Cardiology.*, vol. 17,

no. 2. [New York, N.Y.] :, p. A235, 1991.

[79] S. Venkatraman, T. L. Poh, T. Vinalia, K. H. Mak, and F. Boey, “Collapse pressures of biodegradable stents.,” *Biomaterials*, vol. 24, no. 12, pp. 2105–2111, May 2003.

[80] N. Debusschere, P. Segers, P. Dubruel, B. Verhegghe, and M. De Beule, “A finite element strategy to investigate the free expansion behaviour of a biodegradable polymeric stent,” *J. Biomech.*, vol. 48, no. 10, pp. 2012–2018, 2015.

[81] A. C. Bobel, S. Petisco, J. Ramon Sarasua, W. Wenxin, and P. E. McHugh, “Computational Bench Testing to Evaluate the Short-Term Mechanical Performance of a Polymeric Stent,” *Cardiovasc. Eng. Technol.*, 2015.

[82] A. C. Bobel and P. E. McHugh, “Computational Analysis of the Utilisation of the Shape Memory Effect and Balloon Expansion in Fully Polymeric Stent Deployment,” *Cardiovasc. Eng. Technol.*, vol. 9, no. 1, pp. 60–72, 2018.

[83] B. Gupta, N. Revagade, and J. Hilborn, “Poly(lactic acid) fiber: An overview,” *Prog. Polym. Sci.*, vol. 32, no. 4, pp. 455–482, 2007.

[84] K. Hamad, M. Kaseem, H. W. Yang, F. Deri, and Y. G. Ko, “Properties and medical applications of polylactic acid: A review,” *Express Polym. Lett.*, vol. 9, no. 5, pp. 435–455, 2015.

[85] S. Farah, D. G. Anderson, and R. Langer, “Physical and mechanical properties of PLA, and their functions in widespread applications — A comprehensive review,” *Adv. Drug Deliv. Rev.*, vol. 107, pp. 367–392, 2016.

[86] M. Zilberman, N. D. Schwade, and R. C. Eberhart, “Protein-Loaded Bioresorbable Fibers and Expandable Stents: Mechanical Properties and Protein Release,” *J. Biomed. Mater. Res. - Part B Appl. Biomater.*, vol. 69, no. 1, pp. 1–10, 2004.

[87] N. Grabow *et al.*, “A biodegradable slotted tube stent based on poly(l-lactide) and poly(4-hydroxybutyrate) for rapid balloon-expansion,” *Ann. Biomed. Eng.*, vol. 35, no. 12, pp. 2031–2038, 2007.

[88] L. D. Kimble and D. Bhattacharyya, “In Vitro Degradation Effects on Strength, Stiffness, and Creep of PLLA/PBS: A Potential Stent Material,” *Int. J. Polym. Mater. Polym. Biomater.*, vol. 64, no. 6, pp. 299–310, 2015.

[89] T. A. P. Engels, S. H. M. Söntjens, T. H. Smit, and L. E. Govaert, “Time-dependent failure of amorphous polylactides in static loading conditions,” *J. Mater. Sci. Mater. Med.*, vol. 21, no. 1, pp. 89–97, 2010.

[90] M. L. Dreher, S. Nagaraja, H. Bui, and D. Hong, “Characterization of load dependent creep behavior in medically relevant absorbable polymers.,” *J. Mech. Behav. Biomed. Mater.*, vol. 29, pp. 470–479, Jan. 2014.

[91] H. Y. Ang *et al.*, “Radiopaque Fully Degradable Nanocomposites for Coronary Stents.,” *Sci. Rep.*, vol. 8, no. 1, p. 17409, 2018.

[92] Y. Chen, A. Murphy, D. Scholz, L. M. Geever, J. G. Lyons, and D. M. Devine, “Surface-modified halloysite nanotubes reinforced poly(lactic acid) for use in biodegradable coronary stents,” *J. Appl. Polym. Sci.*, vol. 135, no. 30, p. 46521, Aug. 2018.

[93] T. R. Welch, R. C. Eberhart, and C.-J. Chuong, “The influence of thermal treatment on the mechanical characteristics of a PLLA coiled stent.,” *J. Biomed. Mater. Res. B. Appl. Biomater.*, vol. 90, no. 1, pp. 302–311, Jul. 2009.

[94] W. Schmidt, P. Behrens, C. Brandt-Wunderlich, S. Siewert, N. Grabow, and K. P. Schmitz, “In vitro performance investigation of bioresorbable scaffolds – Standard tests for vascular stents and beyond,” *Cardiovasc. Revascularization Med.*, vol. 17, no. 6, pp. 375–383, 2016.

[95] J. A. Ormiston, B. Webber, B. Ubod, O. Darremont, and M. W. I. Webster, “An independent bench comparison of two bioresorbable drug-eluting coronary scaffolds (Absorb and DESolve) with a durable metallic drug-eluting stent (ML8/Xpedition).,” *EuroIntervention J. Eur. Collab. with Work. Gr. Interv. Cardiol. Eur. Soc. Cardiol.*, vol. 11, no. 1, pp. 60–67, May 2015.

[96] A. Gleadall, “9 - Mechanical properties of biodegradable polymers for medical applications,” in *Woodhead Publishing Series in Biomaterials*, J. B. T.-M. D. of B. P. M. D. Pan, Ed. Woodhead Publishing, 2015, pp. 163–199.

[97] J. P. Nuutinen, C. Clerc, R. Reinikainen, and P. Törmälä, “Mechanical properties and in vitro degradation of bioabsorbable self-expanding braided stents,” *J. Biomater. Sci. Polym. Ed.*, vol. 14, no. 3, pp. 255–266, 2003.

[98] J. S. Soares, J. E. Moore Jr., and K. R. Rajagopal, “Constitutive framework for biodegradable polymers with applications to biodegradable stents,” *ASAIO J*, vol. 54, no. 3, pp. 295–301, 2008.

[99] M. Bartkowiak-Jowsa, R. Będziński, A. Kozłowska, J. Filipiak, and C. Pezowicz, “Mechanical, rheological, fatigue, and degradation behavior of PLLA, PGLA and PDGLA as materials for vascular implants,” *Meccanica*, vol. 48, no. 3, pp. 721–731, 2013.

[100] Q. Luo *et al.*, “Comparative Study of Degradation Behavior of Bioresorbable Cardiovascular Scaffolds,” *Cardiovasc. Eng. Technol.*, vol. 6, no. 1, pp. 71–79, 2015.

[101] D. Hayman, C. Bergerson, S. Miller, M. Moreno, and J. E. Moore, “The effect of static and dynamic loading on degradation of PLLA stent fibers,” *J Biomech Eng*, vol. 136, no. 8, p. 4027614, 2014.

[102] M. L. Dreher, S. Nagaraja, Q. Lu, R. Malinauskas, and B. Batchelor, “Degradation of PLLA Tubes in a Pulsatile Flow Loop as a Model for Cardiovascular Stent Degradation,” in *Biomaterials*, 2015, vol. 8, no. 33, p. 44.

[103] M. L. Dreher, S. Nagaraja, and B. Batchelor, “Effects of fatigue on the chemical and mechanical degradation of model stent sub-units,” *J. Mech. Behav. Biomed. Mater.*, vol. 59, pp. 139–145, 2016.

[104] P.-J. Wang, N. Ferralis, C. Conway, J. C. Grossman, and E. R. Edelman, “Strain-induced accelerated asymmetric spatial degradation of polymeric vascular scaffolds,” *Proc. Natl. Acad. Sci.*, p. 201716420, 2018.

[105] S. K. Saha and H. Tsuji, “Effects of rapid crystallization on hydrolytic degradation and mechanical properties of poly(l-lactide-co-ε-caprolactone),” *React. Funct. Polym.*, vol. 66, no. 11, pp. 1362–1372, 2006.

[106] S. Li, H. Garreau, and M. Vert, “Structure-property relationships in the case of the degradation of massive poly (α-hydroxy acids) in aqueous media,” *J. Mater.*

Sci. Mater. Med., vol. 1, no. 4, pp. 198–206, 1990.

[107] X. H. Zong *et al.*, “Structure and morphology changes in absorbable poly(glycolide) and poly(glycolide-co-lactide) during in vitro degradation,” *Macromolecules*, vol. 32, no. 24, pp. 8107–8114, 1999.

[108] E. A. R. Duek, C. A. C. Zavaglia, and W. D. Belangero, “In vitro study of poly(lactic acid) pin degradation,” *Polymer (Guildf).*, vol. 40, no. 23, pp. 6465–6473, 1999.

[109] H. Tsuji, A. Mizuno, and Y. Ikada, “Properties and Morphology of Poly (L -lactide). III . Effects of Initial Crystallinity on Long-Term In Vitro Hydrolysis of High Molecular Weight Poly (L -lactide) Film in Phosphate-Buffered Solution,” *J. Appl. Polym. Sci.*, pp. 1452–1464, 2000.

[110] X. Yuan, A. F. T. Mak, and K. Yao, “In vitro degradation of poly(L-lactic acid) fibers in phosphate buffered saline,” *J. Appl. Polym. Sci.*, vol. 85, no. 5, pp. 936–943, 2002.

[111] T. Karjalainen, M. Hiljanen-Vainio, M. Malin, and J. Seppälä, “Biodegradable lactone copolymers. III. Mechanical properties of ε-caprolactone and lactide copolymers after hydrolysis in vitro,” *J. Appl. Polym. Sci.*, vol. 59, no. 8, pp. 1299–1304, Feb. 1996.

[112] G. Perego, G. D. Cella, and C. Bastioli, “Effect of molecular weight and crystallinity on poly(lactic acid) mechanical properties,” *J. Appl. Polym. Sci.*, vol. 59, no. 1, pp. 37–43, Jan. 1996.

[113] S. H. M. Sontjens, T. A. P. Engels, T. H. Smit, and L. E. Govaert, “Time-dependent failure of amorphous poly- D , L -lactide : Influence of molecular weight,” vol. 13, pp. 69–77, 2012.

[114] H. Tsuji and Y. Ikada, “Properties and morphology of poly(l-lactide) 4. Effects of structural parameters on long-term hydrolysis of poly(l-lactide) in phosphate-buffered solution,” *Polym. Degrad. Stab.*, vol. 67, no. 1, pp. 179–189, 2000.

[115] H. Tsuji, “Properties and morphologies of poly(L-lactide): 1. Annealing condition effects on properties and morphologies of poly(L-lactide),” *Polymer (Guildf).*, vol. 36, no. 14, pp. 2709–2716, 1995.

[116] H. Tsuji, “In vitro hydrolysis of blends from enantiomeric poly(lactide)s Part 1. Well-stereo-complexed blend and non-blended films,” *Polymer (Guildf).*, vol. 41, no. 10, pp. 3621–3630, 2000.

[117] N. A. Weir, F. J. Buchanan, J. F. Orr, D. F. Farrar, and G. R. Dickson, “Degradation of poly-L-lactide. Part 2: increased temperature accelerated degradation,” *Proc Inst Mech Eng H*, vol. 218, no. 5, pp. 321–330, 2004.

[118] N. Grabow, D. P. Martin, and K. Sternberg, “Absorbable polymer stent technologies for vascular regeneration Niels Grabow , a ∗ David P . Martin , b Klaus-Peter Schmitz a,” vol. 2009, no. September 2009, pp. 744–751, 2010.

[119] Y. Li *et al.*, “The effect of mechanical loads on the degradation of aliphatic biodegradable polyesters,” *Regen. Biomater.*, no. April, pp. 179–190, 2017.

[120] D. E. Thompson, C. M. Agrawal, and K. Athanasiou, “The effects of dynamic compressive loading on biodegradable implants of 50-50% polylactic Acid-polyglycolic Acid.,” *Tissue Eng.*, vol. 2, no. 1, pp. 61–74, 1996.

[121] Y. Z. Wan, Y. L. Wang, L. Y. Zheng, F. G. Zhou, Q. Zhao, and G. X. Cheng, “Influence of external stress on the in vitro degradation behavior of C3D/PLA composites,” *J. Mater. Sci. Lett.*, vol. 20, no. 21, pp. 1957–1959, 2001.

[122] M. Deng *et al.*, “Effect of load and temperature on in vitro degradation of poly(glycolide-co-L-lactide) multifilament braids.,” *Biomaterials*, vol. 26, no. 20, pp. 4327–4336, Jul. 2005.

[123] M. Guo *et al.*, “The effects of tensile stress on degradation of biodegradable PLGA membranes: A quantitative study,” *Polym. Degrad. Stab.*, vol. 124, pp. 95–100, Feb. 2016.

[124] J. F. da S. Soares, “Constitutive modeling for biodegradable polymers for application in endovascular stents,” Texas A&M University, 2008.

[125] ISO, “ISO/TS 17137:2014 Cardiovascular implants and extracorporeal systems -- Cardiovascular absorbable implants.” Standards, International Organization for, Geneva, Switzerland, p. 26, 2014.

[126] R. G. Pauck and B. D. Reddy, “Computational analysis of the radial mechanical performance of PLLA coronary artery stents,” *Med. Eng. Phys.*, vol. 37, no. 1, pp. 7–12, 2015.

[127] A. Schiavone, T.-Y. Qiu, and L.-G. Zhao, “Crimping and deployment of metallic and polymeric stents -- finite element modelling,” *Vessel Plus*, vol. 1, no. 1, pp. 12–21, 2017.

[128] Q. Wang, G. Fang, Y. Zhao, G. Wang, and T. Cai, “Computational and experimental investigation into mechanical performances of Poly-L-Lactide Acid (PLLA) coronary stents,” *J. Mech. Behav. Biomed. Mater.*, vol. 65, pp. 415–427, 2017.

[129] R. Naseem, L. Zhao, Y. Liu, and V. V. Silberschmidt, “Experimental and computational studies of poly-L-lactic acid for cardiovascular applications: recent progress,” *Mech. Adv. Mater. Mod. Process.*, vol. 3, no. 1, p. 13, 2017.

[130] S. K. Eswaran, J. A. Kelley, J. S. Bergstrom, and V. L. Giddings, “Material Modeling of Polylactide,” *Simulia Cust. Conf.*, pp. 1–11, 2011.

[131] A. Muliana and K. R. Rajagopal, “Modeling the response of nonlinear viscoelastic biodegradable polymeric stents,” *Int. J. Solids Struct.*, vol. 49, no. 7–8, pp. 989–1000, 2012.

[132] K. A. Khan and T. El-Sayed, “A phenomenological constitutive model for the nonlinear viscoelastic responses of biodegradable polymers,” *Acta Mech.*, vol. 224, no. 2, pp. 287–305, 2013.

[133] Q. Luo *et al.*, “Degradation Model of Bioabsorbable Cardiovascular Stents,” *PLoS One*, vol. 9, no. 11, p. e110278, 2014.

[134] T. Shazly, V. B. Kolachalama, J. Ferdous, J. P. Oberhauser, S. Hossainy, and E. R. Edelman, “Assessment of material by-product fate from bioresorbable vascular scaffolds,” *Ann Biomed Eng*, vol. 40, no. 4, pp. 955–965, 2012.

[135] J. Ferdous, V. B. Kolachalama, and T. Shazly, “Impact of polymer structure and composition on fully resorbable endovascular scaffold performance,” *Acta Biomater.*, vol. 9, no. 4, pp. 6052–6061, 2013.

[136] S. Prabhu and S. Hossainy, “Modeling of degradation and drug release from a

biodegradable stent coating," *J Biomed Mater Res A*, vol. 80, no. 3, pp. 732–741, 2007.

[137] K. R. Rajagopal and A. S. Wineman, "A constitutive equation for nonlinear solids which undergo deformation induced microstructural changes," *Int. J. Plast.*, vol. 8, no. 4, pp. 385–395, 1992.

[138] K. R. Rajagopal, A. R. Srinivasa, and A. S. Wineman, "On the shear and bending of a degrading polymer beam," *Int. J. Plast.*, vol. 23, no. 9, pp. 1618–1636, 2007.

[139] J. Soares, K. Rajagopal, and J. Jr Moore, "Theoretical Modeling of Cyclically Loaded, Biodegradable Cylinders," in *III European Conference on Computational Mechanics*, C. A. Motasoares, J. A. C. Martins, H. C. Rodrigues, J. C. Ambrósio, C. A. B. Pina, C. M. Motasoares, E. B. R. Pereira, and J. Folgado, Eds. Springer Netherlands, 2006, p. 207.

[140] J. S. Soares, J. E. Moore, and K. R. Rajagopal, "Modeling of deformation-accelerated breakdown of polylactic acid biodegradable stents," *J. Med. Device.*, vol. 4, no. 4, p. 41007, 2010.

[141] J. S. Soares, K. R. Rajagopal, and J. E. Moore Jr., "Deformation-induced hydrolysis of a degradable polymeric cylindrical annulus," *Biomech. Model. Mechanobiol.*, vol. 9, no. 2, pp. 177–186, 2010.

[142] A. Muliana, K. R. Rajagopal, and S. C. Subramanian, "Degradation of an elastic composite cylinder due to the diffusion of a fluid," *J. Compos. Mater.*, 2009.

[143] Y. C. Fung, *Biomechanics: Mechanical Properties of Living Tissues*. New York.: Springer, 1981.

[144] T. Qiu, R. He, C. Abunassar, S. Hossainy, and L. G. Zhao, "Effect of two-year degradation on mechanical interaction between a bioresorbable scaffold and blood vessel," *J. Mech. Behav. Biomed. Mater.*, vol. 78, no. November 2017, pp. 254–265, 2018.

[145] D. Farrar and F. J. Buchanan, "Chapter 9: Modelling of the degradation processes for bioresorbable polymers," in *Degradation rate of bioresorbable materials: Prediction and evaluation*, Elsevier, 2008, pp. 183–206.

[146] C. G. Pitt, F. I. Chasalow, Y. M. Hibionada, D. M. Klimas, and A. Schindler, "Aliphatic polyesters. I. The degradation of poly(ϵ-caprolactone) in vivo," *J. Appl. Polym. Sci.*, vol. 26, no. 11, pp. 3779–3787, 1981.

[147] Y. Wang, J. Pan, X. Han, C. Sinka, and L. Ding, "A phenomenological model for the degradation of biodegradable polymers," *Biomaterials*, vol. 29, no. 23, pp. 3393–3401, 2008.

[148] F. Alexis, "Factors affecting the degradation and drug-release mechanism of poly(lactic acid) and poly[(lactic acid)-co-(glycolic acid)]," *Polym. Int.*, vol. 54, no. 1, pp. 36–46, 2005.

[149] Y. Chen, S. Zhou, and Q. Li, "Mathematical modeling of degradation for bulk-erosive polymers: Applications in tissue engineering scaffolds and drug delivery systems," *Acta Biomater.*, vol. 7, no. 3, pp. 1140–1149, 2011.

[150] G. Perale *et al.*, "A new model of resorbable device degradation and drug

release: transient 1-dimension diffusional model," *J Control Release*, vol. 136, no. 3, pp. 196–205, 2009.

[151] X. Han and J. Pan, "A model for simultaneous crystallisation and biodegradation of biodegradable polymers," *Biomaterials*, vol. 30, no. 3, pp. 423–430, 2009.

[152] Z. Lin *et al.*, "A Monte Carlo simulation study of the effect of chain length on the hydrolysis of poly(lactic acid)," *Chinese J. Polym. Sci.*, vol. 31, no. 11, pp. 1554–1562, 2013.

[153] Lyu *et al.*, "Kinetics and Time−Temperature Equivalence of Polymer Degradation," *Biomacromolecules*, vol. 8, no. 7, pp. 2301–2310, 2007.

[154] H. Samami and J. Pan, "A constitutive law for degrading bioresorbable polymers," *J. Mech. Behav. Biomed. Mater.*, vol. 59, pp. 430–445, Jun. 2016.

[155] T. Zhang, S. Zhou, X. Gao, Z. Yang, L. Sun, and D. Zhang, "A multi-scale method for modeling degradation of bioresorbable polyesters," *Acta Biomater.*, vol. 50, pp. 462–475, 2017.

[156] R. N. Shirazi, F. Aldabbagh, A. Erxleben, Y. Rochev, and P. McHugh, "Nanomechanical properties of poly(lactic-co-glycolic) acid film during degradation," *Acta Biomater.*, vol. 10, no. 11, pp. 4695–4703, 2014.

[157] Y. Wang, X. Han, J. Pan, and C. Sinka, "An entropy spring model for the Young's modulus change of biodegradable polymers during biodegradation.," *J. Mech. Behav. Biomed. Mater.*, vol. 3, no. 1, pp. 14–21, Jan. 2010.

[158] A. V Finn *et al.*, "Pathological correlates of late drug-eluting stent thrombosis: strut coverage as a marker of endothelialization.," *Circulation*, vol. 115, no. 18, pp. 2435–2441, May 2007.

[159] R. P. M. Janssen, L. E. Govaert, and H. E. H. Meijer, "An Analytical Method To Predict Fatigue Life of Thermoplastics in Uniaxial Loading: Sensitivity to Wave Type, Frequency, and Stress Amplitude," *Macromolecules*, vol. 41, no. 7, pp. 2531–2540, Apr. 2008.

.

3 Theory

3.1 Chapter Summary

The theoretical and numerical methods specific to the work completed in this thesis are now presented and discussed. An overview of the physio-chemical equations used to examine polymer degradation and crystallisation is given in Section 3.2, with details on the numerical theory for degradation product diffusion in semi-crystalline polymers provided as part of this. Techniques used to obtain semi-analytical solutions to these equations are discussed in Section 3.3.

An overview of continuum mechanics, and details on the material constitutive laws employed in this thesis are given in Section 3.4. The finite element (FE) method is reviewed, and the numerical techniques used to implement and solve physio-chemical polymer degradation equations are provided in Section 3.5. Finally, concluding remarks on the theoretical methods are outlined in Section 3.6.

3.2 Polymer Degradation Models

An overview of the physio-chemical polymer degradation and crystallisation equations which are adapted and implemented in this thesis to study BPS degradation behaviour is now given.

3.2.1 Biodegradation model

The hydrolytic degradation of biodegradable aliphatic polyesters (represented in **Figure 3.1**) has been described in a biodegradation model [1] through physio-chemical rate equations which capture the changes in the mole

concentration of ester bonds, C_e, and the mole concentration of monomers produced through hydrolysis, C_m, for a general copolymer system [1].

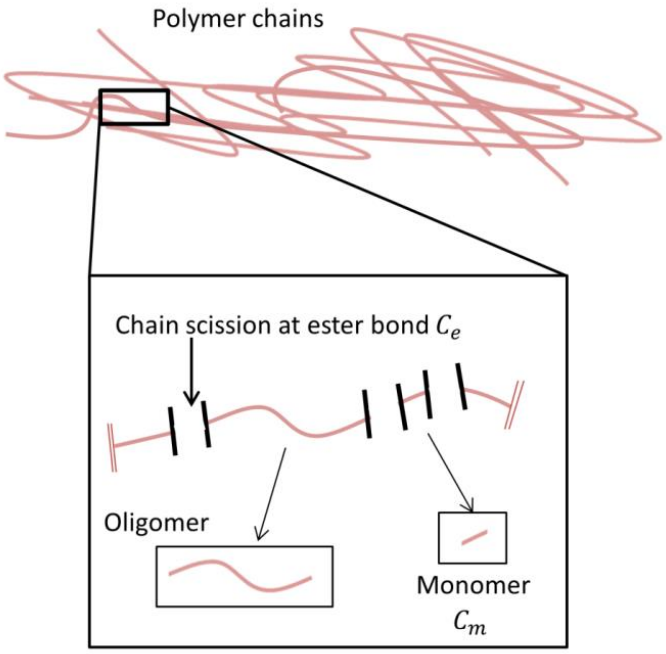

Figure 3.1 Schematic showing the process of chain scission through hydrolysis for a region of amorphous polymer (tangled polymer chains) with C_e and C_m highlighted.

Model governing equations are as follows

$$\frac{\partial C_e}{\partial t} = -(k_1 C_e + k_2 C_e C_m^n) \tag{3.1}$$

$$\frac{\partial C_m}{\partial t} = k_1 C_e + k_2 C_e C_m^n + \nabla \cdot \{D \nabla C_m\} \tag{3.2}$$

where the rates of C_e and C_m are related to an effective diffusion coefficient, D, and to reaction rate constants for hydrolysis, k_1, and autocatalysis, k_2. The kinetic rate constants are directly related to the activation energies required by each degradation mechanism, as discussed in Han *et al*. [2]. The dissociation

of acidic chain-ends is governed by the constant, n, assumed here to take a value of 0.5 [3]. The origins of the half-order power law governing end-scissions, which is based on the catalytic role of the carboxylic acid end-group concentrations, are discussed in Siparsky *et al*. [3].

For this first degradation model formulation, the effects of crystallisation on the degradation rate are not considered, therefore reduction in C_e of the amorphous phase is assumed to be governed by the hydrolysis reaction only, as represented by the variable, H (introduced to account for all of the terms on the right-hand side of Eq. (3.1)), as follows

$$\frac{\partial C_e}{\partial t} = -(k_1 C_e + k_2 C_e C_m^n) = -(H) \tag{3.3}$$

Assuming Fickian diffusion within the polymer matrix, the diffusion behaviour of monomer products is represented by the divergence term on the right-hand side of Eq. (3.2). The correlation between D, and the intrinsic diffusion coefficient, D_0, is given as

$$D = D_0[1 + \alpha\left(1 - \frac{C_m + C_e}{C_{e0}}\right)] \tag{3.4}$$

where C_{e0} is the initial concentration of ester bonds and α is related to the porosity of the structure [4]. Substituting in for D, gives the expression shown in Eq. (3.5), where a vector term, $\boldsymbol{C_m}$, is introduced to represent the total diffusion behaviour of the monomer products.

$$\frac{\partial C_m}{\partial t} = H + \nabla \cdot \left\{ D_0 \left[1 + \alpha \left(1 - \frac{C_m + C_e}{C_{e0}} \right) \right] \nabla C_m \right\} \tag{3.5}$$

$$= H + \nabla \cdot \boldsymbol{C_m}$$

Finally, as shown in Eq. (3.6), the molecular weight, M_w, can be determined when values for C_{e0}, the normalised ester bond concentration, $\bar{C}_e$, and the initial molecular weight, M_{w0}, are known, in this case yielding $\bar{M}_w$, the normalised molecular weight [5].

$$\bar{C}_e = \frac{C_e}{C_{e0}} = \frac{M_w}{M_{w0}} = \bar{M}_w \tag{3.6}$$

The presented model is based on the fundamental assumption that the dominant mechanisms which influence polyester hydrolysis are autocatalysis and degradation product diffusion. Water in the polymer system is assumed to be abundant, hence its concentration does not explicitly appear in the rate equations [1]. It is also assumed that each ester bond cleavage directly produces a monomer fragment (i.e. end scission dominates) and for simplicity, the size distributions of polymer chains and degradation products, as well as any effect of mass or volume loss on the degradation rates, are not considered [1]. In summary, the physical processes of degradation which can be captured by model described above are:

- Hydrolytic random scission of polymer chains which reduces the number of ester chain bonds and increases the concentration of monomers, captured by the rate constant k_1.

- Autocatalytic dissociation of chain-ends which also decreases the number of ester chain bonds and increases the concentration of monomers. This is captured by the rate constant k_2 , and the exponent, n, which accounts for the non-linear dependence on monomer concentration, i.e. more monomers leads to increased monomer production.
- Diffusion of monomers, where the diffusion coefficient is affected by the local molecular weight. Note that the negative term in Eq. (3.4) means that a decrease in ester bonds leads to an increase in the diffusion coefficient.

3.2.2 Simplified theory for polymer crystallinity

Polymer crystallinity encompasses the degradation-induced changes which can occur in highly ordered polymer structures [6], [7]. As discussed in **Chapter 2** for PLLA, such changes take the form of chain alignments, when amorphous regions of the polymer, which are composed of entangled polymer chains, undergo hydrolysis. Chain scissions provide the interwoven polymer chains with extra mobility, allowing them to become packed closely together in crystallite regions [8]. An overview of the simplified crystallinity theory [9] implemented in this thesis for BPS is now given.

As stated in an earlier description [2], [10] of polymer degradation, the rate of polymer chain-scission due to hydrolysis for semi-crystalline polymers can be described by

$$\frac{\partial R_s}{\partial t} = k_1 C_e + k_2 C_e \left(\frac{C_{ol}}{1 - X_c} \right)^{0.5} \tag{3.7}$$

where R_s is defined as the molar number of chain-scissions per unit volume, C_e is the mole concentration of ester bonds in the amorphous polymer, X_c is the volume fraction degree of crystallinity and C_{ol} is the molar number of ester bonds in oligomers per unit volume. Similar to the model described in the previous section, the standard hydrolysis and auto-catalysed degradation reactions are once again governed respectively by reaction rate constants k_1 and k_2. As shown in Eq. (3.8) the time rate behaviour of the oligomer degradation products is dependent on the oligomer production rate due to chain scissions, $\frac{\partial R_{ol}}{\partial t}$, and on the diffusion behaviour

$$\frac{\partial C_{ol}}{\partial t} = \frac{\partial R_{ol}}{\partial t} + (\nabla \cdot (D \nabla C_{ol}) \tag{3.8}$$

where D is an effective diffusion coefficient. An empirical relationship between the mole numbers of oligomers per unit volume and R_s is given as follows (in which α_2 and β are empirical parameters).

$$\frac{R_{ol}}{C_{e0}} = \alpha_2 \left(\frac{R_s}{C_{e0}}\right)^{\beta} \tag{3.9}$$

This initial framework for the chain-scission induced crystallinity of biodegradable polymers [2], [10] was developed based on an extension of the classical Avrami theory [11]–[13]. The inclusion of both differential and integrational equations, which represented the time-dependent nucleation and growth of crystallites, resulted in a complex and difficult to use framework [2], [10].

In a more recently developed simplified version of this framework [9], the number of material parameters is greatly reduced by elimination of the integration equations; the assumption that crystallites which nucleate grow instantly to a finite size is introduced i.e. the growth of crystallites therefore occurs considerably faster than the chain-scission reactions. In the simplified theory, a volume fraction extended degree of crystallinity, X_{ext}, (representing idealised crystal growth without impingement) is introduced, and which is determined by a probability, P_x , that each chain scission will nucleate a crystal which grows to a finite volume, V_c [9]. These parameters are related to Avogadro's constant, η_A, as shown in the following

$$X_{ext} = P_x V_c \eta_A R_s \tag{3.10}$$

A maximum degree of crystallinity, X_{max} is introduced, so that the actual and the proposed extended degree of crystallinity are related by

$$\frac{\partial X_c}{\partial X_{ext}} = X_{max} - X_c \tag{3.11}$$

Based on this simplified theory, the reduction in C_e in the amorphous phase of the polymer originates from both the hydrolysis of the polymer chains (oligomer production rate due to chain scissions, $\frac{\partial R_{ol}}{\partial t}$) and the induced crystallisation of the mobile polymer chains, as follows

$$\frac{\partial C_e}{\partial t} = -\frac{\partial R_{ol}}{\partial t} - \omega \frac{\partial X_c}{\partial t} \tag{3.12}$$

where ω is the inverse molar volume of the crystalline phase. The number-averaged molecular weight of the polymer system, in this case M_n, is determined from [9]:

$$M_n = \frac{(C_e + \omega X_c)M_0}{N_{chains0} + (R_s - \frac{C_{ol}}{m})} \tag{3.13}$$

This updated formula for molecular weight includes the contribution from the initial molar concentration of the polymer chains, $N_{chains0}$, the molar mass of a repeating unit of the polymer, M_0, and m, the average number of repeating units of the oligomers. The simplified theory [9] is found to be efficient in describing the key events of polymer crystallinity with degradation, and it is shown to capture observed experimental crystallinity and molecular weight trends.

3.2.3 Diffusion theory

In the later stages of the work presented in this thesis, diffusion of the degradation products is modelled by more complex equations than that described in Section 3.2.1, to account for the impact of material crystallinity on the diffusion of the oligomer products. The key equations of this diffusion theory [1], [2], [10] are now reviewed.

The effective diffusion coefficient, D, of oligomers formed in semi-crystalline polymers is given by

$$D = D_a\{D_{matrix} + (1.3p^2 - 0.3p^3)(D_{pore} - D_{matrix})\} \tag{3.14}$$

in which p is the porosity of the degrading polymer, D_{pore} is the diffusion coefficient of oligomers in liquid-filled pores and D_{matrix} is the coefficient for oligomers in the polymer matrix. The latter can be determined from

$$D_{matrix} = \left[1.3 \left(\frac{\bar{C}_{ol} + \bar{C}_e}{\bar{C}_{ol} + \bar{C}_e + \frac{X_c}{1 - X_{c0}}} \right)^2 - 0.3 \left(\frac{\bar{C}_{ol} + \bar{C}_e}{\bar{C}_{ol} + \bar{C}_e + \frac{X_c}{1 - X_{c0}}} \right)^3 \right] \tag{3.15}$$

where $\bar{C}_e$ and $\bar{C}_{ol}$ represent the normalised concentrations of ester bonds and oligomers respectively (i.e. $\bar{C}_e = C_e/C_{e0}$;$\bar{C}_{ol} = C_{ol}/C_{e0}$), and where X_{c0} is the initial degree of crystallinity. Oligomer diffusion can be assumed to occur at a much faster rate in the liquid filled pores, formed through bulk degradation, than in the polymer matrix (high ratio of D_{pore}/D_a is assumed, where D_a is a temperature dependant material constant (m^2/s)). Finally, p is given by

$$p = 1 - \{(\bar{C}_{ol} + \bar{C}_e)(1 - X_{c0}) + X_c\} \tag{3.16}$$

3.3 Derivation of a Semi-analytical solution

MATLAB solver R2013b (Mathworks Inc., MA, USA) is used to derive semi-analytical solutions to the physio-chemical governing equations described in Section 3.2. Specifically, the Galerkin method is used to generate the semi-analytical solution to the governing equations of degradation (Eq. (3.1) and Eq. (3.2)) for various polymer plate and film cases (**Chapter 4**), and an ODE solver is employed to solve the simplified crystallinity theory (Eq.'s 3.7 -3.13)

for PLLA degradation at three different temperatures (as described in **Chapter 5**). The semi-analytical solutions are used to verify the predictions of the implemented finite element model (Abaqus/Standard UMATHT) (described below in Section 3.5).

Further information on the Galerkin method of weighted residuals can be found in the following references [14], [15]. The method of weighted residuals involves using trial functions, as given in Eq. (3.17) and Eq. (3.18), for the physio-chemical degradation equations examined in this thesis, to obtain the semi-analytical solution for a one-dimensional geometry. The one-dimensional polymer plate and film geometries examined using these methods are described in **Chapter 4**. Variables $\hat{C}_e$ and $\hat{C}_m$ represent the non-dimensional forms of C_e and C_m respectively; $\bar{x}$ is assigned as the non-dimensional distance through the film thickness; and the unknown trial functions of the normalised time, $\bar{t}$, are denoted by Y_1, Y_2 and Y_3.

$$\hat{C}_m = \frac{1}{2} Y_1(\bar{t})(1 - \bar{x}^2) \tag{3.17}$$

$$\hat{C}_e = Y_2(\bar{t})\bar{x} + Y_3(\bar{t}) \tag{3.18}$$

The trial functions shown above are substituted into non-dimensional forms of Eq. (3.1) and Eq. (3.2), and a set of ordinary differential equations is generated for the variables Y_1, Y_2 and Y_3 [1]. MATLAB solver ODE45 is then used to numerically integrate these equations for the initial conditions $Y_1(0) = 0$, $Y_2(0) = 0$ and $Y_3(0) = 1$. The geometry and applied boundary conditions for each of the cases investigated are described in **Chapter 4**. To summarise, perfect sink boundary conditions are assumed for each of the plate and film

geometries investigated (i.e. where all monomers reaching the outer surface of the film or plate geometry are immediately removed), and the flux of monomers at all other surfaces is assumed to be zero. The solution for $\bar{C}_e$ is determined by averaging $\hat{C}_e$ over the thickness of the film or the plate each time, and compared to finite element predictions for normalised molecular weight for each case. The one-dimensional problems solved using these methods are described in more detail in **Chapter 4**.

The MATLAB solver ODE45 is used to obtain the solution of the governing equations of the simplified crystallinity model (Eq.s 3.7 -3.13) for the cases described in **Chapter 5**. The Arrhenius relation is used to evaluate temperature dependant material parameters for each of the different temperature cases as outlined in **Chapter 5**. Initial conditions of $C_e = C_{e0}(1 - X_{c0}), X_c = X_{c0}$, $C_{ol} = 0$, $X_{ext} = 0$, $R_{ol} = 0$ and $R_s = 0$ are used to generate the solution for the PLLA plate examined each time.

3.4 Continuum Mechanics

The fundamental principles of continuum mechanics relevant to the work presented in this thesis are now outlined. Standard notation is used throughout. Further reading on continuum mechanics can be found in [16]–[18] and the Abaqus Theory Manual (Abaqus/Standard v6.13, Dassault Systems Simulia, RI, USA) [19]. The theory described is applied in this thesis through finite element modelling, described in Section 3.5.

3.4.1 Deformation and stress

The deformation of a body from a reference, undeformed configuration to an updated, or current, configuration is shown in **Figure 3.2**. A point P in the

reference configuration experiences motion from its original position vector $\boldsymbol{X}$ to a new deformed point P', with position vector $\boldsymbol{x}$.

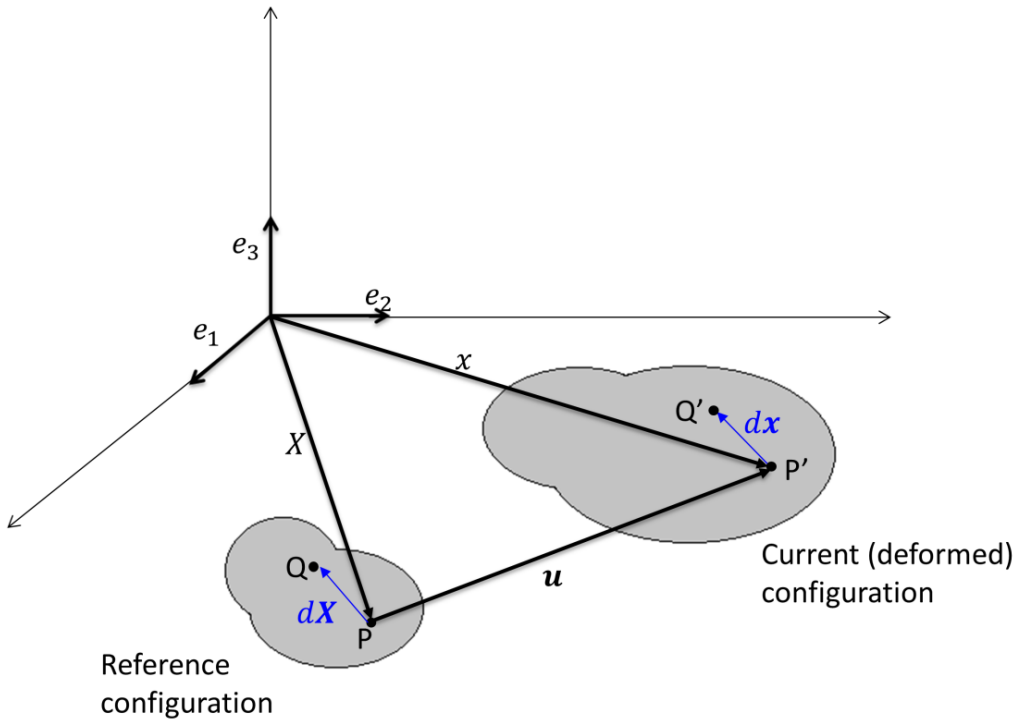

Figure 3.2 Schematic showing a body undergoing motion from a reference to current configuration.

The vector $d\boldsymbol{X}$, which describes the infinitesimal line element between point P and another reference point Q in the body, is transformed to $d\boldsymbol{x}$ in the deformed configuration (**Figure 3.2**). The displacement $\boldsymbol{u}$ is defined as:

$$\boldsymbol{x} = \boldsymbol{X} + \boldsymbol{u} \tag{3.19}$$

The deformation gradient, $\boldsymbol{F}$, describes the transformation of the vector in the reference configuration $d\boldsymbol{X}$ to the corresponding vector in the current configuration $d\boldsymbol{x}$ as follows

$$\boldsymbol{F} = \frac{\partial \boldsymbol{x}}{\partial \boldsymbol{X}} \tag{3.20}$$

A useful strain tensor, the Green-Lagrangian strain tensor, $\boldsymbol{E}$, can be defined relative to the reference configuration as

$$\boldsymbol{E} = \frac{1}{2}\left(\boldsymbol{F}^{\mathrm{T}} \cdot \boldsymbol{F} - \boldsymbol{I}\right) \tag{3.21}$$

where $\boldsymbol{F}^{\mathrm{T}}$ is the transpose of $\boldsymbol{F}$ and $\boldsymbol{I}$ is the identity matrix. For small deformations, this reduces to the infinitesimal strain tensor $\boldsymbol{\varepsilon}$ as shown below.

$$\boldsymbol{\varepsilon} = \frac{1}{2}\left(\nabla \boldsymbol{u} + \nabla^{\mathrm{T}} \boldsymbol{u}\right) \tag{3.22}$$

It is possible to obtain two useful measures of stretch from the deformation gradient, namely the left and right Cauchy-Green strain tensors, $\boldsymbol{B}$ and $\boldsymbol{C}$ respectively.

$$\boldsymbol{B} = \boldsymbol{F} \cdot \boldsymbol{F}^{\mathrm{T}} \tag{3.23}$$

$$\boldsymbol{C} = \boldsymbol{F}^{\mathrm{T}} \cdot \boldsymbol{F} \tag{3.24}$$

The first three invariants of tensors $\boldsymbol{B}$ and $\boldsymbol{C}$ are defined as:

$$I_1 = tr\,(\boldsymbol{C}) = \lambda_1^2 + \lambda_2^2 + \lambda_2^3 \tag{3.25}$$

$$I_2 = \frac{1}{2}[I_1^2 - tr\,(\boldsymbol{C}^2)] = \lambda_1^2\lambda_2^2 + \lambda_2^2\lambda_3^2 + \lambda_1^2\lambda_2^2\lambda_3^2 \tag{3.26}$$

$$I_3 = \det(\boldsymbol{C}) = [\det(\boldsymbol{F})]^2 = J^2 = \lambda_1^2\lambda_2^2\lambda_3^2 \tag{3.27}$$

where the determinant of the deformation gradient $\boldsymbol{F}$, is known as the Jacobian, J (gives the volume change of the body). The deformation can be uniquely decomposed into an orthogonal rotation tensor $\boldsymbol{R}$ and symmetric spatial and material stretch tensors, $\boldsymbol{V}$ and $\boldsymbol{U}$ respectively, where λ_i are the principle stretches of the deformation (i = 1, 2, 3), and the eigenvalues of $\boldsymbol{U}$, the material stretch tensor.

Cauchy stress, $\boldsymbol{\sigma}$, describes the force per unit area acting on the current configuration. Sometimes also referred to as true stress, this symmetric tensor relates the traction $\tilde{\boldsymbol{t}}$ acting on a surface in the current configuration to a unit normal vector to the surface $\hat{\boldsymbol{n}}$.

$$\tilde{\boldsymbol{t}} = \boldsymbol{\sigma} \cdot \hat{\boldsymbol{n}} \tag{3.28}$$

The Cauchy stress can generally be broken down into its two principal components; a hydrostatic stress component which causes volume change and a deviatoric stress governing shape change, generally expressed as follows:

$$\boldsymbol{\sigma} = \boldsymbol{S} - p\boldsymbol{I} \tag{3.29}$$

where $\boldsymbol{S}$ is the deviatoric stress, and p is the hydrostatic pressure, which is determined from

$$p = -tr(\boldsymbol{\sigma})/3 \tag{3.30}$$

Important stress measures in the analysis of materials include the von Mises equivalent stress, $\bar{\sigma}$ (often used for the analysis of elastic-plastic materials), the Kirchhoff stress, $\boldsymbol{K}$, the first Piola-Kirchhoff stress, $\boldsymbol{P}$, which is the force per unit area in the reference configuration, and the second Piola-Kirchhoff stress, $\boldsymbol{\tau}$. Each of these can be defined as follows:

$$\bar{\sigma} = \sqrt{\frac{3}{2} S_{ij} S_{ij}} \tag{3.31}$$

$$\boldsymbol{K} = J\boldsymbol{\sigma} \tag{3.32}$$

$$\boldsymbol{P} = \boldsymbol{F}^{-1} \cdot \boldsymbol{K} \tag{3.33}$$

$$\boldsymbol{\tau} = \boldsymbol{P} \cdot \boldsymbol{F}^{-\mathrm{T}} \tag{3.34}$$

All of the above stress tensor definitions become equal under the assumption of infinitesimal deformation kinematics, and hence can all be represented by the tensor $\boldsymbol{\sigma}$.

3.4.2 Isotropic linear elasticity

Infinitesimal deformation kinematics is the basis for isotropic linear elasticity, which is typically assumed for elastic materials that experience small (< 5%) strains under loading. Isotropic linear elasticity is a reversible mode of deformation that can be represented by Hooke's law (where the stress, $\boldsymbol{\sigma}$ is a linear function of the infinitesimal strain, $\boldsymbol{\varepsilon}$):

$$\sigma_{ij} = \lambda \varepsilon_{kk} \delta_{ij} + 2\mu \varepsilon_{ij} \tag{3.35}$$

where λ and μ are the Lamé elastic constants, and δ_{ij} is the Kronecker delta, when

$$\delta_{ij} = \begin{cases} 1 & i = j \\ 0 & i \neq j \end{cases} \tag{3.36}$$

The Lamé constants can be derived directly from the material's Young's modulus, E, and the Poisson's ratio, ν, through:

$$\mu = \frac{E}{2(1+\nu)} \tag{3.37}$$

$$\lambda = \frac{\nu E}{(1+\nu)(1-2\nu)} \tag{3.38}$$

Finally, the material bulk modulus, K, can be defined as:

$$K = \frac{3\lambda + 2\mu}{3} \tag{3.39}$$

3.4.3 Hyperelasticity

Hyperelastic, or Green elastic, materials are a class of materials which typically exhibit a non-linear elastic response when subjected to moderate or large strain deformations. The most common example of such a material is rubber. The stress-strain relationship for hyperelastic materials derives from a strain energy density potential, W_e, which describes the strain energy stored in the material per unit of deformed volume. This potential can be related to the first Piola-Kirchhoff stress and the true (Cauchy) stress described in the previous section, through the following:

$$\boldsymbol{P} = \frac{\partial U(\boldsymbol{F})}{\partial \boldsymbol{F}} \tag{3.40}$$

$$\boldsymbol{\sigma} = \frac{1}{J}\boldsymbol{F} \cdot \frac{\partial U(\boldsymbol{F})}{\partial \boldsymbol{F}} \tag{3.41}$$

For isotropic hyperelastic materials, W_e is regarded as a function of the three principle invariants (I_1, I_2, I_3) of the right Cauchy-Green deformation tensor $\boldsymbol{C}$:

$$W_e(\boldsymbol{C}) = W_e(I_1, I_2, I_3) \tag{3.42}$$

Hyperelastic laws are often written in terms of their volumetric and isochoric components, U and $\bar{W}$ respectively, as shown.

$$W_e(\boldsymbol{C}) = U(J) + \bar{W}\,(\bar{\boldsymbol{C}}) \tag{3.43}$$

where $\bar{\boldsymbol{C}}$ is the modified right Cauchy-Green strain tensor, defined as follows.

$$\bar{\mathbf{C}} = J^{-2/3}\mathbf{C} \tag{3.44}$$

The hyperelastic constitutive laws used in this thesis include a mechanical material model for PLLA and a reduced polynomial form of strain energy density potential to represent arterial mechanics.

The Knowles model for hyperelastic behaviour [20] is used in the work presented in this thesis to describe the mechanical behaviour of PLLA bioresorbable polymeric stents. As discussed in **Chapter 2**, PLLA displays complex wide ranging mechanical behaviour, including hyperelastic, viscoelastic and plastic comportments. Similar to other thermoplastic polymers, PLLA has been known to experience non-linear deformations at moderate strains [21]–[24]. The Knowles model has previously been used to capture the mechanical performance of PLLA by a number of groups [25], [26], however this hyperelastic model is not wholly representative of the full mechanical behaviour of PLLA, i.e. the Knowles model does not consider plastic or viscoelastic material behaviour and therefore, is used herein to capture elastic behaviour only. The implications of this for the specific approach taken in this thesis to simulate the mechanical behaviour of the PLLA stents are as described in **Chapter 6**.

In this hyperelastic model, the strain energy density potential is given in its decoupled form by

$$W_e = \frac{\mu}{2b}\left\{\left[1 + \frac{b}{n_h}(\bar{I}_1 - 3)\right]^{n_h} - 1\right\} + \frac{1}{D_1}(J-1)^2 \tag{3.45}$$

where n_h is a hardening parameter, b is an empirical curve fitting parameter, D_1 is the inverse of the material bulk modulus and $\bar{I}_1$ is the first invariant of $\bar{\mathbf{C}}$. Assuming an incompressible material (i.e. high value is assumed for the bulk modulus, K), negates the term on the right hand side of Eq. (3.45). This model has been implemented into FE software (Abaqus/Standard) through a user material subroutine, UMAT [27].

A hyperelastic material law is also utilised in this thesis to represent the mechanical behaviour of arterial tissues. Arterial tissue is a complex biological tissue which shows a highly non-linear stress-strain relationship, and there has been much work done in the development of arterial constitutive laws (e.g. [28]–[30]). The polynomial form of strain energy potential is a common type of hyperelastic model, and has been commonly expressed as follows [31]

$$W_e = \sum_{i+j=1}^{N} C_{ij}\,(\bar{I}_1 - 3)^i(\bar{I}_2 - 3)^j + \sum_{i=1}^{N}\frac{1}{D_i}(J-1)^{2i} \tag{3.46}$$

where N is the number of polynomial terms used in the series, C_{ij} (not to be confused with components of the right Cauchy-Green strain tensor), D_i are experimentally measured material parameters and $\bar{I}_1$ and $\bar{I}_2$ are the first and second invariants of $\bar{\boldsymbol{C}}$. A sixth order, reduced form of this polynomial model was applied in this thesis to describe the isotropic deformation of arterial tissue. The specific strain energy density potential for the model used is given as

$$W_e = \sum_{i=1}^{N} C_{i0} (\bar{I}_1 - 3)^i + \sum_{i=1}^{N} \frac{1}{D_i} (J - 1)^{2i} \tag{3.47}$$

where C_{i0} and D_i are the experimentally measured material parameters [29], and $N = 6$.

3.5 The Finite Element Method

Numerical simulations in this thesis are performed using the finite element (FE) method through the commercially available FE solver, Abaqus/Standard (Abaqus/Standard v6.13, Dassault Systems Simulia, RI, USA) [19]. In-depth descriptions of using finite element methods to analyse solid structures can be found in the following [17], [18], [32].

3.5.1 Overview of the finite element method

In the finite element method, a solid body is divided into discrete volumes or elements, which are interconnected at points called nodes (**Figure 3.3**). In the following summary of the theory, matrix/vector (Voigt notation) is used. Quantities such as displacement and temperature can be interpolated throughout the body based on the discrete values measured at the element nodes.

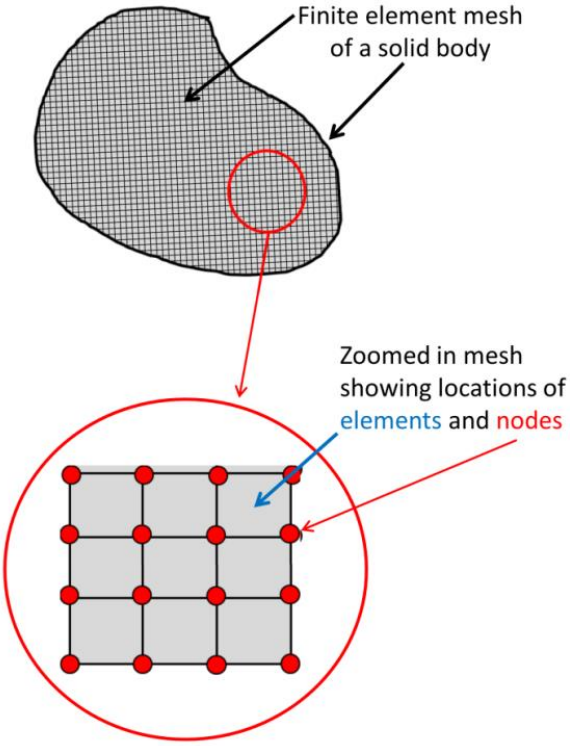

Figure 3.3 A solid body can be divided into discrete regions using finite element analysis (FEA). The use of a finite element mesh allows for formation of regions (elements), which meet at interconnecting points (nodes).

For example, for displacement, this interpolation takes the form

$$\boldsymbol{u} = \boldsymbol{N}_e \boldsymbol{u}_e \tag{3.48}$$

where $\boldsymbol{N}_e$, is the matrix of shape functions for an element e, and $\boldsymbol{u}_e$ is the column vector of nodal displacements for the same element. Species concentration variables, which are also of interest in this work, are interpolated in a similar manner, using the appropriate elements.

In the FE method, the required governing equations are determined for each element and assembled to form a global system of algebraic equations, which describe the behaviour of the body as a whole. Boundary conditions are

applied to this system of equations, allowing for the global equation system to be solved to yield the unknown nodal solution variables. The FE method can be derived from the principle of virtual work, which can be fundamentally written for displacement as

$$\int_V \delta\, \boldsymbol{\varepsilon}^T \boldsymbol{\sigma}\, dV = \int_S \delta\, \boldsymbol{u}^T \boldsymbol{t}\, dS \tag{3.49}$$

In Eq. (3.49) the equilibrium is enforced on the reference volume, V, which is bounded by a surface, S, and where the acting stress vector and surface traction vector are $\boldsymbol{\sigma}$ and $\boldsymbol{t}$, respectively. The vectors $\delta\boldsymbol{\varepsilon}$ and $\delta\boldsymbol{u}$ represent the virtual strain and virtual displacement vectors. The following interpolation holds true for each element e in the finite element mesh

$$\delta\boldsymbol{\varepsilon} = \boldsymbol{B}_e \delta\boldsymbol{u}_e \tag{3.50}$$

$$\delta\boldsymbol{u} = \boldsymbol{N}_e \delta\boldsymbol{u}_e \tag{3.51}$$

where $\boldsymbol{N}_e$ and $\boldsymbol{B}_e$ are the element shape function and shape function matrices, respectively, and $\delta\boldsymbol{u}_e$ is the vector of virtual nodal displacements for the element. Introducing these terms into Eq. (3.49), the finite element approximation can be summed over all the elements in the FE mesh

$$\sum_{el} \int_{V_{el}} \delta\boldsymbol{u}_e \boldsymbol{B}_e^T\, \boldsymbol{\sigma}(\boldsymbol{u}_e)\, dV = \sum_{el} \int_{S_{el}} \delta\boldsymbol{u}_e^T \boldsymbol{N}_e^T\, \boldsymbol{t}\, dS \tag{3. 52}$$

A global expression is then obtained by assembling the element quantities into global quantities, and removing the arbitrary virtual quantities. This global expression takes the form

$$\int_V \widehat{\boldsymbol{B}}^{\boldsymbol{T}} \boldsymbol{\sigma}\, dV = \int_V \widehat{\boldsymbol{N}}^{\boldsymbol{T}} \boldsymbol{t}\, dS \tag{3.53}$$

where the global shape function matrix, $\widehat{\boldsymbol{N}}$ and the global shape function gradient matrix, $\widehat{\boldsymbol{B}}$ are included. It is possible to rearrange this expression further and obtain the global force balance, $\boldsymbol{G}(\boldsymbol{u})$ (which is solved for $\boldsymbol{u}$ which in this case is the global nodal displacement vector for the body):

$$\boldsymbol{G}(\boldsymbol{u}) = \int_V \widehat{\boldsymbol{B}}^{\boldsymbol{T}} \boldsymbol{\sigma}\, dV - \int_V \widehat{\boldsymbol{N}}^{\boldsymbol{T}} \boldsymbol{t}\, dS = 0 \tag{3.54}$$

In the commercially available code Abaqus/Standard, non-linear systems are often solved using implicit integration techniques. The solution methods used for the work presented in this thesis are based on an Abaqus implicit solver, specifically the iterative Newton-Raphson integration scheme. The Newton-Raphson method is utilised with incremental steps in time, t, to determine the nodal displacements at the end of a time increment, using an iterative procedure, as summarised in the following,

$$\boldsymbol{u}_{n_i+1}^{t+\Delta t} = \boldsymbol{u}_{n_i}^{t+\Delta t} - \left[\frac{\partial \mathbf{G}\boldsymbol{u}_{n_i}^{t+\Delta t}}{\partial \boldsymbol{u}}\right]^{-1} \cdot \mathbf{G}(\boldsymbol{u}_{n_i}^{t+\Delta t}) \tag{3.55}$$

In Eq. (3.55), t is the time at the start of the increment, Δt is the value of the time increment used, and n_i is the iteration number. The current estimate of the nodal displacements at the end of the time increment (for iteration n_i), $\boldsymbol{u}_{n_i}^{t+\Delta t}$ is updated to an improved estimate, $\boldsymbol{u}_{n_i+1}^{t+\Delta t}$, at the end of the iteration. Iterations are repeated until a converged solution for $\boldsymbol{u}_{n_i}^{t+\Delta t}$ is found. The Newton-Raphson method is used to solve equations using this iterative process, for each increment, when boundary conditions are applied incrementally over the course of the deformation history.

3.5.2 Modelling Degradation using Abaqus/Standard

The governing equations for the degradation models described above are implemented into the commercially available finite element code Abaqus through use of a thermal analogy. Abaqus/Standard provides the built-in capabilities for a heat transfer analysis, through the thermal user material subroutine UMATHT. It has previously been shown [33] that hydrogen transport can be modelled using this in-built material subroutine. Adopting a similar approach in the current work, correlations are established between the hydrolysis and diffusion reactions of polymer degradation and the transfer of heat and temperature in a physical system. The details of the UMATHT analogy developed for modelling degradation and hydrolysis are now provided. The degradation variables in Eq. (3.1) - (3.6) are given equivalence to variables in the basic energy balance for an uncoupled heat transfer analysis.

The equations which describe the basic energy balance for an uncoupled heat transfer analysis are now presented (and are given in the documentation for Abaqus/Standard [19]). This energy balance relates the material time rate of the internal thermal energy, $\dot{U}$, to the heat flux per unit area of a body, q, and

to the heat supplied externally into the body per unit volume, r, [34] as shown below

$$\int_V \rho \dot{U} dV = \int_S q dS_A + \int_V r dV \tag{3.56}$$

where ρ represents the density of a material with surface area, S_A, and volume, V. A heat flux vector, $\mathbf{f}$ can be defined such that

$$q = -\mathbf{f} \cdot \boldsymbol{n} \tag{3.57}$$

when $\boldsymbol{n}$ is the outward unit vector normal to S_A. Introducing Eq. (3.57) into the energy balance and applying the divergence theorem gives the following:

$$\int_V \rho \dot{U} dV = -\int_V \nabla \cdot \mathbf{f}\, dV + \int_V r dV \tag{3.58}$$

The thermal conductivity matrix, $\mathbf{k}$, relates the heat flux vector to the temperature gradient, $\nabla\theta$, through Fourier's law for heat conduction:

$$\mathbf{f} = -\mathbf{k}\nabla\theta \tag{3.59}$$

Rewriting Eq. (3.58) in pointwise form and incorporating Eq. (3.59) yields

$$\rho \dot{U} = \nabla \cdot \{\mathbf{k}\nabla\theta\} + r \tag{3.60}$$

The material time rate of the internal thermal energy can be related to the time derivative of the temperature $\frac{\partial \theta}{\partial t}$ through the specific heat c_p as follows

$$\dot{U} = c_p \frac{\partial \theta}{\partial t} \tag{3.61}$$

Substituting this into Eq. (3.60) yields

$$\rho c_p \frac{\partial \theta}{\partial t} = \nabla \cdot \{\mathbf{k} \nabla \theta\} + r \tag{3.62}$$

Correspondence between the terms in Eq. (3.62) and the hydrolysis and diffusion mechanisms described in Eq. (3.5) is made in **Table 3.1** . In this representation C_m, is related to the temperature; hydrolysis of the polymer chains, H, is related to the external heat source, and diffusive flux of the monomers, $\boldsymbol{C_m}$, is related to the heat flux term when ρ, the material density and c_c, the specific energy, are included for unit conversion.

Table 3.1 Correspondence between the thermal parameters and the hydrolysis and diffusion parameters

Heat transfer parameters			**Degradation parameters**		
Variable	*Symbol*	*Units*	*Variable*	*Symbol*	*Units*
Temperature	θ	[K]	Monomer concentration	C_m	[mol/m^3]
Thermal energy	$U(\theta)$	[J]	Chemical energy	U_C	[J]
Specific heat	c_p	[J/ (kg K)]	Specific energy	c_c	[Jm^3/ (kg mol)]
Density	ρ	[kg/m^3]	Unity	1	[kg/m^3]
Heat supplied externally	r	[J/ (s m^3)]	Hydrolysis	H	[mol / (week m^3)]
Heat flux per unit area	q	[J/ (s m^2)]	Diffusive flux of monomers	$\boldsymbol{C_m}$	[J/ (week m^2)]

The governing equation for the degradation analysis can therefore be written as

$$\rho c_c \frac{\partial C_m}{\partial t} = \rho c_c H + \nabla \cdot \{\rho c_c \boldsymbol{C_m}\} \tag{3.63}$$

By applying this analogy, simulations are performed on Abaqus/Standard to investigate the degradation of PLA and PLGA plates and films and of BPS. The degradation model described above has been implemented into a number of computational frameworks to investigate the degradation of different polymer structures (as outlined in **Chapter 4**). The governing equations of the degradation model described above have previously been implemented into the commercially available FE program Comsol (Comsol Multiphysics v4. 3b, Comsol, Inc., MA, USA) in a computational investigation of the degradation of PLGA films [34]. Using the classical partial differential equation (PDE) module in Comsol, numerical solutions were obtained at each time step in each element using an implicit backward differentiated formula (BDF) method, with the maximum order of 2 [34]. To allow for comparison with the semi-analytical (MATLAB) and Abaqus/Standard degradation predictions, the Comsol FE model [34] is applied to generate predictions for a PLA plate and film as described in **Chapter 4**.

3.5.3 Modelling Crystallinity using Abaqus/Standard

The physio-chemical equations outlined in Section 3.2 for the polymer crystallinity theory are implemented into Abaqus/Standard via the user material subroutine, UMATHT. A similar approach is used to that described for the thermal analogy implementation of the degradation equations. In this instance, the temperature solution of the Abaqus/Standard solver is used to

represent C_{ol} in the degrading polymer system. A differential equation solver, specifically the fourth order Runge Kutta solution method [35] was initially investigated to obtain the solution of the crystallinity equations. However, full convergence is obtained for the simplified theory equations when the direct Euler method is utilised with a small time increment (solution checked for temporal convergence, which is achieved for a time increment less than or equal to 0.1). FE simulations are performed on Abaqus/Standard using this analogy to investigate the degradation and crystallisation behaviour of PLLA based BPS (as described in **Chapter 5**).

3.6 Conclusion

The numerical and theoretical methods used throughout this thesis have been outlined and reviewed. The theory described herein is applied in the following chapters of this thesis to examine and predict the in-vivo behaviours of BPS. Physio-chemical degradation equations (Section 3.2) have been implemented and examined in a number of computational frameworks, as described in Sections 3.3 – 3.5. A thermal analogy is presented (Section 3.5.2) which enables implementation into the commercially available finite element code, Abaqus (Abaqus/Standard v6.13, Dassault Systems Simulia, RI, USA). The key aspects of continuum mechanics as utilised in this thesis have been reviewed and an overview of the numerical techniques used in FEA has been presented. In the remaining work of this thesis, the degradation of various BPS geometries is predicted and examined using the finite element implementation of the physio-chemical degradation equations (**Chapter 4**). Polymer crystallinity effects are examined for a number of case studies (**Chapter 5**), and a damage formulation is also introduced, where damage due to material degradation (decreasing molecular weight) is incorporated into a

mechanical constitutive law for PLLA (Section 3.4). The final phase of this work involves investigation of a number of case studies to better understand simultaneous degradation and mechanical performance (scaffolding ability) of PLLA based BPS (**Chapter 6**). Key features of the physio-chemical models presented here in capturing the degradation rates of BPS are highlighted and discussed in **Chapter 7**.

References

[1] Y. Wang, J. Pan, X. Han, C. Sinka, and L. Ding, “A phenomenological model for the degradation of biodegradable polymers,” *Biomaterials*, vol. 29, no. 23, pp. 3393–3401, 2008.

[2] X. Han, J. Pan, F. Buchanan, N. Weir, and D. Farrar, “Analysis of degradation data of poly(l-lactide-co-l,d-lactide) and poly(l-lactide) obtained at elevated and physiological temperatures using mathematical models,” *Acta Biomater*, vol. 6, no. 10, pp. 3882–3889, 2010.

[3] G. Siparsky, K. Voorhees, and F. Miao, “Hydrolysis of Polylactic Acid (PLA) and Polycaprolactone (PCL) in Aqueous Acetonitrile Solutions: Autocatalysis,” *J. Environ. Polym. Degrad.*, vol. 6, no. 1, pp. 31–41, 1998.

[4] J. Siepmann and A. Gopferich, “Mathematical modeling of bioerodible, polymeric drug delivery systems.,” *Adv. Drug Deliv. Rev.*, vol. 48, no. 2–3, pp. 229–247, Jun. 2001.

[5] Y. Wang, X. Han, J. Pan, and C. Sinka, “An entropy spring model for the Young’s modulus change of biodegradable polymers during biodegradation.,” *J. Mech. Behav. Biomed. Mater.*, vol. 3, no. 1, pp. 14–21, Jan. 2010.

[6] S. K. Saha and H. Tsuji, “Effects of rapid crystallization on hydrolytic degradation and mechanical properties of poly(l-lactide-co-ε-caprolactone),” *React. Funct. Polym.*, vol. 66, no. 11, pp. 1362–1372, 2006.

[7] S. Li, H. Garreau, and M. Vert, “Structure-property relationships in the case of the degradation of massive poly (α-hydroxy acids) in aqueous media,” *J. Mater. Sci. Mater. Med.*, vol. 1, no. 4, pp. 198–206, 1990.

[8] A. C. Gleadall, “Modelling degradation of biodegradable polymers and their mechanical properties.” Department of Engineering, University of Leicester, 2015.

[9] A. Gleadall, J. Pan, and H. Atkinson, “A simplified theory of crystallisation induced by polymer chain scissions for biodegradable polyesters,” *Polym. Degrad. Stab.*, vol. 97, no. 9, pp. 1616–1620, 2012.

[10] X. Han and J. Pan, “A model for simultaneous crystallisation and biodegradation of biodegradable polymers,” *Biomaterials*, vol. 30, no. 3, pp. 423–430, 2009.

[11] M. Avrami, “Kinetics of phase change. I General theory,” *J. Chem. Phys.*, vol. 7, no. 12, pp. 1103–1112, 1939.

[12] M. Avrami, “Kinetics of Phase Change. II Transformation—Time Relations for Random Distribution of Nuclei.,” *J. Chem. Phys.*, vol. 8, pp. 212–225, 1940.

[13] M. Avrami, “Kinetics of Phase Change. III. Granulation, Phase Change and Microstructure,” *J. Chem. Phys.*, vol. 9, pp. 177–184, 1941.

[14] R. Venkatraman, “Lecture Notes: The Galerkin Method,” no. 1, pp. 1–9, 2011.

[15] N. Friedman, “Numerical methods for PDEs FEM - abstract formulation , the Galerkin method,” 2018.

[16] M. A. Crisfield, “Nonlinear Finite Element Analysis of Solids and Structures volume 2 Advanced Topics,” *Non-Linear Finite Elem. Anal. Solids Struct. Second Ed.*, pp. 31–62, 1996.

[17] P. Wriggers, “Non-Linear Finite Element Analysis of Solids and Structures – Volume 2: Advanced Topics, by Michael Crisfield, Wiley, Chichester, 1997, No. of pages 508, ISBN: 0-471-95649-X.,” *Int. J. Numer. Methods Eng.*, vol. 44, no. 2, p. 305, Jan. 1999.

[18] T. Belytschko, W. Liu Kam, B. Moran, and K. Elkhodary, *Nonlinear Finite Elements for Continua and Structures*, 2nd Editio. Wiley, 2014.

[19] *Abaqus/standard users manual*, Version 6. Dassault Systémes Simulia Corporation, 2013.

[20] J. Knowles, “The finite anti-plane shear field near the tip of a crack for a class of incompressible elastic solids,” *Int. J. Fract.*, vol. 13, no. 5, pp. 611–639, 1977.

[21] R. G. Pauck and B. D. Reddy, “Computational analysis of the radial mechanical performance of PLLA coronary artery stents,” *Med. Eng. Phys.*, vol. 37, no. 1, pp. 7–12, 2015.

[22] M. Bartkowiak-Jowsa, R. Będziński, A. Kozłowska, J. Filipiak, and C. Pezowicz, “Mechanical, rheological, fatigue, and degradation behavior of PLLA, PGLA and PDGLA as materials for vascular implants,” *Meccanica*, vol. 48, no. 3, pp. 721–731, 2013.

[23] P.-J. Wang *et al.*, “Effect of working environment and procedural strategies on mechanical performance of bioresorbable vascular scaffolds,” *Acta Biomater.*, pp. 1–10, 2018.

[24] A. Muliana and K. R. Rajagopal, “Modeling the response of nonlinear viscoelastic biodegradable polymeric stents,” *Int. J. Solids Struct.*, vol. 49, no. 7–8, pp. 989–1000, 2012.

[25] D. Hayman, C. Bergerson, S. Miller, M. Moreno, and J. E. Moore, “The effect of static and dynamic loading on degradation of PLLA stent fibers,” *J Biomech Eng*, vol. 136, no. 8, p. 4027614, 2014.

[26] J. S. Soares, K. R. Rajagopal, and J. E. Moore Jr., “Deformation-induced hydrolysis of a degradable polymeric cylindrical annulus,” *Biomech. Model. Mechanobiol.*, vol. 9, no. 2, pp. 177–186, 2010.

[27] C. Suchocki, “A FINITE ELEMENT IMPLEMENTATION OF KNOWLES STORED-ENERGY FUNCTION : THEORY , CODING AND APPLICATIONS,” *Arch. Mech. Eng.*, vol. LVIII, 2011.

[28] G. Holzapfel, T. Gasser, and R. Ogden, “A New Constitutive Framework for Arterial Wall Mechanics and a Comparative Study of Material Models,” *J. Elast. Phys. Sci. solids*, vol. 61, no. 1–3, pp. 1–48, 2000.

[29] J. D. Humphrey, “Review Paper. Continuum Biomechanics of Soft Biological Tissues,” *Proc. Math. Phys. Eng. Sci.*, vol. 459, no. 2029, pp. 3–46, 2003.

[30] G. A. Holzapfel and R. W. Ogden, *Constitutive modelling of arteries*, vol. 466, no. 2118. 2010.

[31] H. Pouriayevali, Y. B. B. Guo, and V. P. W. P. W. Shim, “A visco-hyperelastic constitutive description of elastomer behaviour at high strain rates,” *Procedia Eng.*, vol. 10, pp. 2274–2279, Jan. 2011.

[32] O. Zienkiewicz, R. Taylor, and J. Z. Zhu, “The Finite Element Method: its Basis and Fundamentals: Seventh Edition,” in *The Finite Element Method: its Basis and Fundamentals: Seventh Edition*, O. C. Zienkiewicz, R. L. Taylor, and J. Z.

B. T.-T. F. E. M. its B. and F. (Seventh E. Zhu, Eds. Oxford: Butterworth-Heinemann, 2013, pp. 1–714.

[33] C.-S. Oh, Y.-J. Kim, and K.-B. Yoon, “Coupled analysis of hydrogen transport using ABAQUS,” *J. Solid Mech. Mater. Eng.*, vol. 4, no. 7, pp. 908–917, 2010.

[34] R. N. Shirazi, W. Ronan, Y. Rochev, and P. McHugh, “Modelling the degradation and elastic properties of poly (lactic-co-glycolic acid) films and regular open-cell tissue engineering scaffolds,” *J. Mech. Behav. Biomed. Mater.*, vol. 54, pp. 48–59, 2016.

[35] W. T. Vetterling, S. A. Teukolsky, W. H. Press, and B. P. Flannery, *Numerical Recipes in F77*. 1992.

4 Modelling of Bioresorbable Polyesters with Applications for Coronary Stents

4.1 Chapter Summary

In this chapter, the previously described Abaqus/Standard degradation model implementation is verified against the semi-analytical solution described in **Chapter 3** for several polymer plate and film geometries. Experimental observations for various polymer materials are then used to validate the predictions of the Abaqus/Standard model for the different geometries and an investigation into the finite element model's ability to capture thickness dependency is carried out (Section 4.3). Using the developed methodology, the physio-chemical degradation behaviours of various BPS geometries are investigated in terms of their dependence on material, boundary conditions, and design (Section 4.3). The impact of thickness on degradation behaviour is highlighted for the polymer plates and films examined (Section 4.4.1), and for the BPS, predictions indicate that there is a notable difference in the molecular weight trends predicted for the different materials and boundary condition assumptions investigated (Section 4.4.2), with autocatalysis emerging as a dominant mechanism controlling the degradation behaviour. Insights into the scaffolding ability of the BPS are obtained using a suggested general relationship between Young's modulus and molecular weight and the emerging trends of this chapter are discussed in Section 4.5.

The work presented herein has been published in the ASME Journal of Medical Devices [1]. Edits are made to the text presented here to (i) remove the methodology, presented in **Chapter 3**, and (ii) to extract the minor contributions to the published paper by co-authors.

4.2 Introduction

Biodegradable polymers are becoming increasingly prevalent in medical device design due to their potential to produce temporary implants which become gradually eroded in the body over time [2]. The hydrolytic degradation behaviour of the synthetic aliphatic polyesters, i.e. poly-glycolic acid (PGA), polylactide (PLA) and their co-polymers, has made them attractive materials for use in numerous medical device applications, for example in biodegradable orthopaedic fixation devices [3], [4], biodegradable drug delivery devices [5]–[7], and more recently in bioresorbable polymeric stents (BPS) [8]–[10]. As discussed in **Chapter 2**, degradation of such polymer materials in-vivo occurs via chemical hydrolysis when an uptake of water molecules into the material matrix induces scission of the backbone polymer chains into monomer fragments which then become naturally metabolized [11]. Notably for the aliphatic polyesters, chemical hydrolysis exhibits autocatalytic effects when a build-up of the acidic chain ends formed leads to accelerated rates of material degradation [12]–[14].

In terms of BPS, developed to restore patency and offer temporary support to vessels, degradation modelling techniques presented to date fall into two main categories: phenomenological and physio-chemical models [15], as reviewed in **Chapter 2**. Phenomenological models for BPS have typically been developed with a focus on the detrimental effects of degradation on the mechanical properties of the polymer [16]–[18]. Although implementation of such models in finite element software allows for prediction of the varying mechanical performance of the bioresorbable polymeric device, there is no explicit representation of the internal physical processes involved in the material degradation, or of their influence on device behaviour. In contrast, physio-chemical models for BPS degradation aim to describe the material

degradation in terms of the inherent physio-chemical reactions which occur in the eroding polymer, for example [19]–[21]. Such models are often based on kinetic reaction-diffusion equations, similar to those presented in [22], [23] , which allow for an improved understanding of the dominant physical and chemical processes involved in the degradation.

In the current chapter, an Abaqus/Standard implementation of the physio-chemical degradation model described in **Chapter 3** is used to investigate the physio-chemical degradation behaviours of various polymeric devices under a range of boundary conditions. Comparisons are made between a semi-analytical (MATLAB) solution and the finite element (FE) predictions for the polymer plates and films investigated, and the degradation behaviour of several BPS geometries are examined using the FE implementation.

4.3 Methods

Two approaches are taken to solve the physio-chemical degradation model equations presented in **Chapter 3**; (i) a semi-analytical approach in MATLAB using the GALERKIN method and (ii) representing the reaction-diffusion equations in Abaqus (Abaqus/Standard, v6.13 Dassault Systems Simulia, Providence, RI, USA). In the case of the former, briefly, a weighted residual error method is used to generate a set of ordinary differential equations for C_e and C_m, which are then solved using the ODE45 function on MATLAB.

In Abaqus, through use of a thermal analogy (described in **Chapter 3**), the degradation model equations are implemented a via user-defined subroutines and solved using the FE method. Correlations are established between the hydrolysis and the diffusion reactions of polymer degradation, and the principal reactions of a heat transfer analysis. A user material subroutine

(UMATHT) is developed to simulate a polymer material's degradation behaviour, and several case studies are examined.

4.3.1 Analysis of polymer plates and films

The semi-analytical MATLAB approach is firstly used for various polymer films and plates. FE simulations are then performed to verify and validate the Abaqus model implementation, and to provide predictions for the degradation behaviours of BPS. In the first instance, a semi-analytical solution using the GALERKIN method (**Chapter 3**) is determined for the one-dimensional case of a 2 mm thick PLA plate and 0.3 mm thick PLA film (experimentally examined in [12]) using the material parameters shown in **Table 4.1**.

Table 4.1 Material parameters for the physio-chemical degradation model, where the fit of the PLLA material constants is achieved with an R^2 value of 0.98

Description	Symbol	PLA	PLGA	PLLA
Initial ester bond concentration $(\mathrm{mol/m^3})$	C_{e0}	17300	17300	17300
Acid dissociation constant [13]	n	0.5	0.5	0.5
Porosity constant [24]	α	4.5	4.5	4.5
Reaction rate constant – hydrolysis $(1/\mathrm{week})$	k_1	0.003	0.014	0.005
Reaction rate constant – autocatalysis $(\sqrt{\mathrm{m^3/mol}}/\mathrm{week})$	k_2	0.002	0.014	0.00055
Diffusion coefficient $(\mathrm{m^2/week})$	D_0	$8.528e-9$	$7e-12$	$6.048e-7$

Model parameters (**Table 4.1**) were initially determined in the work presented by Wang *et al*. [22] which describes the degradation trends of PLA plate and film samples [12]. In the degradation study [12], 2 mm thick plates and 0.3 mm thick films were eroded in phosphate buffer solution, pH 7.4, at 37°C for 30

weeks, with the plates immersed and exposed to media on both sides and the films cast onto dishes and exposed to media on one side only. The one-dimensional model of the plate and the films investigated are shown in **Figure 4.1**(a), while **Figure 4.1**(b) is the representative unit investigated in MATLAB using the GALERKIN method.

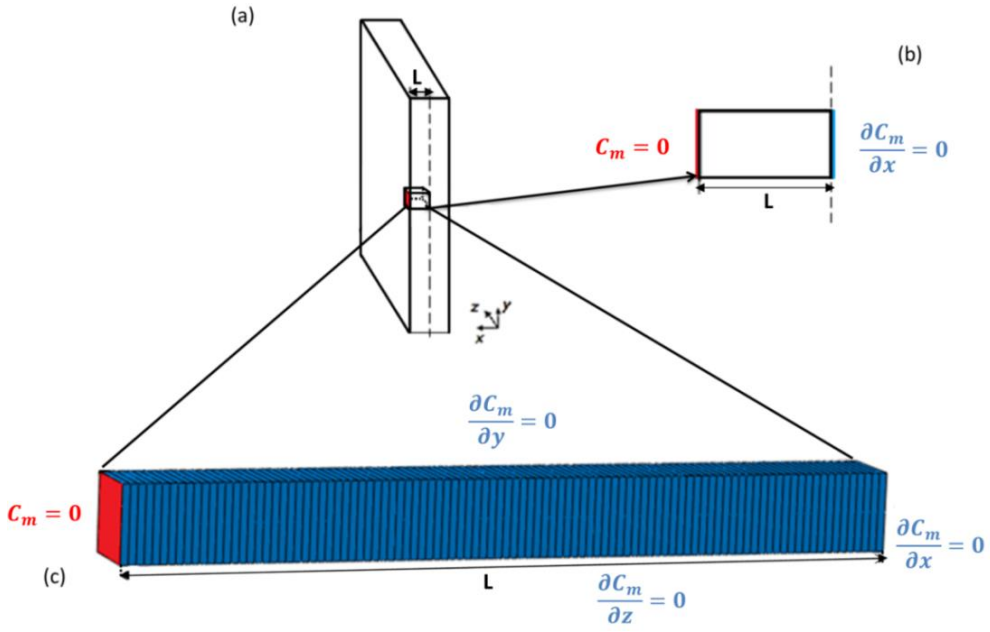

Figure 4.1 For the semi-analytical solution, the dimension L of the films investigated each time is represented using the one-dimensional unit shown in (a) and (b). C_m is assumed to have a value of zero at the assigned free surface (red) and a monomer flux of zero is imposed at the opposite boundary (blue, shown in (b)). The geometry used in each of the finite element investigations is shown in (c) as a representative unit of material (of thickness L). The finite element mesh and boundary conditions applied are also shown. $C_m = 0$ is applied at the free surface on the left hand boundary of the model and all other surfaces are set to impermeable (zero flux) surfaces ((c)).

Boundary conditions, which assume (i) the diffusive flux of monomers to be zero across the centre plane of symmetry for the plate (or the film-substrate interface of the film) and (ii) a monomer concentration of zero at the free surface, are applied as shown in **Figure 4.1**(b). Solutions for the spatial average of the normalised ester bond concentration, $\overline{C}_e$, are obtained as a function of time and, as is outlined in **Chapter 3**, used to determine changes in $\bar{M}_w{}^V$, the volume averaged form of $\bar{M}_w$ (as shown in Eq. (4.1), where $\bar{M}_w$ is

the normalised weight average molecular weight, and C_{e0} is the initial concentration of ester bonds) for the various material geometries investigated.

$$\bar{C}_e = \frac{C_e}{C_{e0}} = \frac{M_w}{M_{w0}} = \bar{M}_w \tag{4.1}$$

The predictions of the semi-analytical model are then compared to those obtained using the FE modelling techniques for the PLA plate and film.

Following this initial validation of the semi-analytical solution, the developed MATLAB code is used to generate the one-dimensional solution for the degradation of a PLGA film (250 μm thick) (as examined in the experimental studies of Shirazi *et al*. [25]). In the experimental work, 250 μm PLGA films were cast onto glass slides and degraded at pH 7.4 and 37°C, and size exclusion chromatography techniques were used to evaluate the changes in molecular weight of the films over a 20 day period [25]. Model parameters (**Table 4.1**) were recently suggested [14] to describe the degradation of the examined PLGA films.

Using the parameters for PLGA in **Table 4.1**, the effect of film thickness on the molecular weight distribution predicted by the MATLAB model for PLGA films measuring 0.25 μm, 2.5 μm, 25 μm, 100 μm, 250 μm, and 2500 μm in thickness is then investigated. Model parameters for poly-L-lactide (PLLA) are fit to the results of an experimental study [26] on PLLA tensile samples (degraded in-vitro for 44 weeks at 37°C and a pH of 7.4) using the FE implementation. An R^2 value is used to evaluate the fit to PLLA experimental data. Model parameters for the three materials (PLA, PLGA and PLLA) are summarised in **Table 4.1**.

Simulations are performed using Abaqus/Standard to investigate the degradation of the PLA plate and film using the material parameters given in

Table 4.1. A 1 mm thick film (representing a 2 mm plate, exposed on both sides) and a 0.3 mm thick film are modelled using the geometry shown in **Figure 4.1** (c) (where L is the thickness of the film in each case).

The FE predictions for $\bar{M}_w{}^V$ in the plate and film over 30 weeks are compared to those obtained with the previously described semi-analytical (MATLAB) model and to the experimental results [12]. Following this, degradation of various PLGA films is simulated in Abaqus/Standard using the same geometry (**Figure 4.1**(c)) and the parameters for PLGA from **Table 4.1**. The predictions for $\bar{M}_w{}^V$ in PLGA films across a range of thicknesses (0.25 µm, 2.5 µm, 25 µm, 100 µm, 250 µm, and 2500 µm), are compared to those of the MATLAB model and to those previously determined with Comsol by Shirazi *et al*. [14].

The FE mesh and boundary conditions used in the Abaqus/Standard simulations are shown in **Figure 4.1**(c), where the through-thickness model dimension, L, is varied to represent the various thicknesses of interest. Boundary conditions, which follow the assumptions stated above for the semi-analytical model, i.e. $C_m = 0$ on a free surface at the outside edge and all other surfaces set as impermeable (with a value of zero monomer flux assigned), are applied to the model (**Figure 4.1**(c)). The solution of the one-dimensional problem in each case is achieved by using a simple through-thickness mesh. Similarly to the semi-analytical solution, the spatial average of $\bar{C}_e$ across all of the integration points though the thickness is output to give $\bar{M}_w{}^V$ versus time for each investigation. In the Abaqus/Standard investigations, 100 quadratic heat transfer elements of type DC3D20 are used. For each one-dimensional case investigated, this mesh density is more than sufficient to achieve converged FE solutions (on increasing the mesh from 100 to 250 elements, a less than 1% change in the solution variables is observed). A

predefined field is applied to set the initial concentration of monomers to zero, signifying that there are no residual monomers present and that hydrolysis starts at time zero in the analysis. In Abaqus/Standard, the hydrolysis and diffusion properties are assigned using the thermal user material subroutine, UMATHT, with the part having a density of 1 kg m^{-3} and a specific energy of 1 J m^3 kg^{-1} mol^{-1}.

4.3.2 Analysis of bioresorbable polymeric stents (BPS)

An investigation into the degradation of BPS is carried out using the Abaqus/Standard implementation of the physio-chemical model (outlined in **Chapter 3**). Model parameters for PLLA are firstly calibrated to fit the experimental degradation data of Weir *et al.* [26]. In this parameter fit, simulations are performed on a film geometry measuring 0.4 mm in thickness (to represent the 0.8 mm thick plate examined in the experimental study [26]), following the same approach as outlined above for the PLA and the PLGA film geometries. Degradation is simulated for 44 weeks. The $\bar{M}_w$ trend reported in the plate for different combinations of the degradation parameters (k_1,k_2 and D_0) is evaluated against the experimental data, when the material is assumed to have a C_{e0} of 17300 mol/m^3 and where the values for n (0.5) [13] and α (4.5) [24] are kept constant. The material parameters shown in **Table 4.1** gave the best fit to the PLLA experimental data.

An open-cell geometry, representative of the ABSORB Bioresorbable Vascular Scaffold (BVS) from Abbott Vascular, is created as a 3D solid. The stent is modelled in its deployed state (external diameter of 2.65 mm), with a strut thickness of 156 μm and width of 150 μm (**Figure 4.2**(a)). A mesh comprising of approximately 250,000 quadratic heat transfer brick (DC3D20) elements is created to allow for 8 elements across the width of each stent strut (Figure

4.**Figure 4.2**(b)). This mesh density is found to be sufficient to give accurate results (i.e. the maximum value of C_e reduces by less than 0.1% when the number of elements is increased to 300000). A study is then performed to investigate the effects of material, strut size and boundary condition on the degradation of the stent. The $\bar{M}_w{}^V$ in the stent is determined and plotted versus time for a period of 104 weeks (24 months) to allow for comparison between the different cases investigated.

To gain an understanding of the influence of material parameters k_1,k_2 and D_0 on the degradation rates, the stent is modelled using the values shown in **Table 4.1** for PLA, PLGA and PLLA. The effects of physiological monomer boundary conditions on stent degradation are examined by considering two extreme boundary condition assumptions. In the first case (stent free surface (SFS)), C_m is set to zero at an assigned free surface on the stent (i.e. the inner surface and internal strut edges, as highlighted in **Figure 4.2**(c)). This echoes the assumption used previously for the plates and films; that any monomers produced on this surface are immediately removed, (i.e. swept away by the actions of blood flow). The remaining stent surface (outer surface) is assumed to be impermeable, with a value of zero monomer flux applied (**Figure 4.2**(c)). This boundary condition represents a stent immediately post-implantation into an artery, where only the monomers produced at the outer stent surface (in contact with the artery) could provide any possible contribution to autocatalysis reactions. This can be considered as an upper bound for the diffusion behaviour in the current context. For the second boundary condition assumption, a fully embedded stent (stent fully embedded (SFE)) is modelled, similar to the approach used in [21]. In this case, this condition can be considered as the lower bound for diffusion in the current context, where monomers are confined on stent surfaces.

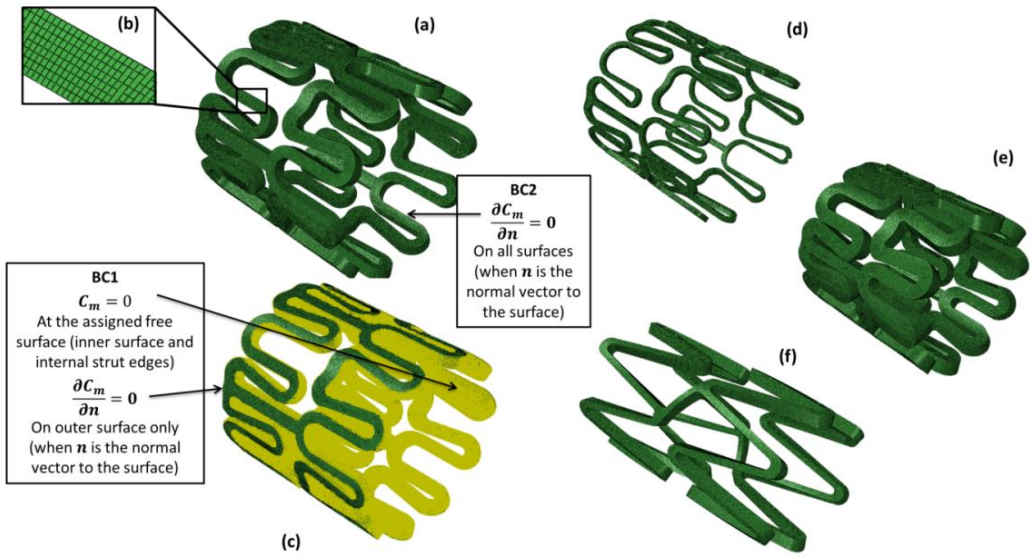

Figure 4.2 A number of different geometries and boundary conditions are investigated for the case of the bioresorbable polymeric stent. The open-cell and zig-zag geometries examined are shown in (a)-(e) and (f) respectively. For the open-cell geometry, the thickness and width of the stent strut are varied uniformly in two dimensions to create three different struts sizes. (a) and (c) show the stent when the struts are of dimensions 156 m thick x 150 µm wide, (d) is for struts 78 µm thick x 75 µm wide and (e) struts 234 µm thick x 225 µm wide. The two boundary conditions investigated, SFS and SFE are also highlighted. The surfaces at which $C_m = 0$ is applied are shown in (c), when the outer surface of the stent is set to an impermeable surface (i.e. $(\partial C_m/\partial n) = 0$), which is the boundary applied to all of the surfaces in (a).

Each of the stent surfaces are modelled as impermeable surfaces, i.e. a zero diffusive monomer flux is applied to each surface (**Figure 4.2**(a)), to represent the case of a stent embedded in an artery which has had significant neo-intimal tissue regrowth occur. This boundary condition assumes that degradation products are unlikely to be immediately washed away by environmental flow, but would instead act as catalysts for further degradation.

The effects of strut size on the degradation rate are investigated for three different strut sizes (78 µm, 156 µm and 234 µm), by varying the thicknesses and width of the stent struts each time (**Figure 4.2**(a), (d), (e)). The influence of geometry on stent degradation is then investigated by including a second stent geometry in the study: a zig-zag helical stent representative of the Igaki-Tamai BPS [8]. The degradation behaviour of this stent is investigated using

Abaqus/Standard for PLA, PLGA and PLLA materials with a strut size of 156 μm and width of 150 μm. The zig-zag geometry used in this study (shown in **Figure 4.2**(f)) is modelled with a mesh of 237000 quadratic heat transfer brick elements (DC3D20).

4.4 Results

4.4.1 Degradation behaviour of PLA and PLGA plates and films

The changes in $\bar{M}_w{}^V$ of the PLA plate and film after 30 weeks, as predicted by the MATLAB and Abaqus/Standard simulations are shown in **Figure 4.3**. The experimental results of Grizzi *et al*. [11] and the predictions of Wang *et al*. [21] are also shown. For all methods investigated, it can be observed that the 2 mm plate degrades faster than the 0.3 mm film, with the plate having a maximum $\bar{M}_w{}^V$ of 3% remaining after 30 weeks, compared to 26% for the film. The FE predictions show good agreement with the trends predicted by the semi-analytical (MATLAB) model, more so for the film geometry than for the plate.

The changes in $\bar{M}_w{}^V$ for PLGA films of different thicknesses, as predicted by the MATLAB and Abaqus/Standard simulations for a 40-day period, are shown in **Figure 4.4**. The predictions of the Abaqus/Standard model for each film thickness show good agreement with previous Comsol model predictions by Shirazi *et al*. [13]. In the work of Shirazi *et al*. [14], a least means square measure was used to fit a FE (Comsol) solution of the degradation model governing equations to experimental data for PLGA films [14], [25]. It can be observed from **Figure 4.4**(a) that while the semi-analytical model shows a close match to the FE predictions for films 0.25 and 2.5 μm thick, it differs to the FE predictions for the 25 μm film, particularly between days 5 and 19. For the case of the 250 μm film (**Figure 4.4**(b)), there is close agreement between

the FE predictions and the experimental data of Shirazi *et al*. [26], whereas the MATLAB model fails to capture the observed experimental degradation behaviour. As highlighted in **Figure 4.4**(c), the semi-analytical model is unable to capture the differences in $\bar{M}_w{}^V$ for the 100, 250, and 2500 µm films. The FE simulations, however, predict faster degradation trends for the thicker films, with the 100 µm films having a $\bar{M}_w{}^V$ of 8.2% remaining after 15 days, compared to 7.31% for the 250 µm film and 6.52% for the 2500 µm film.

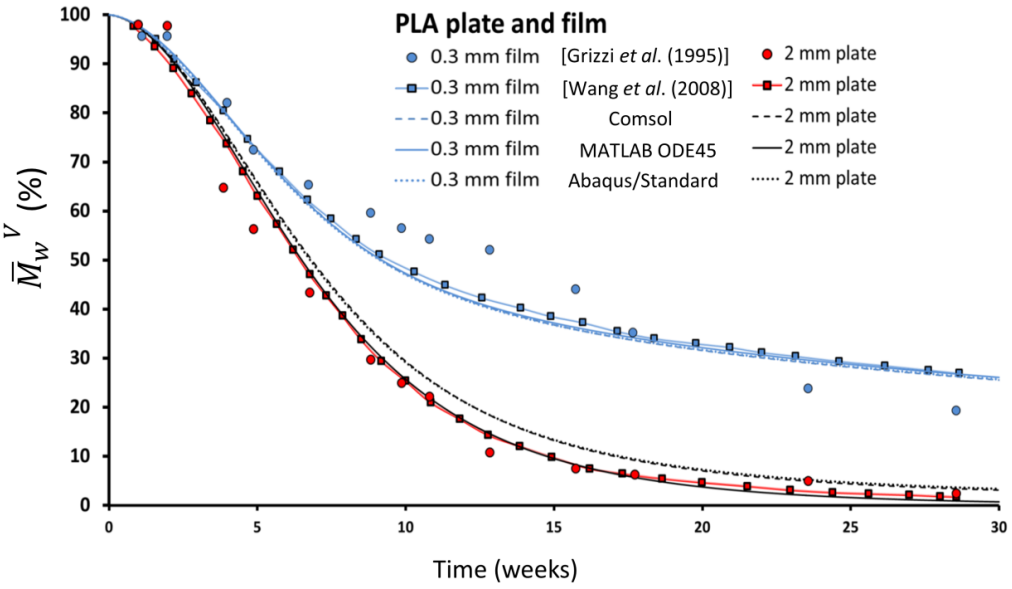

Figure 4.3 The predicted changes in $\bar{M}_w{}^V$ of the PLA plate and film investigated by Grizzi et al.[12] for a degradation period of 30 weeks are shown. The predictions of the MATLAB, Comsol and Abaqus/Standard simulations are compared to those obtained by Wang et al. [22] and also to the experimental data [12].

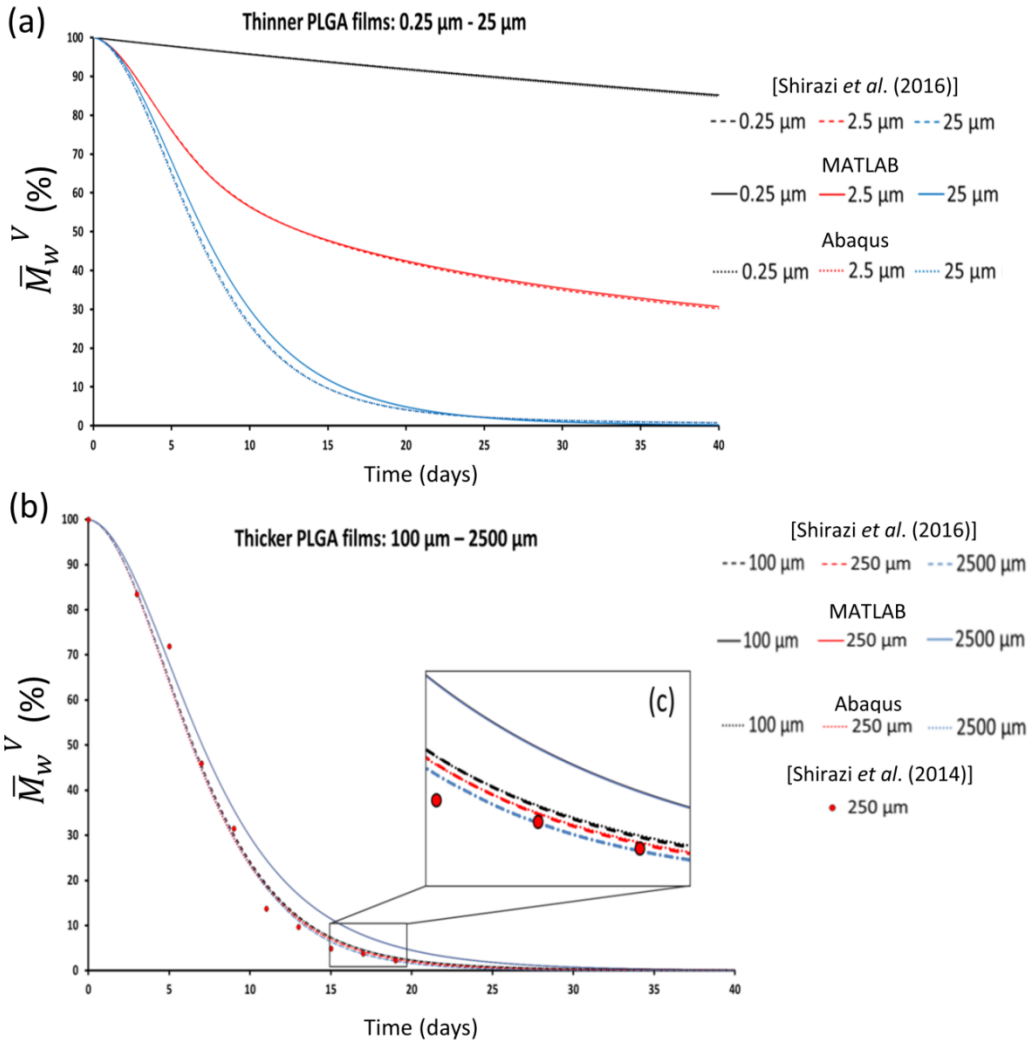

Figure 4.4 The results predicted for the range of PLGA films investigated using the MATLAB and Abaqus/Standard simulations are compared to the Comsol predictions of Shirazi *et al*. [14]. The predictions of $\bar{M}_w^V$ in thinner PLGA films (0.25, 2.5 and 25 µm) are shown in (a) whereas the predictions for the 10, 250 and 2500 µm films are compared in (b). The differences predicted by the semi-analytical and FE models for the thicker PLGA film cases are highlighted in (c).

4.4.2 Degradation behaviour of BPS

For the open-cell stent geometries, **Figure 4.5** compares the Abaqus/Standard predictions of the changes in $\bar{M}_w^V$ for each case investigated. As is evident from the figure, the stent degradation profile is strongly dependent on the material. For the stent free surface (SFS) simulations, $\bar{M}_w^V$ for the PLGA scaffolds has reduced to approximately 21% after 104 weeks. In contrast, the PLA and PLLA stents show much slower

degradation trends, with minimum predicted $\bar{M}_w{}^V$ values of 66% and 60%, respectively.

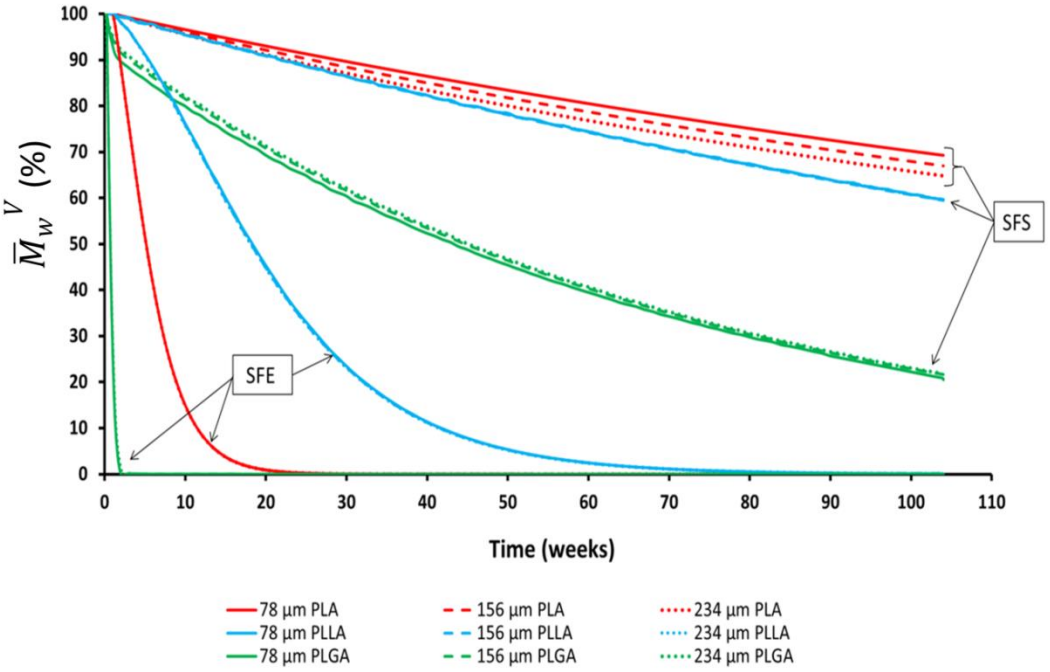

Figure 4.5 The predictions of the Abaqus/Standard simulations carried out on the open-cell stent geometries are shown. Predictions of $\bar{M}_w{}^V$ in various materials, strut size and boundary conditions assumed are compared for a degradation period of 104 weeks.

It can also be observed from **Figure 4.5** that the predicted degradation rates are highly dependent on the assumed boundary conditions. The fully embedded (SFE) assumption results in much faster degradation rates for all materials, in comparison to the SFS case. After 70 weeks, the SFE simulations predict a decrease in $\bar{M}_w{}^V$ of more than 95% for all materials investigated. The strong material dependence is again observed for the SFE simulations; it is interesting to note the reversal in the relative stent degradation rates for the PLA and PLLA materials, with the PLA stent degrading faster than the PLLA stents, in contrast to the SFS case. In relation to stent strut size, it is interesting to observe from **Figure 4.5** that the strut size has almost negligible influence on the degradation rate for PLGA and PLLA; a

slight influence is observed for PLA, with the 234 μm geometry showing a faster degradation rate than that of the 156 μm and 78 μm geometries.

The contour plots in **Figure 4.6** show the spatial distribution in $\bar{M}_w$ and C_m for the open-cell 156 μm stents at 104 weeks. For the SFS boundary condition differences in $\bar{M}_w$ at the inner and outer surfaces of the PLGA and PLA stents are evident, in particular for PLGA, where $\bar{M}_w$ is observed to decrease at a faster rate on the outer surface of the stent; this effect, however, is less evident for PLLA (**Figure 4.6**(a)). Regarding the distribution of degradation products for the SFS cases (**Figure 4.6**(b)), maximum C_m values (located at the outer surfaces) are observed for the PLA stent (0.43 mol/m^3), compared to values of 0.0029 mol/m^3 and 0.0025 mol/m^3 respectively for the PLLA and PLGA stents. Additionally, due to the SFS boundary condition, a high gradient in C_m in the stent strut close to the outer surface is observed (this is most evident for PLA as shown in the insert in **Figure 4.6**(b)), indicating low C_m values (and hence low autocatalysis potential) through most of the strut thickness. In contrast to the SFS case, the fully embedded SFE boundary condition generates high C_m values (and hence, high autocatalysis potential) and low degradation product gradients through the stent strut, as is shown for the example of the PLA material in **Figure 4.6**(c)**.** This is consistent with low $\bar{M}_w$ values (and hence, greater degradation), as shown once again for the PLA SFE case in **Figure 4.6**(a), with $\bar{M}_w$ predicted to reduce to 0% by the end of the 104 week time period. These local spatial distribution observations are fully consistent with the overall degradation trends observed in **Figure 4.5**, as described above.

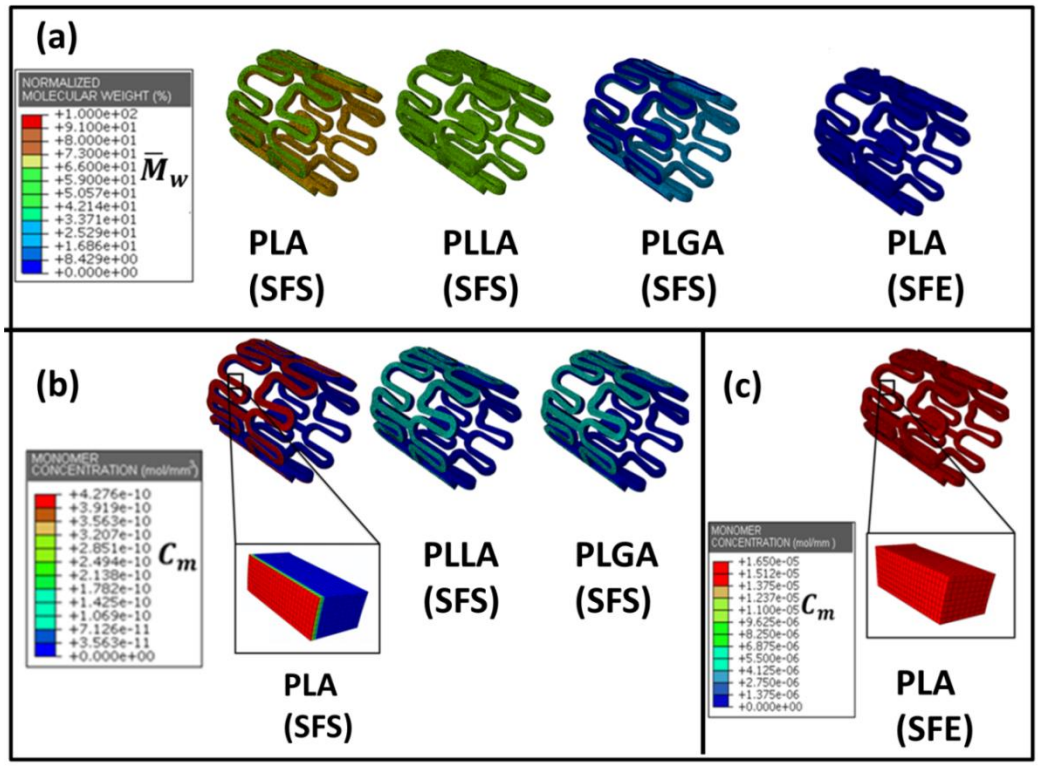

Figure 4.6 The contour plots shown depict $\bar{M}_w$ and C_m in the scaffold (156 x 150 µm struts, multilink geometry) for when various boundary conditions (stent free surface (SFS); stent fully embedded (SFE)) are applied for the PLA, PLLA and PLGA materials. The predictions for $\bar{M}_w$ are shown in (a) for SFS and SFE as labelled, with predictions for C_m shown in (b) for the three materials, with (c) showing the high C_m in PLA under SFE conditions. Inserts highlight the boundary condition driven difference in C_m gradient for PLA.

Figure 4.7 compares the ${\bar{M}_w}^V$ predictions over time for the two stent geometries examined, the zig-zag and the open-cell geometries.

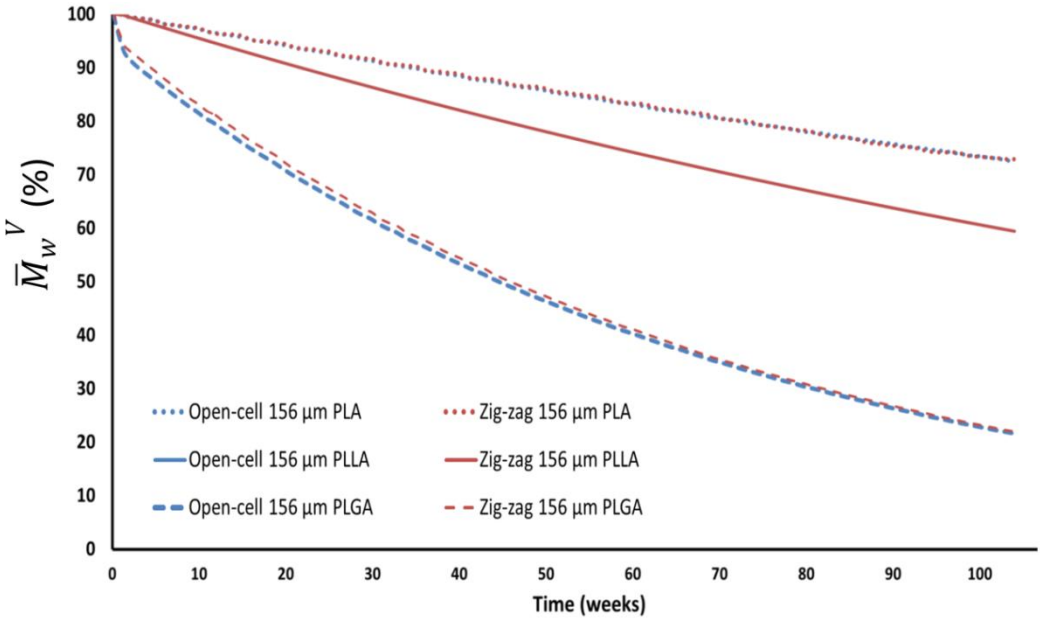

Figure 4.7 The predictions in $\bar{M}_w{}^V$ versus time for the two stent geometries (open-cell and zig-zag) are compared for 104 weeks under SFS conditions.

Little difference in the degradation behaviour is predicted between the two geometries for the three materials investigated. As a final step in this study, a recently suggested empirical relationship between the Young's modulus, E, and the molecular weight of degrading polymers [27] is used to estimate the decrease in mechanical stiffness of the BPS examined. Specifically, the following equation Eq.(4.2) is used here, based on that presented in [27], which describes the relationship between $\bar{M}_w{}^V$ and E, using the initial modulus, E_0, and a modulus degradation rate constant, k_m, that is assumed to take the value of 1400 MPa [27]. The values of E_0 are assumed to be 3500 MPa, 4800 MPa and 2000 MPa for PLA, PLLA and PLGA, respectively [2], [28].

$$E = E_0 + k_m \mathbf{log} \bar{M}_w{}^v \tag{4.2}$$

The value of E calculated in Eq.(4.2) is therefore akin to a "volume averaged" E for the stent structure. The results of this study are presented in **Figure 4.8**, where the predicted decrease in E after 90 weeks for the three polymer

materials is compared for the case of the SFS and SFE boundary condition assumptions. The predictions indicate a much faster decrease in mechanical stiffness for the SFE simulations than that predicted for the SFS case, particularly for the PLA and PLGA materials. The PLLA material shows a more gradual decrease in mechanical stiffness than that observed for the other two materials.

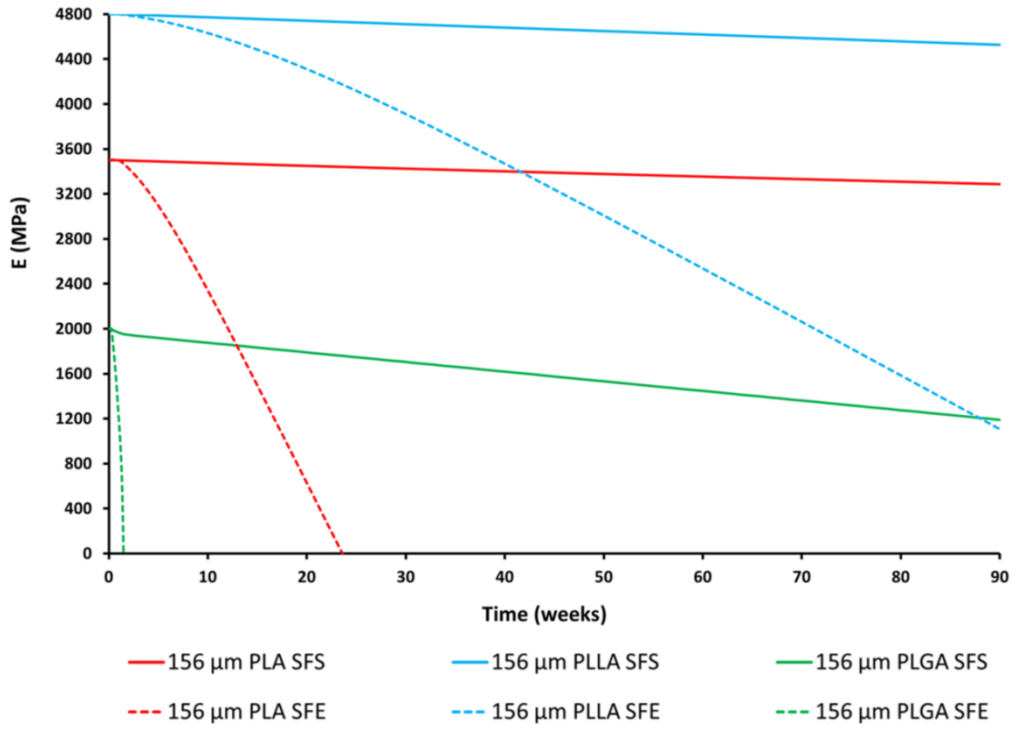

Figure 4.8 The predictions in the Young's modulus, E, for the open-cell 156 µm stents are shown for a time of 90 weeks, when the initial moduli, E_0 are assigned as 3500 MPa, 4800 MPa and 2000 MPa for the PLA, PLLA and PLGA materials and where the value of k_m is 1400 MPa [28].

4.5 Discussion

From the perspective of designing next generation BPS, the bulk degradation behaviour of the polymer material adds considerable complications in comparison to established permanent devices for the treatment of coronary artery disease. Computational modelling offers an efficient framework to predict and provide understanding into the degradation behaviours of bioresorbable medical devices and implants. Development of appropriate

computational modelling techniques for BPS involves consideration of both the physio-chemical aspects of hydrolysis and polymer chain scission, and the impact of this on the mechanical behaviour of the material, in order to suitably evaluate the in-vivo performance of BPS devices.

4.5.1 Summary of modelling work

Computational modelling plays a key role in the analysis and design of medical devices and the development of improved techniques with a principal focus on the degradation behaviour of biodegradable polymers will undoubtedly help to aid the growth and development of bioresorbable technologies. In the current study, a physio-chemical model for the degradation of general polymer materials [22] is implemented into a number of computational frameworks (MATLAB, Comsol and Abaqus/Standard) to investigate the physio-chemical degradation behaviour of polymer plates, films and bioresorbable stents. The Abaqus/Standard and Comsol predictions for $\bar{M}_w{}^V$ in the examined PLA plate and film show close agreement with both the MATLAB semi-analytical model solutions and also with experimental degradation data [12], verifying the FE predictions for the PLA structures. It is important to note that the semi-analytical (MATLAB) approach was initially used to calibrate model parameters for PLA [22], which may explain the very close match between the MATLAB solution derived in this study, the previous predictions [22] and the experiments [12] for the plate and the film. The FE model predictions, using the same material parameter values, but different numerical formulations, are very close to the MATLAB solution for the PLA film, but display an over prediction in $\bar{M}_w{}^V$ of about 3% for the PLA plate.

Using the developed MATLAB code, the $\bar{M}_w{}^V$ for a range of PLGA film thicknesses is determined for 40 days of simulated degradation and compared

to the corresponding Abaqus/Standard predictions and also to the Comsol predictions of Shirazi *et al*. [14]. As previously observed using Comsol [14], and as is demonstrated again here for other modelling frameworks (MATLAB and Abaqus/Standard), the degradation behaviour of PLGA films is observed to be quite dependent on the thickness of the film [14]. A close correspondence of the two FE (Abaqus/Standard and Comsol) solutions is again observed, but it is interesting to note that the MATLAB model predictions fail to capture any thickness dependency for the thicker PLGA films examined (**Figure 4.4**(b)). The relatively high number (>100) of nodes afforded by the FE simulations enables a far more accurate solution for $\bar{M}_w{}^V$ than that allowed by the MATLAB model, which is based on trial functions that display quite a restrictive spatial variation [22]. Overall, these results have verified the successful implementation of the degradation modelling equations into Abaqus/Standard for the first time, and have demonstrated the general predictive capabilities of the modelling frameworks investigated (albeit with the exception of the current form of the semi-analytical model for very thick films).

4.5.2 Influence of material parameters

Using the Abaqus/Standard implementation of the degradation model, the effects of a number of factors (material, strut size, boundary condition assumptions and geometry) on the degradation rates of BPS are examined. From the results of these studies, it is clear to see that for the case of the SFS and SFE simulations alike, the PLGA stents exhibit much faster degradation (in terms of $\bar{M}_w{}^V$) than is observed for the other two materials. This may be explained by the high values of the reaction rate constants, k_1 and k_2, assigned to the PLGA material (**Table 4.1**). Reaction rate constants are included in the degradation model to represent both the normal hydrolytic and

autocatalytic reactions which occur in the degradation of aliphatic polyesters. The hydrolysis constant, k_1, governs the rate at which polymer chains are cleaved through chemical hydrolysis, which is directly related to the reduction in the number average molecular weight. Autocatalysis, commonly observed in the biodegradable polyesters of predominant interest in bioresorbable clinical devices, describes an increased rate of material degradation due to the accumulation of acidic chain ends (formed when the polymer chains are hydrolytically cleaved) within the material matrix [12], [13]. In the implemented degradation model, the influence of autocatalysis is governed by k_2, which controls the augmenting effects that the acidic chain ends have on the material hydrolysis rates. The PLGA stents exhibit more of a dependency on autocatalysis than is observed for the other polymers, especially when compared with the PLLA stents. PLLA is currently the most commercially investigated material for the BPS application, with a number of PLLA based devices already having received market approval in Europe [15], as discussed in **Chapter 2**. The results here support this fact, from the point of view of choosing a polymer with relatively slow degradation characteristics as would be required for the BPS application. In contrast, and as is once again consistent with the results presented here, the use of PLGA is often limited to applications which require faster degradation times, e.g. tissue engineered and drug delivery stents [5], while PLA is generally employed in orthopaedic screws or fixation devices [4].

4.5.3 Influence of monomer boundary condition assumptions

From the present study, it is revealed that there is a significant influence of monomer boundary condition assumption on the predicted degradation rates of the stents investigated, especially for the PLA and PLGA materials, with less of an influence observed for PLLA. For the PLA and PLGA simulations, a

much greater decrease in $\bar{M}_w{}^V$ is observed in the fully embedded (SFE) case than for the free surface (SFS) case, where for the latter case, the inner surface and the internal edges of the stent struts are assumed to be monomer free surfaces (due to the eradicating actions of blood flow), resulting in a low autocatalysis potential. In contrast, in the SFE simulations, the embedding results in a build-up in acidic chain ends (due to monomer build-up), and hence a high autocatalysis potential. As a result, PLA and PLLA show similar degradation trends in the SFS case, with the degradation rate of the PLLA stent being slightly higher than of the PLA stent, which is consistent with the primarily direct hydrolysis driven degradation in this case and the relative values of the hydrolysis constant, k_1 (k_1 for PLLA > k_1 for PLA, see **Table 4.1**). In contrast, a considerable difference exists in the predicted trends for the two materials when the SFE boundary condition is assumed, with $\bar{M}_w{}^V$ reducing much more slowly for PLLA; consistent with the primarily autocatalysis driven degradation in this case due to the relative values of k_2 (k_2 for PLA > k_2 for PLLA, see **Table 4.1**) and the retention of monomers in the material for this embedded condition.

The SFE boundary condition assumption is intended to represent the remodelling of arterial tissue around the stent struts following BPS implantation and the assumed retention of monomers within the tissue during this time. Arterial remodelling is generally thought to occur in the first 6-12 months after implantation [29], with a significant amount of neo-intimal tissue formed around the stent during this time [30]. The current study seeks to investigate the effects of two extreme boundary condition assumptions on the degradation rates of BPS. In reality, the complex interactions between degradation, neo-intimal formation and monomer diffusion would result in a

more intermediate state in-vivo, therefore the actual degradation rates of the materials investigated are expected to be in between the upper and lower bounds predicted in this study.

4.5.4 Strut thickness investigation

Previously, it has been experimentally shown for PLA and PLGA that thicker samples degrade faster than thinner samples [12], [13], [31], [32]. An investigation into the effects of strut thickness on the predicted degradation rates of various stent structures concludes that, for the strut sizes analysed in the current study, there is little difference in predicted $\bar{M}_w{}^V$. Having said this, the dependency is more noticeable for PLA (in the SFS case), in contrast to the other two materials. In an effort to understand this effect, one can look to the competing mechanisms of autocatalysis and monomer diffusion. The spatially heterogeneous degradation rates observed for thicker polyester samples [12] are generally attributed to the catalysing effects of acidic chain ends, and rates are often observed as being higher at the core of the sample compared to the surface (as monomers diffuse out of the polymer material nearer to the surface) [12]. Recently, Shirazi *et al*. [14] showed that a length scale parameter can be derived to better understand the competition which occurs between diffusion of monomer fragments and their catalysing effects on degradation. Eq.(4.3) below shows how this parameter, the "diffusion length", l_{diff}, can be determined from model parameters.

$$l_{diff} = \sqrt{\frac{D_0}{k_2\sqrt{C_{e0}}}} \tag{4.3}$$

As indicated herein, material parameters D_0 and k_2 are respectively linked to the diffusion behaviour of degradation products and their autocatalytic influence. For thicknesses greater than l_{diff}, spatially heterogeneous

degradation due to autocatalysis dominates, whereas for thicknesses less than l_{diff}, monomer diffusion dominates and degradation rates are lower. Previously, l_{diff} has been determined for PLGA as 2 μm [14]. As part of the current study, values of l_{diff}, for PLA (180 μm) and PLLA (2.9 mm) are calculated, using parameters from **Table 4.1**. The maximum strut thickness considered here (234 μm) is two orders of magnitude lower than l_{diff} for PLLA. Firstly, this is consistent with the minimal observed thickness dependence for PLLA, and it also indicates diffusion dominance and low degradation rates for the material; consistent with the results presented herein and as discussed above. The minimum strut thickness considered in the current study (78 μm), is much greater than l_{diff} for PLGA, again leading to the minimal observed thickness dependence for PLGA, and in contrast to PLLA, indicating autocatalysis dominance, which is again consistent with the results presented herein. For PLA however, l_{diff} is within the range of the strut thicknesses considered, indicating that there is a potential for a thickness dependence: in keeping with what is observed for PLA in the SFS condition, where monomer diffusion is allowed. In the SFE condition the observed lack of thickness dependence for PLA is most likely due to the constraint on monomer diffusion out of the strut that, as a result, promotes autocatalysis.

4.5.5 Mechanical scaffolding of PLLA

The molecular weight is generally considered to be one of the most important factors in understanding the degradation of a polymeric device [27]. While consideration of the molecular weight (in particular in its volume averaged form) is interesting to assess the degradation of BPS, a more direct relationship between degradation time and material Young's modulus is arguably of greater interest to the manufacturer. In the current study, and

following on from the general model presented by Gleadall *et al*. [27], an empirical relationship is presented to correlate the volume averaged molecular weight with the volume averaged modulus. Using this to investigate the predictions of decreasing E versus time for the various stent cases, the superiority of the PLLA material, as compared to the PLA and PLGA materials, is highlighted. The PLLA stents show a gradual decrease in mechanical stiffness, even for the fully embedded (SFE) case. In contrast, a rapid decrease in mechanical stiffness is observed for the fully embedded (SFE) PLA and PLGA cases, suggesting that such materials would lose their mechanical integrity long before the recommended vessel scaffolding period has passed. The results shown here provide further evidence to support the established use of PLLA materials in the BPS application.

4.5.6 Model assumptions and limitations

For next generation BPS, a number of complex factors must be considered in the device design and analysis process, including the physio-chemical properties of the polymer and how this influences on the material degradation rates [10]. The effects of arterial tissue remodelling and neo-intimal formation, the mechanical loading environment and residual degradation products on the performance of BPS in-vivo are other important factors to consider [15]. As previously indicated in **Chapter 3**, the specific model formulation presented here has limitations and does not incorporate the effects of material mass or volume loss. The mass loss in the material can be accounted for via diffusion of monomers out of the sample; possible volume changes during degradation (due to water uptake, changes in crystallinity, or otherwise) have not been included here. The results presented clearly verify the validity of the use of the thermal analogy to implement kinetic degradation equations into Abaqus/Standard. This provides a sound platform for the incorporation of

model enhancements, including consideration of the effects of co-polymer ratio and different types of chain scission mechanisms on the degradation, as presented in [33]–[36]. Additionally, the model formulation used in this chapter does not include an explicit representation of polymer crystallisation during degradation. While this is not particularly relevant for PLGA or amorphous forms of PLA, it is important for studying the degradation of semi-crystalline PLLA materials. Once again, the use of an FE framework to model degradation, as presented here, provides a strong basis for the incorporation of these effects, through implementation of crystallisation kinetic equations (for example as presented in [27], [37], [38]) which is the focus of **Chapter 5**. The implementation of the physio-chemical degradation model in Abaqus allows a number of complex numerical techniques to be included in the analysis, namely: contact between the device and surrounding tissue; non-linear material models to capture tissue deformations; finite deformations to capture the large mechanical strains imposed during stent deployment; and, if necessary, fluid structure interactions with pulsatile blood flow. Finally, the use of FE programmes to model material degradation is desirable, as most commercial software programmes offer opportunities to combine several modelling formulations, such as the kinetic formulation examined here, solid mechanics formulations and fluid structure interaction formulations. This would undoubtedly aid the development of more advanced computational techniques for the in-vitro analysis of BPS degradation.

4.6 Conclusion

The current study presents the successful use of the Abaqus/Standard framework from **Chapter 3** to simulate polymer degradation. Model predictions of changes in the normalised molecular weight of various polymeric devices are established and effects of various factors on the degradation of BPS

geometries are examined. Taking this, and a previous Comsol implementation of the physio-chemical degradation model [14], into account, the successful implementation of physio-chemical degradation equations across a number of commercially available computational platforms has now been shown. The formulation implementation presented here will allow for more robust validation of the degradation model in complex and realistic device geometries. The establishment of computational techniques for BPS which can quantify the material degradation and offer possible insight into its effects on the mechanical integrity and scaffolding ability of the stent is beneficial for the future development of BPS. Further experimental testing of biodegradable polymers is important to increase confidence in developed numerical analysis and design methods. In **Chapter 5**, building on the FE framework presented above, equations governing polymer crystallinity are incorporated into the user material subroutine, and investigations into the simultaneous degradation and crystallisation behaviours of semi-crystalline BPS are carried out for a range of conditions.

References

[1] R. Shine *et al.*, “Modeling of Biodegradable Polyesters With Applications to Coronary Stents,” *J. Med. Device.*, vol. 11, no. 2, p. 021007, 2017.

[2] L. S. Nair and C. T. Laurencin, “Biodegradable polymers as biomaterials,” *Prog. Polym. Sci.*, vol. 32, no. 8, pp. 762–798, 2007.

[3] K. Ficek, J. Filipek, P. Wojciechowski, K. Kopec, S.-Z. Ewa, and S. Blazewicz, “A bioresorbable polylactide implant used in bone cyst filling,” *J. Mater. Sci. Mater. Med.*, vol. 27, no. 2, pp. 1–8, 2015.

[4] J. C. Middleton and A. J. Tipton, “Synthetic biodegradable polymers as orthopedic devices.,” *Biomaterials*, vol. 21, no. 23, pp. 2335–2346, Dec. 2000.

[5] S. J. Hollister, “Porous scaffold design for tissue engineering.,” *Nat. Mater.*, vol. 4, no. 7, pp. 518–524, Jul. 2005.

[6] B. Dhandayuthapani, Y. Yoshida, T. Maekawa, and D. S. Kumar, “Polymeric scaffolds in tissue engineering application: a review,” *Int. J. Polym. Sci.*, vol. 2011, 2011.

[7] H. Patel, M. Bonde, and G. Srinivasan, “Biodegradable polymer scaffold for tissue engineering,” *Trends Biomater Artif Organs*, vol. 25, no. 1, pp. 20–29, 2011.

[8] H. Tamai *et al.*, “Initial and 6-month results of biodegradable poly-l-lactic acid coronary stents in humans,” *Circulation*, vol. 102, no. 4, pp. 399–404, 2000.

[9] B. D. Gogas, V. Farooq, Y. Onuma, and P. W. Serruys, “The ABSORB bioresorbable vascular scaffold: an evolution or revolution in interventional cardiology,” *Hell. J Cardiol*, vol. 53, no. 4, pp. 301–309, 2012.

[10] B. Tesfamariam, “Bioresorbable vascular scaffolds: Biodegradation, drug delivery and vascular remodeling,” *Pharmacol. Res.*, vol. 107, pp. 163–171, 2016.

[11] S. Lyu and D. Untereker, “Degradability of Polymers for Implantable Biomedical Devices,” *Int. J. Mol. Sci.*, vol. 10, no. 9, pp. 4033–4065, 2009.

[12] I. Grizzi, H. Garreau, S. Li, and M. Vert, “Hydrolytic degradation of devices based on poly(dl-lactic acid) size-dependence,” *Biomaterials*, vol. 16, no. 4, pp. 305–311, 1995.

[13] G. Siparsky, K. Voorhees, and F. Miao, “Hydrolysis of Polylactic Acid (PLA) and Polycaprolactone (PCL) in Aqueous Acetonitrile Solutions: Autocatalysis,” *J. Environ. Polym. Degrad.*, vol. 6, no. 1, pp. 31–41, 1998.

[14] R. N. Shirazi, W. Ronan, Y. Rochev, and P. McHugh, “Modelling the degradation and elastic properties of poly (lactic-co-glycolic acid) films and regular open-cell tissue engineering scaffolds,” *J. Mech. Behav. Biomed. Mater.*, vol. 54, pp. 48–59, 2016.

[15] E. L. Boland, R. Shine, N. Kelly, C. A. Sweeney, and P. E. McHugh, “A Review of Material Degradation Modelling for the Analysis and Design of Bioabsorbable Stents,” *Ann. Biomed. Eng.*, vol. 44, no. 2, pp. 341–356, 2015.

[16] J. F. da S. Soares, “Constitutive modeling for biodegradable polymers for application in endovascular stents,” Texas A&M University, 2008.

[17] J. S. Soares, J. E. Moore, and K. R. Rajagopal, “Modeling of deformation-

accelerated breakdown of polylactic acid biodegradable stents," *J. Med. Device.*, vol. 4, no. 4, p. 41007, 2010.

[18] D. Hayman, C. Bergerson, S. Miller, M. Moreno, and J. E. Moore, "The effect of static and dynamic loading on degradation of PLLA stent fibers," *J Biomech Eng*, vol. 136, no. 8, p. 4027614, 2014.

[19] S. Prabhu and S. Hossainy, "Modeling of degradation and drug release from a biodegradable stent coating," *J Biomed Mater Res A*, vol. 80, no. 3, pp. 732–741, 2007.

[20] T. Shazly, V. B. Kolachalama, J. Ferdous, J. P. Oberhauser, S. Hossainy, and E. R. Edelman, "Assessment of material by-product fate from bioresorbable vascular scaffolds," *Ann Biomed Eng*, vol. 40, no. 4, pp. 955–965, 2012.

[21] J. Ferdous, V. B. Kolachalama, and T. Shazly, "Impact of polymer structure and composition on fully resorbable endovascular scaffold performance," *Acta Biomater.*, vol. 9, no. 4, pp. 6052–6061, 2013.

[22] Y. Wang, J. Pan, X. Han, C. Sinka, and L. Ding, "A phenomenological model for the degradation of biodegradable polymers," *Biomaterials*, vol. 29, no. 23, pp. 3393–3401, 2008.

[23] Lyu *et al.*, "Kinetics and Time−Temperature Equivalence of Polymer Degradation," *Biomacromolecules*, vol. 8, no. 7, pp. 2301–2310, 2007.

[24] J. Siepmann and A. Gopferich, "Mathematical modeling of bioerodible, polymeric drug delivery systems.," *Adv. Drug Deliv. Rev.*, vol. 48, no. 2–3, pp. 229–247, Jun. 2001.

[25] R. N. Shirazi, F. Aldabbagh, A. Erxleben, Y. Rochev, and P. McHugh, "Nanomechanical properties of poly(lactic-co-glycolic) acid film during degradation," *Acta Biomater.*, vol. 10, no. 11, pp. 4695–4703, 2014.

[26] N. A. Weir, F. J. Buchanan, J. F. Orr, and G. R. Dickson, "Degradation of poly-L-lactide. Part 1: in vitro and in vivo physiological temperature degradation," *Proc Inst Mech Eng H*, vol. 218, no. 5, pp. 307–319, 2004.

[27] A. C. Gleadall, "Modelling degradation of biodegradable polymers and their mechanical properties." Department of Engineering, University of Leicester, 2015.

[28] I. Manavitehrani, A. Fathi, H. Badr, S. Daly, A. Negahi Shirazi, and F. Dehghani, "Biomedical Applications of Biodegradable Polyesters," *Polymers* , vol. 8, no. 1. 2016.

[29] H. Hermawan, D. Dubé, and D. Mantovani, "Developments in metallic biodegradable stents.," *Acta Biomater.*, vol. 6, no. 5, pp. 1693–7, May 2010.

[30] R. S. Schwartz, N. A. Chronos, and R. Virmani, "Preclinical restenosis models and drug-eluting stents: still important, still much to learn.," *J. Am. Coll. Cardiol.*, vol. 44, no. 7, pp. 1373–1385, Oct. 2004.

[31] M. Dunne, I. Corrigan, and Z. Ramtoola, "Influence of particle size and dissolution conditions on the degradation properties of polylactide-co-glycolide particles.," *Biomaterials*, vol. 21, no. 16, pp. 1659–1668, Aug. 2000.

[32] A. C. R. Grayson, M. J. Cima, and R. Langer, "Size and temperature effects on poly(lactic-co-glycolic acid) degradation and microreservoir device performance.," *Biomaterials*, vol. 26, no. 14, pp. 2137–2145, May 2005.

[33] X. Han, J. Pan, F. Buchanan, N. Weir, and D. Farrar, “Analysis of degradation data of poly(l-lactide-co-l,d-lactide) and poly(l-lactide) obtained at elevated and physiological temperatures using mathematical models,” *Acta Biomater*, vol. 6, no. 10, pp. 3882–3889, 2010.

[34] A. Gleadall, J. Pan, M. A. Kruft, and M. Kellomaki, “Degradation mechanisms of bioresorbable polyesters. Part 1. Effects of random scission, end scission and autocatalysis,” *Acta Biomater*, vol. 10, no. 5, pp. 2223–2232, 2014.

[35] A. Gleadall, J. Pan, M. A. Kruft, and M. Kellomaki, “Degradation mechanisms of bioresorbable polyesters. Part 2. Effects of initial molecular weight and residual monomer,” *Acta Biomater*, vol. 10, no. 5, pp. 2233–2240, 2014.

[36] X. Han and J. Pan, “Polymer chain scission, oligomer production and diffusion: a two-scale model for degradation of bioresorbable polyesters,” *Acta Biomater*, vol. 7, no. 2, pp. 538–547, 2011.

[37] A. Gleadall, J. Pan, and H. Atkinson, “A simplified theory of crystallisation induced by polymer chain scissions for biodegradable polyesters,” *Polym. Degrad. Stab.*, vol. 97, no. 9, pp. 1616–1620, 2012.

[38] X. Han and J. Pan, “A model for simultaneous crystallisation and biodegradation of biodegradable polymers,” *Biomaterials*, vol. 30, no. 3, pp. 423–430, 2009.

5 Modelling the Degradation and Crystallisation of Bioresorbable Polymeric Stents

5.1 Chapter Summary

The phenomenon of polymer crystallisation and the important role it has to play during the hydrolytic degradation of bioresorbable PLLA based devices is reviewed in **Chapter 2**. The integration of crystallinity equations into a robust finite element (FE) model for the analysis of material behaviour during polymer degradation provides an efficient means to examine the degradation induced crystallisation of bioresorbable polymers for the BPS application. Following on from the development of the FE material model presented in **Chapter 4**, the inclusion of governing equations for material crystallinity extends the developed material subroutine for use with semi-crystalline polymers.

This chapter presents an experimentally-validated implementation of a simplified version [1] of a previously published theory for polymer crystallinity [2] into Abaqus/Standard (Section 5.2). The addition of an enhanced description of polymer diffusion in the UMATHT analogy allows for the practical analysis of the diffusion of degradation products in semi-crystalline polymers. Analysis of the degradation and crystallisation behaviour of various BPS geometries is performed (Section 5.3), with the predictions for crystallinity, material molecular weight and oligomer flux from the stent examined and discussed in Sections 5.4 to 5.6.

Chapter 5

5.1 Introduction

The successful implementation of bioresorbable polymers for the BPS application revolves around an accurate understanding of the polymer material's degradation behaviour, and the impact that this has on the stents in-vivo performance. For BPS, existing physio-chemical models of polymer degradation very often don't consider the influence of degradation on the mechanical response of the device [3]. Of the bioresorbable polymers utilized in the BPS application, the thermoplastic poly-lactide, PLA and its co-polymers, poly-L-lactide (PLLA), poly-D-lactide (PDLA) and poly-D,L-lactide (PDLLA), are by far the most common polyesters investigated for this application [4].

It has been well documented in the literature that polyesters such as PLLA experience changes in crystallinity during the hydrolytic degradation process [5]–[8], and that such microstructure effects play a significant role in the changing mechanical properties observed for these materials [6], [8]–[10]. Such changes in the degree of polymer crystallinity are a key consideration in the analysis and design of BPS. A computational modelling framework which enables predictions of the precise microstructure changes occurring in a degrading BPS, alongside the resulting impact on its mechanical integrity and scaffolding ability is of significant interest to the community and for future device developments. The previous work presented in this thesis detailed the implementation of a physio-chemical degradation model [11] into the FE software package Abaqus/Standard, allowing for predictions in the degradation rates of various BPS to be made [12]. To further expand on this framework, the governing equations of the simplified polymer crystallinity theory outlined in **Chapter 3** are now included in the Abaqus material model. The effects of strut thickness and applied boundary conditions on the

molecular weight and crystallisation response of BPS under simulated degradation conditions are examined.

5.2 Polymer degradation including effects of crystallinity

The simplified theory outlined in **Chapter 3** (Section 3.2.2) for polymer crystallisation [1] is found to be efficient in describing the key events of polymer crystallinity, and it has previously been proven capable in capturing observed experimental crystallinity and molecular weight trends [1], [13]. In this chapter, an Abaqus/Standard model implementation of the crystallinity equations (Section 3.2.2) is verified against previous simplified model predictions [1], against a semi-analytical (MATLAB) solution, and against experimental data for PLLA [13], [14]. The model variables for the theory outlined in **Chapter 3** are shown in **Table 5.1**, along with their initial conditions.

Table 5.1 Model variables and their initial values.

Description	Symbol	Initial Value	Units
Molar number of chain-scissions per unit volume	R_s	0	[mol/m^3]
Molar concentration of ester bonds	C_e	$C_{e0}(1-X_{c0})$, $[C_{e0}=17300]$	[mol/m^3]
Molar concentration of all the chain units of oligomers available for diffusion	C_{ol}	0	[mol/m^3]
Molar concentration of all the chain units of oligomers produced through chain scission	R_{ol}	0	[mol/m^3]
Degree of crystallinity	X_c	X_{c0}	-
Extended degree of crystallinity	X_{ext}	0	-

5.2.1 Verification of UMATHT predictions

To verify the implemented UMATHT model, Abaqus/Standard simulations are run on a single element cube, with an assumed oligomer flux of zero acting on all surfaces. Hence, no diffusion will occur and these results can be compared to the solutions of [1] and also to the semi-analytical MATLAB solutions to the governing ODEs. As discussed in **Chapter 3**, the model governing differential equations for crystallinity are solved using a direct Euler scheme for the time integration solution of the model variables. For completeness, the experimental degradation data [14] referenced by the predictions of [1] is also shown (**Figure 5.1**). The Arrhenius relation is used to represent the temperature dependant parameters of the implemented crystallinity model, k_1, k_2 and X_{max} ,for each temperature case [15]

$$k_1 = k_{10}e^{-\frac{E_{k1}}{RT}} \qquad k_2 = k_{20}e^{-\frac{E_{K2}}{RT}} \qquad X_{max} = X_{max0}e^{-\frac{E_{Xmax}}{RT}} \qquad (5.1)$$

where $T\ (K)$ is the absolute temperature and $R\ (kJK^{-1}mol^{-1})$ is the universal gas constant. Model parameters from Eq. (5.1) and for the crystallinity equations (Section 3.2.2 in **Chapter 3**) are as reported in **Table 5.2** [1].

As shown in **Figure 5.1**, the UMATHT predictions show an excellent match to both the semi-analytical and the original predictions for the simplified crystallinity model. Total R^2 values of 0.90, 0.91 and 0.89 were given for the UMATHT predictions for each temperature case respectively.

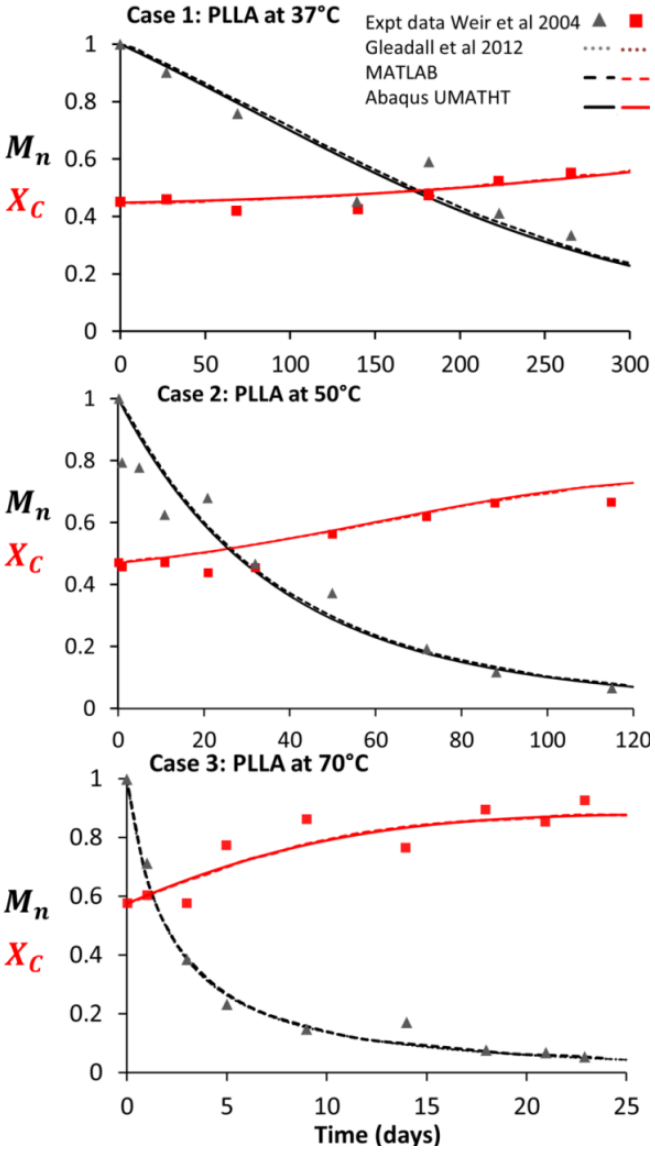

Figure 5.1 Verification of the Abaqus/Standard model simulations (solid lines) was carried out against simplified model predictions of [1] (dotted lines). The Abaqus implementation and a semi-analytical MATLAB solution (dashed line) are also validated for the experimental data of Weir *et al*. (2004) [14] (discrete symbols) from three different degradation scenarios, labelled Case 1-3.

Table 5.2 Fixed parameters in the crystallinity model and their values

Description	Symbol	Value	Units
Pre-exponential constant for reaction rate (k_1)	k_{10}	6.0 E18	[/day]
Pre-exponential constant for reaction rate (k_2)	k_{20}	7.0 E7	[/day]
Pre-exponential constant for maximum crystallinity (X_{max})	X_{max0}	12.2	-
Activation energy for reaction rate (k_1)	E_{k1}	145	[kJ/mol]
Activation energy for reaction rate (k_2)	E_{k2}	75	[kJ/mol]
Activation energy for maximum crystallinity (X_{max})	E_{Xmax}	7.5	[kJ/mol]
Inverse molar volume of the crystalline phase	ω	17300	[mol/m^3]
Probability of crystal being created following chain scission	P_x	0.01	-
Finite volume of crystal growth	V_c	4.19 E-24	[m^3]
Empirical parameter	α	28	-
Empirical parameter	β	2	-
Molar mass of lactic acid	M_0	72	[g/mol]
Average number of repeating oligomer units	m	4	-
Initial molar concentration of polymer chains	$N_{chains0}$	**37°C** 7.85 **50°C** 7.50 **70°C** 7.50	[mol/m^3]
Initial degree of crystallinity	X_{c0}	**37°C** 0.448 **50°C** 0.470 **70°C** 0.575	-

5.2.2 Recalibration of the model parameters for updated diffusion model

Han and co-workers [15] have previously validated a diffusion theory (described in Section 3.2.3 in **Chapter 3**) for PLLA against experimental data for material flux [14]. In summary, oligomer diffusion is assumed to occur at a much faster rate in the liquid filled pores than in the polymer matrix (ratio of $\frac{D_{pore}}{D_a} = 1000$) [15]. The fit of parameters by Han *et al*. [15] was completed using more complex crystallisation theory, incorporating Avrami's differential and integrational equations. Here, a simplified version of this theory is used (as described in **Chapter 3**); therefore, it is necessary to fit new parameters for PLLA at 37°C. As shown in **Figure 5.2**(a), a thin film (representative of the 0.8 mm PLLA samples examined in the experimental work) is simulated, with a finite element mesh of quadratic heat transfer brick elements (DC3D20).

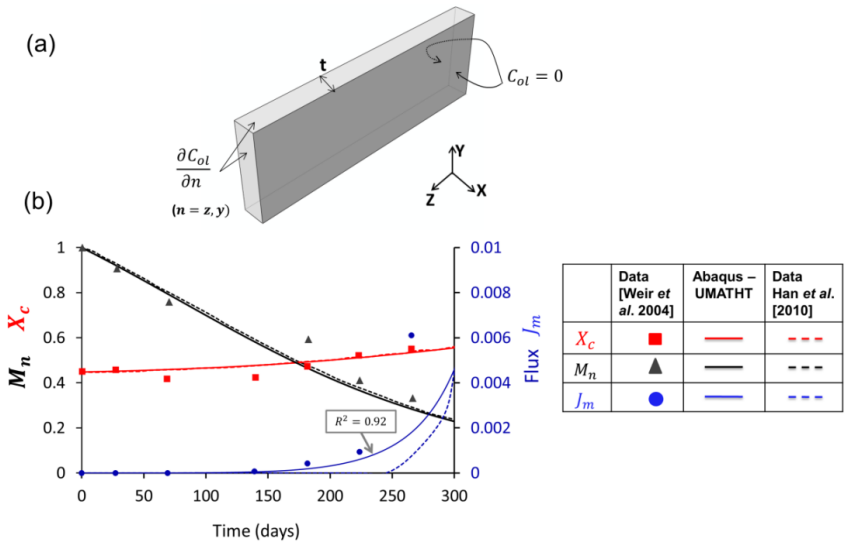

Figure 5.2 A FE model (a) of a thin plate (t =0.8 mm) was simulated to represent the PLLA samples examined in [14]. Mesh density was increased across the plate thickness, the direction for assumed diffusion of oligomers. Perfect sink boundary conditions were applied to the outer surfaces of the plate ($C_{ol} = 0$). For the Abaqus/UMATHT predictions ((b), solid lines), rate and diffusion parameters were calibrated for PLLA at 37°C, to obtain the fit shown to the experimental data [14] ((b), discrete symbols). Abaqus/UMATHT predictions had a R^2 coefficient of correlation of 0.92 to the experimental weight loss data, and capture the experimental trend observed more closely than previous predictions [15] ((b), dashed lines).

It is assumed that any oligomers arriving at the free edge of the plate are removed (i.e. perfect sink boundary conditions for C_{ol} are assigned at the boundary layers at the front and back surfaces of the plate, as depicted in **Figure 5.2**(a)). For completeness, the equations governing the effective diffusion parameter are given here again in Eq. (5.2) – Eq. (5.4).

$$D = D_a\{D_{matrix} + (1.3p^2 - 0.3p^3)\big(D_{pore} - D_{matrix}\big)\} \tag{5.2}$$

$$D_{matrix} = \left[1.3\left(\frac{\bar{C}_{ol} + \bar{C}_e}{\bar{C}_{ol} + \bar{C}_e + \frac{X_c}{1 - X_{c0}}}\right)^2 - 0.3\left(\frac{\bar{C}_{ol} + \bar{C}_e}{\bar{C}_{ol} + \bar{C}_e + \frac{X_c}{1 - X_{c0}}}\right)^3\right] \tag{5.3}$$

$$p = 1 - \{(\bar{C}_{ol} + \bar{C}_e)(1 - X_{c0}) + X_c\} \tag{5.4}$$

An iterative parameter optimisation is performed (using the Abaqus scripting interface, Python, and MATLAB R2013b) to fit the new rate parameters for PLLA at 37°C (shown in **Table 5.3**). This optimisation of k_1 and k_2 supersedes the values of k_{10}, E_{k1}, k_{20}, and E_{k2} above in **Table 5.2** according to Eq. (5.1) as temperature dependent data was not available to fully fit the Arrhenius parameters. All other model parameters are as reported in **Table 5.2**. A final coefficient of determination, R^2, of 0.92 is obtained for the fit to the flux data (i.e. the magnitude of the molar flux, J_m **Figure 5.2**(b)).

Table 5.3 Parameters used in the fitting of the reaction rate and diffusion constants for the simplified crystallinity and diffusion theory implementation

Description	Symbol	Value	Units
Diffusion coefficient	D_a	8.69E-09	[m^2/day]
Reaction rate constant for hydrolysis	k_1	2.28E-06	[/day]
Reaction rate constant for autocatalysis	k_2	2.20E-05	[$\sqrt{\frac{m^3}{mol}}$/day]

5.3 3D application of Crystallinity Model

Once the FE model had been validated and calibrated for PLLA at 37°C, investigations into the degradation and crystallisation behaviour of bioresorbable PLLA stents are performed using Abaqus/Standard. **Figure 5.3**(c) shows the single stent unit which was investigated in the computational study. This unit was chosen to be representative of an open-cell stent geometry modelled in its deployed state (**Figure 5.3**(a)).

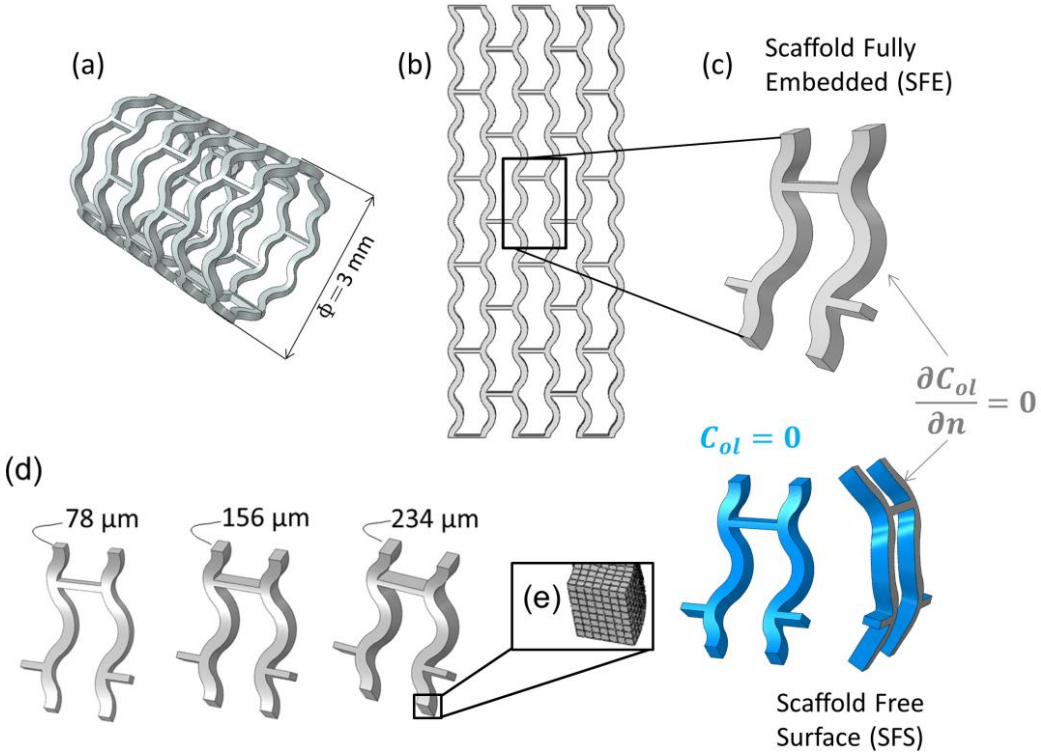

Figure 5.3 A representative unit cell (b) of a generic BPS geometry (deployed to 3 mm) (a) is modelled. The effects of strut size are investigated, with strut thicknesses of 78, 156 and 234 µm modelled (as shown in (d)). Boundary conditions for a stent fully embedded (SFE) ($\frac{\partial C_{ol}}{\partial n} = 0$ every surface) and a stent free surface (SFS) case ($C_{ol} = 0$ on highlighted faces, $\frac{\partial C_{ol}}{\partial n} = 0$ on outer surface) are shown in (c). The FE mesh is shown in insert (e).

A finite element mesh comprising of quadratic heat transfer brick (DC3D20) elements is created, with the mesh density targeted across the width of the stent strut such that each stent has 8 elements across the width of its strut each time (**Figure 5.3**(e)). The effects of strut thickness on the degradation rates of the stent are investigated for three different strut thicknesses (78 µm, 156 µm and 234 µm), as highlighted in **Figure 5.3**(d). The effects of imposed oligomer boundary condition on BPS degradation and crystallisation are also examined by considering two extreme boundary condition assumptions (**Figure 5.3**(c)). In the first instance, the stent fully embedded (SFE) case, the stent is assumed to be fully embedded in neo-intimal tissue following a period of implantation in an artery. Each of the stent surfaces are designated as impermeable surfaces i.e. a zero diffusive flux ($\frac{\partial C_{ol}}{\partial n} = 0$) is applied to each

surface, similar to the approach employed by Ferdous *et al*. in their examination of PLLA stents [16]. Use of this boundary condition assumes that the degradation products formed are unlikely to be immediately washed away by in-vivo blood flow, but would instead be contained on the stent surfaces. For the second boundary condition assumption (stent free surface (SFS)), no oligomers are permitted to remain on the stent's inner surfaces ($C_{ol} = 0$ at the inner surfaces, as highlighted). Any oligomers formed on theses surfaces through degradation are assumed to be swept away by the physiological actions of blood flow. The remaining stent surface is assumed to be impermeable, representing a BPS immediately post-implantation into an artery; where only the oligomers produced at the outer surfaces, in contact with the artery, could provide any possible contribution to autocatalysis reactions. Degradation and crystallisation are simulated for 52 weeks (approximately 1 year) and the resulting average molecular weight and degree of crystallinity of the stent unit in each case are examined. The flux behaviour of degradation products on the surface of the stent in each case is also examined.

5.4 Degradation and Crystallisation of BPS

The normalised M_n and degree of crystallinity, X_c, predicted for the various BPS cases investigated are shown in **Figure 5.4**. Contour plots which highlight the locations of the highest M_n and X_c for the case of the 156 μm stent under each boundary condition assumption (fully embedded (SFE); free surface (SFS)) are shown. A uniform M_n is predicted for the SFE case after 52 weeks, whereas predictions following the application of a free surface (SFS) show a noticeable gradient in the M_n (**Figure 5.4**(a)).

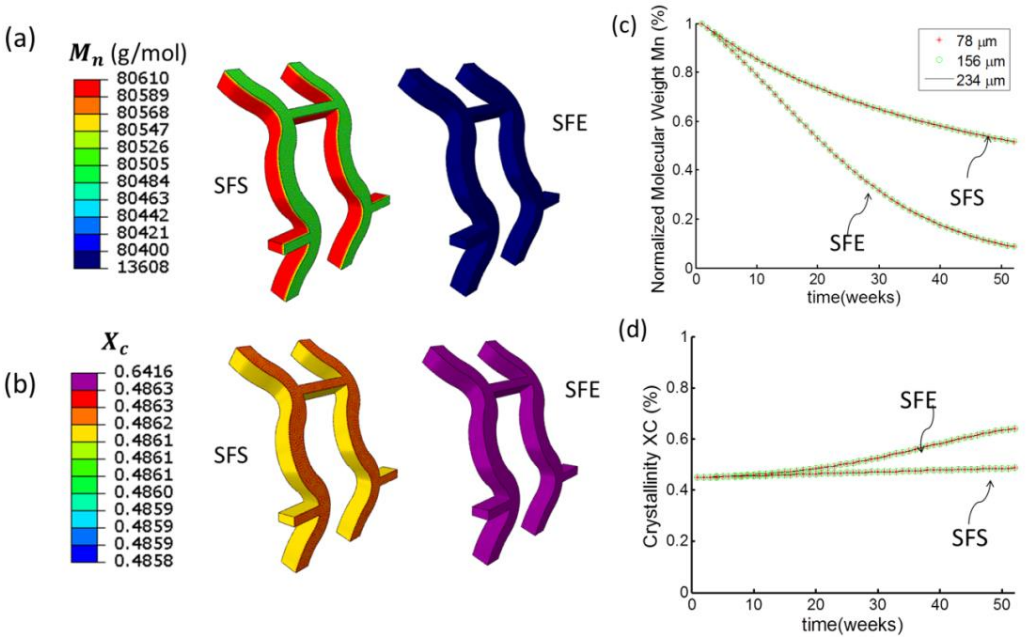

Figure 5.4 The set of contour plots shown in (a) and (b) highlight the differences in predicted values for the case of the 156 µm stent under different boundary condition assumptions. The impact of assumed boundary condition on the predictions for normalised $\mathrm{M_n}$ (c) and $\mathrm{X_c}$ (d) for all of the stents investigated is also depicted. The normalised $\mathrm{M_n}$ of each thickness investigated decreases at a sharper rate in the case of the fully embedded stent than for the free surface condition (c), with a more extreme change in $\mathrm{X_c}$ also observed for the fully embedded case (d).

Predicted values range between 50.7% and 49.8% of the initial M_n (calculated as 158675 g/mol). Similar gradients were predicted for each of the strut thicknesses investigated under the free surface boundary condition. For the SFE, a rapid decrease in the normalised M_n is observed after 1 year of simulated degradation (**Figure 5.4**(a)). This decrease occurs alongside an almost 20% increase in material crystallinity, X_c, as shown in **Figure 5.4**(b).

There was a minimal increase in X_c for the stents modelled with a free surface, with a slight gradient depicted; a maximum X_c of 0.4863 is observed at the outer surface of the stent (**Figure 5.4**(b)). As depicted by the graphs shown in **Figure 5.4**(c)-(d), there is no observed difference in predicted normalised M_n or X_c between the three strut thicknesses investigated. For the SFS cases, values of normalised M_n close to 50% were given for the three strut thickness following the simulated degradation period of 52 weeks, with the more rapid

decrease in normalised M_n (to < 20%) again apparent for the SFE investigations (**Figure 5.4**(c)).

The predicted magnitude of the molar flux (J_m) of the material degradation products from the surface of the stent unit in each case is shown in **Figure 5.5** for the SFS simulations.

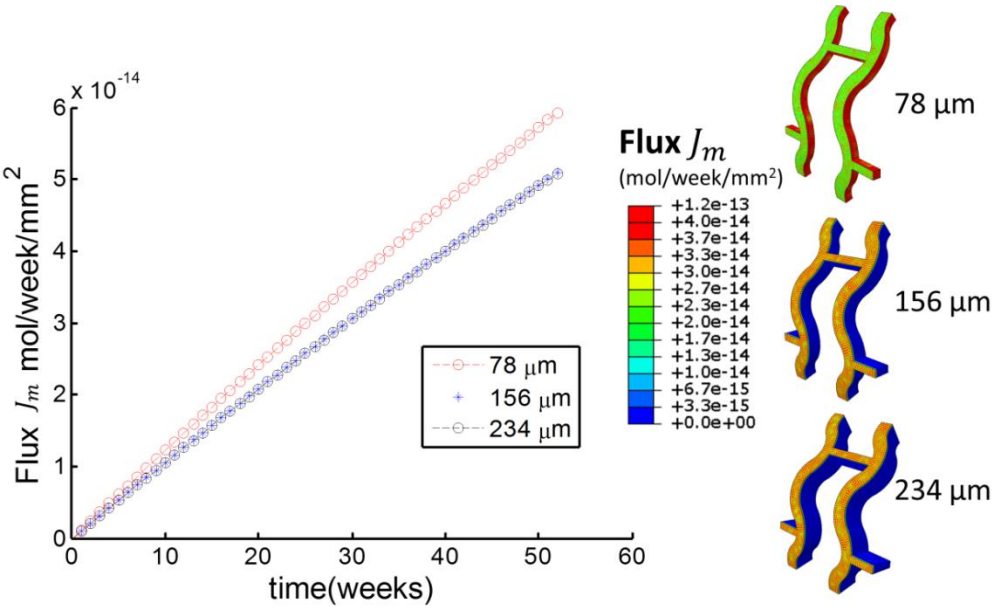

Figure 5.5 The magnitude of molar flux J_m of the material degradation products is plotted for the different thicknesses (78 µm, 156 µm, 234 µm) alongside contour plots which show the location of the maximum J_m. The results shown are for the SFS simulations.

The molar flux of degradation products when SFE is assumed is zero, since all of the oligomers formed through degradation are trapped within the stent. The high flux at the outer surface of the stent units under SFS is highlighted; with the 78 um stent showing slightly a higher flux than the other two cases (for which the predicted molar flux behaviour is very similar).

5.5 Degradation during neo-intimal growth

As a significant finding of the work presented here is the influence that the imposed boundary conditions have on the predicted M_n and X_c trends of the

implanted BPS; these boundary conditions were more closely examined for the case of a representative stent strut (cube of material) (**Figure 5.6**).

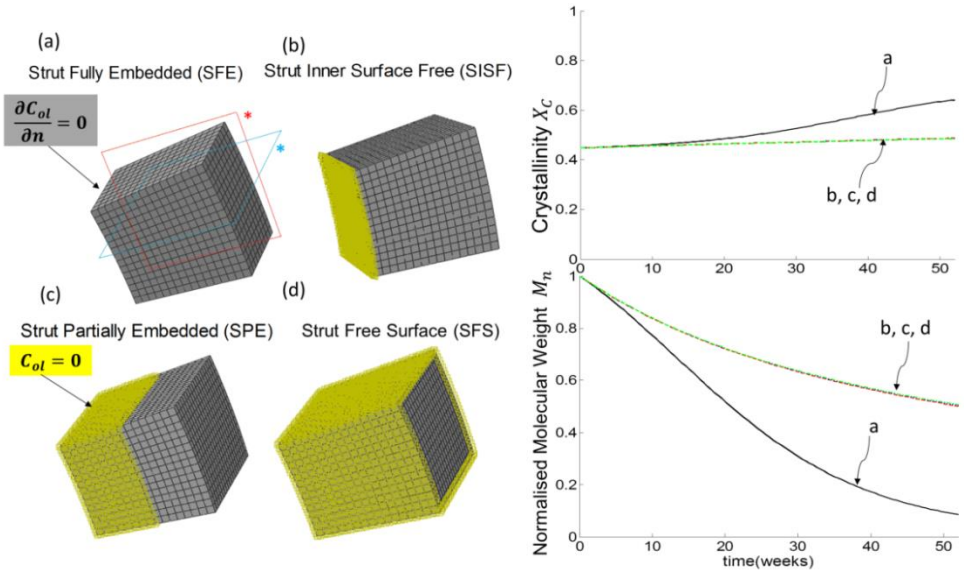

Figure 5.6 A cube of material representing a BPS strut was investigated for four different boundary conditions (a)-(d) as shown on the left. Predictions for the average M_n and X_c of the strut following 52 weeks of simulated degradation are shown on the right. Two planes (as highlighted by the red and blue asterisks) are shown in (a) which reference the location of the cut views shown in **Figure 5.7** below.

Degradation and crystallisation are simulated under four different boundary conditions; strut fully embedded (SFE), strut inner surface free (SISF), strut partially embedded (SPE) and strut free surface (SFS), as shown in **Figure 5.6**. It is found through this investigation that inclusion of a oligomer diffusion condition at any surface of the strut decreases the autocatalysis effect observed for the PLLA material. The predictions for the fully embedded (SFE) case (a) exhibit significantly faster degradations trends than all the other cases ((b)-strut inner surface free (SIFS), (c)-strut partially embedded (SPE) and (d)-strut free surface (SFS)) for which there was no noticeable difference between the predictions for M_n and X_c.

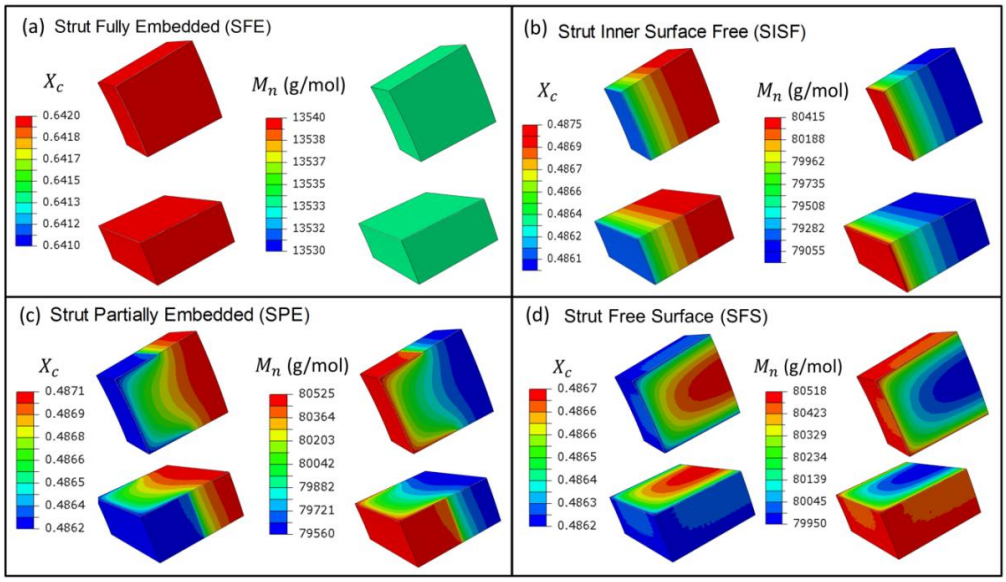

Figure 5.7 Contour plots comparing the predictions of X_c and M_n in the BPS strut (from the previous figure) under the four different boundary conditions investigated are shown. The BPS strut is cut along the two planes (depicted in Figure 5.6 (a)) to give the detailed view of the predictions presented here. The locations of the maximum X_c and M_n are highlighted for the simulations where a degradation product free surface is applied (i.e. cases (b), (c) and (d)).

Contour plots of the crystallinity and molecular weight trends predicted in the representative cube are shown in **Figure 5.7** . The impact of the free surface condition for each of the cases where it is applied to the cube is evident in the presented plots. A maximum X_c of 0.64 is predicted for the fully embedded case (**Figure 5.7** (a)), with the zero flux model also showing the greatest decrease in M_n; final value of predicted M_n reaches 13540 g/mol for the fully embedded cube, and which is constant throughout the cube. A slight gradient in X_C and M_n is depicted for cases (b)-(d), with predicted values for M_n between 80525 g/mol and 79055 g/mol, and X_c ranging from 0.4.875 and 0.4862.

5.6 Discussion

The use of BPS on the global market as a treatment for coronary artery disease has so far been hindered by the high rates of device thrombosis reported at long-term follow up in a number of clinical trials [17], [18]. Such

poor results may be due in part to an inadequate understanding of how exactly BPS degrade within the body, and how the in-vivo environment impacts on and influences this. The application of computational modelling techniques to examine the degradation mechanisms of BPS represents a favourable approach to predict their in-vivo response, and as such computational studies present a key aid to the design and analysis of these devices in their pre-clinical development and testing.

5.6.1 Summary

In the presented work, physio-chemical equations governing polymer degradation and crystallinity behaviour are implemented into FE software through use of a thermal analogy. Building on the work in **Chapter 4**, the computational framework, which uses a thermal analogy to solve the diffusion reaction equations by representing them as the heat equations, is further developed to model a semi-crystalline BPS material, in this case PLLA. The degradation behaviours of a number of BPS geometries under a range of boundary conditions are investigated and a number of key findings related to boundary condition, device thickness and flux of the material leading to material weight loss are revealed.

5.6.2 Impact of polymer crystallinity on degradation rates

In the current work, the inclusion of crystallinity in the model provides further insight into material degradation in a BPS. The impact of X_c on the degradation rates predicted here for BPS is evident when the trends for M_n decrease shown in **Figure 5.4** are compared to those of the previously presented model implementation (**Chapter 4**); predications for M_n show more gradual rates of reduction when material crystallinity is included in the physio-chemical model. As widely reported in the literature, PLLA (a semi-crystalline

polyester) undergoes significant changes in microstructure during the hydrolytic degradation process [5], [7], [8]. Chain scission-induced realignment of polymer chains leads to an increase in the degree of crystallinity, X_c, which along with a corresponding decrease in the amorphous phase of the polymer, is believed to restrict water diffusion into the polymer matrix and reduce the rate of degradation [19]. Thus, the prediction of evolving crystallinity is a key requirement for accurate simulation of BPS degradation.

Along with the expected increased resistance to hydrolysis, formation of tough crystalline regions of higher atomic energies also impacts on the materials mechanical behaviour (as reviewed in **Chapter 2** for the BPS application). A number of experimental investigations into PLLA degradation have reported an increase in the material stiffness during the early stages of degradation [6], [8], [14], [20]–[22]. Investigating the impact of X_c on the mechanical behaviour of PLLA based BPS forms part of the key focus of **Chapter 6**.

5.6.3 Diffusion behaviour in semi-crystalline polymers

Understanding the diffusion behaviour of degradation products in-vivo is needed for the design of bioresorbable polymeric devices, due to both the autocatalytic nature of polymer degradation products, and the anti-inflammatory response that they may impart in-vivo [23]–[25]. Here, physio-chemical equations governing degradation product diffusion in semi-crystalline polymers [2], [15] are implemented alongside the simplified theory for polymer crystallinity [1] to study the in-vivo performance of BPS. Inclusion of the enhanced diffusion theory requires the calibration of rate constants for PLLA. The resulting fit of the Abaqus model's prediction (R^2=0.92) of degradation product flux is shown in **Figure 5.2**. The use of a multifunctional FE framework, such as the Abaqus/Standard implementation here, to

computationally examine BPS degradation presents further possibilities to simulate diffusion of degradation products into the surrounding vessel [26] and to further explore the implications of surface and bulk degradation mechanisms.

5.6.4 Boundary condition assumptions

The predictions of BPS degradation presented in this chapter exhibit a considerable dependency on the assumed degradation product boundary conditions. Similarly to the findings of **Chapter 4**, model predictions of M_n remaining in the fully embedded (SFE) stent after 52 weeks of simulated degradation show a more rapid decrease when compared to predictions for the free surface (SFS) case (**Figure 5.4**(a),(c)). The degree of crystallinity, X_c, predicted for the various stents displays a comparable dependency on applied boundary condition (**Figure 5.4**(b),(d)), with greater increases in X_c observed for the SFE cases compared to SFS. Slight gradients in M_n and X_c are detected throughout the stent in the SFS simulations; with the most noticeable effect observed at the boundary layers of the device (where the degradation product free surfaces are assigned). Closer examination of the degradation product boundary conditions (for the case of a representative BPS strut, **Figure 5.6**) highlighted the dominance of degradation product diffusion from assigned free surfaces over the autocatalytic effect (accelerated degradation observed only in the fully embedded case).

Such observed differences in degradation rate and crystallinity behaviour can be attributed to the autocatalytic nature of PLLA degradation [19], [27]–[29]. In the presented modelling simulations, degradation products are assumed to either (i) remain trapped on the surface of the device (due to the formation of

neo-intimal tissue and stent encapsulation) and act to accelerate degradation reactions or (ii) experience immediate eradication from the designated free surfaces (such that their potential contribution to the degradation reaction is removed).

An enhanced understanding of the formation of neo-intimal tissue and the tissue remodelling process during both the acute and late stages of BPS implantation would enable further improvements in physio-chemical modelling techniques for BPS degradation, perhaps through the inclusion of time variant boundary conditions. Advanced imaging techniques, for example intravascular ultrasound (IVUS) [30] and intracoronary optical coherence tomography (OCT) [31]–[33], have emerged as important tools in the in-vivo analysis of BPS [34]. Such techniques allow for the acquisition of essential data on BPS apposition [35], neo-intimal growth [36], and the effect of degradation behaviour on the vessel wall immediately after implantation and at intermittent follow-up times [37], [38]. The high dependency of PLLA material degradation on residual degradation products highlights the need for the development of more realistic models to describe the tissue remodelling and stent encapsulation processes, similar to those which have been developed for resorbable magnesium stents [39], [40].

5.6.5 Strut thickness and geometry

Polymeric stents are often manufactured with much thicker struts than their permanent metallic counterparts, due to the lower mechanical properties of PLLA and other aliphatic polyesters compared to metals [41]. However, thinner stent struts are desirable as they lead to more flexible devices along with a reduction in its cross sectional profile [42], both of which have beneficial consequences on localised blood flow and the endothelial shear stresses

experienced in-vivo [42]–[44]. The extensively investigated Absorb BVS has a strut thickness in the 150 μm range and it is believed that efforts are underway to develop the next generation BVS with sub-100 μm struts [45]. Strut thickness values within this range were investigated using the modelling techniques developed in this chapter, and predictions of the physio-chemical degradation model are compared. Simulation predictions indicate that changing the strut thickness has little influence on the M_n or X_c in the stent (**Figure 5.4**). This is in agreement with the findings reported in **Chapter 4**, for the earlier model implementation, where it is observed that the device thicknesses investigated must fall within the range of a characteristic diffusion length for a noticeable impact on the degradation rates. It has been widely noted in the literature that strut thickness has a large bearing on the in-vivo performance of the device [42], [43], [46], [47]; therefore, it is practical in this work to consider BPS of various thicknesses in pre-clinical device examination.

Earlier degradation simulations are performed for whole BPS geometries (**Chapter 4**). However, modelling of a full BPS geometry is computationally expensive, and it is found that simulating degradation of a unit cell geometry compared to a full stent resulted in a less than 1% difference in predicted values. Therefore, simulations presented here were carried out for representative stent units (as shown in **Figure 5.2**). The full effects of BPS deployment on its final configuration (e.g. dogboning, resultant flared ends [48]) are not considered for the strut unit examined here; however due to the small dependence on geometry observed for the model predictions in M_n and X_c inclusion of end effects is not expected to be significant.

5.6.6 Modelling limitations/future perspective

The main focus of this chapter was to present the successful implementation of polymer crystallinity theory and evaluate the impact of imposed boundary condition and strut thickness on M_n, X_c and flux, J, predictions for representative BPS. In general, computational modelling of BPS has been undertaken with a focus on the damage based evolution of the material's mechanical properties, with few studies considering the innate microstructural changes which occur in the degrading polymer material [3]. Some of the recent computational studies to examine the effect of degradation on the mechanical properties of a BPS include [49], [50], and [51]. While such studies provide valuable insight into the changes in the load bearing capacity of implanted BPS, and also into the mechanical response of arteries due to BPS implantation, the physio-chemical aspects of the stent degradation are neglected. Modelling frameworks which can adequately capture the key chemical and microstructural changes involved in polyester degradation provide opportunities to gain an enhanced insight into how such devices behave in a clinical setting. Coupling the impact of the physio-chemical model implementation presented here with PLLA mechanical behaviour and examining the clinical effects for BPS makes up the focus of the work presented in **Chapter 6**.

5.7 Conclusion

In conclusion, this chapter presents a computational investigation into the degradation and crystallinity behaviour of the aliphatic polyester material, PLLA, for its use in the BPS application. Representative BPS geometries are simulated in Abaqus/Standard, and the influence of stent thickness on the degradation in M_n and the increase in X_c predicted for examined devices is

revealed to be minor. The extreme boundary condition assumptions considered in this work provide insight into the importance of the fate of the degradation products for BPS composed of bioresorbable aliphatic polyesters in particular. Changing rates of X_c are influenced by the assumed degradation product boundary conditions. The crystallisation of BPS plays a key role in their degradation behaviours and on the resulting in-vivo performance, in particular on the material's mechanical performance (as examined in **Chapter 6**).

References

[1] A. Gleadall, J. Pan, and H. Atkinson, “A simplified theory of crystallisation induced by polymer chain scissions for biodegradable polyesters,” *Polym. Degrad. Stab.*, vol. 97, no. 9, pp. 1616–1620, 2012.

[2] X. Han and J. Pan, “A model for simultaneous crystallisation and biodegradation of biodegradable polymers,” *Biomaterials*, vol. 30, no. 3, pp. 423–430, 2009.

[3] E. L. Boland, R. Shine, N. Kelly, C. A. Sweeney, and P. E. McHugh, “A Review of Material Degradation Modelling for the Analysis and Design of Bioabsorbable Stents,” *Ann. Biomed. Eng.*, vol. 44, no. 2, pp. 341–356, 2015.

[4] S. McMahon *et al.*, “Bio-resorbable polymer stents: a review of material progress and prospects,” *Prog. Polym. Sci.*, vol. 83, pp. 79–96, 2018.

[5] X. H. Zong *et al.*, “Structure and morphology changes in absorbable poly(glycolide) and poly(glycolide-co-lactide) during in vitro degradation,” *Macromolecules*, vol. 32, no. 24, pp. 8107–8114, 1999.

[6] E. A. R. Duek, C. A. C. Zavaglia, and W. D. Belangero, “In vitro study of poly(lactic acid) pin degradation,” *Polymer (Guildf).*, vol. 40, no. 23, pp. 6465–6473, 1999.

[7] S. K. Saha and H. Tsuji, “Effects of rapid crystallization on hydrolytic degradation and mechanical properties of poly(l-lactide-co-ε-caprolactone),” *React. Funct. Polym.*, vol. 66, no. 11, pp. 1362–1372, 2006.

[8] H. Tsuji, A. Mizuno, and Y. Ikada, “Properties and Morphology of Poly (L -lactide). III . Effects of Initial Crystallinity on Long-Term In Vitro Hydrolysis of High Molecular Weight Poly (L -lactide) Film in Phosphate-Buffered Solution,” *J. Appl. Polym. Sci.*, pp. 1452–1464, 2000.

[9] X. Yuan, A. F. T. Mak, and K. Yao, “In vitro degradation of poly(L-lactic acid) fibers in phosphate buffered saline,” *J. Appl. Polym. Sci.*, vol. 85, no. 5, pp. 936–943, 2002.

[10] T. Karjalainen, M. Hiljanen-Vainio, M. Malin, and J. Seppälä, “Biodegradable lactone copolymers. III. Mechanical properties of ε-caprolactone and lactide copolymers after hydrolysis in vitro,” *J. Appl. Polym. Sci.*, vol. 59, no. 8, pp. 1299–1304, Feb. 1996.

[11] Y. Wang, J. Pan, X. Han, C. Sinka, and L. Ding, “A phenomenological model for the degradation of biodegradable polymers,” *Biomaterials*, vol. 29, no. 23, pp. 3393–3401, 2008.

[12] R. Shine *et al.*, “Modeling of Biodegradable Polyesters With Applications to Coronary Stents,” *J. Med. Device.*, vol. 11, no. 2, p. 021007, 2017.

[13] N. A. Weir, F. J. Buchanan, J. F. Orr, and G. R. Dickson, “Degradation of poly-L-lactide. Part 1: in vitro and in vivo physiological temperature degradation,” *Proc Inst Mech Eng H*, vol. 218, no. 5, pp. 307–319, 2004.

[14] N. A. Weir, F. J. Buchanan, J. F. Orr, D. F. Farrar, and G. R. Dickson, “Degradation of poly-L-lactide. Part 2: increased temperature accelerated degradation,” *Proc Inst Mech Eng H*, vol. 218, no. 5, pp. 321–330, 2004.

[15] X. Han, J. Pan, F. Buchanan, N. Weir, and D. Farrar, “Analysis of degradation data of poly(l-lactide-co-l,d-lactide) and poly(l-lactide) obtained at elevated and

physiological temperatures using mathematical models," *Acta Biomater*, vol. 6, no. 10, pp. 3882–3889, 2010.

[16] J. Ferdous, V. B. Kolachalama, and T. Shazly, "Impact of polymer structure and composition on fully resorbable endovascular scaffold performance," *Acta Biomater.*, vol. 9, no. 4, pp. 6052–6061, 2013.

[17] D. Capodanno, "Bioresorbable scaffolds in coronary intervention: Unmet needs and evolution," *Korean Circ. J.*, vol. 48, no. 1, pp. 24–35, 2018.

[18] J. Wykrzykowska *et al.*, "Bioresorbable scaffolds versus metallic stents in routine PCI: the plot thickens," *J. Thorac. Dis.*, vol. 9, no. 8, pp. 2296–2300, 2017.

[19] F. Alexis, "Factors affecting the degradation and drug-release mechanism of poly(lactic acid) and poly[(lactic acid)-co-(glycolic acid)]," *Polym. Int.*, vol. 54, no. 1, pp. 36–46, 2005.

[20] H. Tsuji, "Properties and morphologies of poly(L-lactide): 1. Annealing condition effects on properties and morphologies of poly(L-lactide)," *Polymer (Guildf).*, vol. 36, no. 14, pp. 2709–2716, 1995.

[21] K. J. L. Burg, M. LaBerge, and S. W. Shalaby, "Change in stiffnesss and effect of orientation in degrading polylactide films," *Biomaterials*, vol. 19, no. 7–9, pp. 785–789, 1998.

[22] M. L. Dreher, S. Nagaraja, and B. Batchelor, "Effects of fatigue on the chemical and mechanical degradation of model stent sub-units," *J. Mech. Behav. Biomed. Mater.*, vol. 59, pp. 139–145, 2016.

[23] H. Il Kim *et al.*, "Tissue response to poly(l-lactic acid)-based blend with phospholipid polymer for biodegradable cardiovascular stents," *Biomaterials*, vol. 32, no. 9, pp. 2241–2247, 2011.

[24] J. E. Bergsma, W. C. de Bruijn, F. R. Rozema, R. R. . Bos, and G. Boering, "Late degradation tissue response to poly(L-lactide) bone plates and screws J.E.," *Biomaterials*, vol. 16, pp. 25–31, 1995.

[25] D. Chen *et al.*, "Effect of inflammation on endothelial cells induced by poly-L-lactic acid degradation in vitro and in vivo.," *J. Biomater. Sci. Polym. Ed.*, vol. 29, no. 15, pp. 1909–1919, Oct. 2018.

[26] W. J. Denny, B. M. O'Connell, J. Milroy, and M. T. Walsh, "An analysis of three dimensional diffusion in a representative arterial wall mass transport model," *Ann. Biomed. Eng.*, vol. 41, no. 5, pp. 1062–1073, 2013.

[27] A. Göpferich, "Mechanisms of polymer degradation and erosion," *Biomaterials*, vol. 17, no. 2, pp. 103–114, 1996.

[28] C. G. Pitt and G. Zhong-wei, "Modification of the rates of chain cleavage of poly(ϵ-caprolactone) and related polyesters in the solid state," *J. Control. Release*, vol. 4, no. 4, pp. 283–292, 1987.

[29] M. A. Tracy *et al.*, "Factors affecting the degradation rate of poly(lactide-co-glycolide) microspheres in vivo and in vitro," *Biomaterials*, vol. 20, no. 11, pp. 1057–1062, 1999.

[30] E. Strandberg, J. Zeltinger, D. G. Schulz, and G. L. Kaluza, "Late Positive Remodeling and Late Lumen Gain Contribute to Vascular Restoration by a Non-Drug Eluting Bioresorbable Scaffold," *Circ. Cardiovasc. Interv.*, vol. 5, no. 1, pp. 39–46, 2012.

[31] N. Gonzalo, P. W. Serruys, and E. Regar, “Optical coherence tomography: clinical applications and the evaluation of DES,” *Minerva Cardioangiol.*, vol. 56, no. 5, p. 511—525, 2008.

[32] N. Gonzalo *et al.*, “Reproducibility of quantitative optical coherence tomography for stent analysis.,” *EuroIntervention J. Eur. Collab. with Work. Gr. Interv. Cardiol. Eur. Soc. Cardiol.*, vol. 5, no. 2, pp. 224–232, Jun. 2009.

[33] T. Okamura, P. W. Serruys, and E. Regar, “The fate of bioresorbable struts located at a side branch ostium: serial three-dimensional optical coherence tomography assessment,” *Eur. Heart J.*, vol. 31, no. 17, p. 2179, May 2010.

[34] N. S. van Ditzhuijzen, J. M. R. Ligthart, N. Bruining, E. Regar, and H. M. M. van Beusekom, “Invasive imaging of bioresorbable coronary scaffolds - A review,” *Interv. Cardiol.*, vol. 8, no. 1, pp. 23–35, 2013.

[35] P. W. Serruys *et al.*, “A bioabsorbable everolimus-eluting coronary stent system (ABSORB): 2-year outcomes and results from multiple imaging methods.,” *Lancet*, vol. 373, no. 9667, pp. 897–910, Mar. 2009.

[36] J. Iqbal, “Amaranth Bioresorbable Scaffold - pre-clinical data,” in *PCR Focusgroup*, 2013.

[37] P. W. Serruys *et al.*, “Evaluation of the second generation of a bioresorbable everolimus-eluting vascular scaffold for the treatment of de novo coronary artery stenosis: 12-month clinical and imaging outcomes.,” *J. Am. Coll. Cardiol.*, vol. 58, no. 15, pp. 1578–1588, Oct. 2011.

[38] R. Diletti *et al.*, “ABSORB II randomized controlled trial: a clinical evaluation to compare the safety, efficacy, and performance of the Absorb everolimus-eluting bioresorbable vascular scaffold system against the XIENCE everolimus-eluting coronary stent system in the treatm,” *Am. Heart J.*, vol. 164, no. 5, pp. 654–663, Nov. 2012.

[39] E. L. Boland, J. A. Grogan, C. Conway, and P. E. McHugh, “Computer Simulation of the Mechanical Behaviour of Implanted Biodegradable Stents in a Remodelling Artery,” *Jom*, vol. 68, no. 4, pp. 1198–1203, 2016.

[40] E. L. Boland, J. A. Grogan, and P. E. McHugh, “Computational Modeling of the Mechanical Performance of a Magnesium Stent Undergoing Uniform and Pitting Corrosion in a Remodeling Artery,” *J. Med. Device.*, vol. 11, no. 2, p. 021013, 2017.

[41] S. Mishra, “A fresh look at bioresorbable scaffold technology: Intuition pumps,” *Indian Heart J.*, vol. 69, no. 1, pp. 107–111, 2017.

[42] K. Kolandaivelu *et al.*, “Stent thrombogenicity early in high-risk interventional settings is driven by stent design and deployment and protected by polymer-drug coatings.,” *Circulation*, vol. 123, no. 13, pp. 1400–1409, Apr. 2011.

[43] K. C. Koskinas, Y. S. Chatzizisis, A. P. Antoniadis, and G. D. Giannoglou, “Role of Endothelial Shear Stress in Stent Restenosis and Thrombosis: Pathophysiologic Mechanisms and Implications for Clinical Translation,” *J. Am. Coll. Cardiol.*, vol. 59, no. 15, pp. 1337–1349, 2012.

[44] E. Tenekecioglu *et al.*, “Strut protrusion and shape impact on endothelial shear stress: insights from pre-clinical study comparing Mirage and Absorb bioresorbable scaffolds,” *Int. J. Cardiovasc. Imaging*, vol. 33, no. 9, pp. 1313–1322, 2017.

[45] D. Regazzoli, P. P. Leone, A. Colombo, and A. Latib, “New generation

bioresorbable scaffold technologies: an update on novel devices and clinical results," *J. Thorac. Dis.*, vol. 9(Suppl 9), pp. S979–S985, 2017.

[46] A. Kastrati *et al.*, "Intracoronary stenting and angiographic results: strut thickness effect on restenosis outcome (ISAR-STEREO) trial.," *Circulation*, vol. 103, no. 23, pp. 2816–2821, Jun. 2001.

[47] T. Koppara *et al.*, "Thrombogenicity and early vascular healing response in metallic biodegradable polymer-based and fully bioabsorbable drug-eluting stents," *Circ. Cardiovasc. Interv.*, vol. 8, no. 6, pp. 1–9, 2015.

[48] A. Schiavone, T.-Y. Qiu, and L.-G. Zhao, "Crimping and deployment of metallic and polymeric stents -- finite element modelling," *Vessel Plus*, vol. 1, no. 1, pp. 12–21, 2017.

[49] J. S. Soares, J. E. Moore, and K. R. Rajagopal, "Modeling of deformation-accelerated breakdown of polylactic acid biodegradable stents," *J. Med. Device.*, vol. 4, no. 4, p. 41007, 2010.

[50] A. Muliana and K. R. Rajagopal, "Modeling the response of nonlinear viscoelastic biodegradable polymeric stents," *Int. J. Solids Struct.*, vol. 49, no. 7–8, pp. 989–1000, 2012.

[51] T. Qiu, R. He, C. Abunassar, S. Hossainy, and L. G. Zhao, "Effect of two-year degradation on mechanical interaction between a bioresorbable scaffold and blood vessel," *J. Mech. Behav. Biomed. Mater.*, vol. 78, no. November 2017, pp. 254–265, 2018.

6 Mechanical Performance of Degrading Bioresorbable Polymeric Stents

6.1 Chapter Summary

This chapter presents a computational modelling analysis of the mechanical performance of BPS during long-term degradation. This work builds on that presented in **Chapter 5** by directly linking the developed physio-chemical modelling techniques with constitutive equations for PLLA to examine the impact of physio-chemical degradation on the mechanical performance of PLLA based BPS under a range of loads and boundary conditions. The co-simulation modelling techniques detailed in Section 6.3 enable the dual analysis of polymer degradation and crystallisation, while also capturing the stress strain behaviour of degrading devices. Damage due to degradation is incorporated in the material as described in Section 6.3.2. Representative loading of BPS is achieved through the methods outlined in Section 6.3.3. Finally, the predictions of the simulations are summarised and discussed in Section's 6.4 and 6.5 respectively.

6.2 Introduction

Knowledge of the effects of material degradation on the mechanical integrity of bioresorbable polymeric stents (BPS) is needed to enable device designers to provide accurate predictions into how BPS would respond in the clinical environment. PLLA has emerged as a favourable candidate for BPS design [5], and while the hydrolytic degradation process of this material is well understood, an improved insight into how the physio-chemical degradation behaviour impacts the mechanical performance of PLLA based BPS would enable better device design and enhanced clinical outcomes.

The mechanical properties of PLLA for the BPS application have been investigated in a number of studies using computational techniques [1]–[8]. The effects of geometry and material stiffness on the radial strength and recoil characteristics of BPS were found to have a significant impact on short-term mechanical performance [1]. A similar influence of BPS design variations on the recoil behaviour of the device was also apparent in recent FEA investigations [8]. A slight dependency on expansion technique has also been observed for the stent's short-term mechanical performance (evaluated through stent recoil, dogboning effects) in [2], [3].

Incomplete expansion of a BPS, which also causes decreased vessel stress, has been reported in a study directly comparing the mechanical performance of BPS and metallic stents during crimping and deployment procedures [7]. The long-term fatigue performance of a commercial BPS under pulsatile blood pressure loading demonstrated a risk of fatigue failure at the U-bend regions of the BPS [6]. Other works have examined the long-term degradation dependant mechanical performance of PLLA based BPS, including that of Soares and co-workers [9] who examined the deformation and degradation of several stent designs using a phenomenological damage based model established within a thermodynamic framework [10]. This same framework was used to examine the degradation of a PLLA BPS, when an adaption of the quasi-linear viscoelastic model was used to represent the constitutive mechanical properties of the device, and where the damage variable accounted for the effects of water diffusion through the material [11]. More recently, Qiu *et al*. [12], presented a phenomenological model to capture the degradation behaviour of BPS and examine the mechanical interactions between the stent and a remodelling vessel over a two-year period [12]. Long-

term experimental measurements of radial stiffness and strength for a degrading BPS were used in the model development, and simulations on a geometry representative of the Absorb BVS were performed [12]. While such studies provide a valuable insight into the changing mechanical performance of degrading BPS, the direct impacts of decreasing polymer molecular weight, changes in crystallinity or degradation product diffusion on the long-term radial stiffness and scaffolding ability of BPS have yet to be determined. In this chapter the short and long-term mechanical performance of BPS are investigated for various loads, degradation product boundary conditions and material types.

6.3 Methods

6.3.1 Geometry and mesh generation

Simulated testing of BPS is carried out using Abaqus/Standard (Abaqus/Standard v6.13, Dassault Systems Simulia, RI, USA). Stents are modelled using representative unit geometries of a generic BPS device (Figure 6.1(a)-(c) shows the unwrapping (b) of a generic stent geometry (a) and the selection of the representative unit (c)). The stent unit is modelled in a deployed configuration (3.3 mm diameter).

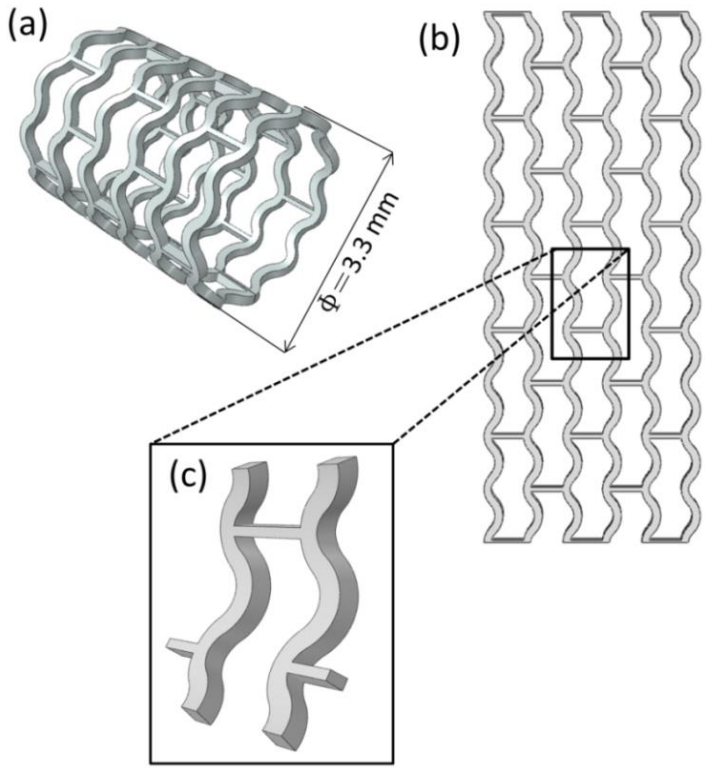

Figure 6.1 Finite element geometry of the BPS representative unit examined. A stent unit cell (c) is selected following the unwrapping (as shown in (b)) of a generic geometry of an expanded BPS geometry (depicted in (a), ϕ = 3.3 mm).

A representative artery geometry with an inner diameter of 3 mm is included in the simulations (for the purposes of applying load to the stent, as discussed below). The artery is modelled as a three layered structure, (**Figure 6.2**(a)) with reference given to the intima, media and adventitia. The thickness of each layer is as given by Holzapfel *et al*. [13], who performed a comprehensive analysis of the histology of coronary arteries in humans. Further details of vessel properties are discussed below.

The artery is meshed using 3D quadratic stress elements (C3D20H), while the BPS is meshed using quadratic coupled temperature-displacement reduced integration elements (C3D20HT). The mesh targeting for both parts is shown in **Figure 6.1**(b), with the mesh density targeted across the strut thickness of

the BPS (**Figure 6.1**(c)). The characteristic element length, l_e of the artery and the BPS are l_e = 0.05 mm and l_e = 0.02 mm respectively.

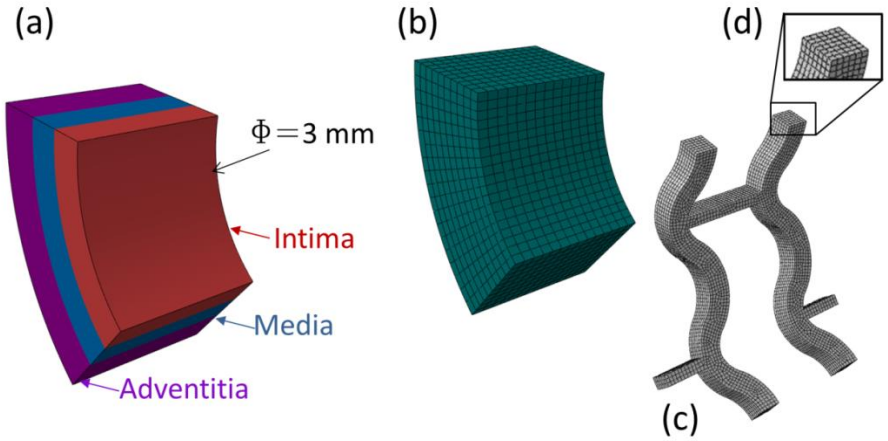

Figure 6.2 Finite element geometry of a representative three-layered artery (a) used to apply loading to the BPS in this study. The BPS is modelled as being deployed in the artery, which has an inner diameter of 3 mm. The mesh of the artery (b) and the deployed BPS (c) are also shown (insert (d) shows mesh density focused across the strut of the BPS).

6.3.2 Material properties

The BPS examined in this study are assigned material degradation properties representative of PLLA at 37°C. The degradation and crystallinity model used to examine the physio-chemical behaviour of the stents has been calibrated for PLLA at this temperature as described in **Chapter 5**. The calibrated material parameters and the remaining material constants for the model which describe the degradation, crystallinity and diffusion behaviours are as shown in **Chapter 5**.

The Knowles hyperelastic model [14] is used to represent the mechanical behaviour of PLLA in this work. The strain energy density potential, W_e, for this constitutive model is given by

$$W_e = \frac{\mu}{2b}\{\left[1 + \frac{b}{n_h}(I_3 - 3)\right]^{n_h} - 1\} \quad (6.1)$$

where μ is the material shear modulus, n_h is a hardening parameter, and b is an empirical constant (b and $n_h > 0$) [14]. As a thermoplastic polymer, PLLA experiences non-linear deformation behaviour at moderate strains [1], [11], [15], [16] and the Knowles model [14] has previously been shown to capture the behaviour of PLLA under isochoric uniaxial extension [17]. The BPS examined in this study are assumed to be fully incompressible [18], [19]. The user subroutine previously developed for representing material degradation and crystallinity (**Chapter 5**) is coupled with a previously published implementation [20] (Abaqus/Standard user material subroutine (UMAT)) of the Knowles model. This coupled UMAT & UMATHT subroutine captures the evolving mechanical behaviour during degradation.

A scalar degradation, or damage, variable, d, is introduced into the model to represent the extent of physio-chemical degradation in the polymer material. Degradation, or damage, is assigned a minimum value of $d = 0$ for an undegraded, undamaged material and a maximum of $d = 1$ for a fully degraded specimen. The degradation variable is initially defined based on the decreasing molecular weight of the material, M_w as shown in **Table 6.1** and Eq. (6.2). In this instance, M_w is assumed to be directly related to the concentration of ester bond linkages remaining in the polymer, C_e, and their initial concentration, C_{e0} (i.e. model does not directly predict M_w). In this first instance (Model 1, **Table 6.1**), the equations governing M_w generation are as described in **Chapter 3** and previously shown in [21] for the original degradation model (i.e. without crystallinity).

$$d_{M_w} = 1 - \bar{M}_w = \left(1 - \frac{C_e}{C_{e0}}\right) \tag{6.2}$$

For the degradation and crystallinity model (as described in **Chapter 3** and used in **Chapter 5** to examine BPS degradation), the degradation variable for Model 2 (**Table 6.1**) is initially considered as being dependent on the normalised number average molecular weight of the semi-crystalline polymer, $\bar{M}_n$ (which is directly computed by the model), and hence is determined from

$$d_{M_n} = 1 - \bar{M}_n = \left(1 - \frac{M_n}{M_{n0}}\right) \tag{6.3}$$

where M_{n0} is the initial value of number average molecular weight.

Finally, for Model 3, the same degradation and crystallinity equations are used; however the degradation variable is now dependent also on the crystallinity. Degradation is defined by Eq. (6.4), which accounts for the changing M_n and the degree of crystallinity, X_c in the material, relative to their original values.

$$d_{X_c} = (1 - \left(\frac{M_n}{M_{n0}}\right)\left(\frac{X_C}{X_{C0}}\right)) \tag{6.4}$$

The three damage formulations described above (Model 1, Model 2 and Model 3) are summarised in **Table 6.1**.

Table 6.1 The key governing equations and degradation variable for each of the models applied to BPS are shown. Further details on the governing equations and can be found in **Chapter's 3-5** and [21] (for Model 1).

Model	Molecular weight	X_c	Governing equations	Damage parameter
1	$\bar{M}_w = \frac{C_e}{C_{e0}}$	NA	$\frac{\partial C_e}{\partial t} = -(k_1 C_e + k_2 C_e C_m^n)$ $\frac{\partial C_m}{\partial t} = k_1 C_e + k_2 C_e C_m^n + \nabla \cdot \{D \nabla C_m\}$ $D = D_0[1 + \alpha\left(1 - \frac{C_m + C_e}{C_{e0}}\right)]$	$d_{M_w} = (1 - \bar{M}_w)$
2	$M_n = \frac{(C_e + \omega X_c) M_0}{N_{chains0} + (R_s - \frac{C_{ol}}{m})}$	$X_{ext} = P_x V_c \eta_A R_s$ $\frac{\partial X_c}{\partial X_{ext}} = X_{max} - X_c$	$\frac{\partial C_e}{\partial t} = -\frac{\partial R_{ol}}{\partial t} - \omega \frac{\partial X_c}{\partial t}$ $\frac{\partial C_{ol}}{\partial t} = \frac{\partial R_{ol}}{\partial t} + (\nabla \cdot (D \nabla C_{ol}))$ $D = D_a\{D_{matrix} + (1.3p^2 - 0.3p^3)(D_{pore} - D_{matrix})\}$ $\frac{\partial R_s}{\partial t} = k_1 C_e + k_2 C_e \left(\frac{C_{ol}}{1 - X_c}\right)^{0.5}$ $\frac{R_{ol}}{C_{e0}} = \alpha_2 \left(\frac{R_s}{C_{e0}}\right)^{\beta}$	$d_{M_n} = \left(1 - \frac{M_n}{M_{n0}}\right)$

Table 6.1 Table 6.1 continued

Model	Molecular weight	$\mathbf{X_c}$	Governing equations	Damage parameter
3	As in Model 2	As in Model 2	As in Model 2	$d_{X_c} = (1 - \left(\frac{M_n}{M_{n0}}\right)\left(\frac{X_C}{X_{C0}}\right))$

Degradation is implemented into the mechanical constitutive law through damage based evolution of the material shear modulus, μ, which is assumed to follow a linear decrease based on the value of d (and where μ_0 represents the initial value of shear modulus).

$$\mu = \mu_0(1 - d) \tag{6.5}$$

The value of μ_0, and the empirical material constant b and hardening parameter, n_h from Eq.(6.1) are as given for PLLA in [22] (and as shown in **Table 6.2**).

Table 6.2 Material parameters for the Knowles hyperelastic model used to represent PLLA mechanical behaviour [22].

Description	Symbol	Value	Units
Shear modulus	μ	612.5	MPa
Empirical constant	b	0.00249	-
Hardening parameter	n_h	8.1 x10^{-5}	-

By way of illustration of the mechanical behaviour of this material, uniaxial tests on a single element cube were performed using the properties shown. **Figure 6.3** shows the stress-strain response of this material for different values of the damage parameter, *d*.

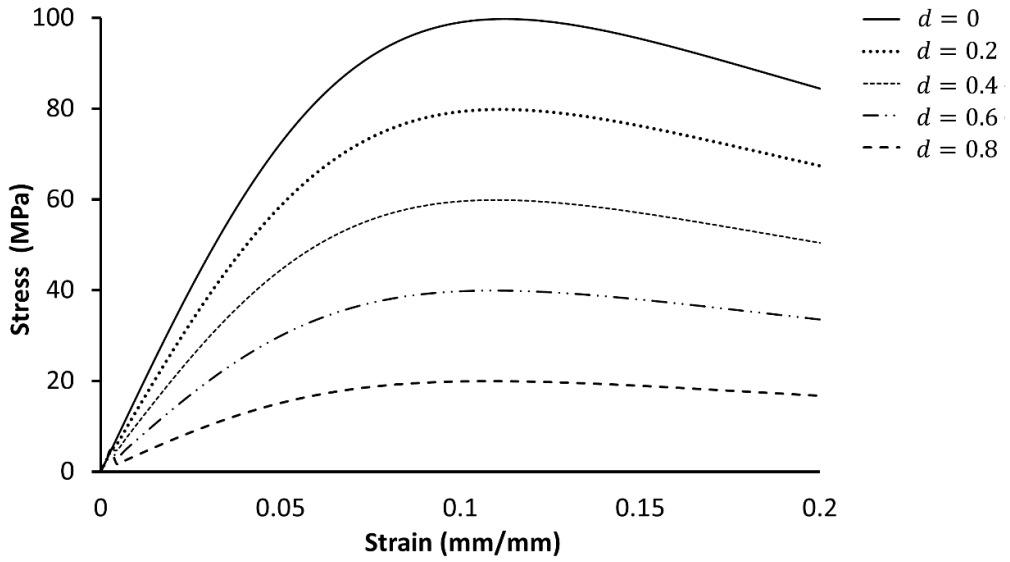

Figure 6.3 The stress strain response (in terms of true stress and true strain) of the PLLA material described in **Table 6.2** is reported for a single element using the UMAT subroutine and for various values of the damage parameter, d.

The introduction of damage into the material constitutive law impacts on the yield stress behaviour of the material, as shown in **Figure 6.3**. As discussed previously in **Chapter 3**, while the Knowles material model is shown to highlight the hyperelastic behaviour of thermoplastics such as PLLA, it does not provide the capabilities to capture any plastic deformation in the material. The maximum stress behaviour seen above in the undamaged case at low strains (e.g. 0.1) is similar to that observed in **Chapter 2** for **Figure 2.5**(a), where the stress reaches a value close to 100 MPa before exhibiting a small decrease (noticeable in particular for the moderate strain case depicted in **Figure 2.5**(a)).

To investigate the effects of heterogeneous material properties on the mechanical behaviour of BPS, simulations are performed on BPS devices sectioned into different regions which are assigned different values of initial crystallinity (**Figure 6.4**Figure 6.4). As shown in **Figure 6.4** (b) an outer surface and inner core are defined for the deployed stent unit, and different

initial crystallinity (X_{c0}) values are assigned to each region, which are outlined in **Figure 6.4**(c).

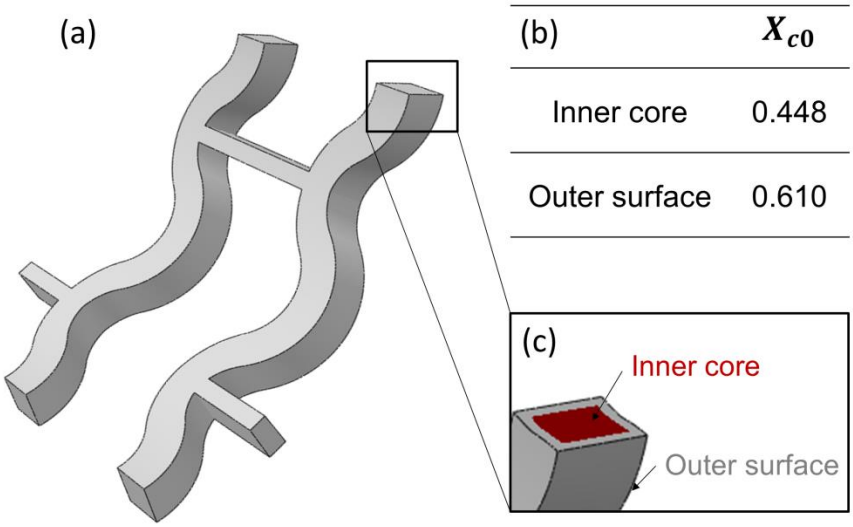

Figure 6.4 Different initial crystallinity values were assigned to separate sections of a BPS (a) as highlighted in (c). The outer surfaces of the stent (grey) are assigned a higher X_{c0} than its inner core (red). Respective values for X_{c0} at the inner core and outer surface are shown in (b).

The mechanical behaviour of the artery is characterised using an isotropic reduced sixth-order hyperelastic model, for which the strain energy density W_e takes the following form

$$W_e = \sum_{i=1}^{N} C_{i0} (\bar{I}_1 - 3)^i + \sum_{i=1}^{N} \frac{1}{D_i} (J - 1)^{2i} \tag{6.6}$$

In Eq. (6.6) N is the number of polynomial terms, C_{i0} and D_i are experimentally measured material parameters and J is the determinant of the material deformation gradient (Jacobian). Material parameters (**Table 6.3**) for each layer are as suggested by [23], based on the experimental testing of arterial tissue reported in [13].

Table 6.3 Values of material coefficients for the isotropic strain energy density function used to represent the behaviour of each arterial layer.

Description	C_{10}	C_{20}	C_{30}	C_{40}	C_{50}	C_{60}
Adventitia	8.27 e-3	0.012	0.52	-5.63	21.44	0.00
Media	6.52 e-3	0.0489	9.26 e-3	0.76	-0.43	0.0869
Intima	6.79 e-3	0.54	-1.11	10.65	-7.27	1.63

6.3.3 BPS loading and simulation of degradation

The main focus of the research undertaken here is the impact of degradation on the long-term mechanical performance of a BPS. Two different methods are used to apply initial loading to BPS based on either (i) a uniform pressure (which idealises the physiological load), or (ii) arterial loading by expansion and recoil of the BPS (with contact between the vessel and BPS). For each method, the BPS is modelled in its deployed state using the stent geometry unit cell and symmetric boundary conditions (**Figure 6.5**) are applied to account for the remainder of the device geometry. The BPS unit is allowed to undergo radial displacement for each loading case (**Figure 6.5**).

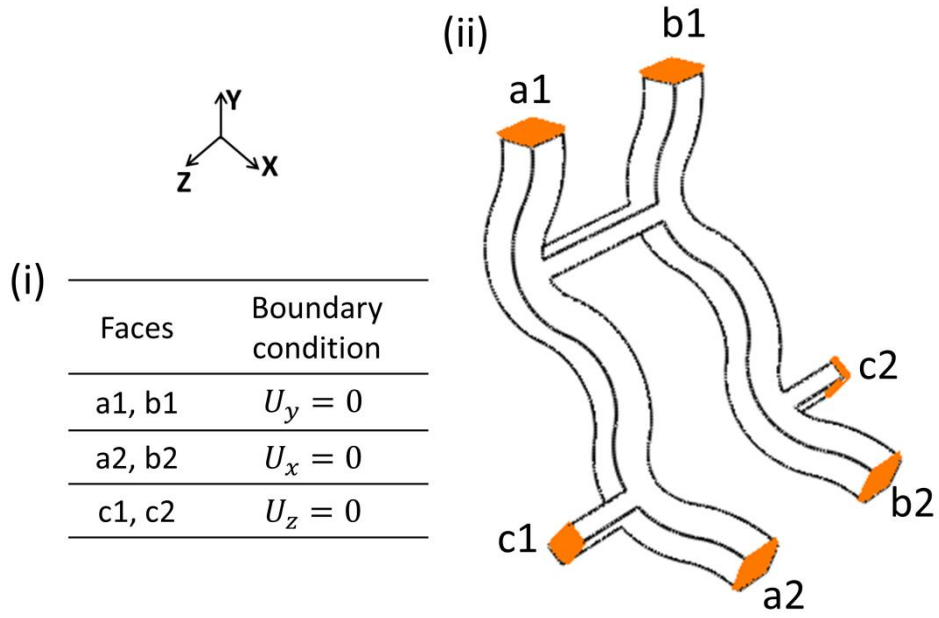

Figure 6.5 Symmetrical boundary conditions listed in the table shown at (i) are applied to the BPS as highlighted in (ii).

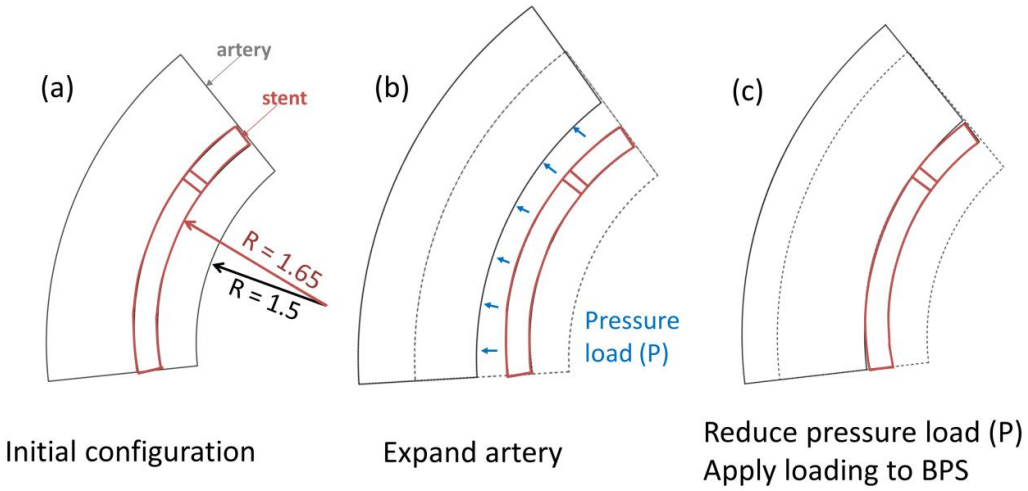

Figure 6.6 Schematic showing the steps involved in the BPS artery loading case, where (a) is the initial setup of the BPS artery assembly, (b) is application of a pressure load at the inner surface of the artery and (c) is reduction of arterial pressure and transfer of loading to the deployed BPS. The dashed lines in (b) and (c) show the original position of the artery before loading.

For the first of the BPS simulations, an inward-acting, uniform, external pressure is applied to the outer surface (to represent vessel loading) of the deployed stent geometry, following previous approaches [24]. In the second set of simulations, an approach similar to that detailed in [25]–[27] is taken to

apply arterial loading to the deployed BPS (**Figure 6.6**). A 5% axial in-situ pre-stretch is applied to the artery, as further described in Zahedmanesh and Lally [28], to account for the biomechanical regulation of the artery that occurs during stent deployment [13], [29]. As is depicted in **Figure 6.6**, the artery is expanded radially following application of a uniform pressure on its internal surface, before being moved over the deployed BPS (**Figure 6.6**(b)). The pressure load is then reduced to a final value of 13.3 kPa (which represents a mean blood pressure of 100 mmHg), allowing the artery to relax onto the BPS, which is over-expanded by 10% [1].

While the above approach neglects any permanent deformation which would be experienced by a BPS during deployment, use of this technique does not affect the degradation modelling approach used, which in its present form is not dependent on either the material stress or strain. Additionally, given that the assumed initial geometry for the stent in this approach is the deployed geometry, i.e. after deployment (plastic deformation) and initial elastic recoil, this allows the elastic-only Knowles model to be used to represent the PLLA mechanical behaviour, as the focus is exclusively on stent elastic deformation from the deployed state due to artery and pressure loading. This general approach for stent loading has previously been applied to successfully examine the degradation and loading of magnesium stents [26], [27]. Contact is initiated between the artery and the BPS unit during the release step, when the artery is allowed to relax back onto the BPS. Contact between the arterial intima layer and the BPS is modelled as *normal hard behaviour*, and assigned a coefficient of friction of 0.25, based on the investigations of [30]. Two degradation boundary condition assumptions are applied to BPS for both loading cases, as shown in **Figure 6.7**. Similar to the degradation boundary

conditions used in **Chapter 5**, stents are modelled as being either fully embedded (SFE) (**Figure 6.7**(a)), where there is no flux on each face of the stent, or as having a free surface condition (SFS), where any degradation products formed on the highlighted free surface (shown in **Figure 6.7**(b)) are immediately removed (representing transport by the blood flow). Degradation is simulated for 2 years or 104 weeks in each case.

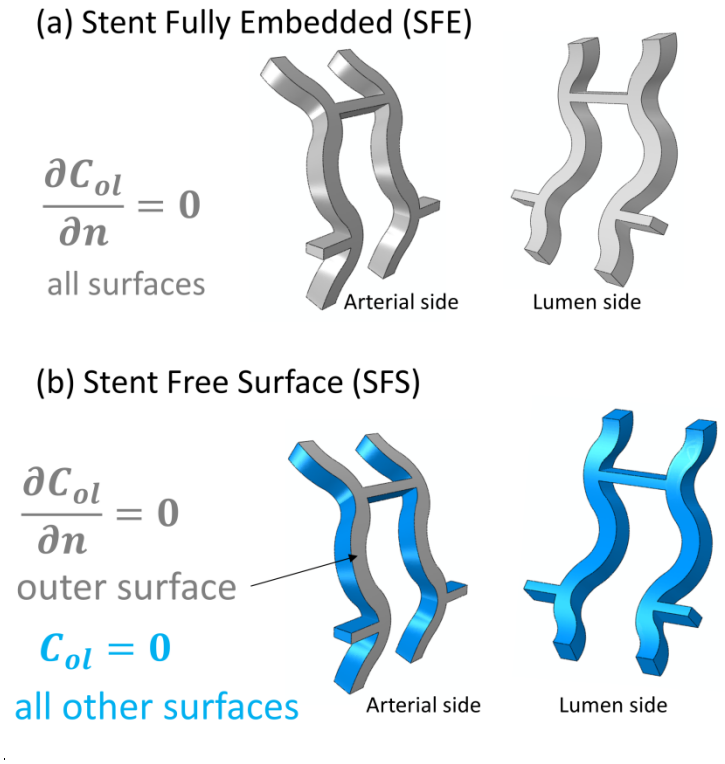

Figure 6.7 Comparison of the two boundary condition assumptions in BPS simulations. A fully embedded stent (SFE), where all the surfaces are considered adiabatic, or of zero flux (grey), is shown in (a). For the stent free surface (SFS) assumption (b) an adiabatic condition is applied to the outer surface of the stent only, with all other surfaces assigned oligomer free conditions ($C_{ol} = 0$, blue).

6.4 Results

6.4.1 Analysis of results

The results of this chapter are presented in two sections. Predictions for the BPS examined under a uniform external pressure are summarised in Section 6.4.2, whereas the arterial loading predictions are presented in Section 6.4.3.

As indicated above, the different degradation model formulations investigated (shown in **Table 6.1** and described in Section 6.3.2) are labelled Model 1, Model 2 and Model 3.

For each of the BPS analysis methods, the following approach is taken to quantify the loss of lumen diameter (ϕ_L) due to the recoil of the degrading BPS:

$$\text{Loss of } \phi_L \ (\%) = \frac{D_I - D_f}{D_I} \tag{6.6}$$

with D_I being the initial internal diameter of the deployed stent geometry at time 0 and D_f the final internal diameter at maximum degradation in each case. The stress distributions during loading and degradation are examined. The damage induced in the BPS for each of the model formulations is also examined under the assumed boundary conditions depicted in **Figure 6.7**. Predictions for the volume averaged M_n, $\overline{M}_n^V$, in uniform (homogeneous) and heterogeneous BPS are shown for both loading cases, alongside changes in X_c. Trends in M_n, X_c and material stiffness μ across a heterogeneous BPS strut at different time points are examined. Finally, for the case of the arterial loading simulations, the maximum principal stresses in the artery and the average radial force acting on the BPS over the 2 year degradation period are investigated.

6.4.2 BPS performance under uniform pressure load

The loss of ϕ_L for each of the cases investigated under a uniform pressure are directly compared in **Figure 6.8**(b) and (c). Lumen loss (which in this idealised simulation is captured as the change in the stent's inner diameter) due to BPS

degradation is highest (5%) in Model 3 simulations under the fully embedded (SFE) condition. The evolution of the degree of material damage for each BPS is compared in **Figure 6.8**(d); it is observed that free surface (SFS) conditions result in a more gradual onset of damage in the homogenous BPS than the SFE assumption. The faster progression of damage in the SFE case brings about the higher rates of ϕ_L loss observed for these stents.

Comparative predictions of the volume averaged M_n, $\bar{M}_n^V$, are depicted in **Figure 6.8**(e). Similar rates of $\bar{M}_n^V$ are observed for each of the models investigated under the assumption of a SFE boundary condition. Model 2 and Model 3 show matching rates of $\bar{M}_n^V$ decrease when SFS degradation is assumed; Model 1 exhibits a more gradual decrease in $\bar{M}_n^V$ in comparison. Rapid increases in X_c are also predicted for the SFE investigations compared to those degraded with SFS assumption (**Figure 6.8**(f)): such sharp increases in material X_c are due to the accelerated change in the concentration of chain scissions, R_s occurring with the auto-catalysed degradation.

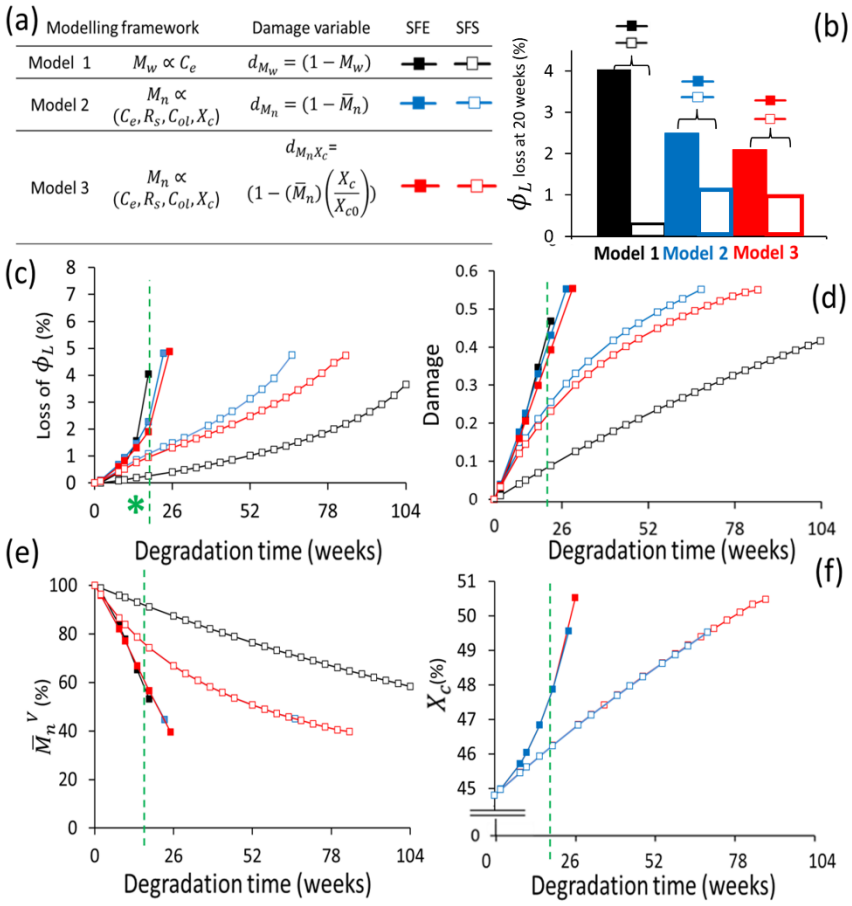

Figure 6.8 The various modelling frameworks and damage formulations applied to uniform BPS are summarised in (a), along with a description for each of the presented data sets. Comparison of the maximum percentage ϕ_L decrease for each of the 6 cases (Model 1, 2, 3 for SFE and SFS conditions as denoted in (a)) after 20 weeks of degradation is shown in (b). Loss of ϕ_L over degradation time is given in (c), where the line referenced by the asterisk (green) highlights the predictions at 20 weeks (corresponding to values in (b)). Plots of the time evolution of material damage, volume averaged M_n and change in X_c are shown in (d)-(f) for each case (data differentiated for each case as explained in (a)).

Von Mises stress values in homogeneous and heterogeneous BPS following degradation for 20 weeks under the assumed boundary conditions are compared in **Figure 6.9**, with maximum principal stress compared in **Figure 6.10**.

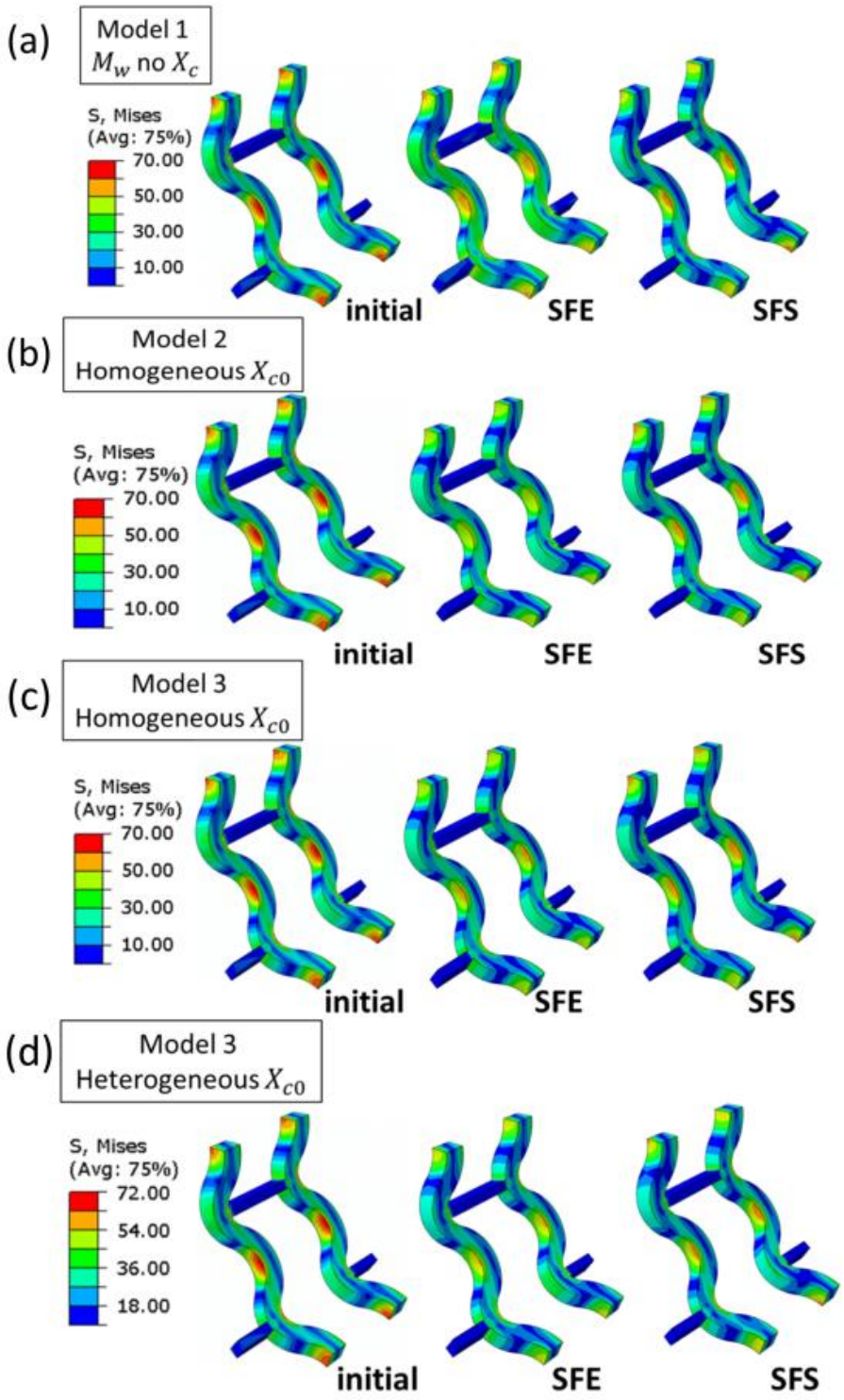

Figure 6.9 Contour plots of Von Mises stress (MPa) in BPS with uniform (homogeneous) ((a)-(c)) and heterogeneous (d) material properties following initial application of external pressure load and 20 weeks of simulated degradation under stent fully embedded (SFE) and stent free surface (SFS) boundary conditions. The stress predictions in each model (Model 1 (a); Model 2 (b); Model 3 (c), (d)) are also compared.

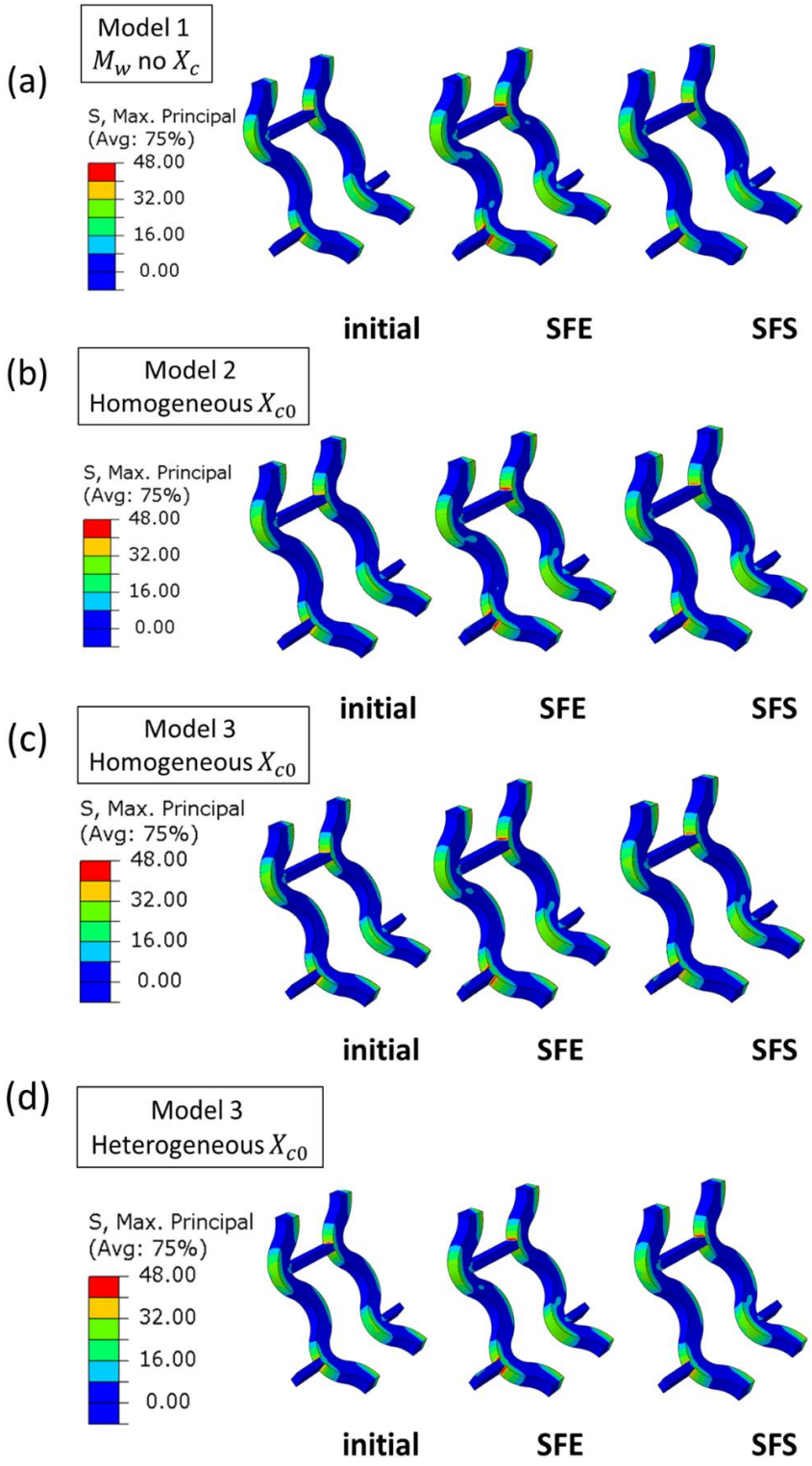

Figure 6.10 Contour plots of maximum principal stress (MPa) in BPS with uniform (homogeneous) ((a)-(c)) and heterogeneous (d) material properties following initial application of external pressure load and 20 weeks of simulated degradation under stent fully embedded (SFE) and stent free surface (SFS) boundary conditions. The stress predictions in each model (Model 1 (a); Model 2 (b); Model 3 (c), (d)) are also compared.

Homogeneous stents (labelled for each model in (a)-(c)) show similar rates of degradation under SFE and SFS conditions. A maximum von Mises stress of 70 MPa is observed (**Figure 6.9**) close to the corners of the U-bend stent strut (i.e. at the middle part of the stent structure) for each model directly after application of the pressure load in homogenous BPS. The highest maximum principal stress in the stents is also observed to close to the U-bend region (**Figure 6.10**). Maximum stress reduces at a slightly faster rate in SFE stents (von Mises values of 57.4 MPa, 59.6 MPa and 61.6 MPa for Model 1, 2 and 3 respectively) than for those degraded with SFS condition (69.7 MPa, 65.6 MPa and 66.2 MPa observed in Models 1, 2 and 3). Heterogeneous BPS **Figure 6.9**(d) (in this case Model 3 applied only) display a marginally higher initial stress than the uniform stents, with this maximum stress reducing by about 4% and 1.4% for SFE and SFS cases respectively. A similar impact of boundary condition on maximum principal stress in the stents is observed; SFE stents display increased values of stress compared to the SFS devices. Less of an effect however, is noted for this variable across the stents for the different models examined.

The loss of ϕ_L due to material degradation for each of the BPS subjected to uniform pressure loading is compared in **Figure 6.11**, in an expansion of the graph shown in **Figure 6.8**(c). Predictions for heterogeneous stents (green markers, **Figure 6.11**(a)) exhibit more gradual trends than the homogeneous devices examined with the same damage model (red markers, **Figure 6.11**(a)).

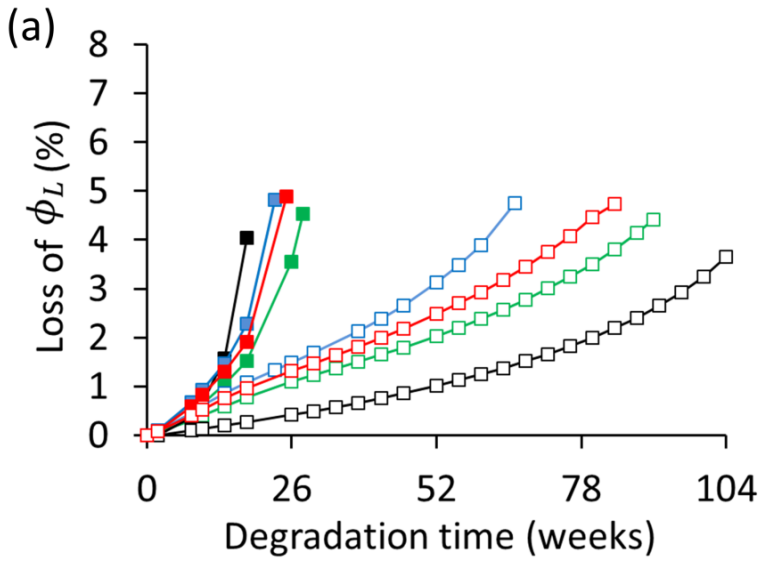

(b)

Model	X_{c0}	SFE	SFS
Model 1	-		
Model 2	Homogeneous		
Model 3	Homogeneous		
Model 3	Heterogeneous (Higher at surface)		

Figure 6.11 Loss of $\boldsymbol{\phi_L}$ due to BPS degradation is compared (a) for each of the cases as outlined in (b), with SFE and SFS referring to fully embedded and free surface boundary conditions respectively.

6.4.3 BPS performance under arterial loading

The loss of ϕ_L predicted for homogeneous BPS is shown in **Figure 6.12**(b) for each of the model cases and boundary conditions examined (as summarised in **Figure 6.12**(a)). BPS modelled under SFE conditions show significantly higher ϕ_L loss (4.8%) than those degraded with SFS condition (predicted loss for SFS between 1.6 and 0.5%). The material damage converges to a maximum in all cases when SFE conditions are considered, as shown in **Figure 6.12**(c). Under SFS conditions, Model 2 and Model 3 predictions of damage show similar rates of increase at the earlier stages of degradation (i.e. each reaches a damage of approximately 0.25 at 18 weeks) before a greater

increase is seen from 18 to 104 weeks for Model 3. The progression of damage in Model 1 simulations exhibits the greatest dependence on the choice of boundary condition. Degradation trends for each of the fully embedded BPS show a significantly faster decrease in $\bar{M}_n^V$ (**Figure 6.12**(d)) with minimal $\bar{M}_n^V$ predicted after 78 weeks for this boundary condition. In comparison, SFS stents display more gradual rates of $\bar{M}_n^V$ degradation. Similarly, a noticeable difference between the SFE and SFS cases is highlighted in the X_c predictions (**Figure 6.12**(e)).

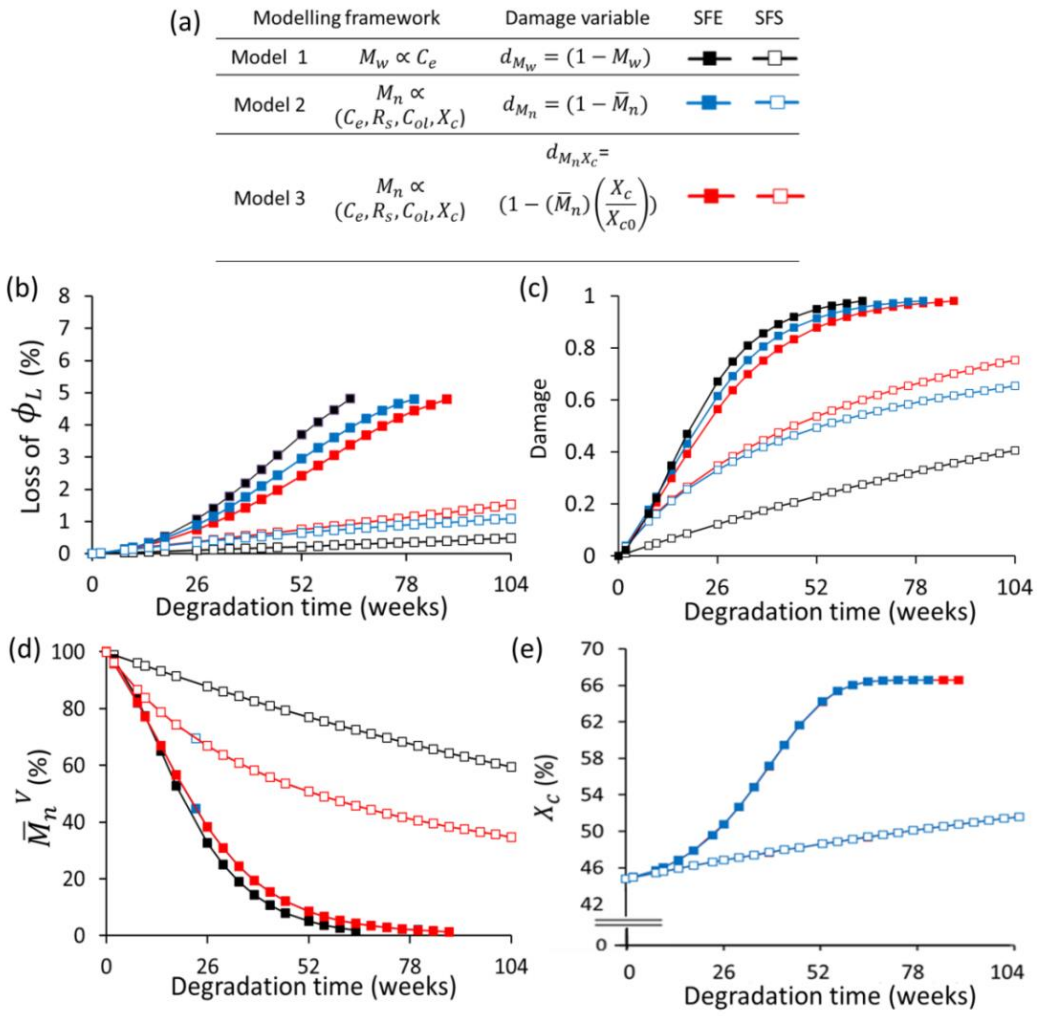

Figure 6.12 The various modelling frameworks and damage formulations applied to uniform BPS under arterial loading are summarised in (a), with reference given to the various data sets. Predictions of ϕ_L loss due to degradation (b), damage (c), volume averaged M_n (d) and X_c (e) are also shown, with the trends for fully embedded (SFE) and free surface (SFS) cases compared.

Comparison of the predicted loss of ϕ_L in BPS subjected to a uniform pressure load (a) and arterial loading (b) are shown in **Figure 6.13**, with a significant difference in the trends predicted for the two cases. Values of predicted ϕ_L loss due to degradation are significantly lower (4.8% and 0.5-1.5% for SFE and SFS simulations respectively) under the applied arterial loading, than that shown in (a) for a uniform pressure (maximum value of 5% in Model 3 SFE simulation). In the case of the arterial loading, vessel compliance reduces the

pressure as lumen diameter is lost, which slows the observed rate of lumen loss.

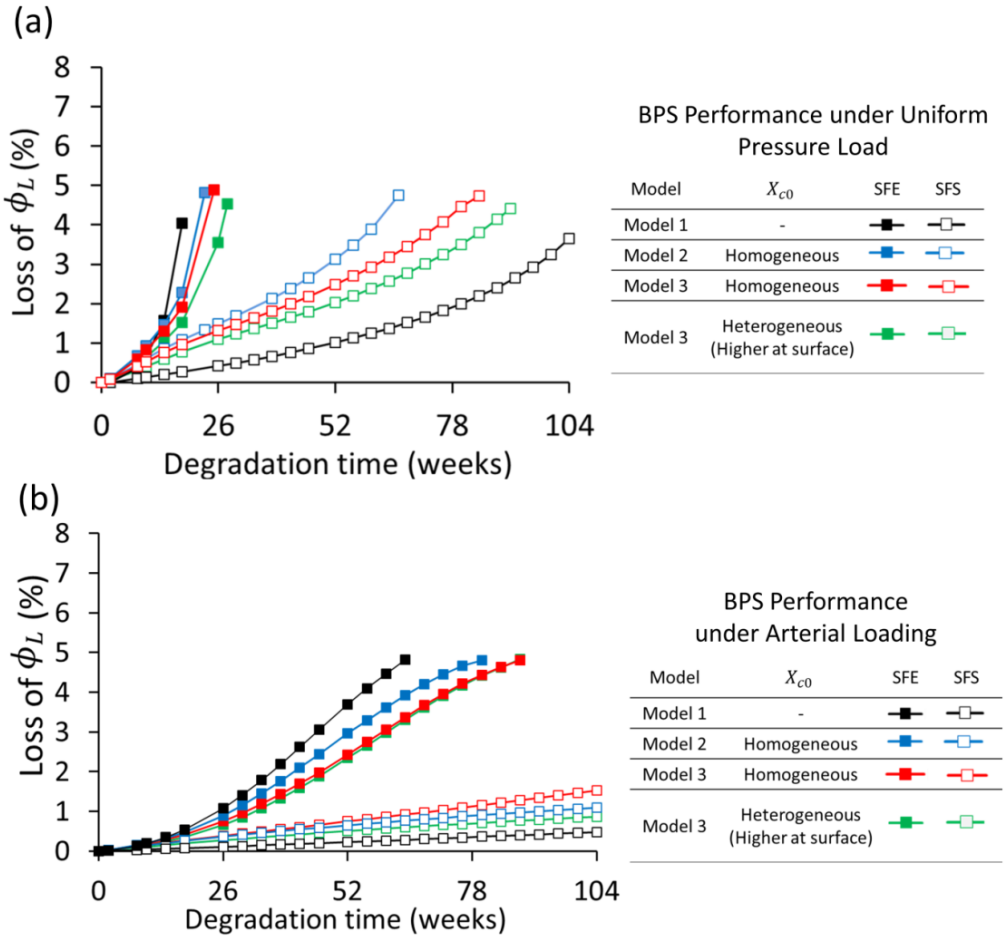

Figure 6.13 Comparison of the predicted loss in ϕ_L due to BPS degradation for the two loading cases; (a) uniform pressure loading and (b) arterial loading simulation. Legends in both indicate the SFE and SFS data, along with model formulation and X_{c0} distribution. The trends for heterogeneous BPS (X_{c0} higher at outer surface) simulations are shown by the green markers.

In **Figure 6.14**, a greater increase in material damage is observed in the homogeneous stents modelled with SFS boundary conditions, compared to heterogeneous stents simulated under the same conditions. This increase in damage corresponds to the higher ϕ_L loss observed for homogeneous free surface BPS. Little differences in ϕ_L loss due to BPS degradation are observed, however, in the homogeneous and heterogeneous BPS modelled under the SFE condition (as compared in **Figure 6.14**(b)). Rates of $\bar{M}_n^V$ decrease show similar trends for each of the SFE simulations; predictions for the outer surface of heterogeneous BPS initially show a more gradual decrease in $\bar{M}_n^V$ with very close agreement later seen for this region, the inner core and the full BPS at later time points (around 52 weeks). SFS simulations also show more gradual rates of $\bar{M}_n^V$ decrease for the outer surface region, with predictions for the inner core and the homogeneous stent both showing the fastest decrease in $\bar{M}_n^V$ for this condition (**Figure 6.14**(c), and insert, which shows overlapping data referenced by the asterisk in (c)). Predicted values of X_c are shown in **Figure 6.14**(e). Significant differences in predicted X_c for homogenous BPS are observed between SFE and SFS simulations; X_c of 67.0% predicted in fully embedded case compared to 51.6% under free surface assumption. Values of X_c in heterogeneous stents show similar dependences on the applied boundary conditions (data referenced by double asterisk in **Figure 6.14**(e) is more closely examined in the insert shown, where data for the inner core of SFS heterogeneous BPS overlaps with predictions for homogenous case).

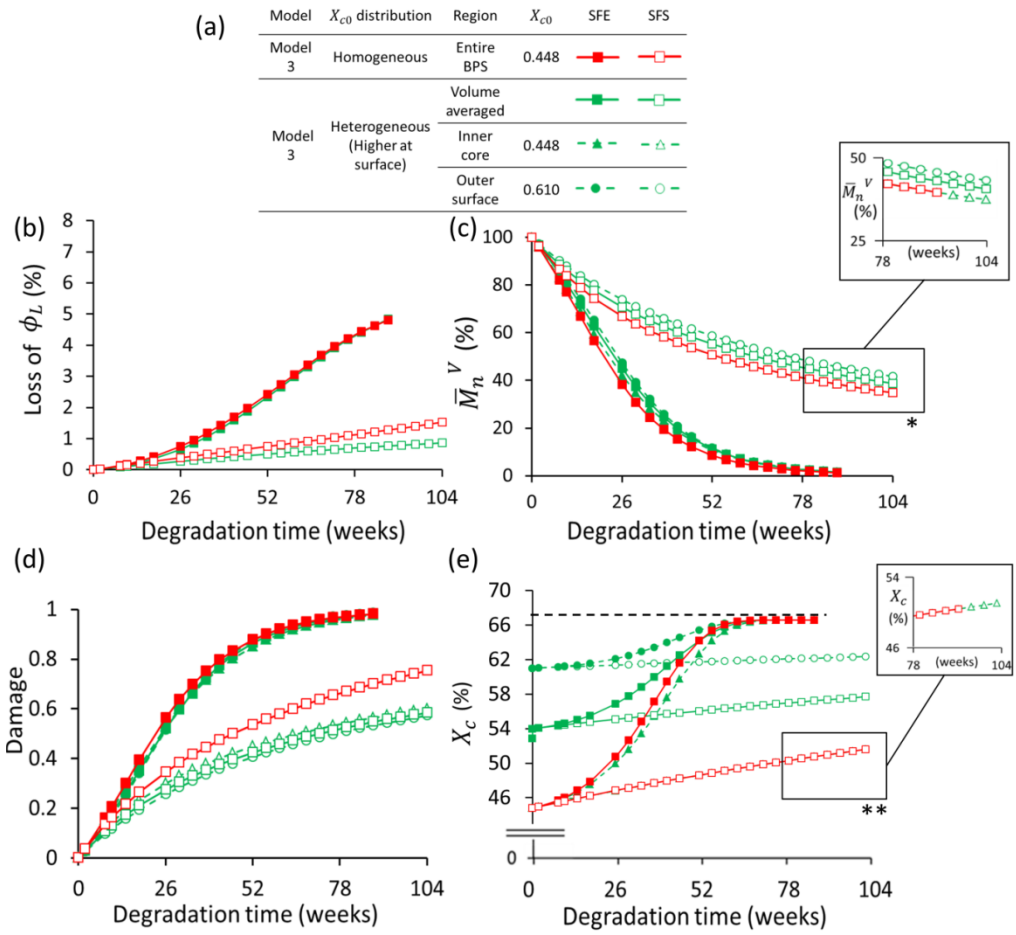

Figure 6.14 Predictions for Model 3 simulations in homogenous (red) and heterogeneous (green) BPS subjected to arterial loading and degraded under SFS and SFE conditions. Volume average trends for M_n^V (c), damage (d) and X_c (e) are shown for the entire BPS in the heterogeneous case alongside the predictions at inner core (dashed line, triangle) and outer surface (dashed line, circles) regions. Inserts at * and ** show the overlapping SFS data and the dashed line in (e) indicates the value of X_{max} (model parameter).

Contour plots of M_n and X_c in each region of heterogeneous BPS are shown in **Figure 6.15** for SFS and SFE boundary conditions. A minimum M_n of 80504 g/mol is predicted at the inner core of stents degraded under SFS conditions, while the outer surface for this condition reaches a value of 93037 g/mol (**Figure 6.15**(b)). In comparison, the M_n predicted in SFE simulations displays less of a gradient than that predicted for the SFS simulation. A maximum M_n (at outer surfaces) of 18455 g/mol is predicted for fully embedded BPS, while the inner core shows a minimum of 16884 g/mol (as highlighted in the insert in

Figure 6.15(d)). Differences in X_c at 52 weeks are predicted across heterogeneous BPS for both boundary conditions. A maximum X_c of 65.4% is predicted after 52 weeks degradation at the outer surface of a heterogeneous BPS examined under SFE conditions, with an X_c of 62.6% predicted at the inner core for this condition (**Figure 6.15**(h)). The SFS predictions show lower values of X_c in comparison; values of 61.7% and 48.6% are given at the outer surface and inner core respectively for this boundary condition.

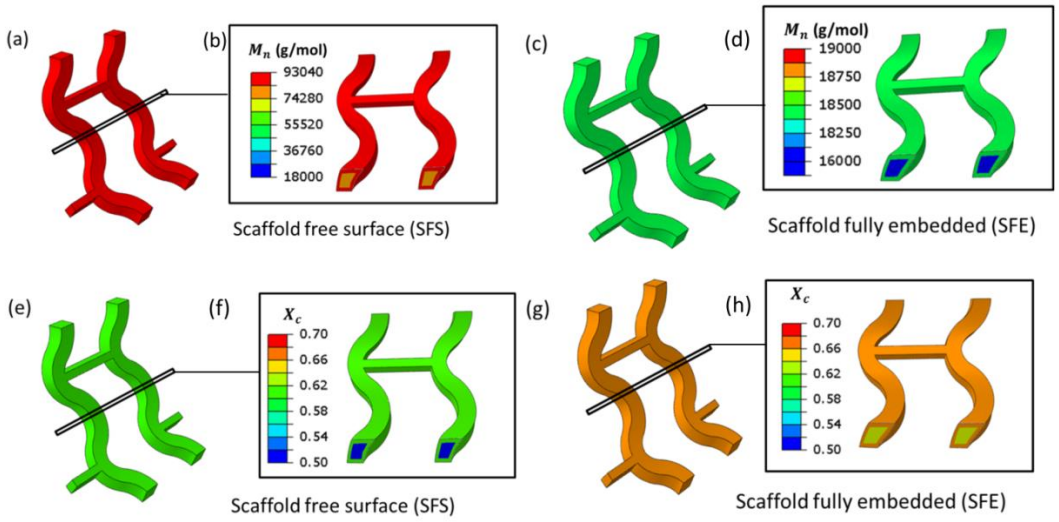

Figure 6.15 Contour plots showing M_n (g/mol, (a)-(d)) and X_c ((e)-(h)) predictions in heterogeneous BPS after 52 weeks of degradation under different boundary condition assumptions (SFS and SFE as described). Inserts highlight the value of M_n ((b), (d)) and X_c ((f), (h)) at the device's inner core in each case.

Changes in M_n, X_c and the resulting materials stiffness μ across a BPS strut degraded under SFS or SFE conditions are examined more closely in **Figure 6.16** for 0, 27, 52, 80 and 104 week time points. Significantly faster degradation in M_n is once more highlighted for SFE stents. In comparison, the SFS simulation shows a lesser decrease in M_n over the investigated degradation time (**Figure 6.16**(a)) with similar differences in M_n predicted across the strut thickness at each time point up to 104 weeks. The X_c predicted across the BPS strut in each case displays the greatest variance at the earlier time points for both SFS and SFE degradation conditions, with the

SFE predictions reaching a maximum X_c of 67% across the full strut at 80 weeks. The material stiffness, μ, exhibits the greatest differences across the strut in the SFS assumption. For the SFE degradation, while the μ values are initially slightly higher at the strut outer surfaces than at the inner core (27 weeks line, **Figure 6.16**(e)) lower stiffness is predicted at the outer surfaces after 52 weeks. This change in stiffness behaviour for the SFE simulations is indicated by the red line in the graph of μ over degradation time shown in **Figure 6.16**(e).

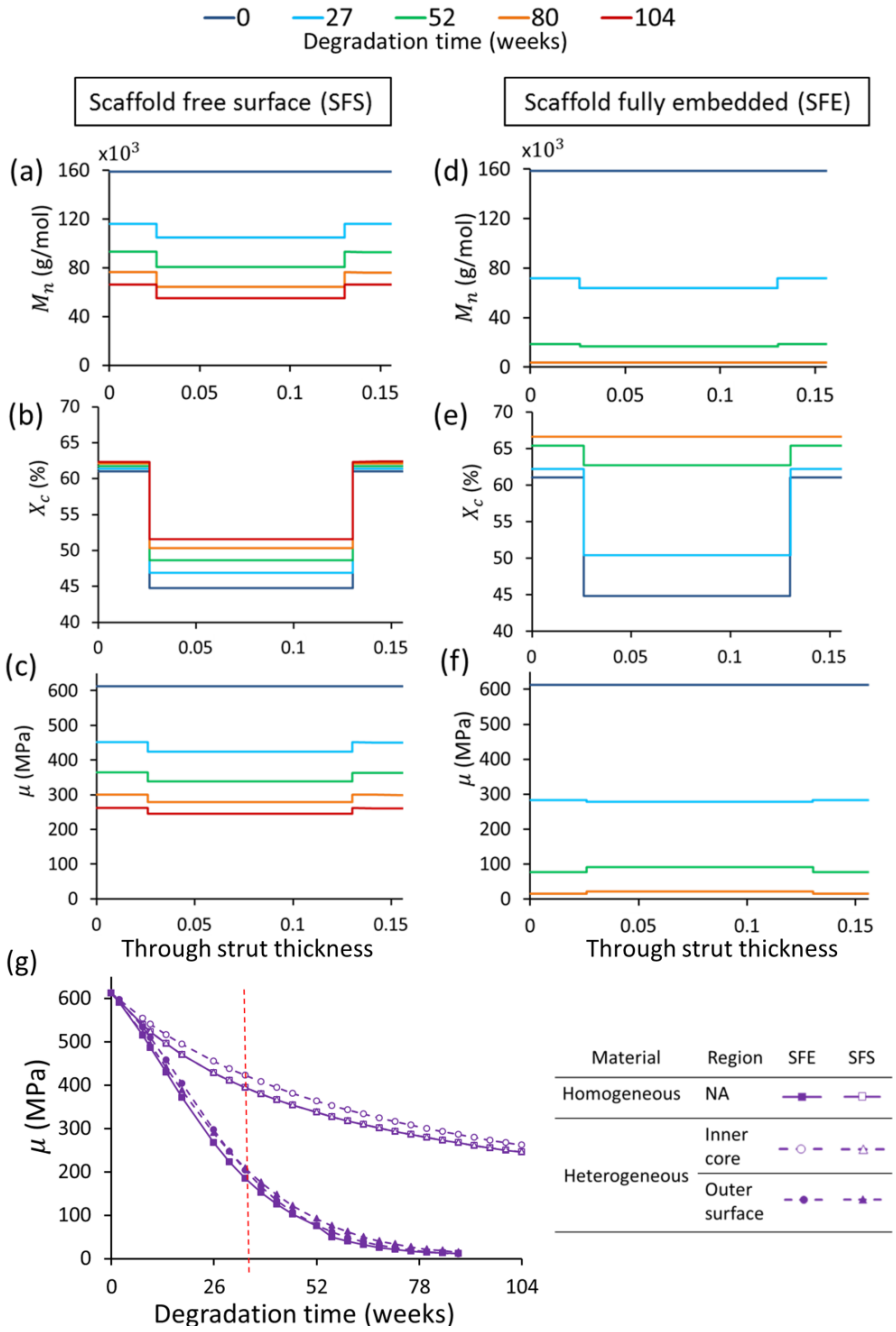

Figure 6.16 Plots showing the changes in M_n, X_c and μ across a BPS strut when heterogeneous material properties are assigned for degradation under stent free surface (SFS; (a)-(c)) and stent fully embedded (SFE; (d)-(f)) boundary conditions. Predictions in μ over the degradation time are included for homogeneous BPS in (g) and compared to the predictions in specific regions of heterogeneous stents (where the legend details the region and boundary condition).

The maximum principal stress in the artery with heterogeneous BPS degradation is examined in **Figure 6.17**. Maximum values of stress are generated in the artery in both cases after contact is initiated with the BPS (day 0 in degradation simulations). Stress shows a gradual decrease for the SFS case in comparison to the SFE simulation, where stress in the artery show a 26% decrease after 189 days, or 27 weeks (compared to 8% for the SFS case at the same time point).

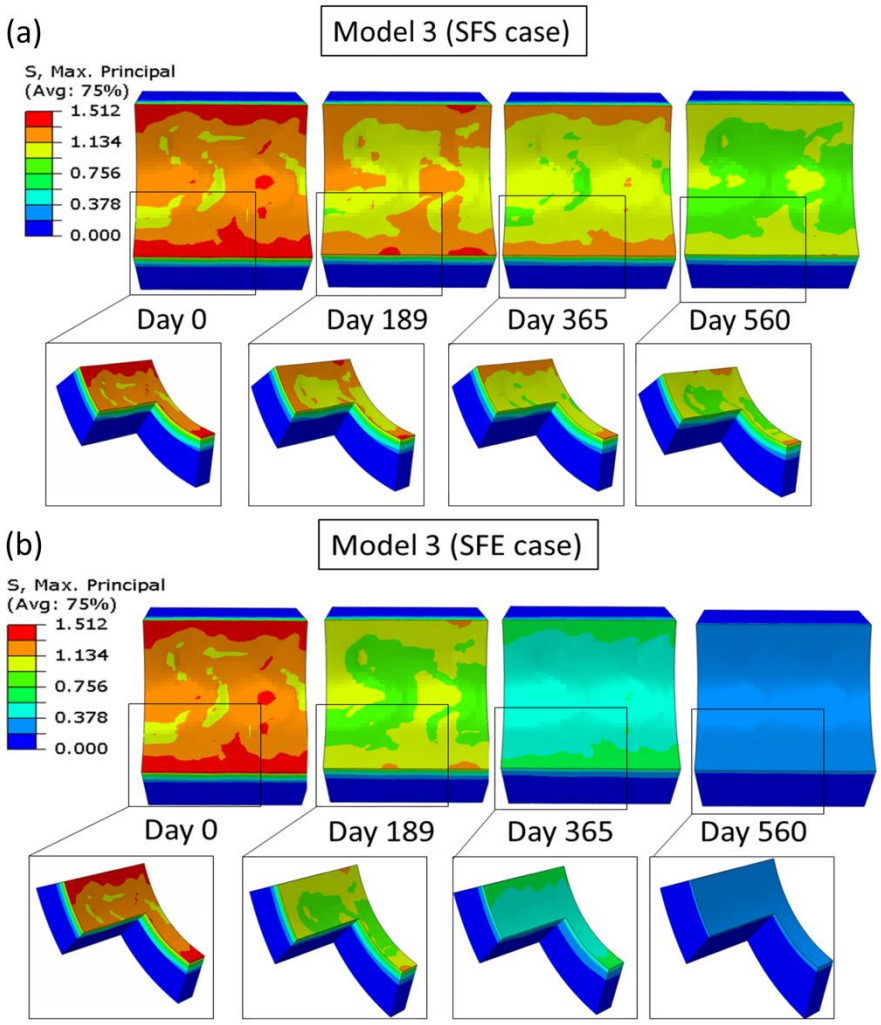

Figure 6.17 The maximum principal stress in the artery following heterogeneous BPS degradation under (a) SFS and (b) SFE conditions is investigated at a number of time points throughout the degradation. Inserts show the distribution and locations of maximum stress values in the three layered artery.

The radial forces acting on BPS during the arterial loading cases are compared in **Figure 6.18**. Radial force, which is reported here as the length normalised radial force (N/mm) [31] is calculated from the average contact pressure acting on the outer surface area of a full BPS (outer surface area of one BPS unit is calculated and approximate number of units in a full BPS of length 12 mm is used to determine total area). Trends for the radial force acting on heterogeneous and homogeneous stents throughout the examined degradation period are compared for SFE and SFS conditions (**Figure 6.18**); a maximum value of 1.45 N/mm is reported in all cases at the initial point of contact with the artery with similar decrease in radial force predicated for each case, with the exception of Model 1 with slightly decreasing force observed under SFS conditions, and more rapid decrease observed for the SFE simulations.

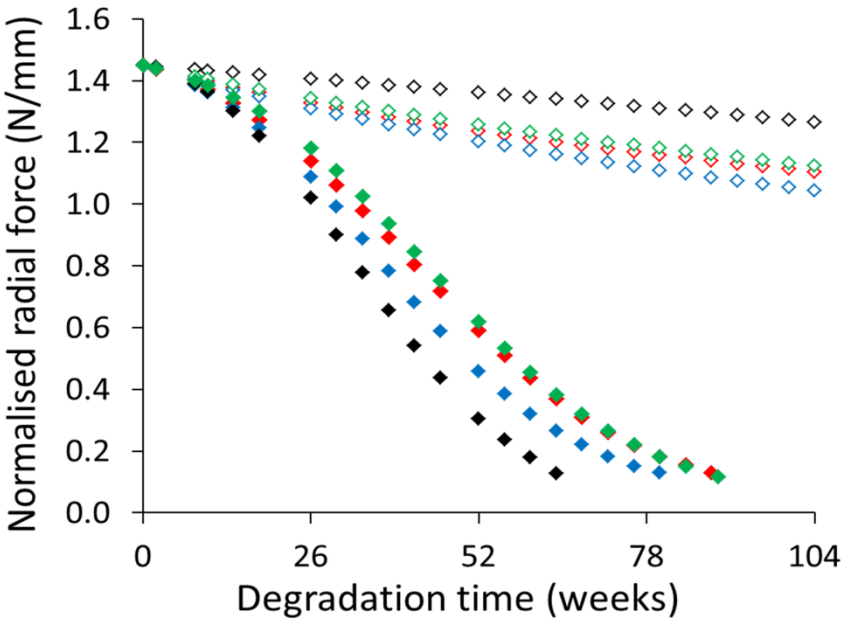

Model	X_{c0}	SFE	SFS
Model 1	Homogeneous	◆	◇
Model 2	Homogeneous	◆	◇
Model 3	Homogeneous	◆	◇
Model 3	Heterogeneous (Higher at surface)	◆	◇

Figure 6.18 Decrease in normalised radial force data (N/mm) acting on the BPS is compared for each model case and for the two degradation boundary conditions, SFE and SFS.

6.5 Discussion

Simulations are presented of coupled material degradation and mechanical behaviour for an idealised, uniform external pressure case and for physiological loading in a vessel. Comparisons are made between the original model implementation [21] and the simplified crystallinity theory [32], where each model is coupled to an appropriate damage based degradation model (**Table 6.1**). Material parameters and device performance, as measured by loss of lumen diameter (ϕ_L) and radial force, are reported as the BPS undergoes degradation. The influence of heterogeneities in the initial crystallinity is investigated.

6.5.1 Summary of key results

Predictions of the loss of ϕ_L for the various BPS cases examined show a dependence on both the loading experienced and on the assumed degradation product boundary conditions. In all cases, BPS examined with fully embedded conditions (SFE) show a much faster decrease in their scaffolding ability than those assumed to have degradation product free surfaces (SFS); predicted ϕ_L loss exhibits gradual trends over the two year period examined when degradation products are allowed to diffuse from the outer surfaces of the device. The percentage loss of ϕ_L measured here is distinct from elastic recoil (which the BPS would experience following crimping and deployment in the artery). This chapter instead considers the impact of degradation on the scaffolding performance (measured through the loss of ϕ_L) during intermediate and late stages of device implantation.

Similar stress behaviour is observed for homogeneous and heterogeneous stents, with again, a strong dependence on the assumed boundary condition revealed for both cases. Interestingly, the BPS subjected to arterial pressure loads display lower values of ϕ_L loss than those degraded under a uniform external pressure load (**Figure 6.13**). The maximum radial force experienced by the BPS reaches a peak value in both loading cases following simulated loading, with different rates of force decrease observed for the various model and material cases examined.

6.5.2 Neo-intimal regrowth: diffusion boundary conditions

As discussed previously in **Chapters 4** and **5**, and as is evident here, the choice of assumed boundary condition has a significant influence on the predicted rates of BPS material degradation. The difference in predicted

behaviour between the two boundary condition assumptions persists in the modelling predictions presented here. An insight into how the stiffness of the material is influenced by the choice of boundary condition is provided in this chapter; stents with initially heterogeneous crystallinity display a change in their location of maximum material stiffness during degradation when fully embedded conditions are assumed. This effect may be more pronounced for different forms of poly-lactide materials, depending on the values of calibrated rate constants for conventional and autocatalytic hydrolysis, as well as the assumed value of maximum crystallinity. Knowledge of the changing locations of maximum stiffness in a degrading BPS is of importance as variations in the mechanical integrity of the stent would impact on its long-term capabilities (for example its fatigue response under pulsatile loading [6], [33]–[35]). BPS degradation product fate and behaviour has recently been computationally investigated for tissue embedded BPS [36], [37], with material degradation kinetics and arterial remodelling emerging as modulating factors in the uptake and concentration of lactic acids in local tissue. Further insight into the environmental response following BPS implantation and degradation in an artery is obtainable through use of advanced imaging techniques, as discussed in **Chapter 5**. Such insight would allow for improvements in the physio-chemical models of BPS degradation behaviour such as presented here.

6.5.3 Importance of X_c

As discussed in **Chapter 5**, degradation driven changes in X_c are known to contribute to the increased stiffness and higher tensile properties often observed for degrading PLLA specimens [35], [38]–[42]. Semi-crystalline poly-lactide materials show higher initial mechanical strength than amorphous

polymers [43], with increased degradation times also apparent for PLLA in comparison to PDLLA (due to the faster hydrolysis of amorphous (disordered) regions ([44], [45])). Investigating the influence of X_c on the scaffolding ability of degrading BPS revealed an improvement in the predicted loss of ϕ_L for the BPS simulated with the implemented crystallinity theory, when fully embedded boundary conditions are assumed. For SFS simulations however, in **Figure 6.12**(b) the inclusion of X_c is shown to induce slightly higher ϕ_L loss, suggesting that the BPS modelled as semi-crystalline (i.e. Model 3) show faster degradation under free surface conditions than those assumed to be amorphous (i.e. Model 1) under the same SFS boundary condition.

Often observed alongside the increasing stiffness is a transition in failure mode of degrading semi-crystalline materials; PLLA elongation at break is reported as inversely proportional to X_c in a number of experimental studies [38], [40], [41]. Further insight into how the in-vivo environment loading impacts on the rates of change of X_c and the effects this has on the overall mechanical performance (for example [35]) would offer improvements to BPS design, and would aid the development of computational modelling techniques for evaluating device performance. Since the presented degradation model formulation is independent of the stress or strain experienced during loading, the degradation characteristics of the homogenous BPS cases are as presented in **Chapter 5**. Focus is therefore brought to $\bar{M}_n^V$ and X_c predictions of heterogeneous stents, which are now discussed.

6.5.4 Modelling heterogeneous BPS properties

The impact of initial crystallinity on degradation has been experimentally investigated for PLLA, with increased rates of degradation observed for

samples with higher initial crystallinities [39], [40]. Experimental measurements of BPS have highlighted differences in polymer alignment and morphology across stents [46], [47], with higher values of crystallinity reported at outer surfaces compared to within the stent core [46]. Such differences have been attributed to the complex material transformations which occur during the device manufacture process, in particular during the crimping step, where the thermal and mechanical strain imparted strongly influence the BPS microstructure [42], [47]. The effect of such material heterogeneities on device degradation behaviour in-vivo is examined through computational predictions, and it is revealed that introducing differences in X_c slightly improves BPS scaffolding ability under the SFS assumption; with comparable ϕ_L loss predicted for both homogenous and heterogeneous cases in the SFE simulations (**Figure 6.14**). An increase in material degradation is observed at the core of heterogeneous BPS for both boundary conditions. Similar trends for X_c are observed for homogenous and heterogeneous stents under SFS conditions. For the heterogeneous case, the differences in X_c across the BPS strut are shown to have an important effect on the material stiffness measured. The faster rate of X_c increase observed in the SFE case leads to an increase in material stiffness at the core of the device after 30 weeks. As discussed above, this change in the location of the maximum stiffness has important implications for the long-term mechanical performance of the device.

6.5.5 Damage based degradation of mechanical properties

Initially damage in PLLA BPS due to degradation is incorporated through changes in the decreasing normalised molecular weight, M_w (Model 1) or $\bar{M}_n$ (Model 2, Model 3) of the polymer. Physio-chemical degradation is governed by the rates of change and diffusion behaviour of ester bonds, C_e, and

monomer products, C_m, in Model 1, while Model 2 equations include the effects of chain scission concentration, R_s, larger oligomer products, C_{ol}, degree of crystallinity, X_c, molar mass of lactic units, M_0, the inverse molar volume of the crystalline phase, ω and the initial molar concentration of polymer chains, $N_{chains0}$ (see **Table 6.1** for details). Model 3 simulations follow the same trends in physio-chemical degradation as Model 2; however the damage parameter in Model 3 is assumed to be dependent on changes in M_n and X_c of the material (Eq. (6.4). In the BPS simulations, damage is initiated in the material immediately after the onset of degradation. As has commonly been observed for the biodegradable polyesters however, mechanical property decrease does not occur until a critical value of M_n is reached [48]–[50].

6.5.6 PLLA material behaviour

As is discussed in **Chapter 2**, PLLA experiences complex mechanical behaviour, including non-linear deformation behaviour at moderate strains, similarly to other thermoplastic polymers [1], [11], [15], [16]. The hyperelastic Knowles model [14] has previously been shown to capture the behaviour of PLLA under isochoric uniaxial extension [17], and has recently been used to represent the mechanical behaviour of PLLA BPS ([17], [22]). In relation to the elastic response of the material, maximum principal stress in the range of40-45 MPa is reported (**Figure 6.10**), which is in the lower stress-strain range (pre stress peak) of the behaviour shown for the Knowles model (**Figure 6.3**) corresponding with the observed experimental behaviour for PLLA seen in **Chapter 2**.

Reductions in maximum Von Mises stress in degrading BPS are predicted for each model (**Figure 6.10**). Stress is revealed to decrease at a more gradual rate in devices assigned the SFS boundary condition than those modelled as SFE, with the observed reduction in stress following a similar trend to [12]. Improvements in the mechanical model of PLLA behaviour presented here, including the addition of plastic [1], [4], or quasi-linear viscoelastic material behaviour [11], [51] would enable more accurate predictions of BPS in-vivo stress state.

In its current form, the degradation modelling framework is a one-way coupling between the physio-chemical properties of the degrading stent and its mechanical stiffness. In future studies, consideration of the impact of in-vivo stress and loading on the physio-chemical degradation constants (e.g. reaction rates, and diffusion coefficients similarly to [52]) would provide more insight into the predicted in-vivo degradation rates. Experimental studies which have examined the impact of in-vivo stress and loading on the degradation behaviour of BPS have shown the importance of static [53], [54] and dynamic loading [22], [35] in accelerating the degradation of the material's tensile properties.

6.5.7 BPS mechanical performance

Radial force testing is often the means through which stents are evaluated for long-term performance [55], [56]. The ability of the device to provide scaffolding support to the vessel wall is characterised by both its radial strength and radial stiffness [57], which are often of particular importance in the polymeric stents, due to polymers exhibiting reduced mechanical properties compared to metallic materials [58].

The impact of BPS degradation on the radial stiffness of the device is evaluated here based on the computational predictions of molecular weight and crystallinity. The average radial force experienced by the BPS in the arterial simulations over the degradation time of 2 years is compared for each of the cases (**Figure 6.18**). Values of initial radial stiffness and strength are similar to those reported in [5] and [12], with predictions for decreasing radial properties for the two examined boundary conditions falling within the range of those observed in [12].

6.5.8 Oversizing and arterial stress

Clinical guidelines for use of BPS include recommendations for device deployment, and in general a pre-dilation, sizing, post-dilation (PSP) strategy is observed by clinicians who are implanting BPS in diseased arteries [59], [60]. Consideration of such guidelines in the computational modelling of BPS deployment is important in order to simulate realistic stresses in both the device and the artery. BPS examined in the current chapter are modelled in a deployed state, with 10% over expansion in the artery, similarly to [1]. Despite experimental evidence showing BPS to be capable of high expansion before experiencing strut fractures [61], instructions for clinical use advise against expanding the stent beyond 0.5 mm greater than its nominal diameter [62].

BPS deployment and implantation produce high stresses in the arterial wall, which can often trigger stent restenosis [63]–[65] or stent thrombosis [66], [67] due to vessel injury (which may occur as a result of over-expansion, incomplete BPS expansion or strut fracture during deployment). Predictions of the maximum principal stresses generated in the artery reveals an average decrease of 17% in stress in the intima layer with BPS degradation; SFS

simulations display high areas of arterial stress even at later time points, compared to SFE cases, which exhibit a sharp drop off in stress. This observed decrease in maximum principal stress is in agreement with that reported in [12], which investigated the mechanical interactions between degrading BPS in a combined artery and plaque model. Knowledge of the stress values in diseased arteries treated with BPS possessing heterogeneous degradation behaviours offers insight into the expected in-vivo response. Arterial remodelling is influenced by the shear stresses which endothelial cells in the arterial wall are exposed to during implantation [63], [68], [69]. Including the influence of shear stress on the arterial remodelling process in-vivo in a computational framework would allow for enhanced analysis of BPS performance in-vivo [70].

6.6 Conclusion

In conclusion, the work presented in this chapter demonstrates the ability of the developed FE model to provide predictions into the physio-chemical degradation behaviour and the mechanical performance of PLLA based BPS. The type of loading applied, degradation product boundary conditions and non-uniform crystallinity are all revealed to be important factors in prediction of the final scaffolding ability of the device. The emergent significant factors from this chapter are discussed, along with the other main findings of this thesis, in **Chapter 7**.

References

[1] R. G. Pauck and B. D. Reddy, “Computational analysis of the radial mechanical performance of PLLA coronary artery stents,” *Med. Eng. Phys.*, vol. 37, no. 1, pp. 7–12, 2015.

[2] N. Debusschere, P. Segers, P. Dubruel, B. Verhegghe, and M. De Beule, “A finite element strategy to investigate the free expansion behaviour of a biodegradable polymeric stent,” *J. Biomech.*, vol. 48, no. 10, pp. 2012–2018, 2015.

[3] A. C. Bobel, S. Petisco, J. Ramon Sarasua, W. Wenxin, and P. E. McHugh, “Computational Bench Testing to Evaluate the Short-Term Mechanical Performance of a Polymeric Stent,” *Cardiovasc. Eng. Technol.*, 2015.

[4] A. C. Bobel and P. E. McHugh, “Computational Analysis of the Utilisation of the Shape Memory Effect and Balloon Expansion in Fully Polymeric Stent Deployment,” *Cardiovasc. Eng. Technol.*, vol. 9, no. 1, pp. 60–72, 2018.

[5] Q. Wang, G. Fang, Y. Zhao, G. Wang, and T. Cai, “Computational and experimental investigation into mechanical performances of Poly-L-Lactide Acid (PLLA) coronary stents,” *J. Mech. Behav. Biomed. Mater.*, vol. 65, pp. 415–427, 2017.

[6] T. Y. Qiu, L. G. Zhao, and M. Song, “A Computational Study of Mechanical Performance of Bioresorbable Polymeric Stents with Design Variations,” *Cardiovasc. Eng. Technol.*, vol. 10, no. 1, pp. 46–60, 2018.

[7] A. Schiavone, T.-Y. Qiu, and L.-G. Zhao, “Crimping and deployment of metallic and polymeric stents -- finite element modelling,” *Vessel Plus*, vol. 1, no. 1, pp. 12–21, 2017.

[8] T. Y. Qiu, M. Song, and L. G. Zhao, “A computational study of crimping and expansion of bioresorbable polymeric stents,” *Mech. Time-Dependent Mater.*, vol. 22, no. 2, pp. 273–290, 2018.

[9] J. S. Soares, J. E. Moore, and K. R. Rajagopal, “Modeling of deformation-accelerated breakdown of polylactic acid biodegradable stents,” *J. Med. Device.*, vol. 4, no. 4, p. 41007, 2010.

[10] K. R. Rajagopal, A. R. Srinivasa, and A. S. Wineman, “On the shear and bending of a degrading polymer beam,” *Int. J. Plast.*, vol. 23, no. 9, pp. 1618–1636, 2007.

[11] A. Muliana and K. R. Rajagopal, “Modeling the response of nonlinear viscoelastic biodegradable polymeric stents,” *Int. J. Solids Struct.*, vol. 49, no. 7–8, pp. 989–1000, 2012.

[12] T. Qiu, R. He, C. Abunassar, S. Hossainy, and L. G. Zhao, “Effect of two-year degradation on mechanical interaction between a bioresorbable scaffold and blood vessel,” *J. Mech. Behav. Biomed. Mater.*, vol. 78, no. November 2017, pp. 254–265, 2018.

[13] G. Holzapfel, G. Sommer, T. Gasser, and P. Regitnig, “Determination of layer-specific mechanical properties of human coronary arteries with nonatherosclerotic intimal thickening and related constitutive modeling,” *Am. J. Physiol. Heart Circ. Physiol.*, vol. 289, pp. H2048-58, Dec. 2005.

[14] J. Knowles, “The finite anti-plane shear field near the tip of a crack for a class of incompressible elastic solids,” *Int. J. Fract.*, vol. 13, no. 5, pp. 611–639,

1977.

[15] M. Bartkowiak-Jowsa, R. Będziński, A. Kozłowska, J. Filipiak, and C. Pezowicz, “Mechanical, rheological, fatigue, and degradation behavior of PLLA, PGLA and PDGLA as materials for vascular implants,” *Meccanica*, vol. 48, no. 3, pp. 721–731, 2013.

[16] P.-J. Wang *et al.*, “Effect of working environment and procedural strategies on mechanical performance of bioresorbable vascular scaffolds,” *Acta Biomater.*, pp. 1–10, 2018.

[17] J. S. Soares, K. R. Rajagopal, and J. E. Moore Jr., “Deformation-induced hydrolysis of a degradable polymeric cylindrical annulus,” *Biomech. Model. Mechanobiol.*, vol. 9, no. 2, pp. 177–186, 2010.

[18] J. Lunt, “Large-scale production, properties and commercial applications of poly lactic acid polymers,” *Polym. Degrad. Stab.*, vol. 59, no. 1–3, pp. 145–152, 1998.

[19] D. Garlotta, “A Literature Review of Poly (Lactic Acid),” vol. 9, no. 2, 2002.

[20] C. Suchocki, “A FINITE ELEMENT IMPLEMENTATION OF KNOWLES STORED-ENERGY FUNCTION : THEORY, CODING & APPLICATIONS,” vol. LVIII, 2011.

[21] R. Shine *et al.*, “Modeling of Biodegradable Polyesters With Applications to Coronary Stents,” *J. Med. Device.*, vol. 11, no. 2, p. 021007, 2017.

[22] D. Hayman, C. Bergerson, S. Miller, M. Moreno, and J. E. Moore, “The effect of static and dynamic loading on degradation of PLLA stent fibers,” *J Biomech Eng*, vol. 136, no. 8, p. 4027614, 2014.

[23] F. Gervaso, C. Capelli, L. Petrini, S. Lattanzio, L. Di Virgilio, and F. Migliavacca, “On the effects of different strategies in modelling balloon-expandable stenting by means of finite element method,” vol. 41, pp. 1206–1212, 2008.

[24] J. Bedoya, C. A. Meyer, L. H. Timmins, M. R. Moreno, and J. Moore James E., “Effects of Stent Design Parameters on Normal Artery Wall Mechanics,” *J. Biomech. Eng.*, vol. 128, no. 5, pp. 757–765, Apr. 2006.

[25] C. Lally and P. J. Prendergast, “Simulation of In-stent Restenosis for the Design of Cardiovascular Stents BT - Mechanics of Biological Tissue,” G. A. Holzapfel and R. W. Ogden, Eds. Berlin, Heidelberg, Heidelberg: Springer Berlin Heidelberg, 2006, pp. 255–267.

[26] E. L. Boland, J. A. Grogan, C. Conway, and P. E. McHugh, “Computer Simulation of the Mechanical Behaviour of Implanted Biodegradable Stents in a Remodelling Artery,” *Jom*, vol. 68, no. 4, pp. 1198–1203, 2016.

[27] E. L. Boland, J. A. Grogan, and P. E. McHugh, “Computational Modeling of the Mechanical Performance of a Magnesium Stent Undergoing Uniform and Pitting Corrosion in a Remodeling Artery,” *J. Med. Device.*, vol. 11, no. 2, p. 021013, 2017.

[28] H. Zahedmanesh and C. Lally, “Determination of the influence of stent strut thickness using the finite element method: Implications for vascular injury and in-stent restenosis,” *Med. Biol. Eng. Comput.*, vol. 47, no. 4, pp. 385–393, 2009.

[29] L. Cardamone, A. Valentín, J. F. Eberth, and J. D. Humphrey, “Origin of axial

prestretch and residual stress in arteries," *Biomech. Model. Mechanobiol.*, vol. 8, no. 6, pp. 431–446, Dec. 2009.

[30] F. Ju, Z. Xia, and K. Sasaki, "On the finite element modelling of balloon-expandable stents," *J. Mech. Behav. Biomed. Mater.*, vol. 1, no. 1, pp. 86–95, 2008.

[31] ASTM, "ASTM F3067 - 14 Guide for Radial Loading of Balloon Expandable and Self Expanding Vascular Stents." 2014.

[32] A. Gleadall, J. Pan, and H. Atkinson, "A simplified theory of crystallisation induced by polymer chain scissions for biodegradable polyesters," *Polym. Degrad. Stab.*, vol. 97, no. 9, pp. 1616–1620, 2012.

[33] J. Li, Q. Luo, Z. Xie, Y. Li, and Y. Zeng, "Fatigue life analysis and experimental verification of coronary stent," *Heart Vessels*, vol. 25, no. 4, pp. 333–337, 2010.

[34] M. Azaouzi, A. Makradi, and S. Belouettar, "Fatigue life prediction of cardiovascular stent using finite element method," *Comput. Methods Biomech. Biomed. Engin.*, vol. 15, no. sup1, pp. 93–95, Sep. 2012.

[35] M. L. Dreher, S. Nagaraja, and B. Batchelor, "Effects of fatigue on the chemical and mechanical degradation of model stent sub-units," *J. Mech. Behav. Biomed. Mater.*, vol. 59, pp. 139–145, 2016.

[36] T. Shazly, V. B. Kolachalama, J. Ferdous, J. P. Oberhauser, S. Hossainy, and E. R. Edelman, "Assessment of material by-product fate from bioresorbable vascular scaffolds," *Ann Biomed Eng*, vol. 40, no. 4, pp. 955–965, 2012.

[37] J. Ferdous, V. B. Kolachalama, and T. Shazly, "Impact of polymer structure and composition on fully resorbable endovascular scaffold performance," *Acta Biomater.*, vol. 9, no. 4, pp. 6052–6061, 2013.

[38] N. A. Weir, F. J. Buchanan, J. F. Orr, D. F. Farrar, and G. R. Dickson, "Degradation of poly-L-lactide. Part 2: increased temperature accelerated degradation," *Proc Inst Mech Eng H*, vol. 218, no. 5, pp. 321–330, 2004.

[39] E. A. R. Duek, C. A. C. Zavaglia, and W. D. Belangero, "In vitro study of poly(lactic acid) pin degradation," *Polymer (Guildf).*, vol. 40, no. 23, pp. 6465–6473, 1999.

[40] H. Tsuji, A. Mizuno, and Y. Ikada, "Properties and Morphology of Poly (L -lactide). III . Effects of Initial Crystallinity on Long-Term In Vitro Hydrolysis of High Molecular Weight Poly (L -lactide) Film in Phosphate-Buffered Solution," *J. Appl. Polym. Sci.*, pp. 1452–1464, 2000.

[41] H. Tsuji, "Properties and morphologies of poly(L-lactide): 1. Annealing condition effects on properties and morphologies of poly(L-lactide)," *Polymer (Guildf).*, vol. 36, no. 14, pp. 2709–2716, 1995.

[42] K. J. L. Burg, M. LaBerge, and S. W. Shalaby, "Change in stiffnesss and effect of orientation in degrading polylactide films," *Biomaterials*, vol. 19, no. 7–9, pp. 785–789, 1998.

[43] H. Tsuji, "Poly(lactide) stereocomplexes: Formation, structure, properties, degradation, and applications," *Macromol. Biosci.*, vol. 5, no. 7, pp. 569–597, 2005.

[44] M. Vert, "Aliphatic Polyesters : Great Degradable Polymers That Cannot Do Everything," pp. 538–546, 2005.

[45] K. Fukushima, J. Luis, and M. Yang, “Comparison of abiotic and biotic degradation of PDLLA , PCL and partially miscible PDLLA / PCL blend,” *Eur. Polym. J.*, vol. 49, no. 3, pp. 706–717, 2013.

[46] P.-J. Wang, N. Ferralis, C. Conway, J. C. Grossman, and E. R. Edelman, “Strain-induced accelerated asymmetric spatial degradation of polymeric vascular scaffolds,” *Proc. Natl. Acad. Sci.*, p. 201716420, 2018.

[47] A. Ailianou, K. Ramachandran, M. B. Kossuth, J. P. Oberhauser, and J. A. Kornfield, “Multiplicity of morphologies in poly (l-lactide) bioresorbable vascular scaffolds,” *Proc. Natl. Acad. Sci.*, vol. 113, no. 42, pp. 11670–11675, 2016.

[48] R. N. Shirazi, W. Ronan, Y. Rochev, and P. McHugh, “Modelling the degradation and elastic properties of poly (lactic-co-glycolic acid) films and regular open-cell tissue engineering scaffolds,” *J. Mech. Behav. Biomed. Mater.*, vol. 54, pp. 48–59, 2016.

[49] A. S. Maxwell and P. E. Tomlins, “New approaches to mapping through-thickness variations in the degradation in poly (lactide-co-glycolide),” *Polym. Degrad. Stab.*, vol. v. 96, no. 5, pp. 1015-1021–2011 v.96 no.5, 2011.

[50] H. Tsuji, “Autocatalytic hydrolysis of amorphous-made polylactides: effects of L-lactide content, tacticity, and enantiomeric polymer blending,” *Polymer (Guildf).*, vol. 43, no. 6, pp. 1789–1796, 2002.

[51] C. Suchocki, “A QUASI-LINEAR VISCOELASTIC RHEOLOGICAL MODEL FOR THERMOPLASTICS AND RESINS,” *J. Theor. Appl. Mech. Appl.*, pp. 117–129, 2013.

[52] G. N. Gatica, B. Gomez-vargas, and R. Ruiz-baier, “Analysis and mixed-primal finite element discretisations for stress-assisted diffusion problems,” *Comput. Methods Appl. Mech. Engrg.*, vol. 337, pp. 411–438, 2018.

[53] J. F. da S. Soares, “Constitutive modeling for biodegradable polymers for application in endovascular stents,” Texas A&M University, 2008.

[54] J. S. Soares, J. E. Moore Jr., and K. R. Rajagopal, “Constitutive framework for biodegradable polymers with applications to biodegradable stents,” *ASAIO J*, vol. 54, no. 3, pp. 295–301, 2008.

[55] B. W. Kaebnick, B. D. Gogas, and S. B. King III, “Interventional Cardiology,” 2nd ed., 2007, pp. 3–13.

[56] F. Migliavacca, L. Petrini, M. Colombo, F. Auricchio, and R. Pietrabissa, “Mechanical behavior of coronary stents investigated through the finite element method.,” *J. Biomech.*, vol. 35, no. 6, pp. 803–811, Jun. 2002.

[57] W. Schmidt, P. Behrens, and K.-P. Schmitz, “Biomechanical Aspects of Potential Stent Malapposition at Coronary Stent Implantation BT - World Congress on Medical Physics and Biomedical Engineering, September 7 - 12, 2009, Munich, Germany,” 2009, pp. 136–139.

[58] C. M. Agrawal, K. F. Haas, D. A. Leopold, and H. G. Clark, “Evaluation of poly(L-lactic acid) as a material for intravascular polymeric stents,” *Biomaterials*, vol. 13, no. 3, pp. 176–182, 1992.

[59] C. Tamburino *et al.*, “Contemporary practice and technical aspects in coronary intervention with bioresorbable scaffolds: a European perspective.,” *EuroIntervention J. Eur. Collab. with Work. Gr. Interv. Cardiol. Eur. Soc. Cardiol.*, vol. 11, no. 1, pp. 45–52, May 2015.

[60] L. Ortega-Paz *et al.*, “Predilation, sizing and post-dilation scoring in patients undergoing everolimus-eluting bioresorbable scaffold implantation for prediction of cardiac adverse events: Development and internal validation of the PSP score,” *EuroIntervention*, vol. 12, no. 17, pp. 2110–2117, 2017.

[61] J. A. Ormiston, B. Webber, B. Ubod, O. Darremont, and M. W. I. Webster, “An independent bench comparison of two bioresorbable drug-eluting coronary scaffolds (Absorb and DESolve) with a durable metallic drug-eluting stent (ML8/Xpedition).,” *EuroIntervention J. Eur. Collab. with Work. Gr. Interv. Cardiol. Eur. Soc. Cardiol.*, vol. 11, no. 1, pp. 60–67, May 2015.

[62] A. Abizaid *et al.*, “Serial Multimodality Imaging and 2-Year Clinical Outcomes of the Novel DESolve Novolimus-Eluting Bioresorbable Coronary Scaffold System for the Treatment of Single De Novo Coronary Lesions,” *JACC Cardiovasc. Interv.*, vol. 9, no. 6, pp. 565–574, 2016.

[63] E. R. Edelman and C. Rogers, “Pathobiologic responses to stenting.,” *Am. J. Cardiol.*, vol. 81, no. 7A, pp. 4E-6E, Apr. 1998.

[64] R. Hoffmann and G. S. Mintz, “Coronary in-stent restenosis - Predictors, treatment and prevention,” *Eur. Heart J.*, vol. 21, no. 21, pp. 1739–1749, 2000.

[65] G. S. Mintz *et al.*, “In-stent restenosis: The Washington Hospital Center experience,” *Am. J. Cardiol.*, vol. 81, no. 7 A, pp. 7E-13E, 1998.

[66] K. Kolandaivelu *et al.*, “Stent thrombogenicity early in high-risk interventional settings is driven by stent design and deployment and protected by polymer-drug coatings.,” *Circulation*, vol. 123, no. 13, pp. 1400–1409, Apr. 2011.

[67] S. Puricel *et al.*, “Bioresorbable Coronary Scaffold Thrombosis: Multicenter Comprehensive Analysis of Clinical Presentation, Mechanisms, and Predictors,” *J. Am. Coll. Cardiol.*, vol. 67, no. 8, pp. 921–931, 2016.

[68] A. M. Malek, S. L. Alper, and S. Izumo, “Hemodynamic Shear Stress and Its Role in Atherosclerosis,” *JAMA*, vol. 282, no. 21, pp. 2035–2042, Dec. 1999.

[69] J. J. Wentzel *et al.*, “Relationship between neointimal thickness and shear stress after Wallstent implantation in human coronary arteries.,” *Circulation*, vol. 103, no. 13, pp. 1740–1745, Apr. 2001.

[70] E. L. Boland, J. A. Grogan, and P. E. McHugh, “Computational modelling of magnesium stent mechanical performance in a remodelling artery: Effects of multiple remodelling stimuli.,” *Int. j. numer. method. biomed. eng.*, vol. 35, no. 10, p. e3247, Oct. 2019.

7 Discussion and Conclusion

7.1 Chapter Summary

The main outcomes of the work presented in this thesis are now summarised and discussed. An overview of thesis structure is given in Section 7.2, with key findings highlighted in Section 7.3. Considerations for the modelling requirements for BPS regulatory approval are presented (Section 7.4) and future perspectives for this area are given (Section 7.5). Finally, concluding remarks are outlined in Section 7.6.

7.2 Thesis Overview

In **Chapter 1**, the concept of bioresorbable polymeric stents (BPS) is introduced as a treatment for coronary artery disease and several of the main challenges facing their widespread clinical use are discussed. A review of the relevant background literature is given in **Chapter 2**, with a focus on the degradation and mechanical behaviours of PLLA (currently the prevalent material for the BPS application). A critical review of the state of the art in computational modelling techniques for BPS degradation is also presented. The theoretical methods employed in this thesis are presented in **Chapter 3**. In **Chapter 4**, a finite element implementation of a physio-chemical degradation model is verified and simulations are performed on various polymeric devices, with insight provided on the impact of boundary condition and device design on degradation rates. Material crystallinity equations are included in the computational framework in **Chapter 5**, and the diffusive flux of degradation products is evaluated. Finally, in **Chapter 6**, simulations are performed to investigate the long-term degradation and mechanical performance of BPS.

7.3 Main Findings of Thesis

Bioresorbable polymeric stents are undergoing development as the next innovation in PCI. Unlike their predecessors, bare metal and drug eluting stents, which demonstrated almost immediate success [1], [2], BPS have faced a number of challenges in their adoption onto the global marketplace. Such challenges include the realisation of optimal device degradation rates, strut thickness, strut fracture and late BPS recoil, as discussed in **Chapter 1**. The development of comprehensive and robust computational modelling techniques to investigate BPS degradation would present opportunities to address such challenges.

As reviewed in **Chapter 2**, the mechanical behaviour of PLLA is highly dependent on testing and processing temperatures, loading rate, and material microstructure. Through adaption of processing and manufacturing techniques it is possible to tailor the mechanical properties of PLLA for use in the BPS application. Furthermore, creation of innovative materials by blending PLLA with other degradable polymers, or through addition of degradable nanoparticles, would enable further advancements in BPS design [3], [4].

7.3.1 Computational modelling techniques for BPS

Computational modelling of BPS has typically focused on the short-term mechanical performance of the device in the absence of degradation. A critical review of the computational modelling techniques developed to predict and analyse the degradation of BPS indicates that such modelling methods can generally be split into two main classes; phenomenological and physio-chemical models, with each having distinct advantages and limitations in capturing BPS degradation behaviour.

In an attempt to bridge the gap between the phenomenological damage based and physio-chemical approaches, implementation of physio-chemical degradation equations into a finite element (FE) modelling programme is demonstrated herein, through substitution of physio-chemical degradation and crystallisation equations into the constitutive laws of the heat equation and use of a thermal analogy (**Chapter 3**). The modelling framework developed allows predictions of the physio-chemical aspects of BPS degradation (i.e. decreasing molecular weight, crystallinity, and degradation product diffusion) alongside predictions of their subsequent impact on mechanical performance.

7.3.2 Degradation of polymer materials

The influence of material degradation rate constant on the predicted values of molecular weight, M_w, in several BPS geometries is highlighted in **Chapter 4**. The significantly faster degradation in M_w predicted for PLGA devices is consistent with the known degradation lifetime of this material [5]. PLGA is often chosen for degradable drug-eluting coatings on stents as its faster degradation rates are desirable for the controlled delivery of anti-proliferative drugs to reduce restenosis during the early stages of stent implantation [6], [7]. PLLA has become the most widely investigated polymer for the BPS application, as discussed in **Chapter 2**.The longer degradation times of PLLA are believed to show benefits for both healing of the artery wall and restoration of vessel vasomotion [8].

7.3.3 Degradation in mechanical properties

The influence of degradation in M_w on material Young's modulus for a range of materials is investigated (**Chapter 4**) using a suggested general relationship [9]; PLLA exhibits longer lasting mechanical integrity, compared to PLA and PLGA. Semi-crystalline poly-lactide materials show higher initial mechanical

strength than amorphous polymers [10], with longer degradation times also apparent (due to the faster hydrolysis of amorphous (disordered) regions ([11], [12])).

In **Chapter 6**, examination of the loss of lumen diameter (ϕ_L) of PLLA based BPS using a coupled co-simulation modelling framework provides insight into their long-term scaffolding ability. Loss of ϕ_L is often reported as a primary endpoint in clinical studies of BPS in-vivo performance [13]; the predictions of lumen loss for BPS in **Chapter 6** show a mutual reliance on the damage formulation used (e.g. Model 1, Model 2, Model 3) and the degradation product boundary condition. The predicted trends for BPS radial force show a similar reliance on model and degradation product assumption.

7.3.4 Impact of polymer crystallinity

The influence of the degree of crystallinity, X_c, on the degradation of PLLA BPS is examined and reduced degradation rates are noted for semi-crystalline BPS modelled under SFE conditions (**Chapter 5**). It is possible to capture material mass loss through flux of degradation products using the updated diffusion theory; as outlined in **Chapter 5** rate constants for PLLA are calibrated for the model. The interplay between diffusion, degradation and crystallisation is investigated for a BPS strut under various boundary conditions, with degradation product diffusion emerging as dominant over autocatalysis reactions, and a minor influence seen for the investigated gradient nature of the applied boundary condition.

An influence of X_c on the predicted loss of ϕ_L for the PLLA BPS examined in **Chapter 6** is observed; inclusion of X_c is seen to provide improved scaffolding ability to the devices examined under SFE conditions. As reported and discussed in **Chapter 6**, examining the interactions between X_c and the

material stiffness of BPS highlighted a late stage increase in material stiffness at the core of stents degraded under SFE conditions. Degradation driven changes in X_c are believed to contribute to the increased stiffness and higher tensile properties often observed for degrading PLLA specimens [14]–[17].

7.3.5 BPS design

A minimal influence of geometry and strut thickness on the degradation trends predicted for BPS is observed in **Chapter 4** and **5**. As discussed in **Chapter 4**, by comparing the respective values of diffusion length, l_{diff}, of each material to the characteristic length scale (i.e. the strut thickness), the maximum strut thickness investigated for PLLA is found to be lower than the value of l_{diff} determined for heterogeneous degradation to dominate over degradation product diffusion in this material. Less of an increase in material porosity (i.e. formation of large voids) is seen with spatially homogeneous degradation, and hence the mechanical integrity of the material for this degradation mechanism is expected to persist until extreme loss of mass is observed. For the PLLA devices examined in **Chapter 5**, the material flux predictions exhibit a slight dependency on thickness.

As discussed in **Chapter 1**, strut thickness plays a critical role in the clinical outcomes of BPS during the initial implantation stage [18], [19], and in the occurrence of late stage ISR or stent thrombosis [20], [21]. The thickness of a deployed BPS influences the shear stresses imparted on the vessel wall, impacting endothelialisation [22] and the arterial remodelling process [21], which has significant consequences for the formation of device degradation boundary conditions.

7.3.6 Degradation product boundary conditions

The numerical predictions in **Chapters 4**-**6** show a considerable dependency on the imposed degradation product boundary conditions. Significant increases in the predicted rates of chain scission (hydrolysis), formation of crystalline regions and loss of ϕ_L are apparent for BPS where degradation products are considered to be confined, or 'embedded' within neo-intimal tissue regrowth (i.e. SFE condition), compared to when BPS are assigned degradation product free surfaces (i.e. SFS condition). The assumption of the immediate removal of the degradation products from free surfaces represents the eradicating actions of in-vivo blood flow, which lessens the autocatalytic effects observed for PLLA degradation [23], [24], and which brings about the more gradual rates of degradation observed for the SFS cases. The autocatalytic nature of polyester degradation has been widely investigated in experimental studies (for example, in [25]–[27]), while few computational studies of BPS have considered this phenomenon [28], [29].

7.4 Thesis Implications and Impact on Modelling for BPS

The findings of the modelling work presented in this thesis highlight a number of areas of importance for the development of improved design and analysis techniques for BPS, and the enhancement of the regulatory guidelines surrounding modelling for BPS regulatory approval. Guidance documents published by the FDA for intravascular stents and associated delivery systems recommend the implementation of finite element analysis (FEA) to evaluate the stress/strain behaviour and assess the fatigue and durability performance of such devices [30]. Specific detailed guidelines on the FEA requirements for bioresorbable stents however, are yet to be published [31], although the American Society of Mechanical Engineering (ASME) has recently released a

Verification and Validation (V&V 40) document for the computational modelling of medical devices [32], which seeks to further advance the in-silico techniques used to assess medical device performance for regulatory approval. The adoption of such new standards, alongside improved insights into polymer and BPS degradation mechanisms, will enable more accurate models to be developed.

As a first implication of the work presented herein, the important role of stent endothelialisation in accurate prediction of device degradation rates is highlighted. The considerable impact of device boundary condition on the damage predicted for BPS examined herein (e.g. in **Chapter 6**, 10% damage predicted for SFS after 26 weeks vs. 48% for SFE following the same time period) highlights the need for accurate knowledge of tissue response. BPS degradation in-vivo occurs alongside several key tissue responses (e.g. inflammation, endothelial and smooth muscle cell (SMC) proliferation, neo-intima formation and endothelialisation during the early stages of implantation, followed by neo-intimal remodelling (NIR) [33]). The majority of this active response of arterial tissue post stent implantation, which greatly influences the surrounding boundary conditions, is generally believed to occur within the first 3-6 months [34], [35], suggesting that the two extreme degradation product boundary conditions considered in this thesis in reality transform and fluctuate throughout the lifetime of the implanted device. Alongside this, incomplete vessel healing which leads to uncovered struts [36] would further impact the diffusion behaviours of degradation products. In-vivo animal and clinical studies designed to evaluate the tissue response alongside BPS performance would provide essential information for enhancement of BPS degradation models. In recent computational studies of bioresorbable magnesium stents (BRMS), NIR has recently been shown to have a significant impact on the

mechanics of the stent [37]–[39], as well as noticeable effects on the in-vivo degradation rates [40].

Another implication of the work presented in this thesis relates to the material degree of crystallinity X_c; the inclusion of X_c has many consequences for modelling the performance (both degradation and mechanical aspects) of BPS, therefore, degradation-driven changes in X_c of degrading polymer materials are an important consideration for BPS design and analysis. Variations in X_c have recently been observed throughout examined BPS [41], [42]; such differences are often attributed to the effects of different material processing methods or device crimping procedures [17], [41] The inclusion of heterogeneous material properties in BPS (as examined in **Chapter 6**) demonstrates an improvement in the scaffolding ability predicted for SFS and SFE devices Computational investigation and prediction of the changing X_c in a device over the course of its degradation allows for insight into the expected mechanical response at different regions and as such should be taken into consideration in the development of modelling techniques.

The anticipated fate of degradation products is also shown here to be dependent on X_c, with the diffusion behaviour of both monomers and oligomers impacted by the formation of crystalline regions; X_c has previously been shown to significantly impact the concentration of lactic acids in a defined critical zone in an arterial wall [29]. Inclusion of degradation product diffusion into and through the surrounding arterial tissue (similarly to [28], [29], [43]) as well as the representation of atherosclerotic plaques [44], would add further dimensions to a modelling frameworks for BPS analysis.

The impact of mechanical loading (i.e. uniform external pressure, vs. arterial loading) on the loss of ϕ_L predicted for the BPS examined here is revealed to

be significant. Consideration of the mechanical boundary conditions acting on the device during degradation should form part of BPS modelling developments. In the presented work, the application of arterial loading produces more gradual rates of ϕ_L loss; this is considered to more closely follow an expected in-vivo response. The interactions between the artery and the BPS transform with degradation, therefore further enhancements to this framework, e.g. to include NIR, is required.

In its current form, the presented degradation modelling framework is a one-way coupling between the physio-chemical properties of the degrading stent and its mechanical stiffness. The different damage formulations examined herein (Model 1, Model 2, Model 3) to investigate BPS mechanical performance represent first approximations of the link between physio-chemical degradation and the mechanical properties of the material. Experimental studies which have examined the impact of in-vivo stress and loading on the degradation behaviour of BPS have shown the importance of static [45] and dynamic loading [14], [46] in accelerating the degradation of the material's tensile properties.

An increased interest in polyester chemistry, composite materials, and adaptive manufacturing and processing techniques will enable BPS with suitable mechanical properties, enhanced design and tailored degradation rates to be developed from combinations of polymer and composite materials. The modelling framework presented in this work enables the degradation and mechanical performance of several polymeric materials, along with composite materials and polymers enhanced with degradable nanoparticles, to be computationally investigated.

As discussed in **Chapter 2**, further work is needed to advance the computational modelling techniques used to examine the degradation behaviours of polymeric materials for the BPS application. Multi-scale and multi-physical models which take into account both the physio-chemical and phenomenological damage-based effects of material degradation, which can offer further insight into and capture the impact and influences of the complex in-vivo environment (dynamic loads, blood flow, tissue remodelling etc.) and which provide opportunities for robust and rigorous validation to experimental data would improve the design and analysis outcomes for BPS. The various implications of the work presented herein present opportunities to improve modelling techniques for BPS design and analysis, while also providing possible enhancement to the regulatory guidelines surrounding such techniques.

7.5 Future Perspective

A number of suggestions for the future development and enhancement of the computational modelling techniques for BPS degradation are now outlined and briefly discussed.

Appropriate understanding of neo-intimal formation during early BPS implantation, and NIR during late stage BPS erosion would enable the development of more realistic physio-chemical degradation modelling techniques. Timescales for tissue regrowth around implanted struts show wide variation for different material and device designs [18]. Insights into the in-vivo tissue response to BPS implantation can be gained through use of advanced imaging techniques (e.g. OCT, IVUS as discussed in **Chapter 5** [47]–[49]),which can aid quantification of the in-vivo degradation product boundary conditions which exist for BPS. As discussed above, the impact of NIR on the

mechanical performance of bioresorbable stents has recently been investigated for BRMS [37]–[39]. Adaptation of the techniques used to examine BRMS for the analysis of BPS is now achievable, however, is reliant on further knowledge of the stent encapsulation and NIR processes during BPS implantation.

Due to the high dependency of polyester material degradation on residual degradation products, residual monomers have received increasing interest in recent years, including further understanding of the effect of various polymer processing techniques on their formation [50]. Further insight into the fate of degradation products in-vivo may be achieved through experimental [51], [52] or computational means [28], [43]. Due to expected high-costs and lengthy timescales that would be required to experimentally investigate degradation product diffusion through, or accumulation in, arterial tissue during BPS degradation, the use of computational modelling presents an effective means to assess and predict such behaviours and provide further insights into the autocatalysis effect, and the potential for adverse tissue response [53]–[55] following accumulation of lactic acids in local tissue. The inclusion of degradation product transport into and diffusion through surrounding arterial tissue represents another possible avenue for future investigation. The thermal analogy presented in this thesis provides a sound basis to build on the implementation of the physio-chemical degradation equations and similar to [43], examine the diffusion behaviour of degradation products in compressed anisotropic arterial tissue.

Through the presented FE implementation of the physio-chemical degradation and crystallisation equations, robust validation of the degradation model in complex and realistic device geometries is now possible for BPS. Strut

thickness is shown to have a negligible influence on the degradation predictions of the BPS examined herein; however examining the influence of thickness on BPS mechanical performance, as well as on its interactions with a diseased artery, provide opportunities for further investigation. The inclusion of a biodegradable drug-eluting coating on the surface of the BPS would also improve the model prediction capabilities. Possibilities exist to combine the degradation framework presented here with formulations governing drug release from a biodegradable polymeric coating, similarly to that presented in [56]–[58].

One of the main limitations of the modelling work presented here is the lack of direct experimental degradation data for BPS. Further experimental testing of biodegradable polymers and of BPS is important to increase confidence in developed numerical analysis and design methods. The conventional experimental testing techniques developed for permanent BMS and DES have been unsuccessful in adequately evaluating BPS [59]. As revealed in the review of the experimental literature in **Chapter 2**, the arrangement and execution of long-term experiments to examine BPS degradation and mechanical performance is a many factored and iterative process. Efforts to design enhanced experiments to study the long-term creep behaviour of PLLA based BPS would represent a significant step towards better device design. Alongside this, the impact of in-vivo conditions (e.g. pulsatile blood flow) on degradation, crystallisation and mechanical performance are important considerations (as reviewed for biodegradable polyesters in [60]).

The development of computational modelling techniques for BPS behaviour is also dependent on improved understanding of the impacts of loading on the physio-chemical degradation. In future studies, consideration of the impact of

in-vivo stress and loading on physio-chemical degradation (e.g. by inclusion of either stress-dependant reaction rates, or diffusion coefficients as presented in Gatica *et al*. [61]) would aid the accuracy of model predictions. Further development of novel experimental techniques to provide for inclusion of stress or strain-based loading during long-term device degradation would aid the validation and enhancement of computational modelling techniques. The modelling framework presented in this thesis offers an efficient means for the inclusion of the above described future work steps.

7.6 Concluding remarks

A recent review of the hydrolytic degradation of bioresorbable polymer based biomaterials [62] concluded that a complex knowledge based approach is needed to achieve an enhanced understanding of the complete aspects of hydrolytic degradation. The findings presented herein back this statement, with the computational investigations of physio-chemical degradation and scaffolding performance of several BPS revealing a significant reliance on device boundary condition, material reaction constants and microstructure, and type of loading experienced. Several critical and suitable areas for future research in this area have been identified (Section 7.5), In conclusion, the work presented in this thesis provides some novel insights into the degradation behaviours of bioresorbable polymeric stents (BPS) for the treatment of coronary artery disease, and an adaptable computational modelling framework for physio-chemical and damage based degradation is presented.

References

[1] D. L. Fischman *et al.*, “A Randomized Comparison of Coronary-Stent Placement and Balloon Angioplasty in the Treatment of Coronary Artery Disease,” *N. Engl. J. Med.*, vol. 331, no. 8, pp. 496–501, Aug. 1994.

[2] D. Ardissino *et al.*, “Sirolimus-eluting vs uncoated stents for prevention of restenosis in small coronary arteries: a randomized trial.,” *JAMA*, vol. 292, no. 22, pp. 2727–2734, Dec. 2004.

[3] Y. Chen, A. Murphy, D. Scholz, L. M. Geever, J. G. Lyons, and D. M. Devine, “Surface-modified halloysite nanotubes reinforced poly(lactic acid) for use in biodegradable coronary stents,” *J. Appl. Polym. Sci.*, vol. 135, no. 30, p. 46521, Aug. 2018.

[4] H. Y. Ang *et al.*, “Radiopaque Fully Degradable Nanocomposites for Coronary Stents.,” *Sci. Rep.*, vol. 8, no. 1, p. 17409, 2018.

[5] L. S. Nair and C. T. Laurencin, “Biodegradable polymers as biomaterials,” *Prog. Polym. Sci.*, vol. 32, no. 8, pp. 762–798, 2007.

[6] W. C. Carlyle *et al.*, “Enhanced drug delivery capabilities from stents coated with absorbable polymer and crystalline drug,” *J. Control. Release*, vol. 162, no. 3, pp. 561–567, 2012.

[7] T. Xi *et al.*, “In vitro and in vivo changes to PLGA/sirolimus coating on drug eluting stents,” *Biomaterials*, vol. 31, no. 19, pp. 5151–5158, 2010.

[8] A. Colombo and E. Karvouni, “Biodegradable stents: ‘Fulfilling the mission and stepping away,’” *Circulation*, vol. 102, no. 4, pp. 371–373, 2000.

[9] A. C. Gleadall, “Modelling degradation of biodegradable polymers and their mechanical properties.” Department of Engineering, University of Leicester, 2015.

[10] H. Tsuji, “Poly(lactide) stereocomplexes: Formation, structure, properties, degradation, and applications,” *Macromol. Biosci.*, vol. 5, no. 7, pp. 569–597, 2005.

[11] M. Vert, “Aliphatic Polyesters : Great Degradable Polymers That Cannot Do Everything,” pp. 538–546, 2005.

[12] K. Fukushima, J. Luis, and M. Yang, “Comparison of abiotic and biotic degradation of PDLLA , PCL and partially miscible PDLLA / PCL blend,” *Eur. Polym. J.*, vol. 49, no. 3, pp. 706–717, 2013.

[13] A. Abizaid *et al.*, “Serial Multimodality Imaging and 2-Year Clinical Outcomes of the Novel DESolve Novolimus-Eluting Bioresorbable Coronary Scaffold System for the Treatment of Single De Novo Coronary Lesions,” *JACC Cardiovasc. Interv.*, vol. 9, no. 6, pp. 565–574, 2016.

[14] M. L. Dreher, S. Nagaraja, and B. Batchelor, “Effects of fatigue on the chemical and mechanical degradation of model stent sub-units,” *J. Mech. Behav. Biomed. Mater.*, vol. 59, pp. 139–145, 2016.

[15] N. A. Weir, F. J. Buchanan, J. F. Orr, D. F. Farrar, and G. R. Dickson, “Degradation of poly-L-lactide. Part 2: increased temperature accelerated degradation,” *Proc Inst Mech Eng H*, vol. 218, no. 5, pp. 321–330, 2004.

[16] H. Tsuji and Y. Ikada, “Properties and morphology of poly(l-lactide) 4.

Effects of structural parameters on long-term hydrolysis of poly(l-lactide) in phosphate-buffered solution," *Polym. Degrad. Stab.*, vol. 67, no. 1, pp. 179–189, 2000.

[17] K. J. L. Burg, M. LaBerge, and S. W. Shalaby, "Change in stiffnesss and effect of orientation in degrading polylactide films," *Biomaterials*, vol. 19, no. 7–9, pp. 785–789, 1998.

[18] T. Koppara *et al.*, "Thrombogenicity and early vascular healing response in metallic biodegradable polymer-based and fully bioabsorbable drug-eluting stents," *Circ. Cardiovasc. Interv.*, vol. 8, no. 6, pp. 1–9, 2015.

[19] B. P. Murphy, P. Savage, P. E. McHugh, and D. F. Quinn, "The stress-strain behavior of coronary stent struts is size dependent.," *Ann. Biomed. Eng.*, vol. 31, no. 6, pp. 686–691, Jun. 2003.

[20] A. Kastrati *et al.*, "Intracoronary stenting and angiographic results: strut thickness effect on restenosis outcome (ISAR-STEREO) trial.," *Circulation*, vol. 103, no. 23, pp. 2816–2821, Jun. 2001.

[21] K. Kolandaivelu *et al.*, "Stent thrombogenicity early in high-risk interventional settings is driven by stent design and deployment and protected by polymer-drug coatings.," *Circulation*, vol. 123, no. 13, pp. 1400–1409, Apr. 2011.

[22] C. Simon, J. C. Palmaz, and E. A. Sprague, "Influence of topography on endothelialization of stents: clues for new designs.," *J. Long. Term. Eff. Med. Implants*, vol. 10, no. 1–2, pp. 143–151, 2000.

[23] A. Göpferich, "Mechanisms of polymer degradation and erosion," *Biomaterials*, vol. 17, no. 2, pp. 103–114, 1996.

[24] F. Alexis, "Factors affecting the degradation and drug-release mechanism of poly(lactic acid) and poly[(lactic acid)-co-(glycolic acid)]," *Polym. Int.*, vol. 54, no. 1, pp. 36–46, 2005.

[25] I. Grizzi, H. Garreau, S. Li, and M. Vert, "Hydrolytic degradation of devices based on poly(dl-lactic acid) size-dependence," *Biomaterials*, vol. 16, no. 4, pp. 305–311, 1995.

[26] G. Siparsky, K. Voorhees, and F. Miao, "Hydrolysis of Polylactic Acid (PLA) and Polycaprolactone (PCL) in Aqueous Acetonitrile Solutions: Autocatalysis," *J. Environ. Polym. Degrad.*, vol. 6, no. 1, pp. 31–41, 1998.

[27] X. Yuan, A. F. T. Mak, and K. Yao, "In vitro degradation of poly(L-lactic acid) fibers in phosphate buffered saline," *J. Appl. Polym. Sci.*, vol. 85, no. 5, pp. 936–943, 2002.

[28] T. Shazly, V. B. Kolachalama, J. Ferdous, J. P. Oberhauser, S. Hossainy, and E. R. Edelman, "Assessment of material by-product fate from bioresorbable vascular scaffolds," *Ann Biomed Eng*, vol. 40, no. 4, pp. 955–965, 2012.

[29] J. Ferdous, V. B. Kolachalama, and T. Shazly, "Impact of polymer structure and composition on fully resorbable endovascular scaffold

performance," *Acta Biomater.*, vol. 9, no. 4, pp. 6052–6061, 2013.

[30] Food and Drug Administration, "Guidance for Industry and FDA Staff Non-Clinical Engineering Tests and Recommended Labeling for Intravascular Stents and Associated Delivery Systems," 2010.

[31] Food and Drug Administration, "ASTM-FDA Workshop on Absorbable Medical Devices:Lessons Learned from Correlations of Bench Testing and Clinical Performance," *U.S Food and Drug Administration - Public Workshop*, 2012. [Online]. Available: http://www.fda.gov/MedicalDevices/NewsEvents/WorkshopsConferences/ucm312601.htm. [Accessed: 30-Apr-2015].

[32] ASME, *Assessing Credibility of Computational Modeling through Verification and Validation: Application to Medical Devices*, V V 40-2. 2018.

[33] E. R. Edelman and C. Rogers, "Pathobiologic responses to stenting.," *Am. J. Cardiol.*, vol. 81, no. 7A, pp. 4E-6E, Apr. 1998.

[34] T. Kobayashi *et al.*, "Neointimal characteristics comparison between biodegradable-polymer and durable-polymer drug-eluting stents: 3-month follow-up optical coherence tomography light property analysis from the RESTORE registry," *Int. J. Cardiovasc. Imaging*, no. 0123456789, 2019.

[35] S. Nishio *et al.*, "Long-term (>10 Years) clinical outcomes of first-in-human biodegradable poly-l-lactic acid coronary stents: Igaki-Tamai stents," *Circulation*, vol. 125, no. 19, pp. 2343–2352, May 2012.

[36] A. V Finn *et al.*, "Pathological correlates of late drug-eluting stent thrombosis: strut coverage as a marker of endothelialization.," *Circulation*, vol. 115, no. 18, pp. 2435–2441, May 2007.

[37] E. L. Boland, J. A. Grogan, C. Conway, and P. E. McHugh, "Computer Simulation of the Mechanical Behaviour of Implanted Biodegradable Stents in a Remodelling Artery," *Jom*, vol. 68, no. 4, pp. 1198–1203, 2016.

[38] E. L. Boland, J. A. Grogan, and P. E. McHugh, "Computational Modeling of the Mechanical Performance of a Magnesium Stent Undergoing Uniform and Pitting Corrosion in a Remodeling Artery," *J. Med. Device.*, vol. 11, no. 2, p. 021013, 2017.

[39] E. L. Boland, J. A. Grogan, and P. E. McHugh, "Computational modelling of magnesium stent mechanical performance in a remodelling artery: Effects of multiple remodelling stimuli.," *Int. j. numer. method. biomed. eng.*, vol. 35, no. 10, p. e3247, Oct. 2019.

[40] J. A. Grogan, B. J. O'Brien, S. B. Leen, and P. E. McHugh, "A corrosion model for bioabsorbable metallic stents," *Acta Biomater.*, vol. 7, no. 9, pp. 3523–3533, 2011.

[41] A. Ailianou, K. Ramachandran, M. B. Kossuth, J. P. Oberhauser, and J. A. Kornfield, "Multiplicity of morphologies in poly (l-lactide) bioresorbable vascular scaffolds," *Proc. Natl. Acad. Sci.*, vol. 113, no.

42, pp. 11670–11675, 2016.

[42] P.-J. Wang, N. Ferralis, C. Conway, J. C. Grossman, and E. R. Edelman, “Strain-induced accelerated asymmetric spatial degradation of polymeric vascular scaffolds,” *Proc. Natl. Acad. Sci.*, p. 201716420, 2018.

[43] W. J. Denny, B. M. O’Connell, J. Milroy, and M. T. Walsh, “An analysis of three dimensional diffusion in a representative arterial wall mass transport model,” *Ann. Biomed. Eng.*, vol. 41, no. 5, pp. 1062–1073, 2013.

[44] C. Conway, J. P. McGarry, and P. E. McHugh, “Modelling of Atherosclerotic Plaque for Use in a Computational Test-Bed for Stent Angioplasty,” *Ann. Biomed. Eng.*, vol. 42, no. 12, pp. 2425–2439, 2014.

[45] J. S. Soares, J. E. Moore Jr., and K. R. Rajagopal, “Constitutive framework for biodegradable polymers with applications to biodegradable stents,” *ASAIO J*, vol. 54, no. 3, pp. 295–301, 2008.

[46] D. Hayman, C. Bergerson, S. Miller, M. Moreno, and J. E. Moore, “The effect of static and dynamic loading on degradation of PLLA stent fibers,” *J Biomech Eng*, vol. 136, no. 8, p. 4027614, 2014.

[47] N. Gonzalo, P. W. Serruys, and E. Regar, “Optical coherence tomography: clinical applications and the evaluation of DES,” *Minerva Cardioangiol.*, vol. 56, no. 5, p. 511—525, 2008.

[48] N. Gonzalo *et al.*, “Reproducibility of quantitative optical coherence tomography for stent analysis.,” *EuroIntervention J. Eur. Collab. with Work. Gr. Interv. Cardiol. Eur. Soc. Cardiol.*, vol. 5, no. 2, pp. 224–232, Jun. 2009.

[49] T. Okamura, P. W. Serruys, and E. Regar, “The fate of bioresorbable struts located at a side branch ostium: serial three-dimensional optical coherence tomography assessment,” *Eur. Heart J.*, vol. 31, no. 17, p. 2179, May 2010.

[50] K. Paakinaho, H. Heino, J. Väisänen, P. Törmälä, and M. Kellomäki, “Effects of lactide monomer on the hydrolytic degradation of poly(lactide-co-glycolide) 85L/15G,” *J. Mech. Behav. Biomed. Mater.*, vol. 4, no. 7, pp. 1283–1290, 2011.

[51] H. A. von Recum, R. L. Cleek, S. G. Eskin, and A. G. Mikos, “Degradation of polydispersed poly(L-lactic acid) to modulate lactic acid release,” *Biomaterials*, vol. 16, no. 6, pp. 441–447, 1995.

[52] N. Artzi *et al.*, “In vivo and in vitro tracking of erosion in biodegradable materials using non-invasive fluorescence imaging.,” *Nat. Mater.*, vol. 10, no. 9, pp. 704–709, Sep. 2011.

[53] H. Il Kim *et al.*, “Tissue response to poly(l-lactic acid)-based blend with phospholipid polymer for biodegradable cardiovascular stents,” *Biomaterials*, vol. 32, no. 9, pp. 2241–2247, 2011.

[54] W. J. van der Giessen *et al.*, “Marked inflammatory sequelae to implantation of biodegradable and nonbiodegradable polymers in

porcine coronary arteries.," *Circulation*, vol. 94, no. 7, pp. 1690–1697, Oct. 1996.

[55] D. Chen *et al.*, "Effect of inflammation on endothelial cells induced by poly-L-lactic acid degradation in vitro and in vivo.," *J. Biomater. Sci. Polym. Ed.*, vol. 29, no. 15, pp. 1909–1919, Oct. 2018.

[56] G. Perale *et al.*, "A new model of resorbable device degradation and drug release: transient 1-dimension diffusional model," *J Control Release*, vol. 136, no. 3, pp. 196–205, 2009.

[57] P. Arosio, V. Busini, G. Perale, D. Moscatelli, and M. Masi, "A new model of resorbable device degradation and drug release - part I: zero order model," *Polym. Int.*, vol. 57, no. 7, pp. 912–920, 2008.

[58] Y. Chen, S. Zhou, and Q. Li, "Mathematical modeling of degradation for bulk-erosive polymers: Applications in tissue engineering scaffolds and drug delivery systems," *Acta Biomater.*, vol. 7, no. 3, pp. 1140–1149, 2011.

[59] R. Naseem, L. Zhao, Y. Liu, and V. V. Silberschmidt, "Experimental and computational studies of poly-L-lactic acid for cardiovascular applications: recent progress," *Mech. Adv. Mater. Mod. Process.*, vol. 3, no. 1, p. 13, 2017.

[60] Y. Li *et al.*, "The effect of mechanical loads on the degradation of aliphatic biodegradable polyesters," *Regen. Biomater.*, no. April, pp. 179–190, 2017.

[61] G. N. Gatica, B. Gomez-vargas, and R. Ruiz-baier, "Analysis and mixed-primal finite element discretisations for stress-assisted diffusion problems," *Comput. Methods Appl. Mech. Engrg.*, vol. 337, pp. 411–438, 2018.

[62] D. Hofmann, M. Entrialgo-Castaño, K. Kratz, and A. Lendlein, "Knowledge-based approach towards hydrolytic degradation of polymer-based biomaterials," *Adv. Mater.*, vol. 21, no. 32–33, pp. 3237–3245, 2009.